UNIVERSITÀ DELLA CALABRIA

Department of Pharmacy, Health, and Nutritional Science

PhD in Translational Medicine

XXXVI cicle

"Next-Generation vesicular systems in Nanomedicine: building blocks for personalized therapeutics"

SSD CHIM-09

Supervisor
Prof.ssa Rita Muzzalupo

PhD student
Dott.ssa Martina Romeo

PhD Coordinator
Prof.ssa Stefania Catalano

STEFANIA
CATALANO
20.05.2024
10:10:52
GMT+01:00

Anno Accademico: 2023/2024

ABSTRACT

The emergence of nanotechnology has not only revolutionized the field of drug formulation but has also ushered in a new era of personalized therapeutic interventions. Over the past few years, nanoscale-controlled release systems have emerged as game-changers, exhibiting extraordinary potential in augmenting therapeutic effectiveness while concurrently mitigating the adverse effects associated with traditional medications. This novel cohort of nanocarriers, comprising a rich array of materials including lipids, polymers, and non-ionic surfactants, stands as a testament to the versatility and ingenuity of nanotechnological advancements. By harnessing their unique properties, nanovehicles offer a precision-targeted approach to drug delivery, homing in on specific pathological sites with unprecedented accuracy. Moreover, the inherent adaptability of nanocarriers allows for bespoke modifications tailored to individual therapeutic needs, whether it be bolstering drug stability, facilitating permeation across biological barriers, or orchestrating sophisticated "intelligent" systems for targeted cancer therapy.

Not only does this approach promise to enhance therapeutic outcomes, but it also presents a more efficient and cost-effective alternative to the traditional pursuit of novel pharmacologically active compounds. As such, the convergence of nanotechnology and drug delivery represents a compelling frontier in the quest for optimized therapeutic interventions, holding profound implications for the future of medicine.

Introduction

Introduction

I. Structure of thesis

The following thesis, based on the research activities carried out in the Pharmaceutical Technology group belonging of the Department of Pharmacy, Health and Nutrition (University of Calabria) is made up into five sections, focusing on the development of new drug delivery systems for various pharmaceutical applications. The following titles summarizes the sections composing the entirety of the thesis: innovative nanosystems based on pharmacologically active molecules with self-association capacity (surfadrug) Chapter 1, Innovative nanosystems for drug delivery, Chapter 2, Multifunctional nanosystems for cancer therapy, Chapter 3, Nanosystems for topical and transdermal drug delivery, and Chapter 4, Intelligent stimulus-responsive nanosystems for drug delivery.

II. Drug Delivery Systems

In the last century, nanotechnology has experienced significant growth, leading to important innovations and applications in various areas of science. Indeed, nanotechnology has enabled medical, diagnostic and therapeutic treatments to be advanced and the quality of healthcare to be improved. The application of nanotechnology has led to the production of nanomaterials as carriers of active substances that enhance their action that could promote their action. Indeed, nanoscale design has made it possible to overcome the limitations of conventional drug delivery. The small size and large surface area of nanoscale particles allow them to be engineered to bind, adsorb, or transport target molecules, enabling targeted therapy [1]. These functional platforms protect the payload by preventing its premature decomposition in the biological environment and improve its bioavailability, blood persistence and cellular uptake [2]. The release of therapeutic molecules from vesicular systems is widely used to deliver hydrophilic and/or lipophilic drugs. Vesicles are nanostructures composed of an aqueous core and a lipid bilayer, typically between 10 and 1000 nm in size, which can encapsulate hydrophilic drugs in the core or lipophilic drugs in the lipid bilayer. These vesicular drug delivery systems are called VDDS (vesicular drug delivery systems). Nanosystems with different shapes and sizes (nanoparticles, polymers, dendrimers, emulsions, liposomes, etc.) can be formulated with different materials that control cellular uptake and promote permeation **Figure 1**.

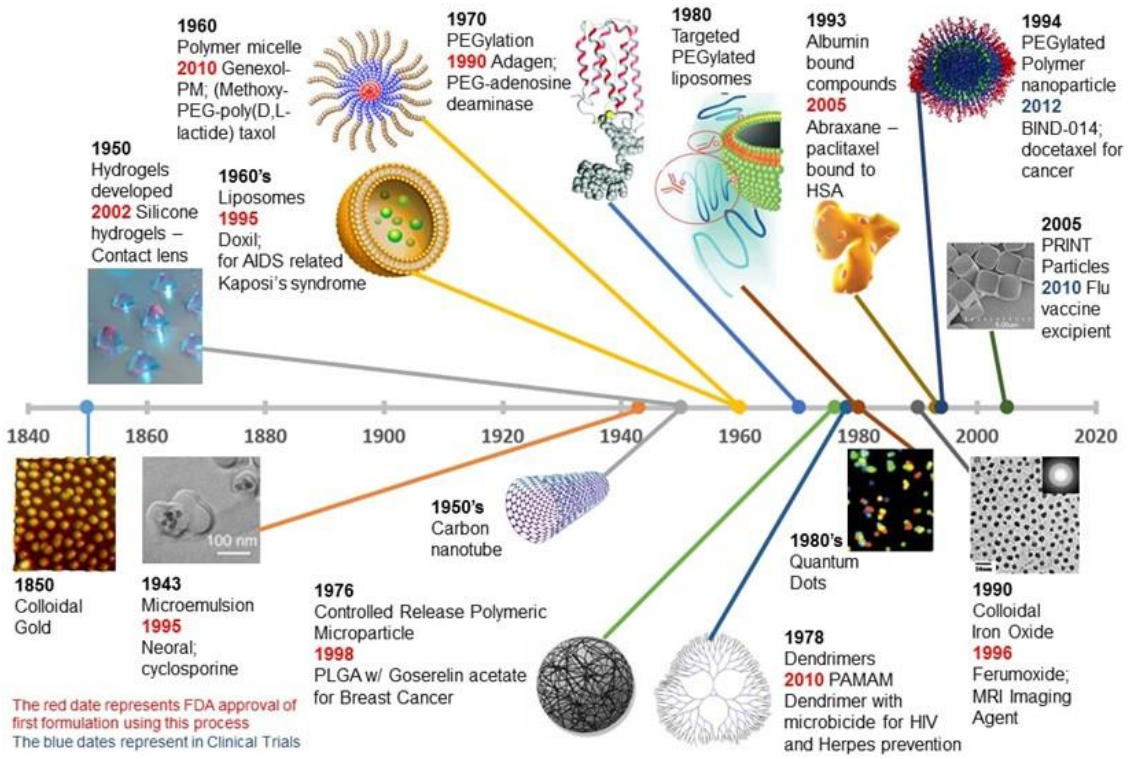

Figure 1. Different micro and nanosystems used for therapeutic and diagnostic application.

The considerable interest in nanocarriers is linked to the side effects and disadvantages of classical therapeutic treatments. Many therapeutic agents are used to treat various diseases, but their use is limited by their susceptibility to biodistribution in the human body and the resulting side effects. The use of nanocarriers for the delivery of pharmacologically active molecules offers significant advantages, including:

- Ability to move efficiently in the blood stream, through the intestinal epithelia by means of facilitated diffusion, membrane transport and receptor/ligand-mediated transport;
- Facilitated absorption of the transported drug due to their physicochemical properties;
- Excellent membrane permeability;
- Good biocompatibility and degradability;
- Improved drug solubility;
- Improved drug chemical stability and photostability;
- Improved drug bioavailability.

To date, great quantities of materials, such as polymers, lipids, and inorganic materials, have been developed and used as drug carriers to control the release behaviour of payloads [3,4] making drugs "smart". Therefore, given their unique properties, nanosystems offer new opportunities for the treatment of numerous pathologies.

III. Multifunctional Nanosystems in Cancer Therapy

The main objective of nanosystems as delivery agents is to deliver drugs with high selectivity to target tissues. The encapsulation of bioactive compounds in drug delivery systems (DDS) increases the stability of active substances and facilitates local therapies by enhancing the bioactivity of the drug, counteracting its degradation and facilitating it reaching the target tissue at the desired therapeutic levels and times. Nanosystems can be made smart by targeting strategies that allow the drug to be concentrated only where needed. The targeting of the administered active substance can be active or passive. Passive targeting consists of the passive accumulation of the drug in the diseased area. Within the tumour environment, in fact, blood vessels have a different nature from physiological ones, due to their irregular organisation and structure: non-conforming diameter, bulges, abnormal permeability, absence of basement membrane. Moreover, when diffusion within the tumour microenvironment is poor, a process of neoangiogenesis is triggered and it leads to the production of new vessels for the supply of oxygen and nutrients [5]. These neovases are more permeable than physiological ones; therefore, nanosystems with a smaller pore size are able to overcome the endothelium and circulate longer in the interstitial space. The plasma permanence of the drug also increases because solid tumours have a deficient lymphatic drainage system, resulting in preferential accumulation (Figure 2) of the nanocarriers by extravasation [6].

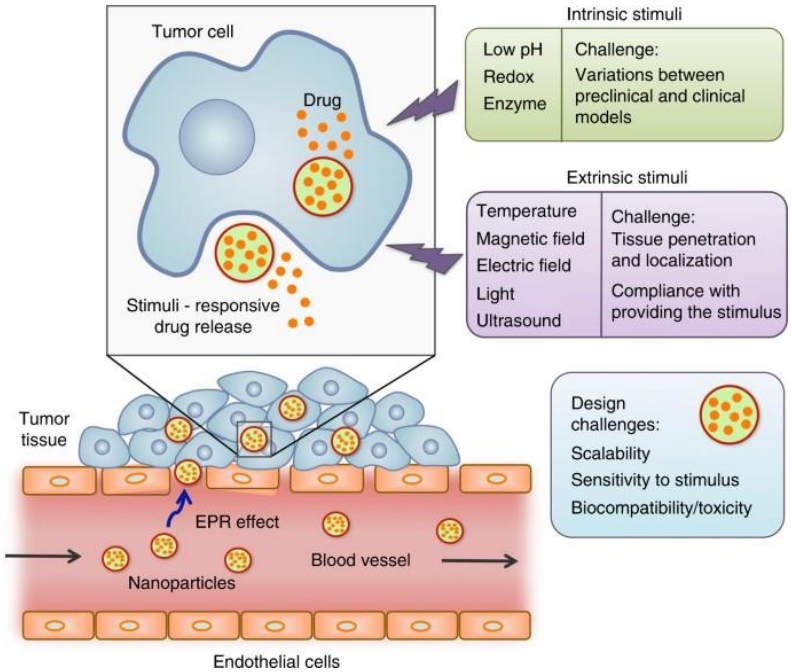

Figure 2. Illustration of passive targeting mechanism

The combination of permeable blood vessels and poor drainage is recognised as the effect of enhanced permeation and retention (EPR). The accumulation of nanosystems in pathological tissue competes with absorption in the liver and EPR [7]. Consequently, vectors must circulate for days before they reach a concentration that has a noticeable pharmacological effect. One important approach is the design of nanosystems capable of responding to stimuli (**Figure 2**) typical of the tumour microenvironment [8]. In this way, the formulations remain in circulation in an inactive form, to be activated upon internalisation in the tumour cells. The stimuli that can be exploited are:

- the extracellular pH of solid tumours, which is more acidic than that of healthy tissue [9];
- the hypoxia typical of the tumour habitat, as the abnormal microcirculation is unable to guarantee the correct supply of oxygen;
- up-regulation of enzymes such as metalloproteases [10], topoisomerases or PARPs increases the activation of nanosystems in situ;
- hyperthermia is indicative of a pathological condition because normally the body temperature is around 37°C and remains constant despite changing external thermal conditions. Instead, following the activation of an inflammatory process, there is the release of heat mediated by the production of an inflammation mediator which is histamine; this promotes a condition of vasodilation and hyperemia (increased blood volume).

Therefore, it is possible to design nanosystems by chemically or physically combining materials of different natures that respond with morphological or surface alterations only when they come into contact with the specific microenvironment for which they were designed. This will make it possible to create site-specific systems and reduce the side effects associated with classic drug therapies. In addition to internal stimuli, due to the specific characteristics of the tumour environment, there are also external stimuli, such as magnetic radiation, application of an electric field and ultrasound. Active targeting, on the other hand, is achieved by conjugating directing agents such as monoclonal antibodies, peptide sequences or small molecules such as folic acid and transferrin onto the surface of the carrier systems, so that the system is only recognised and intercepted by target cells [11]. In this case, the targeting is therefore linked to the interaction of the specific ligand with antigens and receptors overexpressed by the diseased cells compared to normal cells **Figure 3**.

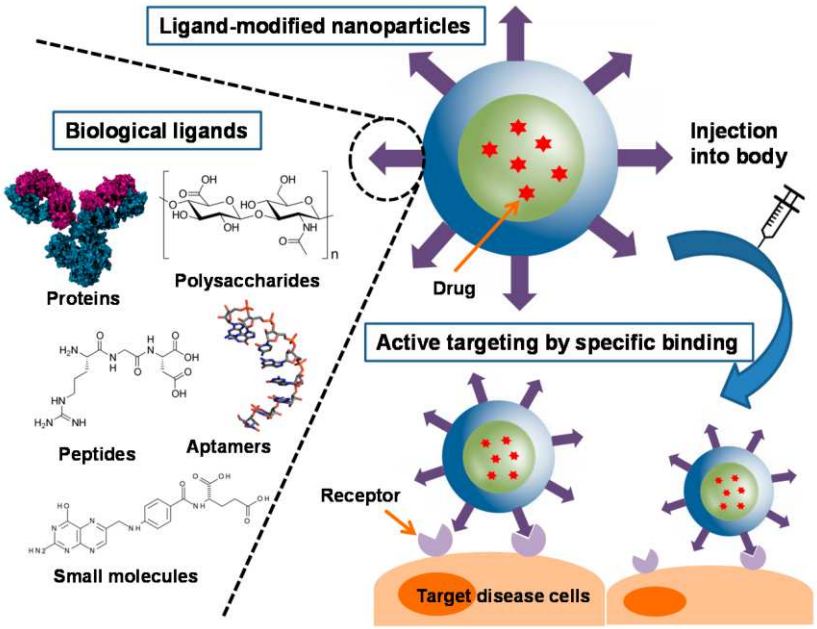

Figure 3. Illustration of active targeting mechanism

In this way, the system selectively targets the pathological microenvironment and actively affects the tumour vasculature. This leads to the destruction of the vessel endothelium and blocks the supply of oxygen and nutrients, resulting in cell death. The factors considered for surface modification of nanosystems are mainly peptides, folates, transferrin, antibodies, hyaluronic acid, proteins and vitamins, **Table 1**. These have numerous targets, including endothelial growth factors (VEGF or EGF); adhesion molecules (VCAM); metalloproteases (MMP) [12]; luteinising hormone (LH-RH); transferrin receptor (TfR) and chemokine receptor (CXCR). Therefore, modified and functionalised nanovectors are used to discriminately target tumour cells that overexpress the corresponding receptors, in order to improve the targeted release and cellular uptake of anticancer drugs, which are precisely delivered to diseased cells, reducing toxic effects on normal tissues [13].

A promising approach in nanotechnology therefore, lies in the development of multifunctional vesicles, simultaneously exploiting multiple targeting strategies. The combination of active and passive targeting could lead to increased safety and efficacy of the systems, ensuring a high degree of specificity for target cells. Multifunctional nanovesicles can simultaneously perform multiple functions such as: imaging, drug monitoring, targeted delivery and controlled release, improving the accurate diagnosis of therapies of disease.

Table 1. Types of ligands

Carbohydrates	Hyaluronic acid
Small molecules	Folic acid
Peptides	Transferrin Apo-E
Antibodies	Cetuximab Trastuzumab
Synthetic molecules	TPB (4-Carboxybutyl triphenylphosphonium bromide)

IV. Nanosystems for topical and transdermal drug delivery

Skin administration has always been of great interest in the pharmaceutical field, due to its ease of administration, high flexibility, controlled drug release, controlled therapeutic effect, etc. The skin, in fact, represents one of the body's main defence mechanisms against foreign agents. Anatomically, it can be divided into three layers: the hypodermis layer (layer of subcutaneous fat), the connective dermis and the epidermis (layer of stratified avascular cells). The epidermis in turn consists of five layers, the stratum germinativum (basal layer), the stratum spinosum (spiny layer), the stratum granulosum (granular layer), the stratum lucidum and the stratum corneum. The stratum corneum, consisting of 15-20 layers of keratin-filled corneocytes, is in fact considered the main obstacle to transdermal permeation of many substances [14]. Indeed, when the skin barrier is not compromised and the stratum corneum is intact, it is only accessible to small, relatively lipophilic, and uncharged molecules with a partition coefficient between 1 and 3 and weighing less than 800 Da.

Since the ongoing request for localised drug delivery, administration through the skin can be a good application approach. Cutaneous administration can be of two types:

- topical: in which a drug is administered at the skin site of action, resulting in a higher concentration of the localised drug and reduced systemic effects [15];
- transdermal: involves transporting the drug through the skin to the systemic circulation to reach therapeutic levels.

In both cases, this administration is advantageous because it avoids first-pass metabolism and the gastrointestinal tract, thus improving the bioavailability of the drug. It improves patient compliance, as it is a convenient and painless administration, thus useful for paediatric or comatose patients. In addition, transdermal administration ensures a controlled release of the drug, thus reducing fluctuations in plasma concentration that occur with other routes of administration. [14]. Since cutaneous permeation is limited by the stratum corneum, nanotechnology aims to develop systems capable of temporarily

modifying the structural and biochemical characteristics of the skin in order to ensure the access of drugs to the body. To date, several systems have been designed that can reversibly reduce the stratum corneum barrier, modifying its structure and favouring the formation of additional pathways for the passage of exogenous molecules. One of the key advancements lies in the utilization of nanosystems, which harness sophisticated permeation enhancers adept at amplifying drug permeability [16]. These nanosystems include both lipid nanoparticles and vesicular systems. [17,18]. Their small size facilitates the transport of the drug through the skin and ensures its release, because their occlusive effect on the skin determines its hydration and elasticity, facilitating its permeation. [19]. Permeation enhancers, also known as potentiators, include polar low-molecular-weight solvents (ethanol, propylene glycol, dimethyl sulphoxide) and amphiphilic compounds containing a polar head and a hydrophobic domain, such as fatty acids -dodecylazepan-2-one (azone), dodecyl-2-dimethylaminopropanoate (DDAIP)[20] .

Also influencing the skin permeation of nanocarriers are some of their chemical-physical properties. For instance, it is well documented that the skin permeation of nanocarriers is influenced by their size. Vesicles with a diameter ≥ 600 nm are unable to penetrate deeper skin layers, whereas vesicles with a diameter ≤ 300 nm allow the release of their contents into the deep layers by penetrating through the transfollicular pathway. Particles with a size ≤ 100 nm, on the other hand, are suitable for deep penetration of the skin, resulting in the onset of the action [21]. Another parameter of great importance is shape. Disc-shaped, cylindrical, and hemispherical vesicles may be more successful than classic spherical particles in avoiding absorption by phagocytic cells. [22]. The surface charge strongly influences the permeation of the transported drugs. Since the skin is negatively charged, it is expected to treat and thus diffuse cationic nanoparticles more than neutral and anionic ones. Hydrophobicity and hydrophilicity are also determining factors. Several studies have indeed shown that the surface hydrophobicity of nanoparticles strongly influences their penetration, but also absorption and biodistribution. [23,24]. Driven by the need to improve skin penetration of conventional vesicles, new ultra-deformable vesicles were also designed through structural and chemical modifications of liposomes. [25]. These include ethosomes, which, due to the presence of ethanol affecting their average size, zeta potential, stability, and drug entrapment efficiency, make them more effective than classical liposomes. Transferosomes, ultra-deformable vesicles that improve the deformability of double layers, mainly by varying their interfacial tension. [26]. Or cubosomes, which involve the use of an amphiphilic non-ionic triblock

copolymer of polyethylene oxide (PEO) and propylene polyoxide (PPO), which are among the most commonly used stabilisers [27]. Study of topical and transdermal absorpition is performed through the application of *in vitro* methods as Franz diffusion cells, *in vivo* as open-flow skin microperfusion, *ex vivo* methods as a tape stripping method. Therefore, various vesicle materials can be used to promote skin permeation, such as certain phospholipids, surfactants, lipids and small molecules (**Table 2**). This chemical enhancer act increasing (and optimizing) the thermodynamic activity of the drug when functioning as a co-solvent, increasing the partition coefficient of the drug to promote its release from the vehicle into the skin, conditioning the stratum corneum to promote drug diffusion and promoting penetration and establishing drug reservoir in this stratum. An ideal chemical enhancer should be pharmacologically inert, non-toxic, non-allergenic, chemically and physically chemically and physically compatible with nanosystems and economical. Furthermore, after its removal, the SC should immediately and completely recover its normal barrier function.

Table 2. Example of skin permeations enhancers

Skin permeations enhancers	
Small Molecule Solvents	Ethanol Propylene Glycol Dimethylsulfoxide Dimethylacetamide Decanol
Sufactants	N-Lauroylsarcosine Span 20 Spsn 80 Ascorbyl Palmitate Glycerol Monolaurate Span 80 Tween 80 Sodium Lauryl Sulphate
Peptides	Cell-Penetrationg Peptides (TAT, Penetratin, Arginine Oligomers), Antimicrobial Peptides (Magainin)
Fatty Acids	Linoleic Acid Oleic Acid Palmitic Acid Lauric Acid
Glycols	Propylen Glycole Dypropylene Glycol
Polymer	Chitosan

V. Vesicular Systems

In recent years, the pharmaceutical industry has placed great emphasis on the development of new drug delivery systems as innovative tools for diagnosis and therapy. This has led to the development of a wide variety of nanocarriers made of different materials, which are described in the following sections.

V.I Liposomes and Niosomes

Among the various DDS, great attention has been paid to niosomes. Niosomes have been developed as a better alternative to liposomes. They have a different chemical composition of the bilayer, which offers several advantages. They are hollow systems, consisting of an aqueous core bordered by one or more bilayers formed by surfactants; they are much more stable than liposomes as they are not degraded by the phospholipolytic enzymes of the stratum corneum as happens to phospholipids, and the surfactant structure is similar to that of epidermal ceramides allows them to assemble the corneous lamellae and reduce epidermal dehydration. The unique structures of niosomes make them capable of encapsulating both hydrophilic and lipophilic substances. Surfactants are substances capable of lowering the surface tension of a liquid (liquid/air interface) and/or the interfacial tension between two liquids or between a liquid and a solid. They generally consist of organic molecules with amphiphilic characteristics, i.e. containing both hydrophilic and hydrophobic (lipophilic) groups. From a chemical point of view, surfactants can be classified based on the characteristics of the hydrophilic portion of the molecule. The following categories can therefore be identified: anionic surfactants, cationic surfactants, amphoteric surfactants or zwitterionic surfactants. The most used non-ionic surfactants in the design of vesicles as release systems include ethers; esters, of which the best known are sorbitans, most frequently called Span, or ether-esters, of which the best known are polyoxyethylene sorbitans, also called Tween. The choice of surfactant is a critical factor to consider when designing such systems. Indeed, it is well known how the molecular structure of the surfactant clearly influences the size, stability, drug entrapment efficiency, pharmacokinetics, pharmacodynamics and targeting properties of vesicular systems [28]. Surfactants used in niosomal systems include Gemini surfactants. These comprise two hydrophobic chains and two polar head groups, covalently connected by a spacer group. Gemini surfactants have attracted much attention as they exhibit a very high aggregation capacity with

correspondingly low CMC values [29]. Further attention is paid to amino acid-based surfactants, both single-chain and gemini-type, as they derive from amino acid compounds and are less toxic, more biodegradable and with high encapsulation capabilities compared to classic surfactants. Niosomes are therefore liposomes based on non-ionic surfactants [30]. They are similar to liposomes in shape and geometry, but offer several advantages, thanks to their reduced tendency to aggregate and greater stability. As regards the physical stability of liposomes, this is determined by the type of phospholipids used, i.e. their head and the nature of the fatty acids. The instability of liposomes could also be related to the possible leakage of the contents from the vesicles, this could occur due to the presence of oxidizing agents or due to possible aggregation or fusion of the vesicles themselves. In addition to the problems of chemical-physical stability, linked to the storage time, there are also stability problems in biological systems, because once introduced into the blood circulation, liposomes are subject to both opsonization mediated by immunoglobulins, complement factor proteins, both by fibronectin which stimulate the reaction of macrophages, and with plasma proteins and lipoproteins which destroy the vesicular structure. Furthermore, liposomes are fragile systems; therefore, care is required in their handling to keep the vesicles intact and allow them to perform the intended controlled release. Therefore, precisely to overcome these limitations linked to the lack of stability of liposomes in the nanoencapsulation of active ingredients, the use of niosomes has been proposed **Table 3**.

Table 3. Niosome and Liposome differences

	Niosome	**Liposome**
Components	Surfactant	Phospholipid
Components avaibility	High	Low
Component purity	Good	Variable
Preparation and storage	No specific condition required	Inert atmosphere, low temperature
Stability	Very good	Low
Cost	Low	High
Toxicity	Low	Low
Dimension	< 1 μm	3 μm

Unfortunately, although a notable variety of such nanocarriers have been developed over time, success appears to be limited to a few formulations [31], this because it has been seen that niosomes also have a series of disadvantages, such as a low drug encapsulation capacity.

V.II Self-assembled drugs

To overcome the limitations induced by niosomal systems, the use of pharmacologically active molecules, with an amphiphilic structure, for the creation of the bilayer has been proposed. Many of the pharmacologically active compounds used for the preparation of niosomal systems are amphiphilic molecules, which tend to self-associate and interact with biological membranes in the same way as classic surfactants. These pharmacologically active compounds have been identified in some studies with the term “surfadrug” [32]. The structure and characteristics of amphiphilic drug molecules influence their association in aqueous solution and consequently their interaction with biological membranes. Typically, amphiphilic molecules, such as surfactants, of sub-colloidal dimensions, when present at low concentrations in a liquid medium tend to exist separately. As the concentration increases, and over a narrow concentration range, they form aggregates made up of multiple molecules, called "micelles". The concentration at which they form is called the critical micelle concentration (CMC), and the number of molecules that aggregate to form the micelle is called the "aggregation number". Therefore, in aqueous medium, surfadrugs can exist as monomers or can aggregate into micelles, bilayers, depending on the concentration, hydrophilic-hydrophobic balance, and preparation method. They therefore tend to form different structures, which can interconvert depending on pH, temperature, ionic strength, and concentration. Several drugs have shown the ability to self-associate, including phenothiazine [33], analgesic drugs [34], antibiotics, Tricyclic antidepressants [35, 36], local anesthetics [37, 38], anticancer drugs [39] etc… **Table 4.**

Table 4. Class of surfadrugs and relative Critical Micellar Concentration (M).

Class	Drug	CMC (M)
Antibiotics	Streptomycin	$9.0x10^{-5}$
	Actinomycin D	$1.0x10^{-4}$
Analgesic	Dextropropoxyphene	$1.0x10^{-1}$
Local anesthetics	Dibucaine HCl	$6.6x10^{-2}$
	Tetracaine HCl	$1.3x10^{-1}$
Tricyclic antidepressants	Amitriptyline HCl	$3.6x10^{-2}$
	Clomipramine HCl	$2.2x10^{-2}$
	Imipramine HCl	$4.7x10^{-2}$
Phenothiazines	Trifluopromazine	$4.5x10^{-3}$
	Chlorpromazine HCl	$1.9x10^{-2}$
	Trifluoperazine	$4.2x10^{-5}$

Chemically, surfadrugs contain one or more flexible, hydrophobic aromatic nuclei, to which an ester group or a charge-carrying N atom is directly attached, or which include a pyridine-like N atom; and it is precisely the flexibility of the aromatic ring that makes these drugs resemble typical surfactants in their associative behaviour [40]. Surfactant drugs with quite different chemical structures have been reported to self-associate and bind to membranes, causing them to rupture and solubilize, similar to a detergent [41]. These molecular characteristics mean that the use of an amphiphilic drug in the design of nanocarriers, in addition to minimizing the use of other excipients, speeds up clinical trials. So much so that excipients are substances that certainly contribute to the characteristics of the product, such as stability, biopharmaceutical profile, organoleptic properties, patient satisfaction, etc., however they can often determine various risks for the patient such as: allergic reactions and anaphylaxis; food intolerance; drug interactions. Furthermore, surfadrug-based nanocarriers can be used to deliver other drugs and achieve combination therapy. Surfadrug-based DDSs could therefore represent a great innovation in the pharmaceutical field, due to their dual function: that relating to the pharmacological nature of the molecule and that relating to the technological properties of the vehicles obtained such as biocompatibility and formulation versatility. The latter, deriving from the different characteristics of the niosomes, such as size, any net surface charges, fluidity of the double layer etc... which can be modified in relation to the application requirements.

V.III Polymeric micelles

Polymeric micelles are core-shell structures synthesized to form amphiphilic block copolymers in aqueous solution [42, 43]. Indeed, they are composed of two separate

functional segments: the inner core, responsible for drug loading capacity, and the outer shell, which controls pharmacokinetic (PK) behaviour in vivo. Several conventional features of these polymeric micelles, such as enhanced solubilization of poorly hydrophobic drugs, exhibiting a sustained release profile, and most importantly, protection of the encapsulated cargo from degradation by various enzymes and even metabolism, make them favourable candidates for the administration of drugs. [44]. They represent an innovative tool to overcome problems related to drug administration, such as low solubility in water and poor permeability of the drug through biological membranes. Micelles are formed from a polymer solution, when the concentration of the latter exceeds the Critical Micellar Concentration (CMC) and a certain threshold temperature known as the critical micelle temperature (CMT) [45,46]. The CMC value is one of the most important parameters to define its thermodynamic stability and kinetic stability, the latter indicates the tendency of the micelles to disassemble over time when the system is diluted below the CMC [47].

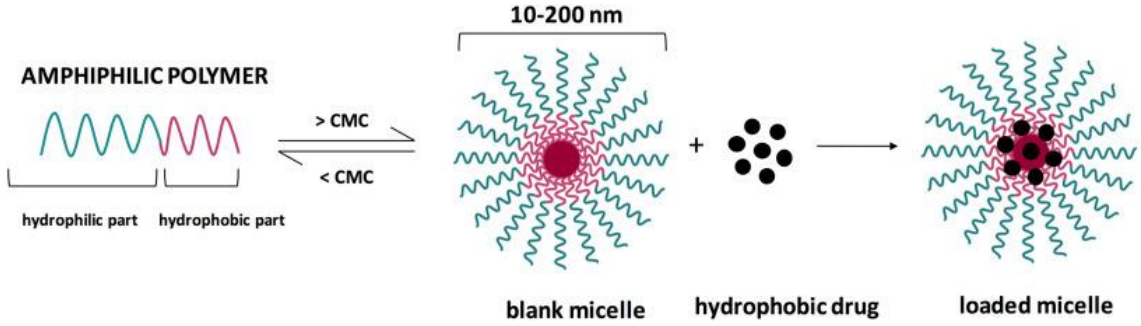

Figure 4. Formulations of polymeric micelles

The most used polymers to produce micelles are amphiphilic block copolymers, including polystyrene and polyethylene glycol, triblock copolymers such as poloxamers but also graft copolymers e.g. G-chitosan [48,49]. Drugs can be encapsulated either during their preparation or at a later stage, depending on the characteristics of the drug and the preparation method used. Practically insoluble drugs can be incorporated into these micelles by various known techniques, such as physical loading by the solvent evaporation or dialysis method, or by chemical conjugation or other emulsification techniques. Chemical conjugation usually involves the formation of a stronger covalent bond, such as an amide bond between the end groups of the drug molecule and the polymer chain. The loading obtained with this technique is quite robust and with adequate combinatorial chemistry it is possible to tailor a higher loading percentage based on the chemical characteristics of the drug molecule's surface and polymer structure [50]. The stable and robust binding can lead to some problems with the splitting and release of the

drug molecule into the blood circulation, in the presence of enzymes. For this reason, suitable groups that can easily degrade in contact with enzymes must be inserted into specific sites between the drug molecule and the polymer chain.

Polymeric micelles exhibit favourable characteristics, such as small size, long circulation, ease of production, reduced toxicity, and the ability to alter the drug internalization pathway and subcellular localization, reducing the efflux effect of P-glycoprotein (P-gp) and consequently they exert a different mechanism of action than the encapsulated drugs [51,52]. Their size is adequate since, in combination with the pathophysiological characteristics of solid tumor tissues, they lead to an increase in the permeability and retention (EPR) effect in solid tumors [53,54] and allow passive targeting towards tumors solid [55]. Compared to newer DDSs, such as liposomes, niosomes and nanoparticles, micelles possess greater drug encapsulation capacity, generally smaller size, easier preparation, and sterilization processes and good solubilization properties, unfortunately they are associated with lower stability in fluids environments physiological body fluids.

V.IV Polymeric nanoparticles

Among DDSs, polymeric nanoparticles represent a key tool for improving the bioavailability of drugs or their release at the specific site of action. Nanoparticles (NPs) are colloidal solid particles with dimensions between 10 and 1000 nm. They can have a spherical, branched or shell structure and consist of biodegradable and non-biodegradable polymers in which drugs are incorporated by dissolution, adsorption, and attachment or by encapsulation. Polymeric nanoparticles have been widely used in recent years due to their ease of processing, design and good biocompatibility. Compared to microparticles, NPs allow sustained and controlled drug release, site-specific targeting and a large surface-to-volume ratio. By doing so, these systems make it possible to reduce the drug dose required and the frequency of administration, ensuring better patient compliance [56]. Nanoparticles are synthesized by size reduction using either top–down methods such as milling, high-pressure homogenization and sonication or bottom–up processes like reactive precipitation and solvent displacement. Polymers are macromolecules generated by joining one or more monomer units to form a linear or branched chain. By selecting the right monomer, a polymer with the desired specific properties can be obtained. Many polymers are in fact synthesised from the corresponding monomers, giving rise to a wide range of structures and applications, such as optimising specificity. But natural polymers are also used, including chitosan, collagen, albumin and gelatin. These natural polymers

have high application potential as they possess intrinsic properties such as biocompatibility, biodegradability and ease of surface modification.

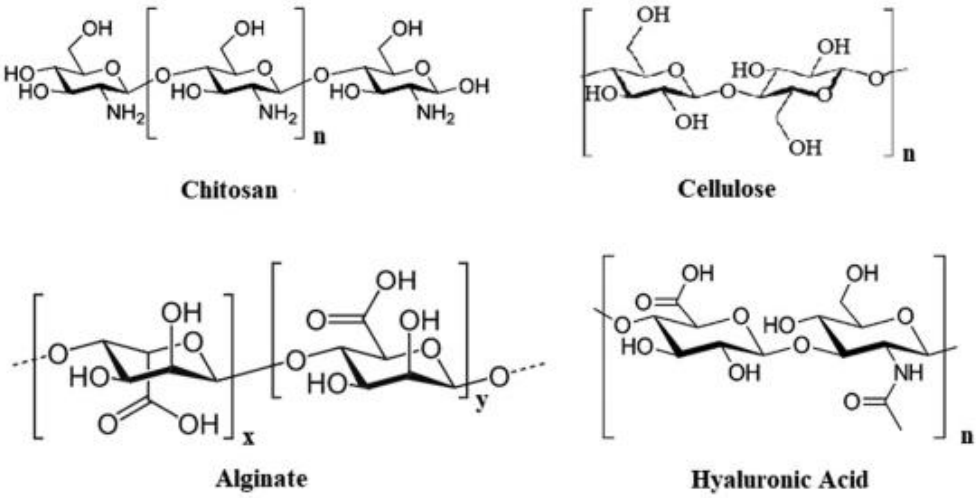

Figure 5. Molecular structure of natural polymers.

The release of the active ingredient from NPs depends on the properties of the polymer and the encapsulated drug. For non-biodegradable polymers, the release is a function of the rate of diffusion of the drug through the polymer matrix. For biodegradable polymers, it is a function of matrix degradation, resulting in drug release, solubilisation and diffusion through channels formed in the matrix because of its erosion [57]. In the case of both biodegradable and non-biodegradable polymers, the so-called 'burst' effect occurs, which consists of the rapid release of a percentage of drug adsorbed onto the surface of the nanoparticle.

Chitosan, for example, is a derivative of chitin, produced by its partial deacetylation. In nature, it is abundant in the shells of crustaceans and in the cell walls of fungi. The degree of deacetylation influences its properties of hydrophobicity, solubility, and toxicity. Chitosan with a high degree of deacetylation has a molecular weight-dependent toxicity. While chitosan with a low degree of deacetylation acts as an absorption enhancer at both molecular weights [58]. Therefore, the molecular weight of chitosan also influences its properties. From the degree of acetylation and the molecular weight also depends on the speed of drug release. Therefore, it is possible to modulate the release rate of a drug, depending on the desired action, by choosing from various types of chitosan. Another distinctive feature is its polycationic nature, which translates into the ability to form cross-links with different polyanions that, through gelation, lead to the development of nanoparticles, as well as being responsible for biological activities such as

mucoadhesiveness [59], antimicrobial [60] and antioxidant activity [61]. Chitosan NPs are used for various types of administration, including parenteral, oral, ocular, topical, intranasal. Chitosan NPs are of great interest in cancer therapy, as the ideal goal would be to develop therapeutic agents with effective toxicity on cancer cells without affecting normal cells. These nanoparticles can indeed be modified, e.g. with aptamers, antibodies or small molecules, to target specific tissues in order to prevent non-specific interactions, increase local drug concentration and reduce systemic side effects [62]. For example, doxorubicin loaded with chitosan NPs showed a regression of tumour growth and an increase in the survival rate of tumour-implanted rats after the fourth administration. There are several methods of preparing chitosan NPs, but the most common is ionotropic gelation, which exploits the cross-linking between the positively charged primary amine groups of chitosan and the negative groups of an anionic substance.

V.V Liquid Lyotropic Crystals

Lyotropic liquid crystals (LLCs) are self-assembling nanomaterials, usually consisting of water and one or more surfactants in defined ratios. They have attracted much attention as drug delivery systems. Depending on the concentration of the components and the temperature, they can be divided into mesophases: cubic, hexagonal (H_2) and lamellar (Lα). They possess anisotropic physical properties, except for the cubic phases, such as refractive index, dielectric constant, elastic behaviour, or viscosity. Cubic mesophases can comprise a curved bicontinuous bilayers and two aqueous nanocannels interpenetrating but not in contact, or be composed by separated spheres being either water or oil continuous and discontinuous in the other phase [63]. This mesophase can be used to deliver drugs of a hydrophilic, lipophilic, or amphiphilic nature. Lipophilic drugs will be in the lipid bilayer, hydrophilic drugs near the polar head or in the aqueous channels, and amphiphilic drugs at the interface [64]. Typically, cubic phases are transparent, viscous, semi-solid gels [65], which makes them difficult to handle. Furthermore, they are optically isotropic and are therefore often called viscous isotropic phases. In hexagonal mesophases, molecular aggregates are organised in closed, extended columnar structures of hexagonal order [66] **Figure 6**.

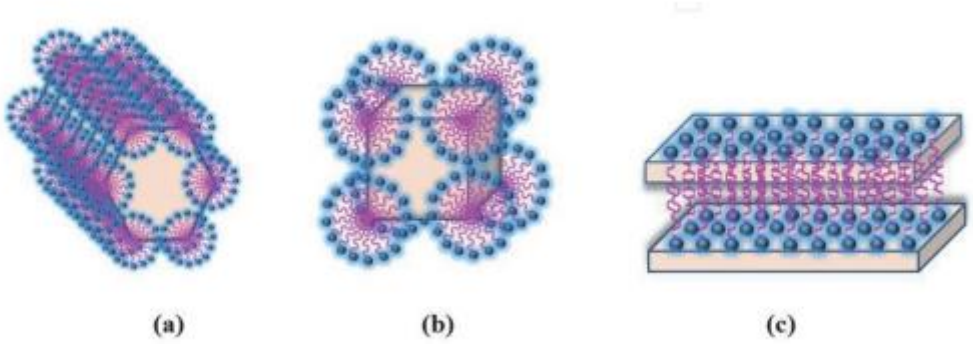

Figure 6. Liquid crystalline phases: a) hexagonal phase (b) cubic phase (c) Lamellar phase

Polymers used to obtain the hexagonal mesophases include glycerate-based surfactants such as oleylglycerate and phytanylglycerate. These phases appear birefringent when observed between crossed polarisers and show optical structures under a polarized light microscope [67]. The lamellar mesophase, on the other hand, is an arrangement in which the hydrophilic head groups are in contact with the

aqueous environment and the hydrophobic groups are arranged to avoid water. It is a fairly fluid phase, and the double layers can easily slide over each other. Due to the alternating arrangement of the lipophilic double layers, it exhibits interesting solubility properties. Furthermore, it shows a similarity to the organisation of the intercellular lipid matrix of the skin, especially the stratum corneum [68]. According to the phase diagram of structuring lipids **(Figure 7)**, the transition from lamellar to cubic phases can be completed by heating from room temperature to body temperature or by swelling with water. Thus, lamellar phases with inherently fluid properties can serve as precursors of viscous cubic phases.

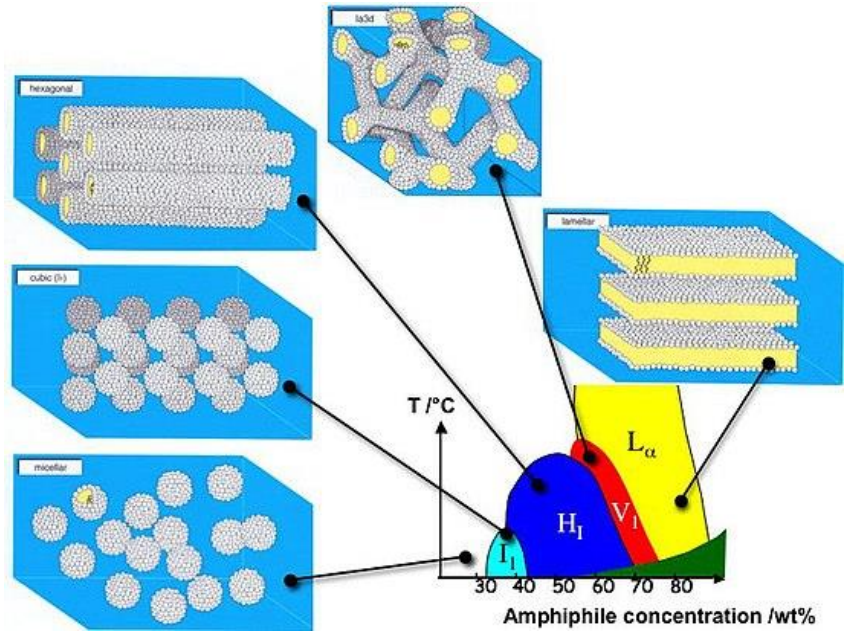

Figure 7. Typical phase diagram of an amphiphilic molecule forming lyotropic phases.

Among the most commonly used polymers for the production of LLCs are pluronic surfactants. Pluronic surfactants, poloxamer block copolymers, are synthetic three-block copolymers consisting of repeating units of ethylene oxide (EO) and propylene oxide (PO), denoted by the general formula (PEO)n(PPO)m(PEO)n. These surfactants are non-ionic, water-soluble macromolecules with amphiphilic properties, due to the alternation of hydrophobic propylene oxide (PPO) chains and hydrophilic ethylene oxide (PEO) chains. When Pluronic surfactants come into contact with a solvent such as water, which is selective for hydrophilic building blocks (PEO), and an oily solvent, which is selective for lipophilic building blocks (PPO), they structure themselves into the various LLC gel phases. Various bioactive molecules, such as

chemical drugs, peptides and proteins, can be solubilised in both aqueous and oil phases and be protected from hydrolysis or oxidation.

Therefore, liquid crystalline phases are used as DDS as they offer numerous advantages. For example, the high viscosity makes localised application of drugs to the skin possible and allows them to remain on the skin surface during application. LLCs show good penetration due to the low surface tension at the oil/water interface, facilitating the progressive diffusion of biologically active substances into the skin and systemic circulation [69]. These systems also make it possible to increase the solubility of transported drugs when they are insoluble or poorly soluble in an aqueous environment, allowing high concentrations to be achieved in the system. In addition, they make it possible to control the speed of release and increase the chemical stability of drugs. Their production is not extremely complex, has a low energy input and is rather inexpensive. Liquid crystal gels can be prepared by simply mixing the aqueous phase with the lipid phase using vortex or ultrasound.

Reference

[1] Khizar, S., Alrushaid, N., Khan, F. A., Zine, N., Jaffrezic-Renault, N., Errachid, A., & Elaissari, A. (2023). Nanocarriers based novel and effective drug delivery system. *International Journal of Pharmaceutics*, *632*, 122570.

[2] Mazzotta, E., Romeo, M., & Muzzalupo, R. (2024). Vesicular drug delivery systems: a novel approach in current nanomedicine. *Molecular Pharmaceutics and Nano Drug Delivery*, 135-159.

[3] Annabi N, Tamayol A, Uquillas JA, Akbari M, Bertassoni LE, Cha C. et al. 25th anniversary article: rational design and applications of hydrogels in regenerative medicine. *Advanced Materials.* 2014; 26:85–124.

[4] Stumpel JE, Gil ER, Spoelstra AB, Bastiaansen CW, Broer DJ, Schenning AP. Stimuli-Responsive Materials Based on Interpenetrating Polymer Liquid Crystal Hydrogels. *Advanced Functional Materials.* 2015; 25:3314–20.

[5] Dnyaneshwar Kalyane, Nidhi Rava l, Rahul Maheshwari, Vishakha Tambe, Kiran Kalia, Rakesh K. Tekade. ―Employment of enhanced permeability and retention effect (EPR): Nanoparticle-based precision tools for targeting of therapeutic and diagnostic agent in cancer‖. Materials Science and Engineering: C 2019

[6] Palmer, T.N., Caride, V.J., Caldecourt, M.A., Twickler,J.,Abdullah, V., The mechanism of liposome accumulation in infarction, Biochim Biophysic Acta,1984,797,363.

[7] Leroux, J.C., De Jaeghere, F., Anner, B., Doelker,E., Gurny, R., An investigation on the role of plasma and serum opsoninson the internalization of biodegradable poly(D,L-lactic acid) nanoparticles by human monocytes, Life Sci,1995,57,695

[8] Jinzhi Du, Lucas A. Lane, Shuming Nie. ―Stimuli-responsive nanoparticles for targeting the tumor microenvironment‖. Journal of Controlled Release 2015

[9] Matthew G. Vander Heiden, Lewis C. Cantley,Craig B. Thompson. ―Understanding the Warburg Effect: The Metabolic Requirements of Cell Proliferation‖. Scence Mag 2009

[10] C.M. Overall, O. Kleifeld. ―Tumour microenvironment — opinion: validating matrix metalloproteinases as drug targets and anti-targets for cancer therapy‖. Nat. Rev. Cancer 2006

[11] Torchilin, V.P., Trubetskoy, V.S., Which polymers can make nanoparticulate drug carriers long circulating, Adv. Drug Deliver. Rev.,1995,16, 141-155

[12] Fakhar ud Din, Waqar Aman, Izar Ullah, Omer Salman Qureshi, Omer Mustafà, Shumaila Shafique, Alam Zeb. Effective use of nanocarriers as drug delivery systems for the treatment of selected tumors. International Journal of Nanomedicine 2017

[13] Lin Huang, Jia Liu, Fan Gao, Qian Cheng, Bo Lu, Hua Zheng, Haixing Xu, Peihu Xu, Xianzheng Zhang and Xuan Zeng. A dual-responsive, hyaluronic acid targeted drug delivery system based on hollow mesoporous silica nanoparticles for cancer therapy. Journal o Materials Chemistry B 2018

[14] Paudel, K. S., Milewski, M., Swadley, C. L., Brogden, N. K., Ghosh, P., & Stinchcomb, A. L. (2010). Challenges and opportunities in dermal/transdermal delivery.*Therapeutic delivery*,*1*(1), 109-131.

[15] Rastogi, V., & Yadav, P. (2012). Transdermal drug delivery system: An overview. *Asian Journal of Pharmaceutics (AJP)*,*6*(3). (sia questa che la successiva)

[16] Mitragotri, S. (2013). Devices for overcoming biological barriers: the use of physical forces to disrupt the barriers.*Advanced drug delivery reviews*,*65*(1), 100-103.

[17] Xu, L., Wang, X., Liu, Y., Yang, G., Falconer, R. J., & Zhao, C. X. (2022). Lipid nanoparticles for drug delivery.*Advanced NanoBiomed Research*,*2*(2), 2100109.

[18] Carter, P., Narasimhan, B., & Wang, Q. (2019). Biocompatible nanoparticles and vesicular systems in transdermal drug delivery for various skin diseases.*International journal of pharmaceutics*,*555*, 49-62.

[19] Samimi, S., Maghsoudnia, N., Eftekhari, R. B., & Dorkoosh, F. (2019). Lipid-based nanoparticles for drug delivery systems.*Characterization and biology of nanomaterials for drug delivery*, 47-76.

[20] K. Vavroka, J. Zbytovska, A. Hrabalek, Amphiphilic Transdermal Permeation Enhancers: structure-activity relationships. Current Medical Chemistry 2005, 12(19): 2273-91

[21] Verma, D. D., Verma, S., Blume, G., & Fahr, A. (2003). Liposomes increase skin penetration of entrapped and non-entrapped hydrophilic substances into human skin: a skin penetration and confocal laser scanning microscopy study.*European Journal of Pharmaceutics and Biopharmaceutics*,*55*(3), 271-277.

[22]Gomathi, T., Rajeshwari, K., Kanchana, V., Sudha, P. N., & Parthasarathy, K. (2019). Impact of nanoparticle shape, size, and properties of the sustainable nanocomposites.*Sustainable polymer composites and nanocomposites*, 313-336.

[23] Cedervall, T., Lynch, I., Foy, M., Berggård, T., Donnelly, S. C., Cagney, G., ... & Dawson, K. A. (2007). Detailed identification of plasma proteins adsorbed on copolymer nanoparticles. *Angewandte Chemie International Edition*, *46*(30), 5754-5756.

[24] Semple, S. C., Chonn, A., & Cullis, P. R. (1998). Interactions of liposomes and lipid-based carrier systems with blood proteins: Relation to clearance behaviour in vivo.*Advanced drug delivery reviews*,*32*(1-2), 3-17.

[25] Phatale, V., Vaiphei, K. K., Jha, S., Patil, D., Agrawal, M., & Alexander, A. (2022). Overcoming skin barriers through advanced transdermal drug delivery approaches. *Journal of controlled release*, *351*, 361-380.

[26] Deng, P., Masoud, R. E., Alamoudi, W. M., & Zakaria, M. Y. (2022). Employment of PEGylated ultra-deformable transferosomes for transdermal delivery of tapentadol with boosted bioavailability and analgesic activity in post-surgical pain. *International Journal of Pharmaceutics*, *628*, 122274.

[27] Wang, J. Y., Chin, J., Marks, J. D., & Lee, K. Y. C. (2010). Effects of PEO− PPO− PEO triblock copolymers on phospholipid membrane integrity under osmotic stress. *Langmuir*, *26*(15), 12953-12961.

[28] Muzzalupo, R., & Tavano, L. (2015). Niosomal drug delivery for transdermal targeting: recent advances. Research and reports in transdermal drug delivery, 4, 23-33.

[29] Mahale, N. B., Thakkar, P. D., Mali, R. G., Walunj, D. R., & Chaudhari, S. R. (2012). Niosomes: novel sustained release nonionic stable vesicular systems—an overview. *Advances in colloid and interface science*, *183*, 46-54.

[30] Journal Of Pharmacy And Experimental Medicine. Niosome: A Novel Drug Delivery System. Ms. Shubhangi V. Shekade Assistant professor, Department of pharmaceutics, Dr. D.Y. Patil Institute of Pharmaceutical Sciences and Research, Pimpri, Pune 411018. 10 May 2021.

[31] Tavano, L., Mazzotta, E., & Muzzalupo, R. (2017). Nanovesicular formulations for cancer gene therapy. Current pharmaceutical design, 23(35), 5327-5335.

[32] Tavano, L., Mazzotta, E., & Muzzalupo, R. (2018). Innovative topical formulations from diclofenac sodium used as surfadrug: The birth of Diclosomes.*Colloids and Surfaces B: Biointerfaces*,*164*, 177-184.

[33] Attwood, D., Florence, A. T., & Gillan, J. M. N. (1974). Micellar properties of drugs: properties of micellar aggregates of phenothiazines and their aqueous solutions.*Journal of pharmaceutical sciences*, *63*(6), 988-993.

[34] Attwood, D., & Tolley, J. A. (1980). Self-association of analgesics in aqueous solution: association models for codeine, oxycodone, ethylmorphine and pethidine.*Journal of Pharmacy and Pharmacology*, *32*(1), 761-765.

[35] Atherton, A. D., & Barry, B. W. (1985). Photon correlation spectroscopy of surface active cationic drugs. *Journal of Pharmacy and Pharmacology*,*37*(12), 854-862.

[36] Attwood, D., Mosquera, V., Garcia, M., Suarez, M. J., & Sarmiento, F. (1995). A comparison of the micellar properties of structurally related antidepressant drugs. *Journal of colloid and interface science*, *175*(1), 201-206.

[37] Frezzatti Jr, W. A., Toselli, W. R., & Schreier, S. (1986). Spin label study of local anesthetic-lipid membrane interactions. Phase separation of the uncharged from and bilayer micellization by the charged form of tetracaine.*Biochimica et Biophysica Acta (BBA)-Biomembranes*, *860*(3), 531-538.

[38] Fernández, M. S., & Calderón, E. (1980). Formation of micelles and membrane action of the local anesthetic tetracaine hydrochloride. *Biochimica et Biophysica Acta (BBA)-Biomembranes*,*597*(1), 83-91.

[39] King, S. Y. P., Basista, A. M., & Torosian, G. (1989). Self-association and solubility behaviors of a novel anticancer agent, brequinar sodium. *Journal of pharmaceutical sciences*, *78*(2), 95-100.

[40] Attwood, D. (1995). The mode of association of amphiphilic drugs in aqueous solution. Advances in colloid and interface science, 55, 271-303.

[41] Schreier, S., Malheiros, S. V., & de Paula, E. (2000). Surface active drugs: self-association and interaction with membranes and surfactants. Physicochemical and biological aspects. *Biochimica et Biophysica Acta (BBA)-Biomembranes*,*1508*(1-2), 210-234.

[42] Wakaskar, R. R. (2018). General overview of lipid–polymer hybrid nanoparticles, dendrimers, micelles, liposomes, spongosomes and cubosomes.*Journal of drug targeting*,*26*(4), 311-318.

[43] Wakaskar, R. R. (2018). Brief overview of nanoparticulate therapy in cancer.*Journal of Drug Targeting*,*26*(2), 123-126.

[44] Gong, J., Chen, M., Zheng, Y., Wang, S., & Wang, Y. (2012). Polymeric micelles drug delivery system in oncology.*Journal of Controlled Release*,*159*(3), 312-323.

[45] Wakaskar, R. R. (2015). Effect of peripheral shell cross-linking on the efficacy of a hydrophobic vascular disrupting agent physically loaded in core-shell polymeric micelles.

[46] Wakaskar, R. R. (2017). Passive and active targeting in tumor microenvironment. *Int J Drug Dev Res*,*9*(2), 37-41.

[47] Owen, S. C., Chan, D. P., & Shoichet, M. S. (2012). Polymeric micelle stability. *Nano today*,*7*(1), 53-65.

[48] Yadav, H. K., Almokdad, A. A., Sumia, I. M., & Debe, M. S. (2019). Polymer-based nanomaterials for drug-delivery carriers. In *Nanocarriers for drug delivery* (pp. 531-556). Elsevier.

[49] Jiang, G. B., Quan, D., Liao, K., & Wang, H. (2006). Preparation of polymeric micelles based on chitosan bearing a small amount of highly hydrophobic groups. *Carbohydrate Polymers*, *66*(4), 514-520.

[50] Wakaskar, R. R. (2017). Cancer therapy with drug delivery systems. *J Pharmacogenomics Pharmacoproteomics*, *8*, e158.

[51] Mikhail, A. S., & Allen, C. (2009). Block copolymer micelles for delivery of cancer therapy: transport at the whole body, tissue and cellular levels. *Journal of Controlled Release*, *138*(3), 214-223.

[52] Maeda, H., Wu, J., Sawa, T., Matsumura, Y., & Hori, K. (2000). Tumor vascular permeability and the EPR effect in macromolecular therapeutics: a review. *Journal of controlled release*, *65*(1-2), 271-284.

[53] Torchilin, V. (2011). Tumor delivery of macromolecular drugs based on the EPR effect. *Advanced drug delivery reviews*, *63*(3), 131-135.

[54] Zhang, Y., Huang, Y., & Li, S. (2014). Polymeric micelles: nanocarriers for cancer-targeted drug delivery. *Aaps Pharmscitech*, *15*, 862-871.

[55] Tiyaboonchai, W. (2003). Chitosan nanoparticles: a promising system for drug delivery. Naresuan Univ J 11: 51–66.

[56] Panyam J., Dali M.M., Sahoo S.K., Ma W., Chakravarthi S.S., Amidon G.L., Labhasetwar V. (2003). Polymer degradation and in vitro release of a model protein from poly (D, L-lactide-co-glycolide) nano and microparticles. *Journal of Controlled Release*, 92: 173-187.

[57] Nagpal, K., Singh, S. K., & Mishra, D. N. (2010). Chitosan nanoparticles: a promising system in novel drug delivery. *Chemical and Pharmaceutical Bulletin*, *58*(11), 1423-1430.

[58] Chopra S., Mahdi S., Kaur J., Igbal Z., Talegaonkar S., Ahmad F.J. (2006). Advances and potential applications of chitosan derivatives as mucoadhesive biomaterials in modern drug delivery. Journal of Pharmacy and Pharmacology; 58: 1021-1032.

[59] Rabea E.I., Mohamed E.T., Stevens C.V., Smagghe G., Steurbaut W. (2003). Chitosan as antimicrobial agent: applications and mode of action. Biomacromolecules; 4: 1457-1465.

[60] Sun T., Zhou D., Xie J., Mao F. (2007). Preparation of chitosan oligomers and their antioxidant activity. European Food Research and Technology; 225: 451-456.

[61] Mazzotta, E., De Benedittis, S., Qualtieri, A., & Muzzalupo, R. (2019). Actively targeted and redox responsive delivery of anticancer drug by chitosan nanoparticles. *Pharmaceutics*,*12*(1), 26.

[62] Drummond, C. J., & Fong, C. (1999). Surfactant self-assembly objects as novel drug delivery vehicles. *Current opinion in colloid & interface science*, *4*(6), 449-456.

[63] Sagalowicz, L., Leser, M. E., Watzke, H. J., & Michel, M. (2006). Monoglyceride self-assembly structures as delivery vehicles. *Trends in Food Science & Technology*, *17*(5), 204-214.

[64] Spicer, P. T., Hayden, K. L., Lynch, M. L., Ofori-Boateng, A., & Burns, J. L. (2001). Novel process for producing cubic liquid crystalline nanoparticles (cubosomes). *Langmuir*, *17*(19), 5748-5756.

[65] Laughlin, R. (1995). Correction. the aqueous phase behavior of surfactants. *Journal of the American Chemical Society*, *117*(42), 10603-10603.

[66] Muzzalupo, R., Tavano, L., Nicoletta, F. P., Trombino, S., Cassano, R., & Picci, N. (2010). Liquid crystalline Pluronic 105 pharmacogels as drug delivery systems: preparation, characterization, and in vitro transdermal release. *Journal of drug targeting*, *18*(5), 404-411.

[67] Roux, D., Safinya, C. R., & Nallet, F. (1994). Lyotropic Lamellar L α Phases. *Micelles, Membranes, Microemulsions, and Monolayers*, 303-346.

[68] Lise Sylvest Nielsen, Lise Sylvest Helledi & Lene Schubert. “Release Kinetics of Acyclovir from a Suspension of Acyclovir Incorporated in a Cubic Phase Delivery System.” Drug Development and Industrial Pharmacy, 27:10, (2001): 1073-1081,

[69] Boyd, B. J., Whittaker, D. V., Khoo, S. M., & Davey, G. (2006). Lyotropic liquid crystalline phases formed from glycerate surfactants as sustained release drug delivery systems. *International journal of pharmaceutics*, *309*(1-2), 218-226.

Chapter 1: Innovative nanosystems for drug delivery

1. Innovative nanosystems for drug delivery

1.1 Lidosomes: Innovative Vesicular Systems Prepared from Lidocaine Surfadrug

Martina Romeo [1], Elisabetta Mazzotta [1], Ida Daniela Perrotta [2] and Rita Muzzalupo [1]

1 Department of Pharmacy, Health and Nutritional Sciences, University of Calabria, 87036 Arcavacata di Rende, Italy
2 Centre for Microscopy and Microanalysis (CM2), Department of Biology Ecology and Earth Sciences, University of Calabria, 87036 Arcavacata di Rende, Italy

Pubblished on *Pharmaceutics* 2022, *14*(10), 2190

Abstract: Lidocaine is a local anesthetic drug with an amphiphilic structure able to self-associate, under certain conditions, in molecular aggregates playing the role of both carrier and drug. The aim of this study was to determine the optimal conditions for obtaining vesicular carriers, called lidosomes. The new formulations were obtained using both lidocaine and lidocaine hydrochloride and different hydration medias (distilled water, acid, and basic aqueous solution). Lidosomes formulations were characterized in terms of size, ζ-potential, drug retained, stability formulation, and ex vivo permeation profile. Moreover, lidosomes were incorporated in two different gel structures: one based on carboxymethylcellulose and one based on pluronic F-127 to achieve suitable properties for a topical application. Results obtained showed that lidocaine showed a better performance to aggregate in vesicular carriers in respect to hydrochloride form. Consequently, only formulations comprised of lidocaine were studied in terms of skin permeation performance and as carriers of another model drug, capsaicin, for a potential combined therapy. Lidocaine, when in form of vesicular aggregates, acted as percutaneous permeation enhancer showing better permeation profiles with respect to drug solutions. Moreover, lidosomes created a significant drug depot into the skin from which the drug was available for a prolonged time, a suitable feature for a successful local therapy.

1. Introduction

Painkillers are the most widely used local anasthetics, which reversibly inhibit pain impulse transmission by blocking voltage-dependent channels.

Among them, Lidocaine (LID), or Xylocaine, is an amino-type anasthetic largely employed in clinical practice, since its binding ability to voltage-gated sodium channels of excitable membranes results in the inhibition of action potential depolarization and the

conduction of noxious stimuli to the central nervous system [1]. LID is an efficacious local anesthetic at fast onset and low systemic toxicity. Further, LID exhibits a short action duration and antiarrhythmic activity and, thus, its administration needs caution due to these cardiovascular effects.

LID performance could be improved by nanotechnology approaches that could in- crease resistance time on the skin, in order to allow the penetration into corneum stratum and pain receptors underlying desensitization [2,5]. Nanoscale drug delivery systems (DDS) have been designed as inert systems that can transport drugs at the target site with high selectivity and controllable kinetic release profile [6,7]. Various DDS, such as niosomes, liposomes, transferosomes, and solid lipid nanoparticles, have already been employed to improve LID efficacy due to the role of these systems as skin permeation enhancers able to increase drug permeability, and consequently, ensure a higher drug accumulation at the target site and thus, an improved analgesic effect [8,11]. Their better permeation ability allows for lower drug doses and could reduce cardiovascular side effects [12,13]. LID possesses an interesting amphiphilic structure that allows it to act as a surface- active drug.

The ability to aggregate in micelles depends on the drug chemical structure and the balance between drug–water interaction and hydrophobic interaction (i.e., solute–solute interaction). Shaik and co-workers [14] investigated the aggregation properties of Lidocaine Hydrochloride (LIDHCL) in water and found that at specific concentrations it formed micelles due to the establishment of hydrophobic interactions between the amide bond (CH_2CONH) and the methyl side group of the benzene ring.

In our previous study, we demonstrated the ability of other surfadrugs, such as Cromolyn and Diclofenac Sodium, to form at specific conditions in vesicular structures, while simultaneously playing the role of both bilayer constituent and drug [15,16]. These innovative nanosized vesicles offered several advantages, such as the ability for better skin permeation and the possibility to avoid the use of additional excipients, improving formulation biosafety, and increasing drug loading [17]. Considering these findings, we decided to study, for the first time, the aggregation properties of lidocaine as vesicle structures (lidosomes, LD) and to find the best experimental conditions to achieve nano-size carriers with physicochemical properties suitable for topical applications. LD were also included in gel created of carboxymethylcellulose (CMC) or pluronic F-127, while ex vivo permeation studies were carried out to investigate drug permeation profile. Moreover, surfadrug-based vesicles may also be used as carriers of other drugs for a

potential synergic therapy. In this light, a further step forward had been taken in this work with respect to the previous study, since vesicles comprised of surfadrugs and loaded with a model drug, capsaicin (CA), were designed and their skin permeation performance was simultaneously investigated to predict their role for a potential synergic therapy.

Materials and Methods

Chemicals

Lidocaine Hydrochloride monohydrate (LIDHCl), Lidocaine (LID), Capsaicin (CA), and pluronic F-127 were purchased from Sigma-Aldrich (Milan, Italy, purity 99%); Carboxymethyl cellulose was purchased from Polichimica S.R.L (Bologna, Italy); the organic solvents were supplied from Sigma-Aldrich (Milan, Italy).

Lidosomes Preparation

Niosomes based on LID and LIDHCl were prepared by a thin layer evaporation [18]. Accurately weighed quantities of the drug were dissolved in ethanol into a round-bottom flask. The solvent was evaporated through the application of reduced pressure and constant rotation to form a thin lipid film. The lipid film was then hydrated with 10 mL of distilled water, acid, or basic solution (pH 5.5 or 7.9, respectively) at 60 ◦C for 30 min, to form large multilamellar vesicles (MLV). After preparation, dispersions were left to equilibrate at 25 ◦C overnight. The reduction of vesicular size was achieved by sonication conducted in an ultrasonic bath at 60 ◦C for 30 min. The amplified mechanical vibrations generated small unilamellar vesicles (SUV) from MLVs. Subsequently, the vesicles were purified by exhaustive dialysis for 4 h in distilled water using Visking tubing (Spectra/Por®, cut-off 12–14 kDa), manipulated before use according to Fenton's method [19]. After purification, formulations were stored at 4◦C until the subsequent experiments. LD loaded with CA (LD-CA) in a 9:1 molar ratio were subsequently prepared by using the same method. CA together with LID were dissolved in ethanol. The LD-CA was purified by exhaustive dialysis for 4 h using an 80:20 hydroalcoholic solution as a medium. Details on vesicles compositions are reported in Table 1.

Table 1. Composition details of lidosomal formulations developed using LID and LIDHCl and various hydration solutions.

Formulation	LID (mg)	CA (mg)	Hydration Medium
LD HCl A	14		H2O
LD HCl B	27		H2O
LD 5.5 A	27		H_2O pH 5.5
LD 5.5 B	30		H_2O pH 5.5
LD	30		H2O
LD:CA	27	4	H2O
LD 7.9	30		H_2O pH 7.9
LD HCl 7.9	30		H_2O pH 7.9

Furthermore, LD gel formulations were prepared to ensure they were suitable for skin application. Specifically, we decided to formulate two different gels, using two different polymers: F127 and CMC. In fact, F127 was widely known as a skin permeation enhancer, thus we compared its performance with that of an inert polymer. To this purpose, 5 mL of LD solution was added to 0.150 g of CMC or 0.900 g of block copolymer and homogenized in accordance with the procedure reported in [20].

Niosomal Characterization

LD diameter, size distribution, and ζ-potential were determined by Zetasizer ZS Malvern Instruments Ltd. (Malvern, U.K.) at 25 ± 0.1 ◦C. After the samples were purified by dialysis, all analyses were conducted in triplicate and expressed as mean ± standard deviation. The morphology of lidosomes was determined by Transmission Electron Microscopy (TEM) and the images were obtained with TEM ZEISS EM 10. Two drops of formulations placed on a copper grid with a nitrocellulose covering were stained with phosphotungstic acid (2%, *w*/*v*) and left to dry at room temperature before the microscopy observation. The stability of the niosomes was evaluated by storing the formulation at 4 ◦C for three months and monitoring diameter, PI and ζ-potential initially after 15 days, and then every month. Each analysis was carried out in triplicate.

Determination of the Amount of LID in Vesicular Systems

The amount of LID retained in the vesicles was determined after sample purification by exhaustive dialysis. A total of 1 mL of purified and 1 mL of non-purified LD were diluted

in 100 mL of ethanol, and the LID concentration was measured spectrophotometrically (Thermo Fisher scientific evolution 201/220, Waltham, MA, USA) at 262 nm corresponding to the LID wavelength. The drug content retained in the formation of vesicles structure (DL%) was calculated according to the following Equation (1):

$$DL\% = \frac{C_{dr}}{C_{d_i}} \times 100$$

where C_{dr} is the initial drug concentration measured after purification process and C_{di} is drug concentration used for the preparation of vesicles.

For the LD:CA formulation, purification was carried out using 80:20 hydro-alcoholic solution as a medium for dialysis. The encapsulation efficiency (E%) of CA and DL% of LID in the formulation LD:CA was determined by HPLC (Varian 920-LC Series Liquid Chromatograph) equipped with a chromatographic column C18 reverse phase. The mobile phase used was 0.1% phosphoric acid: acetonitrile (50:50 *v/v*) at pH 2.4. The wavelength used for analysis was 280 nm for CA and 210 nm for LID. The CA E% was calculated using the following Equation (2):

$$EE\% = \frac{C_{CA\ in\ lidosomes}}{C_{CAi}} x\ 100 \quad (2)$$

where $C_{CA\ in\ lidosomes}$ is the drug concentration measured after the purification process, while C_{CAi} represents the initial drug concentration. All experiments were conducted in triplicate and expressed as mean ± standard deviation (SD).

***Ex-Vivo* Permeation Study**

Skin permeation profiles of the formulations proposed in this work were evaluated using vertical Franz diffusion cells for 24 h at 37 ◦C using rabbit ear skin obtained from a local farmer, as reported elsewhere [17]. The skin was frozen in advance at −18 ◦C and pre-equilibrated in a physiological solution at room temperature for 1 h before the experiments. A portion of skin was placed between the two compartments with the epidermal part in contact with the receptor compartment. The effective diffusion area of cells was 0.416 cm2. The donator compartment was charged with 0.3 mL of the niosomal sample in all exper- iments and covered by Parafilm to prevent water loss, while the acceptor compartment was loaded with 5.5 mL of medium. Specifically, the medium used was distilled water for LD and LD 5.5 B formulations, while a hydro-alcoholic solution

(80:20 water:ethanol) for that LD:CA. At regular intervals, the medium was removed to be analysed and restored with equal volume of fresh medium, maintained at a temperature of 37 ◦C. The amount of LID in the receptor solution was analysed by UV-vis spectrometry, whereas HPLC was employed to investigate the amount of LID and CA released from LD:CA formulation. Skin permeation of free LID and LID gel was also investigated as the control with the same conditions. All experiments were performed in triplicate and expressed as mean ± SD.

Skin LID Retention Studies

The LID amount retained into the skin was evaluated after skin permeation studies. To this purpose, the piece of skin was removed from the Franz diffusion cells, placed in 10 mL of ethanol and magnetically stirred for 2 h. Then, the solution was filtered using 0.22 μm Millipore membrane filters and analysed by UV-vis spectroscopy or HPLC chromatography to evaluate the amount of LID and CA accumulated into the skin. All experiments were conducted in triplicate and expressed as mean ± standard deviation.

Statistical Analysis

All experiments were performed in triplicate and the results were expressed as mean ± SD. Statistical analysis was performed using a Student's *t*-test and *p* values of ≤0.05 were considered statistically significant.

Results and Discussion

LID is a local anasthetic largely employed for topical therapy and other medical and chirurgical procedures, such as skin sores treatment and wound sutures. Its main use is for parenteral way, typically for intravenous way, instead, less frequent is intramuscular administration [21]. The chemical structure of LID suggests the possibility of aggregation in aqueous solution, typical of amphiphilic drugs. In literature, conflicting data are shown; in fact, some authors reported that LID did not lead to the formation of micelles, while in other studies a critic micellar concentration value of 0.12–0.13 mol kg^{-1} was reported [22,23]. For this reason, we decided to investigate the ability of both LIDHCl and LID to form vesicles. Using LIDHCl, we obtained systems that were poorly populated by LD. In fact, vesicular solution appeared only slightly opalescent and the amount of LID retained in the vesicle's formation was very low. Conversely, the use of LID, already with a

quantity of 27 mg but even better with 30 mg, led to obtaining homogeneous vesicular systems with good DL%. The hydration of the lipid film was carried out both in distilled water and in aqueous acid (pH 5.5) or basic (pH 7.9) solution. The size of the LD, depending on the quantity of LID and the hydrating medium used, were between 430 and 574 nm with a PI in the range 0.22–0.27, indicating a homogeneous and narrow size distribution. The negative ζ−potential obtained with LIDHCl may have seemed unusual considering the positive charge of LIDHCl. In order to better investigate the developed formulations, vesicular systems based on both LIDHCl and LID were prepared using for the hydration process solutions with pH equal to the pKa of the drug (pKa = 7.9). In fact, when the pH was equal to the pKa, the drug was present in equal concentrations, both as LID and LIDHCl. The LD obtained, both with the lipid film prepared with LID and with LIDHCl, had a high negative ζ−potential, about −30 mV, and a high DL% that contributed to their formation, over 60%. This could be since only the neutral LID form represented the main constituent of vesicle bilayer, while LIDHCl participated only in a small percentage. Consequently, negative zeta potential values obtained may have been due to the arrangement of amphiphilic molecules with a neutral polar group in their structure, such as that present in LID. In addition, we investigated the use of LD as drug carriers and used the formulation obtained from 30 mg of LID to load a model drug, CA. Table 2 reported all characterization data for the formulations prepared.

Table 2. Physico-chemical characterization of lidosomes prepared at different concentrations and pH: Hydrodynamic diameter, P.I, ζ−potential, DL%, and E% at 25 °C. Results are the average of three different independent experiments ± standard deviation.

Formulation	Diameter (nm)	I.P.	ζ-Potential (mV)	DL(%) LID	E(%) CA
LD HCl A	707 ±15	0.249	−13.0 ±0.709	2.13% ±0.2	-
LD HCl B	506 ±12	0.288	−14.3 ±1.190	1.19% ±0.7	-
LD 5.5 A	430 ±10	0.264	−26.1 ±0.900	19.5% ±0.5	-
LD 5.5 B	574 ±11	0.271	−27.6 ±0.833	35.6% ±0.3	-
LD	437 ±10	0.229	−23.5 ±0.208	37.1% ±0.2	-
LD:CA	519 ±14	0.277	−23.1 ±0.493	67.5% ±0.2	87.75% ±0.8
LD 7.9	512 ±11	0.287	−31.2 ±0.666	61.2% ±0.3	-
LD HCl 7.9	612 ±13	0.277	−30.5 ±0.351	64.8% ±0.6	-

The morphological analysis showed that LD formulations were spherical, homogeneous in shape and size (Figure 1), with regular and well-defined edges.

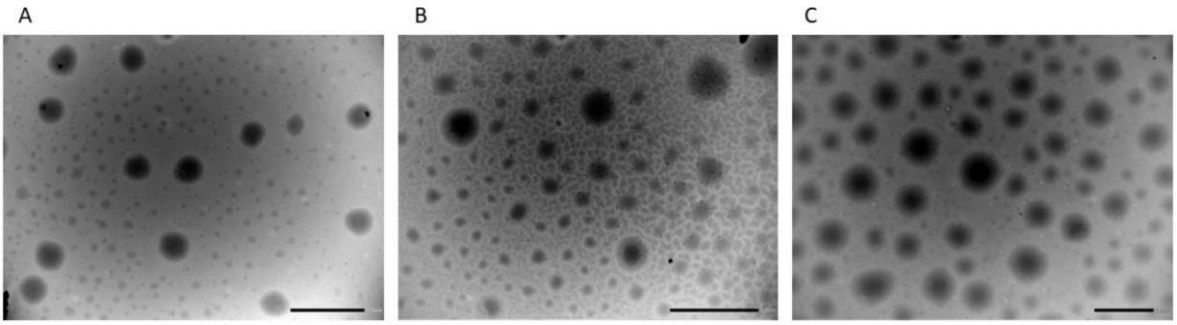

Figure 1. Typical TEM photomicrograph of lidosomes: (**A**) LD 5.5B; (**B**) LD 7.9, and (**C**) LD formulations. Bar is 1 μm.

LD Stability

The stability of LD was evaluated monitoring physical-chemical properties of samples stored at 4 ◦C for three months and the results are depicted in Table 3. The LD 5.5 B formulation showed a higher size stability than the LD formulation, but no significant changes in DL% and ζ -potential values were observed with either for two months.

Table 3. Stability analysis of LD stored at 4 ◦C evaluated by measuring diameter, P.I., ζ−potential, and DL%. Data was collected at specific time points, up to 3 months, and expressed as mean of three independent experiments ± SD.

Formulations	Time (day)	Diameter (nm)	P.I.	ζ-potential (mV)	DL %
LD	0	437 ± 10	0.229	−23.5 ± 0.208	37.1 ± 0.2
	15	321 ± 9	0.235	−23.2 ± 0.907	36.9 ± 0.3
	30	305± 11	0.295	−22.3 ± 0.819	37.3 ± 0.2
	60	253± 9	0.180	−21.4 ± 0.896	36.7 ± 0.5
	90	175 ± 9	0.294	−19.3 ± 0.451	36.8 ± 0.4
LD 5.5 B	0	574 ± 15	0.271	−27.6 ±0.833	35.6 ± 0.3
	15	570 ± 17	0.204	−27.5 ± 0.173	34.3 ± 0.2
	30	520 ± 19	0.235	−27.4 ± 0.864	34.4 ± 0.3
	60	506 ± 19	0.215	−25.7 ± 0.366	33.4 ± 0.2
	90	501± 18	0.276	−26.5 ± 0.456	33.3 ± 0.2

Ex-Vivo Permeation Studies

Lidosomes

Ex vivo skin penetration efficiency of LD, LD 5.5 B, and LD:CA, was evaluated using the Franz diffusion apparatus. The permeation profile as a function of time of LD and LD 5.5 B samples are shown in Figure 2 and compared with LID solution. As observed, 308 µg/cm2 corresponding at 38.38% of drug permeated after 24 h by LD, with respect at almost 214.84 µg/cm2 corresponding at 27.89% by LD pH 5.5. However, skin permeations obtained were always higher than those obtained from LID solution, 122.96 µg/cm2 corre- sponding to 5.68%. This suggests that LID, when in the form of vesicular aggregates, act as percutaneous permeation enhancer. This better permeation ability could be ascribed to two different mechanisms. Generally, permeation increases with carrier lipophilicity, probably due to better interaction with the skin layers [17]. Moreover, the skin permeation of amphiphilic molecules depends on their structure [24]. Indeed, as reported in the literature, non-ionic surfactants can interact with both keratin and lipids, altering the lipid layer of the skin and thus making this membrane more permeable [25]. Instead, regarding ionizable compounds, the chemical form that provides better skin permeation is the non-ionised form, as it has a lower polarity and high logP, which provides better affinity for the stratum corneum, which must be crossed to promote absorption after topical application [26].

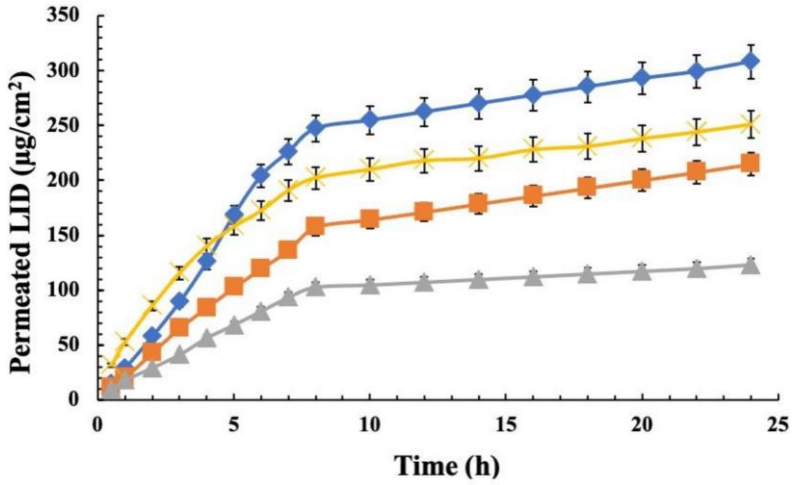

Figure 2. LID permeation profile through rabbit ear skin at 37 ◦C over 24 h using Franz diffusion cells from various formulations: (◆) LD; (■) LD 5.5 B; (**X**) LD 7.9; (▲) LID SOL. Data are represented as mean ± SD (n = 3).

LID exhibits both behaviours, being an ionizable drug with an amphiphilic structure. Both aspects can, therefore, influence its skin permeation.

To achieve a localised pharmacological effect, it would be desirable for the drug to accumulate in the upper layers of the skin [27]. In fact, the formation of intracutaneous drug depot would be suitable to prolong drug duration of action over the time leading to better treatment outcomes. Therefore, we decided to investigate the amount of drug accumulated into the skin after skin permeation studies and the results are reported in Table 4. Data showed that LD led to a higher drug depot into the skin, with respect that obtained with LID solution. In particular, the amount of LID retained increased with the pH increase, since the acid-base balance of LID increases the concentration of the neutral species, which are more affinity to skin bilayer.

Table 4. Amount of LID (μg/cm^2) retained into the skin after 24 h of ex-vivo permeation study carried out for 24 h using Franz cell apparatus.

Formulation	LID Retained into Skin (μg/cm^2)
LD	387.02
LD 5.5 B	352.16
LD 7.9	545.67
LID SOL	165.87

Gel Formulations and Combined Drug Therapy

Gels have proved to be an advantageous vehicle for drug administration over the skin for their long retention time and ability to slow and prolong drug absorption. Specifically, we decided to investigate the effect of two different gel structure on LD skin permeation, one based on CMC, which does not lead to the creation of structured gels, and one based on pluronic F-127, a well-known pluronic surfactant capable of giving gel-like cubic phase at specific concentrations [28].

Ex-vivo skin permeation profiles of CMC LD gel and CMC LID gel are shown in Figure 3A. In this case, skin permeation capacity of LID by LD gel was significantly higher than that achieved by LID gel. In fact, only 11.66% of LID permeated after 24 h from LID-CMC gel. Conversely, a permeation two times higher equal to 20.21% was observed when the drug is in the form of vesicular aggregates, confirming their role as a percutaneous permeation enhancer. Instead, similar performances were observed comparing permeation profile of LD from CMC and F127 gel as shown in Figure 3B. Anyway, a slightly higher amount of LID was retained into the skin with LD-CMC gel compared to that obtained with LD- F-127 (about 450 μg/cm2, 353 μg/cm2, respectively). These skin depot results were advantageous when an analgesic local effect was required, since the

drug was made available in high concentrations for longer times, prolonging drug effects. Finally, to test the possibility of using LD as a carrier of other pharmacological active molecules, CA was used as a model drug and the effect of CA encapsulation on physical-chemical and permeation properties of LD was investigated. As reported in Table 2, physical-chemical parameters were not affected by CA loading in the vesicular structure and high drug content of both drugs (67% LID DL% and 88% E% CA) were observed. The amount of LID and CA permeated was found to be 89.90 µg/cm^2 and 126.65 µg/cm^2, respectively, as shown in Figure 4. Instead, the amount of drug retained in the skin resulted to be about 399 µg/cm^2 and 20.50 µg/cm^2 for LID and CA, respectively. Considering that, the proposed system based on the co-delivery of LID and CA could be very interesting topical tools for pain relief able to prolong and improve pharmacological efficacy through synergic effect.

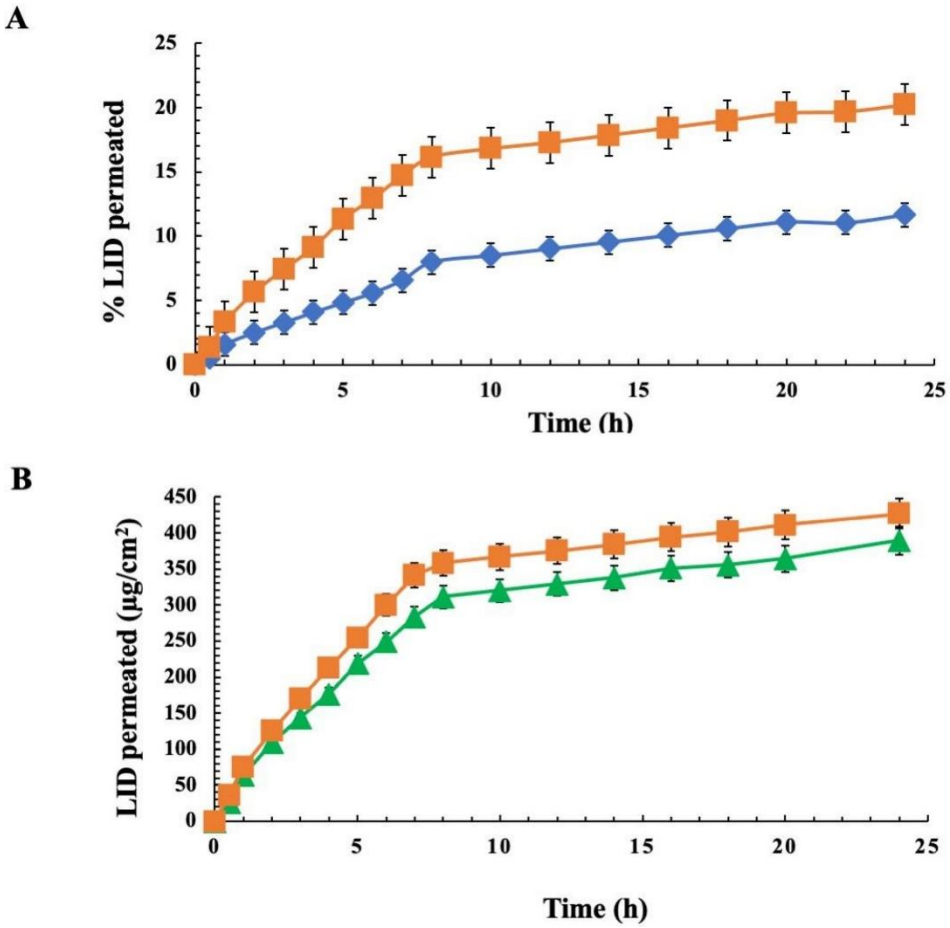

Figure 3. Comparison of LID permeation profiles through rabbit ear skin at 37 ◦C from several gel formulations: (**A**) (◆) Gel LID vs. (■) LD gel CMC; (**B**) (▲) LD gel F-127 vs. (■) LD gel CMC. Results are expressed as mean mean ± SD (n = 3).

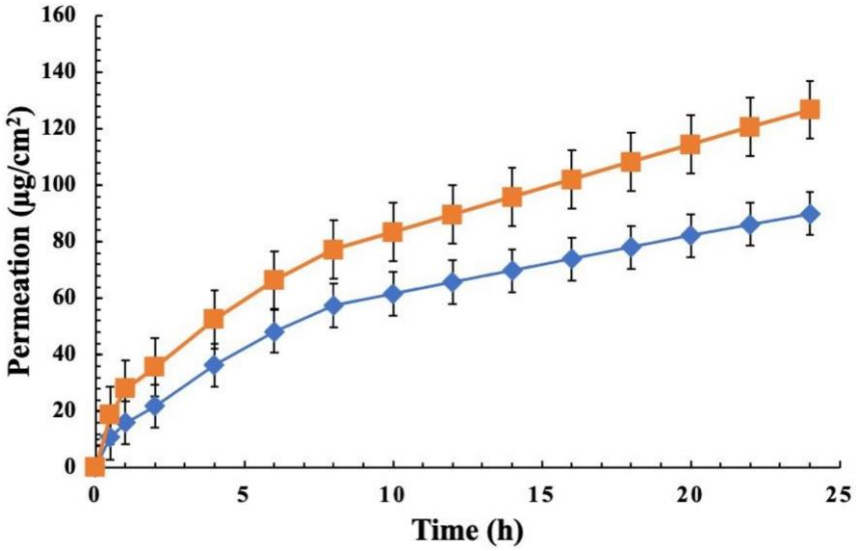

Figure 4. Permeation profile of (◆) LID and (■) CA simultaneously released from LD:CA formulation through rabbit ear skin at 37 °C over 24 h. Results are expressed as mean mean ± SD (n = 3).

Conclusions

In this work, aggregation properties of an analgesic drug lidocaine in vesicles (lidosomes) have been investigated using various experimental conditions. Specifically, vesicles were prepared using both lidocaine and lidocaine hydrochloride and different pH in the preparation process. From the experimental data, we concluded that Lidocaine formed vesicle structures with nanometric size, spherical morphology, and good stability at least for 3 storage months. Particularly interesting were the results of the ex-vivo permeation studies that highlighted an enhanced LID skin permeation and a higher drug depot in the skin when in the form of vesicular aggregates with respect to the free drug. Moreover, the work evaluated as well as the ability of lidosomes to act as carriers of a model drug, capsaicin, and the obtained results revealed the formation of a reservoir of both drugs into the skin, suggesting the great potentiality of these system to be used in synergic therapeutic treatment of pain relief. However, this paper represents only a preformulation evaluation, and further studies in the future are necessary to investigate the in vivo efficacy of these systems for their consideration as clinically viable formulations.

References

[1] Sarheed, O.; Dibi, M.; Ramesh, K.; Drechsler, M. Fabrication of Alginate-Based O/W Nanoemulsions for Transdermal Drug Delivery of Lidocaine: Influence of the Oil Phase and Surfactant. *Molecules* **2021**, *26*, 2556.

[2] Wang, Y.; Wang, S.; Shi, P. Transcriptional transactivator peptide modified lidocaine-loaded nanoparticulate drug delivery system for topical anesthetic therapy. *Drug Deliv.* **2016**, *23*, 3193–3199.

[3] Liu, Y.; Cheng, M.; Zhao, J.; Zhang, X.; Huang, Z.; Zang, Y.; Ding, Y.; Zhang, J.; Ding, Z. Transdermal Delivery of Lidocaine-Loaded Elastic Nano-Liposomes with Microneedle Array Pretreatment. *Biomedicines* **2021**, *9*, 592.

[4] Zhao, Z.Q.; Zhang, B.L.; Chu, H.Q.; Liang, L.; Chen, B.Z.; Zheng, H.; Guo, X.D. A high-dosage microneedle for programmable lidocaine delivery and enhanced local long-lasting analgesia. *Biomater. Adv.* **2022**, *133*, 112620.

[5] Li, Y.; Liao, X.; Zheng, B. Studies on local anesthetic lidocaine hydrochloride delivery via photo-triggered implantable polymeric microneedles as a patient-controlled transdermal analgesia system. *J. Biomater. Sci. Polym. Ed.* **2022**, *33*, 155–173.

[6] Mukherjee, B. Editorial (thematic issue: "Nanosize drug delivery system"). *Curr. Pharm. Biotechnol.* **2013**, *14*, 1221.

[7] Yasamineh, S.; Yasamineh, P.; Kalajahi, H.G.; Gholizadeh, O.; Yekanipour, Z.; Afkhami, H.; Eslami, M.; Kheirkhah, A.H.; Taghizadeh, M.; Yazdani, Y.; et al. A state-of-the-art review on the recent advances of niosomes as a targeted drug delivery system. *Int. J. Pharm.* **2022**, *624*, 121878.

[8] Shakiba-Maram, N.; Avarvand, O.K.; Mohtasham, N.; Ahmady, A.Z. Lidocaine Hydrochloride Nanoparticles Preparation using Multiple Emulsions and its Physicochemical Evaluation. *Int. J. Nanosci.* **2021**, *20*, 2150022.

[9] Vigato, A.A.; Machado, I.P.; del Valle, M.; da Ana, P.A.; Sepulveda, A.F.; Yokaichiya, F.; Franco, M.K.K.D.; Loiola, M.C.; Tófoli, G.R.; Cereda, C.M.S.; et al. Monoketonic Curcuminoid-Lidocaine Co-Deliver Using Thermosensitive Organogels: From Drug Synthesis to Epidermis Structural Studies. *Pharmaceutics* **2022**, *14*, 293.

[10] Qi, Y.; Yao, X.; Du, X.; An, S. Local anesthetic lidocaine-encapsulated polymyxin–chitosan nanoparticles delivery for wound healing: In vitro and in vivo tissue regeneration. *Drug Deliv.* **2021**, *28*, 285–292.

[11] Daryab, M.; Faizi, M.; Mahboubi, A.; Aboofazeli, R. Preparation and Characterization of Lidocaine-Loaded, Microemulsion-Based Topical Gels. *Iran. J. Pharm. Sci.* **2022**, *21*, e123787.

[12] Li, L.; Zhang, Y.; Han, S.; Qu, Z.; Zhao, J.; Chen, Y.; Chen, Z.; Duan, J.; Pan, Y.; Tang, X. Penetration enhancement of lidocaine hydrochlorid by a novel chitosan coated elastic liposome for transdermal drug delivery. *J. Biomed. Nanotechnol.* **2011**, *7*, 704–713.

[13] Omar, M.M.; Hasan, O.A.; El Sisi, A.M. Preparation and optimization of lidocaine transferosomal gel containing permeation enhancers: A promising approach for enhancement of skin permeation. *Int. J. Nanomed.* **2019**, *14*, 1551–1562.

[14] Shaikh, V.R.; Dagade, D.; Hundiwale, D.G.; Patil, K.J. Volumetric studies of aqueous solutions of local anesthetical drug compounds [hydrochlorides of procaine (PC HCl), lidocaine (LC HCl) and tetracaine (TC HCl)] at 298.15 K. *J. Mol. Liq.* **2011**, *164*, 239–242.

[15] Tavano, L.; Nicoletta, F.P.; Picci, N.; Muzzalupo, R. Cromolyn as surface active drug (surfadrug): Effect of the self-association on diffusion and percutaneous permeation. *Colloids Surf. B. Biointerfaces* **2016**, *139*, 132–137.

[16] Tavano, L.; Mazzotta, E.; Muzzalupo, R. Innovative topical formulations from diclofenac sodium used as surfadrug: The birth of Diclosomes. *Colloids Surf. B Biointerfaces* **2018**, *164*, 177–184.

[17] Malhotra, M.; Jain, N.K. Niosomes: A Controlled and Novel Drug Delivery System. *Indian Drugs* **1994**, *31*, 81–86.

[18] Bangham, A.D.; Standish, M.M.; Watkins, J.C. Diffusion of univalent ions across the lamellae of swollen phospholipids. *J. Mol. Biol.* **1965**, *13*, 238–252, IN26–IN27.

[19] Fenton, R.R.; Easdale, W.J.; Er, H.M.; O'Mara, S.M.; McKeage, M.J.; Russell, P.J.; Hambley, T.W. Preparation, DNA binding, and in vitro cytotoxicity of a pair of enantiomeric platinum (II) complexes, [(R)-and (S)-3-aminohexahydroazepine] dichloro-platinum (II). Crystal structure of the S enantiomer. *J. Med. Chem.* **1997**, *40*, 1090–1098.

[20] Antunes, F.E.; Gentile, L.; Rossi, C.O.; Tavano, L.; Ranieri, G.A. Gels of Pluronic F127 and nonionic surfactants from rheological characterization to controlled drug permeation. *Colloids Surf. B Biointerfaces* **2011**, *87*, 42–48.

[21] Golzari, S.E.; Soleimanpour, H.; Mahmoodpoor, A.; Safari, S.; Ala, A.

Lidocaine and Pain Management in the Emergency Department: A Review Article. *Anesthesiol. Pain Med.* **2014**, *3*, e15444.

[22] Shaikh, V.R.; Dagade, D.; Terdale, S.S.; Hundiwale, D.G.; Patil, K.J. Activity and Activity Coefficient Studies of Aqueous Binary Solutions of Procaine, Lidocaine, and Tetracaine Hydrochloride at 298.15 K. *J. Chem. Eng. Data* **2012**, *57*, 3114–3122.

[23] Hata, T.; Matsuki, H.; Kaneshina, S. Effect of local anesthetics on the bilayer membrane of dipalmitoylphosphatidylcholine: Interdigitation of lipid bilayer and vesicle–micelle transition. *Biophys. Chem.* **2000**, *87*, 25–36.

[24] Arora, P.; Mukherjee, B. Design, development, physicochemical, and in vitro and in vivo evaluation of transdermal patches containing diclofenac diethylammonium salt. *J. Pharm. Sci.* **2002**, *91*, 2076–2089.

[25] Walters, K.A.; Bialik, W.; Brain, K.R. The effects of surfactants on penetration across the skin. *Int. J. Cosmet. Sci.* **1993**, *15*, 260–271.

[26] Yasir, M.; Som, I.; Bhatia, K. Status of surfactants as penetration enhancers in transdermal drug delivery. *J. Pharm. Bioallied Sci.* **2012**, *4*, 2–9.

[27] Tewes, F.; Corrigan, O.I.; Healy, A.M. Surfactants in Pharmaceutical Products and Systems. In *Encyclopedia of Pharmaceutical Science and Technology*, 4th ed.; CRC Press: Boca Raton, FL, USA, 2013; pp. 3464–3476.

[28] Nascimento, M.H.M.; Franco, M.K.K.D.; Yokaichyia, F.; de Paula, E.; Lombello, C.B.; de Araujo, D.R. Hyaluronic acid in Pluronic F-127/F-108 hydrogels for postoperative pain in arthroplasties: Influence on physico-chemical properties and structural requirements for sustained drug-release. *Int. J. Biol. Macromol.* **2018**, *111*, 1245–1254.

1.2 Ammonium Glycyrrhizate: a natural biosurfactant for the design of innovative nanocarriers.

Elisabetta Mazzotta[1], Martina Romeo[1], Zakaria Hafidi[2], Lourdes Perez[2], Ida Daniela Perrotta[3], Rita Muzzalupo[1]

1 Department of Pharmacy, Health and Nutritional Sciences, University of Calabria, via P. Bucci, 87036 Arcavacata di Rende (CS), Italy;
2 Department of Surfactants and Nanobiotechnology, Institute for Advanced Chemistry of Catalonia (IQAC-CSIC), 08034 Barcelona, Spain
3 Centre for Microscopy and Microanalysis (CM2), Department of Biology Ecology and Earth Sciences, University of Calabria, 87036 Arcavacata di Rende, Italy

Pubblished on Journal of molecular liquids 2024, 124291.

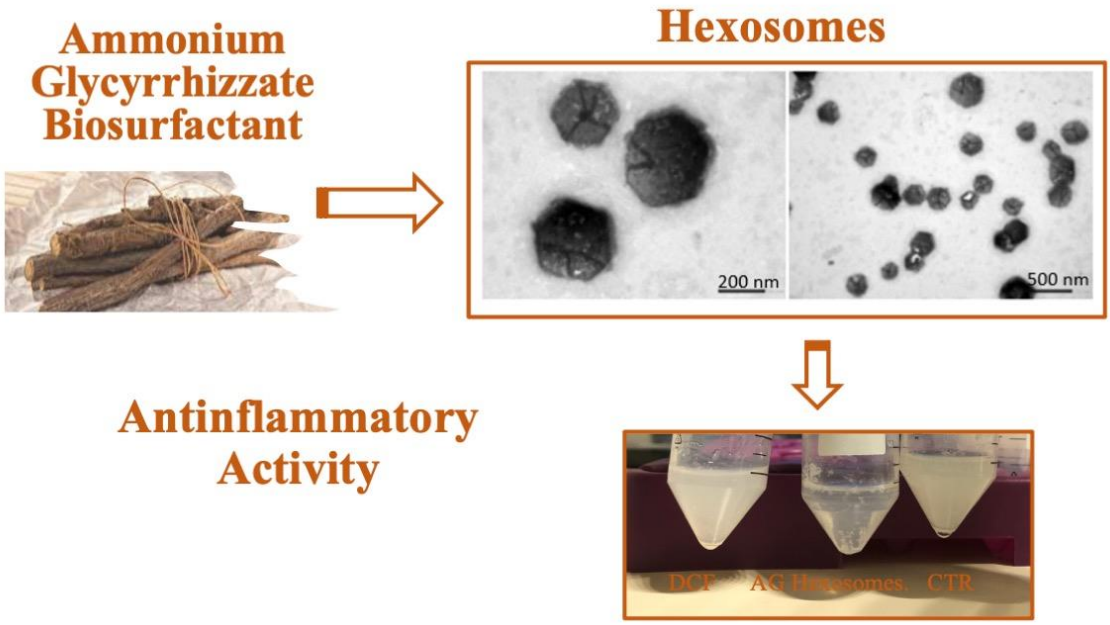

Grafical abstract

Abstract

In this paper, the surfactant properties of Ammonium Glycyrrhizate, a bioactive compound present in Licorice root were studied. Considering the ability of this bioactive molecule to form micelles, we investigated for the first time the self-assemble of Ammonium Glycyrrhizate in vesicle structures. The organization of Ammonium Glycyrrhizate in vesicles allows to increase its bioavailability and, so, efficacy but also to use them as carrier of other drugs for potential combination therapy. Niosomes made up of Ammonium Glycyrrhizate were prepared using thin layer evaporation technique without the use of additional excipients and characterized in term of size, polydispersion index, Zeta potential and colloidal stability. Moreover, the performance of these innovative vesicles as carriers of hydrophilic drug (Fluorescein sodium) or a lipophilic

molecule (Curcumin), was evaluated. Nanocarriers showed nanometric sizes, hexagonal shape, high colloidal stability and ability to encapsulate both hydrophilic and hydrophobic molecules. These vesicles did not showed cytotoxicity nor antimicrobial activity. Moreover, it was found that these niosomes enhanced skin permeation and diffusion in several media and an important ability to interact with mucin. Considering its antinflammatory nature, *in vitro* inhibition of albumin denaturation assay was also carried out to test if the drug maintains these properties also when organized in colloidal structures. The obtained results highlighted an important antinflammatory activity suggesting the potential role of these nanodevices alone or loaded with other therapeutic molecules for the treatment of inflammatory-based diseases.

***Keywords*:**
Biosurfactant, niosomes, ammonium glycyrrhizate, skin permeation enhancer, mucoadhesive drug delivery systems, antinflammatory activity.

1. Introduction

In recent years, an increased interest has been addressed to the rational design of tailored nanomedicines able to deliver payload with tuneable release to the action site at which it is required in a manner dependent on the therapeutic need. To improve nanocarriers performance, a new line of research has arisen focusing on the study of the self-aggregation ability of amphiphilic drugs in several colloidal structures leading to the development of drug self-delivery systems (DSDSs). DSDSs exploit drugs nanoscale properties to realize intracellular delivery by themselves without the help of nanocarriers. This innovative approach allows to overcome several drawbacks related to traditional nanodevices such as the low drug loading efficiency, carrier-induced toxicity and immunogenicity, and the complexity of synthetic process.

Amphiphiles drugs are like surfactants owing the simultaneous presence of hydrophilic as well hydrophobic properties conferring them strong surface activity and the ability to self-assemble into nanoaggregates. Amphiphilic moieties may be intrinsically present in active structure of the drug or may be covalent conjugated with cleavable or non-cleavable linkage to it in order to confer appropriate HLB to induce self-assembling process [1]. Very interesting are biosurfactants, naturally occurring surfactants or surfactants synthesised from natural components that are water-soluble surface-active species. Among them, triterpenoid sapon ins present in different plant species exhibit a high surface activity. Licorice root is a endemic plant of Mediterranean countries that

contain several bioactive compounds with anti-inflammatory, antioxidative, antimicrobial, anticancer properties [2], and , more recently, a potential role in the treatment of coronavirus infections. From a technological point of view, very interesting is the presence in this plant of Ammonium Glycyrrhizate (AG), an amphiphilic molecule with surface active properties. Indeed, AG has a bola structure consisting in an aglycon skeleton as the hydrophobic part and two glucuronic acids as hydrophilic groups at both ends of the hydrophobic groups. Thanks to this amphiphilic structure, AG, when used at the concentration 5 mM, has been shown excellent surface activity, leading to the formation of forms rod-like micelles involving non-covalent interactions and hydrophilic and hydrophobic interplays [3].

Various research groups improved the application of this compound as a potential anti-inflammatory drug using certain drug delivery systems such as non-ionic surfactant vesicles [4] and chitosan nanoparticles [5] enhancing the permeation through the skin stratum corneum and, hence promoting pharmacological activity. In literature, the ability of AG to self-assemble in micelles was widely reported [6, 7, 8].

Anyway, aggregation capacity of AG in vesicle structures has never been investigated. Considering that, the main goal of this study is to evaluate for the first time the potentiality of AG not only as anti-inflammatory drug but also as carrier constituent with low toxicity, high biodegradability and permeation enhancer properties. Vesicles were prepared using thin layer evaporation method and characterized evaluating size, ζ-potential, drug entrapment efficiency, stability and biocompatibility. Release profile was determined *in vitro* both using the Franz diffusion cell apparatus and cellulose membranes in different media in order to investigate their potentiality to be employed across different administration routes such as topical, oral and nasal delivery for the treatment of various inflammatory-based diseases. Additionally, we have investigated if the loading on the device of a hydrophilic drug Fluorescein sodium (FL) or a lipophilic molecule Curcumin (CUR) affect biosurfactant aggregation ability, nanocarrier physicochemical properties and the performance of the device as carriers. Vesicles were further checked for hemolysis and antibacterial properties against various bacteria strains as a prerequisite for its biocompatibility. Finally, we evaluated if the drug, also when organized in vesicle bilayers, maintains its anti-inflammatory potential using egg albumin denaturation method.

2. Materials and methods

2.1 Chemicals

Monoammonium Glycyrrhizate (AG), Diclofenac sodium (DCF), mucin, basic fucsin, periodic acid were purchased by Sigma Aldrich, Milan, Italy, purity ≥ 97%. The organic solvents used, were supplied by VWR International SRL and Sigma Aldrich.

2.2Vesicle preparation

Thin layer evaporation method was used for vesicle preparation as previously reported [9]. AG (45 mg) was firstly dissolved in methanol and then, organic solvent was removed under reduced pressure at 40 °C using a rotary evaporator leading to a formation of thin film on the flask inner wall. After that, the dried film was rehydrated using 10 ml of distilled water at 60°C for 30 min and left to equilibrate overnight. Next, samples were subjected to sonication for 30 min to achieve niosomes with uniform size distribution and then, stored at 4°C until the subsequent experiments.

Moreover, vesicle loaded with CUR (2.44 x 10^{-3} M) and FL (5 x 10^{-4} M) were prepared to test the ability of these vesicle as carrier of other active molecules. CUR-loaded niosomes were obtained by dissolving CUR in the initial surfactant solution, evaporating it to form a thin lipid film and then hydrating it with 10 mL of distilled water. While FL-loaded vesicles were prepared hydrating the thin layer film of AG with FL aqueous solution at 60 °C for 30 min. Next, both AG NIO CUR and AG NIO FL were subjected to sonication for 30 min and then stored at 4°C for the subsequent experiments.

2.3 Physico-chemical characterization.

Vesicles were characterized in term of size, size distribution and ξ-potential by Zetasizer ZS Malvern Instrument Ltd (Malvern, U.K.). The samples were diluted sufficiently with distilled water and measured at 25 °C. The measurements were done in triplicate and expressed as average values ± standard deviation. The morphology of vesicles made up of AG was examined by Transmission Electron Microscopy (TEM) using TEM ZEISS EM 10, operating at an acceleration voltage equal to 80 kV. Two drops of formulations placed on a copper grid with a nitrocellulose covering were stained with phosphotungstic acid (2%, w/v) and left to dry at room temperature before the microscopy observation. The stability of the niosomes was evaluated by storing the formulation at room temperature for three-months monitoring diameter, PI and ζ-potential values.

2.4 Determination of association and encapsulation efficiency

Drug association efficiency (DE %) was determined by analysing the ratio between the amount of biosurfactant aggregated in vesicle structure and the total initial biosurfactant used for the vesicle preparation. To this end, unentrapped AG was removed from niosomal dispersion by exhaustive dialysis for 4 hours using Visking tubing (Spectra/Por®, cut-off 12–14 kDa). The amount of AG retained in vesicle formation was evaluated spectrophotometrically at 250 nm corresponding to the AG wavelength using a UV–VIS spectrophotometer (Thermo Fisher scientific evolution 201/220, Waltham, MA, USA) after dilution of 1 ml purified sample in 10 ml of methanol. DE % was calculated according to the following equation:

$$DE\% = (C_{drug\ retained}/C_{drug\ tot.}) \times 100$$

Where $C_{drug\ retained}$ refers the amount of drug retained after dialysis process and $C_{drug\ tot}$ represents the initial amount of the drug added to the formulation.

The amount of drug encapsulated in vesicle bilayer (EE %) was evaluated using the same technique and analysing spectrophotometrically the concentration of CUR and FL at 420 and 480 nm, respectively.

2.5 *In vitro* mucoadhesion assay

Mucin-particle method was used to investigate mucoadhesive properties of the developed vesicles made up of AG measuring the changes in size and zeta potential upon mucin interaction. First, a soluble fraction of mucin (0.5% w/v) was prepared according to procedures reported in literature [10]. Vesicles were, then, incubated in mucin aqueous solution at different concentration (0.2-0.5 mg/ml) at 37 °C for 1 h and their physicochemical parameters after mucin contact were determined. The amount of mucin adsorbed was evaluated by colorimetric method using periodic acid/Schiff assay.

2.6 *In vitro* release studies

In vitro release studies of niosomal formulations were performed under sink conditions in several media in order to mimic different body districts such as systemic circulation, nasal, intestinal and gastric tract conditions. Aliquots (1 ml) of niosomal suspension or free AG at the same concentration was placed in dialysis bags manipulated before use (Visking dialysis tubes, 20/30 cut-off: 12,000–14,000 Da), and suspended in 50 mL of medium. At set time points, 2 mL of the medium were withdrawn at predetermined time

intervals an exchanged with the fresh medium and analysed by UV-VIS spectrophotometry at 258 nm. Each experiment was carried out in triplicate. The percentage of AG released was evaluated applying the following formula:

$$\% \text{ of Drug released} = Ct / C_0 \times 100$$

Where: C_0 is initial drug concentration and C_t the drug concentration released over time. To simulate systemic circulation, release studies were carried out in PBS (0.01 M, pH 7.4) at 37 °C. Instead, vesicles were first incubated for 2 h in HCl 0.01 M solution and then placed in PBS (0.01 M, pH 6.8) for the rest of the experiment to mimic gastrointestinal conditions. In order to simulate nasal administration, simulant nasal electrolyte solution (SNES) was prepared [11]. Moreover, the nanocarrier ability to release FL and CUR were investigated. Specifically, the controlled release of CUR anf FLwas investigated in PBS pH 7.4/ethanol (7:3 v/v) mixture and gastrointestinal conditions as described above.

2.7 *Ex-vivo* permeation study

Percutaneous permeation profiles were evaluated using Franz diffusion cells for 24 hours at 32°C as previously described [12]. Rabbit ear skins obtained from local breeders were placed into the Franz cells with a diffusional area equal to 0.786 cm^2 between the donor and receptor compartment where dermis faced the receptor fluid. Next, the donor compartment was loaded with 0.3 mL of niosome samples, the acceptor compartment was filled with 8.6 ml of distilled water maintained at 32 ± 0.5 ◦ C. At the pre-determined time intervals, the receiver medium was removed and spectrophotometrically analysed.

At the end of skin permeation experiments, the amounts of AG retained in the skin was determined. To this goal, the skin was rinsed three times with distilled water and the incubated for 1 h with 10 mL of ethanol, under magnetic stirring. Subsequently, the solutions were filtered 0.22 μm Millipore membrane filters and analysed via UV-Vis. Each experiment was performed in triplicate.

2.8 Antimicrobial activity

The antimicrobial activity was determined *in vitro* using a broth microdilution assay to obtain the minimal inhibitory concentration (MIC) defined as the lowest concentration that inhibits the development of visible growth after 24 h of incubation at 37°C [13].

Antimicrobial assays were carried out using 4 Gram positive bacteria and 3 Gram negative bacteria: *Bacilus subtilis* ATCC 6633, *Staphylococcus aureus* ATCC 29213,

Staphylococcus epidermidis ATCC 12228, *Listeria monocytogenes* ATCC 15313, *Enterococcus faecalis* ATCC 29212, *Acinetobacter baumanniii* ATCC 19606, *Klebsiella pneumoniae ATCC 4352* and *Escherichia coli* ATCC 25922

Serial dilutions of the compound, between 376 and 14.75 μg mL^{-1} were dispersed in Mueller–Hinton broth (MHB), and 200 μL of these were added in the corresponding wells of a 96-well polypropylene microtiter plate. The nutrient broth starter culture of each bacterial strain (10 μL) was added to achieve final inoculum of ca. 5 x 10^{-5} colony-forming units (CFU) per mL. Nutrient broth medium without the compound served as growth control. The development of turbidity in an inoculated medium is a function of growth and reflects an increase in both mass and cell number. The MIC was defined as the lowest concentration of antibacterial agent that inhibited development of visible growth after 24 h of incubation at 37 ºC. To confirm this observation, 20 μL of resazurin at 0.015% w/v was added to each well and left to react for approximately 2 h at 37 °C. After the incubation period, the indicative of bacterial growth, i.e., changing from blue to pink, confirmed the MIC value. To obtain the MBC, the antimicrobial concentration corresponding to at least 3 log reductions of viable cells, an aliquot of 10 μL of the MIC well and the 2 concentrations immediately above were seeded over agar MH and incubated for 24 h at 37 °C. The MBC were determined as the lowest concentration in which no colonies were observed on the agar plates.

2.9 Hemolytic activity

The determination of hemolytic activity was carried out on fresh rate blood using an adaptation of the method described by Pape et al. [14].

For the preparation of erythrocyte suspensions, rabbit blood was supplied by the Animal Experimentation Unit (Instituto de Química Avanzada de Cataluña - IQAC). Erythrocytes were washed three times in PBS (pH 7.4) and suspended in PBS at a cell density of $8x10^9$ cells/mL. To determine the hemolytic activity a series of different volumes of a niosomal solution (3760 μg/mL), ranging from 10 to 130 μL, were placed in small Eppendorf tubes containing 25 μL of erythrocyte suspension and PBS was added to each tube to a total volume of 1 mL. Samples were shaken for 10 minutes at room temperature and the tubes were then centrifuged (5 min at 10000 rpm). The percentage of hemolysis was determined by comparing the absorbance (575 nm) of the supernatant of the samples with that of the control totally hemolyzed with distilled water using the follow formula:

$$\%\ Haemolyis = 100x\ (Abs_{test\ compound})/(Abs_{Basal\ haemolytic\ activity})$$

Each analysis was performed in triplicate.

2.10 *In vitro* antinflammatory activity.

Anti-inflammatory activity of AG niosomes was evaluated by protein denaturation assay [15]. Briefly, reaction mixture was prepared consisting of 2.8 mL of phosphate buffer saline pH 6.8, 0.2 mL of fresh egg albumin and 2 mL of sample at different concentration. A similar volume of distilled water served as negative control, while diclofenac sodium (DCF) at various concentrations was used as reference drug. The mixtures were first placed in incubator at 37 °C for 15 min and then heated to 70 °C for 5 min. After that, samples were cooled, and absorbance was spectrophotometrically measured at 660 nm. Inhibition activity of protein denaturation was calculated using the following equation:

$$Inhibition\ activity\ (\%) = 100x\ (A\ control - A\ sample)/A\ control$$

where A control is the absorbance of negative control and A sample is the absorbance of the sample. The drug concentration for 50% inhibition (IC50) was determined from the dose–response curve by plotting percentage inhibition against treatment concentration.

3.Results and discussions

3.1 Niosomes characterization

Ammonium glycyrrhizate, a monodesmosidic triterpenoid saponin, exhibits directly or after metabolization a wide range of biological activities such as anti-inflammatory, anti-fungal, anti-viral, anti-cancer and cholesterol lowering functions [2]. Recently, these classes of natural compounds have been also emerged as biosurfactants for their high surface activity, adsorption to different interfaces and surfaces and their ability to self-assemble into different aggregates [16]. This AG similarity to surfactants is due to the presence in their structure of a hydrophobic component which is a triterpenoid aglycon linked to a hydrophilic glycon consisting of two linked d-glucuronic acid groups by glycoside bonds [17]. It has been recently demonstrated the AG ability to adsorb at the air/water interface and to form micelles in solution [18]. But, to best of our knowledge, there is no study focusing to investigate AG ability to form vesicles before us. Hence, we prepared vesicle aggregates made up of AG via thin-film hydration method using a concentration higher to the CMC reported in literature (3.7 mM) [19]. Preliminarly, we

used 90 mg of AG for niosomes preparation but the vesicles obtained undergo to gelification overnight. So, we decided to test lower AG amounts (45 mg and 22.5 mg). The measurements carried out by DLS Table 1, indicated that the 45 mg AG formed homogeneous vesicular structures with a mean diameter size of 610.5 nm and a narrow size distribution as demonstrated by the low PI value (0.231) obtained without the use of additional excipients. Conversely, formulations prepared using 22.5 mg of AG exhibited a mean diameter of 593.2 nm, a PI equal to 0.304 and low particle concentration. Considering the high count rate of AG niosomes prepared with 45 mg of AG, we used these formulations for the next experiments. As expected, due to the hydrophilic anionic group of AG, a high negative ζ -potential (-28.2 ± 0.53 mV) was recorded indicating a good colloidal stability and preventing potential instability phenomena, such as aggregation, agglomeration, and/or flocculation. The formation of vesicles was also confirmed by TEM analysis: Figure 1 clearly underlines the presence of hexagonal vesicles with a staggered/irregular profile and sizes like that obtained with DLS analysis. AG probably forms polyhedral bilayer membranes characterized by flat faces connected by ridges and vertices with high local curvature, and are energetically favorable compared to spherical vesicles [20].

Table 1. Physicochemical characterization of empty and FL and CUR loaded AG NIO in terms of mean diameter, P.I, ξ-potential, AG association efficiency (DE%) and drug encapsulated in vesicle bilayer (EE%).

FORMULATIONS	Diameter (nm)	P.I	ξ-potential (mV)	(DE%)	(EE%).
AG NIO	610.5 ± 5.3	0.231	-28.2 ± 0.53	86.33	-
AG NIO- FL	500.4 ± 6.9	0.216	- 27.4 ± 1.84	58.30	58.02
AG NIO CUR	334.1 ± 3.4	0.153	-22.4 ± 0.50	74.88	90.03

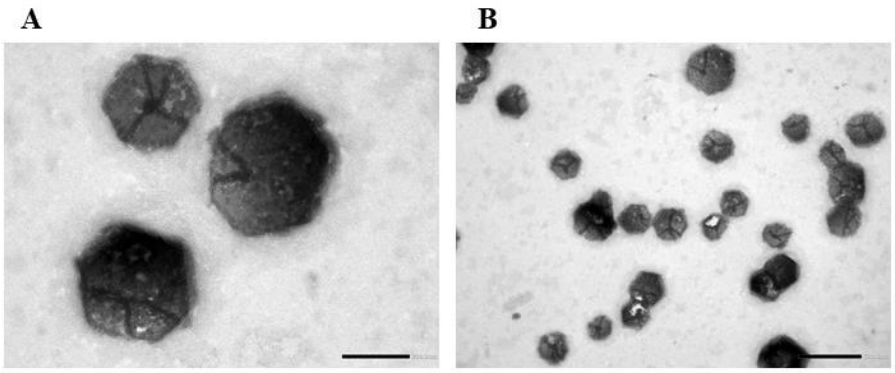

Figure 1. Typical photomicrographs of AG NIO formulation: A) scale 200nm and B) 500nm

AG seems to possess an optimal fluidity of the hydrophobic chains resulting in the formation of hexagonal aggregates without the presence of any membrane additive. Probably, this morphology is due to the surfactant hydrophilic lipophilic balance that possesses rather hydrophobic characteristics (log P=4.637) and led to the formation of hexagonal shaped vesicles. As reported in literature, natural-like branched-chain glycolipids with high hydrophobic character form hexagonal structure in aqueous solution [21, 22]. In fact, Ahmad and coworkers [21] investigated the aggregation properties of two glycolipids with same branched alkyl chain lengths but different headgroup demonstrating the formation of unilamellar vesicles in the case of more hydrophilic surfactant and, instead, hexosome dispersions for that with a more pronounced hydrophobic character. This type of hexagonal organization is commonly observed for saponin surfactant class. Indeed, saponins can form highly viscoelastic networks through intermolecular hydrogen bonds between neighboring sugar residues [23]. Moreover, AG aggregation capability in niosomes was very high as demonstrated by the high value of DE % obtained (86.33 %).

The loading of FL and CUR did not affect AG ability to form regular and stable vesicles homogenous in size. Specifically, the incorporation of CUR in vesicle bilayer led to a significant size decrease (Table 1) due to that this compound acts as a membrane condensing agent. This behaviour has been already observed by Kotenkov et al. [24]. AG NIO also exhibited a high ability to encapsulate both hydrophilic and hydrophobic molecules as highlighted by the EE% values obtained for FL and CUR, 58.02 and 90.03%, respectively. The loading of both drugs, instead, significantly affects the vesicle morphology, in this case spherical niosomes were obtained (data not reported).

Next, we investigated the colloidal stability of niosomes stored at 25 ± 1 °C for 90 days by assessing changes in physicochemical parameters. Interestingly, no sedimentation was found in any sample. Moreover, after 3 months, size distribution, ζ-potential and DE % were not significantly different from the initial preparation. Only a little increase of vesicle size and reduction of ζ-potential values was recorded just after 30 days with some little variations up to 90 days (Table 2).

Table 2. Stability of AG niosomes evaluated measuring diameter, P.I., ξ-potential, D.E. at specific time points up to 3 months. Data are expressed as mean of three different experiments ± SD.

Times (days)	Diameter (nm)	P.I.	ξ-potential (mV)	AG DE %
0	610.5 ± 5.3	0.231	-28.2 ± 0.529	86.33 ± 0.87
30	666.8 ± 4.9	0.221	- 25.3 ± 0.415	83.68 ± 1.32
60	680.6 ± 3.8	0.212	-26.8 ± 0.764	84.00 ± 0.95
90	678.3 ± 5.1	0.278	-22.5 ± 0.865	82.91 ± 3.67

In the search for of novel and efficient drug delivery systems, considerable attention has been focused on the nanodevices with low irritancy potential able to influence the therapeutic use. To verify the compatibility and safety of AG vesicles, their hemolytic effect and antimicrobial activity were investigated considering the reported antibacterial properties of AG metabolite. Antimicrobial activity of AG NIO was tested against a range of representative Gram-positive and Gram-negative bacteria by determining their MIC, the concentration required to completely inhibit microorganism growth, and the MBC, the concentration of surfactants required to kill microorganisms. It has been found that at the highest concentration used, 376 μM, the formulation did not exhibit activity against any of the tested bacteria. These results were confirmed by MBC as bacterial growth was not observed for any strain at the highest concentration of NIO AG. Lack of anti-bacterial activity could be advantageous since confer them inert nature making them to be good candidates for drug delivery applications without any cross-reactivity. Haemolytic activity is also an important factor to be considered in the design of biocompatible pharmaceutical carriers. Even in this case, it has been observed that in the concentration range investigated (45-582 μM) NIO AG did not exhibit any hemolytic activity. Therefore, it seems that AG vesicles can be considered safe carriers representing new devices useful in various administration routes.

Mucoadhesion is a key factor to be considered in the design of nanodevices for oral and nasal delivery since as a result of the adhesion, the residence time of nanocarriers at the absorption site results prolonged improving drug absorption. Consequently, mucoadhesive properties of the designed vesicles were evaluated monitoring nanoparticle interaction with mucin at different concentration. To this purpose, changes in physicochemical parameters after mucin interaction were evaluated and the results are reported in Table 3.

Table 3. Physicochemical characterization of AG NIO contacted with mucin at various concentrations after 1 h at 37 °C

Sample	Diameter (nm)	P.I.	ξ-potential (mV)	Mucin Adsorbed (mg/ml)
AG NIO	610.5 ± 5.3	0.231	-28.2 ± 0.529	-
AG NIO-Mucin 0.2 mg/ml	647.2 ± 3.7	0.020	-27.3 ± 1.88	0.037
AG NIO-Mucin 0.3 mg/ml	971.9 ± 6.5	0.292	-24.8 ± 0.551	0.130
AG NIO-Mucin 0.4 mg/ml	923.3 ± 8.1	0.229	-9.01 ± 1.15	0.188
AG NIO-Mucin 0.5 mg/ml	899.3 ± 4.4	0.229	-6.97 ± 0.804	0.193

An increase in particle size as well as reduction of zeta potential values in a manner dependent on the amount of mucin absorbed on particle surface was observed. This increase of particles sizes indicates an interaction between vesicles and mucin and, so, the mucoadhesive properties of vesicles able increase the residence time at the action site resulting in prolonged drug absorption. In general, the mucoadhesive behaviour of nanocarriers is dependent on both the high specific surface area resulting in a sharp increase in the interface that establishes the bond with the mucosa and the chemical groups (eg, hydroxyl, amine, sulfate, and carboxyl groups) available on carrier surface able to establish electrostatic interactions, hydrogen bonding, and hydrophobic interactions with mucin glycoprotein. Considering the negative surface charge of the developed formulations, interaction with mucin do not occur via electrostatic force but probably trough hydrogen bonding and hydrophobic effects leading to “non-specific” interaction and a physical entanglement between vesicles and mucin [25]. Particle size intensity distribution after interaction with mucin at various concentrations was also showed in Fig.2. Vesicles that interacted with the lowest amount of mucin used presented a single broader population than the uncoated niosomes. Increasing mucin amount, a bimodal size distribution occurred as before interaction but with populations with increased sizes. The higher amount of mucin absorbed on particle surface resulted also in a higher instability according to their important ζ-potential reduction.

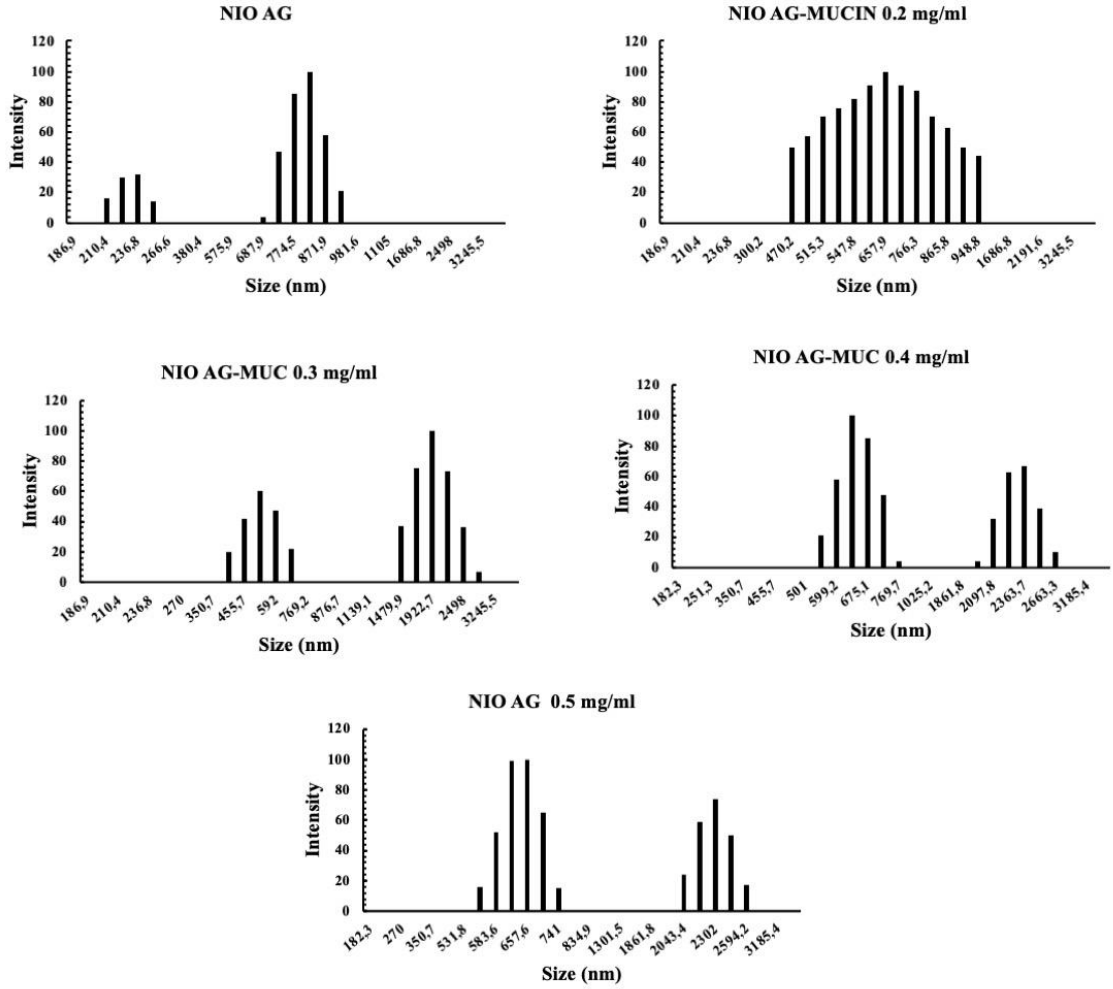

Figure 2. Intensity-based size distribution as detected by DLS for niosomes after interaction for 1 h at 37 °C with mucin at several concentrations.

These results highlighted the mucoadhesive nature of the developed formulations that if associated to an enhanced penetration. These results indicate that these new niosomes could be very successful for oral and nasal delivery systems.

3.2 *Ex-vivo* permeation studies

The AG niosomes developed in this work have been designed for inflammatory based diseased. In this regard, multi-experimental setup has been carried out in order to evaluate various potential administration routes of the developed AG NIO. Franz type diffusion cells were used to perform *ex vivo* skin permeation studies to evaluate the topical and transdermal profile of the niosomal systems and the results are shown in Figure 3A. AG NIO exhibited an increased skin permeation equal to 162.74 μg/cm^2 compared to free AG that had a cumulative permeation of 104.93 μg/cm^2 after 24 h. The poor permeation rate of AG solution could be due to its high molecular weight that limits its spontaneous

permeation through the skin. Moreover, this increased skin permeation is also associated with a higher drug skin retention: in fact, the amount of drug retained after 24 h resulted be equal to 789.49 μg/cm^2 for NIO AG respect that obtained with AG solution equal to 693.40 μg/cm^2. This indicates that when AG organized in nanoscale vesicles acts as skin permeation enhancer showing a higher skin permeation and a higher drug depot in the stratum corneum respect the drug solution.

3.3 *In vitro* release studies

The release studies of AG NIO were evaluated in various fluids simulating parenteral, oral and nasal administration in order to assess if these vesicles can be employed across different administration routes such as topical, oral and nasal delivery. As shown in Figure 3B, C and D, cumulative amounts of AG released from niosome formulations in the all media used in this study were found to be higher than that observed for AG solution. This higher bioavailability may be due to a relatively high surface area of AG exposed to the fluids, thereby increasing its solubilization leading to a more rapid release of AG [26]. Probably, this behaviour may be due to both the low AG solubility in water and the fact that, at the concentration used, free AG forms micelles that decrease its interaction with water resulting in a decreased dissolution rate. Clearly, micelles and vesicles differ in the molecular-scale organization, the higher size of vesicles results in a slightly lower effective viscosity giving rise to less motional freedom within the smaller structures [27]. Moreover, the hydrophobic core zones of micelle are significantly less exposed toward aqueous medium, which contributes to slow release time into aqueous medium [28].
To mimic the behaviour of AG NIO in the gastro-intestinal tract after oral intake, *in vitro* release profiles simulating the different steps of human digestion were evaluated: pH 2 (2h stomach) and pH 6.8 (up to 24h small intestinal). AG and AG NIO showed low release in the stomach (pH=2) implying drug protection (Figure 3D).

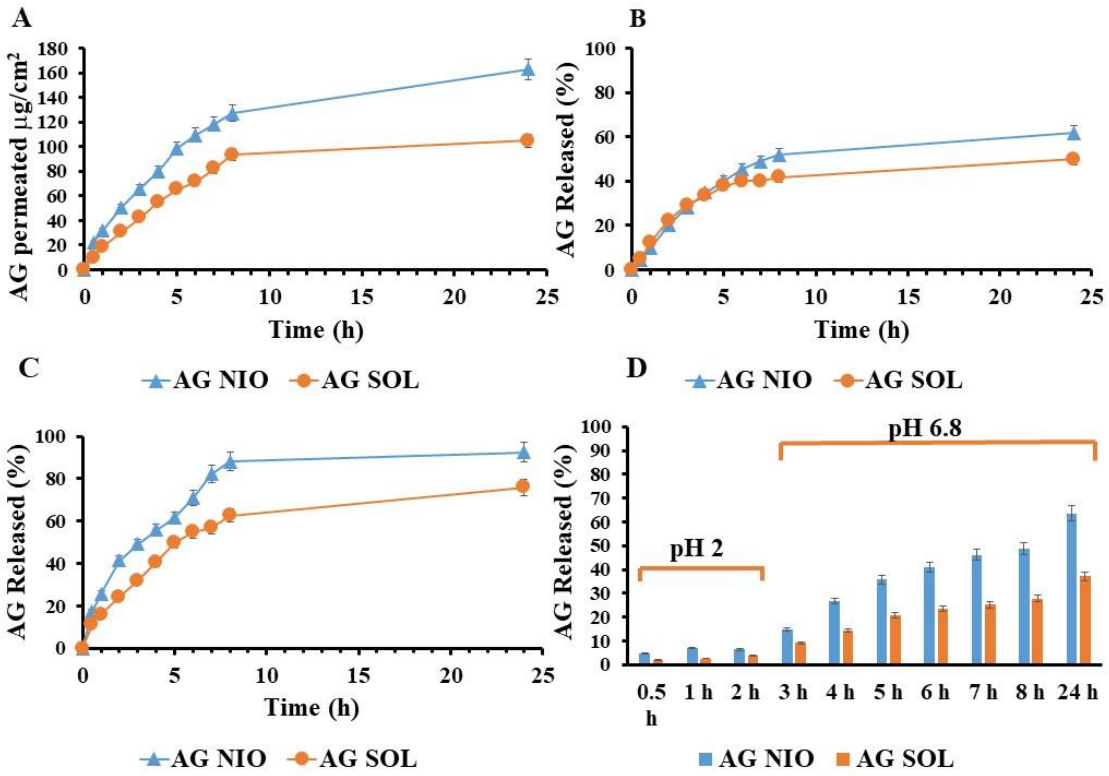

Figure 3. Permeation and release studies: A) *Ex-vivo* permeation of free AG solution and AG NIO; B) *in vitro* release of AG solution and AG NIO in PBS pH 7.4; C) *in vitro* release of AG solution and AG NIO in SNES fluid; D) *in vitro* release of AG solution and AG NIO in gastrointestinal simulant fluid

However, an increased release was observed in intestinal conditions (pH=6.8), this behaviour results desirable for oral delivery systems demonstrating that the AG bioavailability was pronouncedly enhanced.

Moreover, we investigated the potentiality of AG niosomes as nasal drug delivery systems since this route results be very interesting not only for the treatment of local and pulmonary disease but also for the possibility to reach brain bypassing blood-brain barrier and hepatic first pass metabolism. For this regard the release of AG was carried out in SNES fluid ((Figure 3C). It was also observed that, in this medium, the release of AG from the AG NIO solution was faster than that of drug solution suggesting the enhanced dissolution profile and solubility in SNES achieved when organized in vesicle nanostructure. This increased diffusion associated with the ability of the device to interact with mucoadhesive biological surface contributes to a better drug absorption.

In addition, we prepared vesicle loaded with a hydrophobic (CUR) or hydrophilic (FL) molecule as model drug and investigated their release profile. The release of CUR anf FL was carried out in gastrointestinal and physiologic simulant fluid. At pH=7.4 (Fig. 4C and 4D) a sustainable release of FL and CUR with time was observed with a maximum of 20.28 % of CUR, 17.22 and 26.27 % of FL after 24 h. In these conditions the release of

free FL and CUR were much more rapid, more than 70% in 5 hours. This slow release indicates the high stability of encapsulated substance and the possibility to use them as long-lasting delivery systems.

Interesting results were obtained in the gastrointestinal medium. At pH=2 a high release of FL and CUR from the free drug solution was observed indicating that these drugs will release in the stomach and consequently can be potentially degraded. However, very slow release at pH=2 was observed when these molecules were incorporated in AG NIO.

It should be noted that AG NIO act as carrier and as drug given the biological activity of the AG. Moreover, when the AG NIO incorporate other drugs these nanodevices can have numerous therapeutic applications.

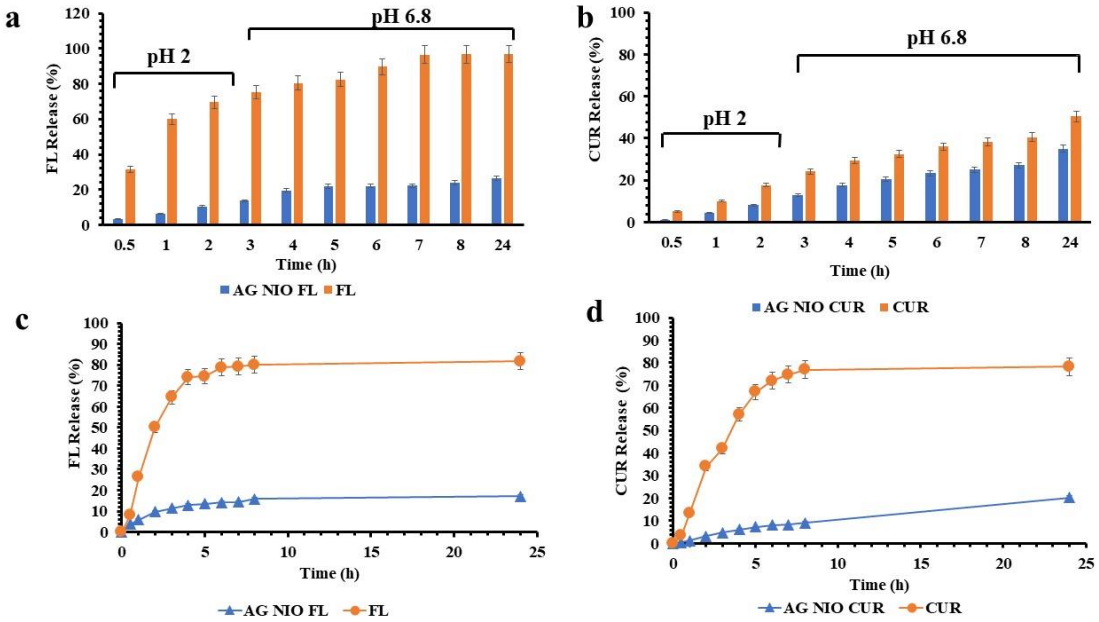

Figure 4. *In vitro* release profile of CUR and FL from AG NIO and free solution of: a) FL in gastrointestinal simulant fluid; b) FL in PBS pH 7.4 ; c) CUR in PBS pH 7.4/Ethanol (7:3 v/v).

3.4 *In vitro* antinflammatory assay

It is well documented that protein denaturation leading to the loosing of their biological activity is involved in the formation of inflammatory disorders [15]. Therefore, the ability of both free AG and AG NIO to inhibit egg albumin denaturation have been investigated (49-147 mg/mL) to predict their potential anti-inflammatory action mechanism and the results are summarized in Figure 5.

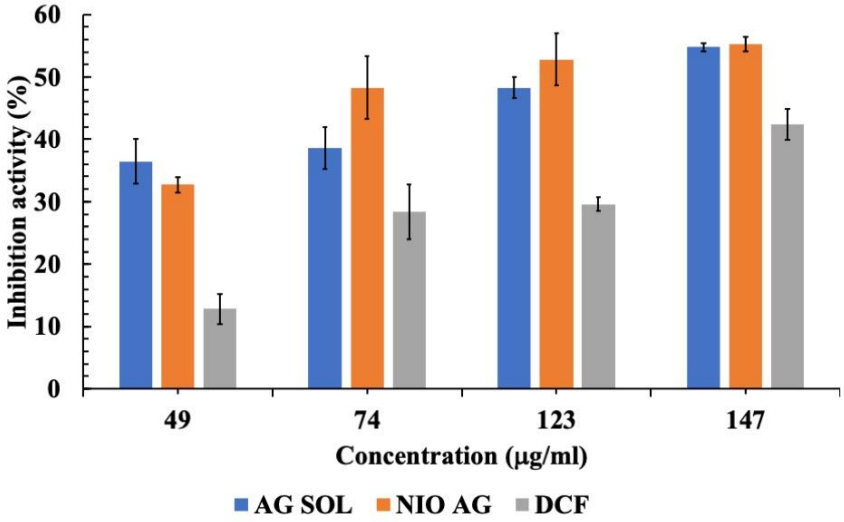

Figure 5. Inhibition activity of AG solution, AG NIO and Diclofenac sodium solution in the egg albumin denaturation method. Data are presented as mean ± SD.

Results revealed that free AG inhibited thermally induced albumin denaturation in a dose dependent manner with a IC50 equal to 118.15 µg/mL. Moreover, even when organized in vesicular structures, AG maintains its capacity to control protein denaturation involved in the inflammatory process evidenced by the similar IC50 values obtained (110.11 µg/mL). The inhibitory activity was also compared with a standard anti-inflammatory drug DCF and at all concentration tested, AG and AG NIO showed a higher inhibitory activity than DCF, that exhibited an IC50 of 179.47 µg/mL. These results highlighted that when AG is organized in vesicles its pharmacokinetic profile is improved by reducing the use of other carrier excipients, increasing drug loading and, also, maintaining the anti-inflammatory activity. In this light, these nanodevices could be used as carrier of other drugs for potential synergic therapies.

Conclusions

A successful application of drug delivery systems, a promising area of nanomedicine, still depends on our capability as scientists to design efficient, biocompatible and eco-friendly vehicles. This manuscript reports, for the first time, the use of a biosurfactant with anti-inflammatory properties, the ammonium glycyrrhizate (AG) present in a Mediterranean plant, to prepare a drug self-delivery system.

This biosurfactant (AG) form suitable homogeneous and biocompatible vesicles with high stability and great drug loading without the use of additional excipients. AG niosomes appear to be a versatile nanocarriers able to behave as drug percutaneous permeation enhancers after topical application, and, also, as mucoadhesive delivery systems in the case of oral and nasal administration

These AG based vesicles exhibited important anti-inflammatory properties assessed through the albumin denaturation inhibition assay suggesting their great potentiality in the treatment of inflammatory based diseases. Moreover, these AG nanodevices successfully encapsulated a hydrophobic (CUR) and a hydrophilic (FL) molecule giving rise to a sustained release with time for both compounds.

The obtained results indicate that AG NIO act simultaneously as both carrier and therapeutic drug. In addition, these vehicles can encapsulate other medicines, thus expanding their therapeutic properties. The strategy used in this paper represents a great innovation from a technological viewpoint suggesting the potentiality to use amphiphilic drugs not only for their pharmacological activity but also as a carrier of other substances in combined or synergic therapies.

Reference

[1] J. Xi, & H. Liu, (2020). Recent Advances in the Design of Self-Delivery Amphiphilic Drugs and Vaccines. *Advances in Therapy*, *3* (2), 1900107, DOI: 10.1002/adtp.201900107.

[2] Y. J. Kwon, D. H. Son, T. H. Chung, & Y. J. Lee. (2020)**.** A review of the pharmacological efficacy and safety of licorice root from corroborative clinical trial findings. *Journal of Medicinal Food*, *23*(1), 12-20, DOI: 10.1089/jmf.2019.4459.

[3] K. Matsuoka, M. Arima, Y. Goto, S. Yada, & T. Yoshimura. Micelle Formation of Monoammonium Glycyrrhizinate. **(**2021). *Journal of Oleo Science*, *70*(7), 911-918, DOI: 10.5650/jos.ess21046.

[4] D. Paolino, R. Muzzalupo, A. Ricciardi, C. Celia, N. Picci, & M. Fresta, M., (2007). In vitro and in vivo evaluation of Bola-surfactant containing niosomes for transdermal delivery. *Biomedical microdevices*, 9, 421-433.

[5] T. W. Wang, Q. Xu, Y. Wu, A. J. Zeng, M. Li, & H. Gao, (2010). Quaternized chitosan (QCS) nanoparticles as a novel delivery system for ammonium glycyrrhizinate, *Journal of Nanoscience and Nanotechnology*10(11), 7402-7405.

[6] O.Y. Selyutina, N.E. Polyakov (2019). Glycyrrhizic acid as a multifunctional drug carrier -From physicochemical properties to biomedical applications: A modern insight on the ancient drug. *International Journal of Pharmaceutics*, 25 (559),271-279, DOI: 10.1016/j.ijpharm.2019.01.047

[7] K. Matsuoka, R.Miyajima, Y. Ishida, S. Karasawa, T. Yoshimura, (2016). Aggregate formation of glycyrrhizic acid. *Colloids and Surfaces A: Physicochemical and Engineering Aspects*, 500, 112-117

[8] M. Hussain, (2019). Molecular dynamics simulations of glycyrrhizic acid aggregates as drug-carriers for paclitaxel. *Current drug delivery*, 16(7), 618-627.

[9] R. Muzzalupo, L. Tavano, R. Cassano, S. Trombino, T. Ferrarelli, & N. Picci, (2011). A new approach for the evaluation of niosomes as effective transdermal drug delivery systems. *European Journal of Pharmaceutics and Biopharmaceutics*, *79*(1), 28-35, DOI: 10.1016/j.ejpb.2011.01.020.

[10] B. Menchicchi, J. P. Fuenzalida, K. B. Bobbili, A. Hensel, M. J. Swamy, & F. M. Goycoolea, (2014). Structure of chitosan determines its interactions with mucin. *Biomacromolecules*, *15*(10), 3550-3558, DOI: 10.1021/bm5007954.

[11] D. M. Vasa, Z. Bakri, M. D. Donovan, L. A. O'Donnell, & P. L. Wildfong, (2021). Evaluation of Ribavirin–Poloxamer Microparticles for Improved Intranasal Absorption. *Pharmaceutics*, *13*(8), 1126, DOI: 10.3390/pharmaceutics13081126.

[12] M. Romeo, E. Mazzotta, I. D. Perrotta, & R. Muzzalupo, (2022). Lidosomes: Innovative Vesicular Systems Prepared from Lidocaine Surfadrug. *Pharmaceutics*, 14, 2190, DOI: 10.3390/pharmaceutics14102190.

[13] J. B. Patel, F. C. Tenover, J. D. Turnidge, & J. H. Jorgensen, (2011). Susceptibility test methods: dilution and disk diffusion methods. *Manual of clinical microbiology*, 1122-1143, DOI: 10.1128/9781555816728.ch68.

[14] W. J. Pape, U. Pfannenbecker, & U. Hoppe, (1987). Validation of the red blood cell test system as in vitro assay for the rapid screening of irritation potential of surfactants. Journal of Biochemical and Molecular Toxicology, *1*(4), 525-536.

[15] D. B. Aidoo, D. Konja, I. T. Henneh, & M. Ekor, (2021). Protective effect of bergapten against human erythrocyte hemolysis and protein denaturation in vitro. *International Journal of Inflammation*, *2021,* DOI: 10.1155/2021/1279359.

[16] J. Penfold, & R. K. Thomas, (2019). Adsorption properties of plant based bio-surfactants: Insights from neutron scattering techniques. Advances in Colloid and Interface Science, *274*, 102041, DOI: 10.1016/j.cis.2019.102041.

[17] E. Tykarska, S. Sobiak, & M. Gdaniec, (2012). Supramolecular Organization of Neutral and Ionic Forms of Pharmaceutically Relevant Glycyrrhizic Acid-Amphiphile Self-Assembly and Inclusion of Small Drug Molecules. *Crystal Growth & Design*, *12*(4), 2133-2137, DOI: 10.1021/cg300160c.

[18] I. M. Tucker, A. Burley, R. E. Petkova, S. L. Hosking, J. Penfold, R. K. Thomas, ... & J. Doutch, (2021**).** Adsorption and self-assembly properties of the plant based biosurfactant, Glycyrrhizic acid. *Journal of Colloid and Interface Science*, *598*, 444-454, DOI: 10.1016/j.jcis.2021.03.101.

[19] K. Matsuoka, R. Miyajima, Y. Ishida, S. Karasawa, & T. Yoshimura, (2016). Aggregate formation of glycyrrhizic acid.*Colloids and Surfaces A: Physicochemical and Engineering Aspects, 500*, 112-117, DOI: 10.1016/j.colsurfa.2016.04.032.

[20] C. A. Haselwandter, & R. Phillips, (2011). Elastic energy of polyhedral bilayer vesicles. *Physical Review E, 83*, 061901. DOI: 10.1103/PhysRevE.83.061901

[21] N. Ahmad, R. Ramsch, J. Esquena, C. Solans, H. A. Tajuddin, & R. Hashim, (2012). Physicochemical characterization of natural-like branched-chain glycosides toward formation of hexosomes and vesicles. *Langmuir*, *28*(5), 2395-2403., DOI: 10.1021/la203736b.

[22] M. Rosa, M. Rosa Infante, M. D. G. Miguel, & B. Lindman, (2006). Spontaneous formation of vesicles and dispersed cubic and hexagonal particles in amino acid-based catanionic surfactant systems. *Langmuir*, *22*(13), 5588-5596, DOI: 10.1021/la053464p.

[23] F. Rinaldi, P. N. Hanieh, L. K. N. Chan, L. Angeloni, D. Passeri, M. Rossi,... & C. Marianecci, (2018). Chitosan glutamate-coated niosomes: A proposal for nose-to-brain delivery. *Pharmaceutics*, *10*(2), 38, DOI: 10.3390/pharmaceutics10020038.

[24] S. A. Kotenkov, O. I. Gnezdilov, A. V. Khaliullina, O. N. Antzutkin, R. S. Gimatdinov, A. V. Filippov, (2019). Effect of cholesterol and curcumin on ordering of DMPC bilayers. Applied Magnetic Resonance, 50, 511–520.

[25] M. I. Adamczak, Ø. G. Martinsen, G. Smistad, & M. Hiorth, (2017)**.** Polymer coated mucoadhesive liposomes intended for the management of xerostomia. *International Journal of Pharmaceutics*, *527*(1-2), 72-78, DOI: 10.1016/j.ijpharm.2017.05.032.

[26] X. Huang, Y. Liu, Y. Zou, X. Liang, Y. Peng, D. J. McClements, & K. Hu, (2019)**.** Encapsulation of resveratrol in zein/pectin core-shell nanoparticles: Stability, bioaccessibility, and antioxidant capacity after simulated gastrointestinal digestion. *Food Hydrocolloids*, *93*, 261-269, DOI: 10.1016/j.foodhyd.2019.02.039.

[27] S. A. Stevenson, & G. J. Blanchard, (2006). Investigating internal structural differences between micelles and unilamellar vesicles of decanoic acid/sodium decanoate. *Journal of Physical Chemistry B*, *110*(26), 13005-13010, DOI: 10.1021/jp062129m.

[28] F. Avila-Salas, A. Pereira, M. A. Rojas, M. Saavedra-Torres, R. Montecinos, S. Bonardd, … & C. Saldías, (2017). An experimental and theoretical comparative study of the entrapment and release of dexamethasone from micellar and vesicular aggregates of PAMAM-PCL dendrimers. *European Polymer Journal*, *93*, 507-520, DOI: 10.1016/j.eurpolymj.2017.06.023.

1.3 Formulations and characterization of novel drug delivery systems based on Folic acid

Introduction

The increase in scientific knowledge in recent years has led to the pharmaceutical industry's increased interest in developing new drug delivery systems. This has made it possible to improve the therapeutic efficacy of the drug, increase the stability of the encapsulated drug and minimise side effects. These new delivery systems fall into the category of DDS (drug delivery systems). In particular, niosomes are spherical vesicular systems consisting of surfactants, arranged to form a lipid bilayer bordering a hydrophilic core [1]. Although several types of these nanocarriers have been developed, success is limited to a few formulations [2]. With the aim of overcoming the limitations induced by niosomal and liposomal systems, nanotechnology has proposed the use of pharmacologically active molecules with an amphiphilic structure to make the bilayer. These molecules have been defined by many authors as surfadrugs, and indeed possess the ability to self-associate in an aqueous environment and interact with biological membranes in the same way as classical surfactants [3]. Folic acid (FA), also known as vitamin B9, is a B-complex vitamin required for the transfer of carbon units in the intermediate metabolism of amino acid synthesis and in the production of S-adenosyl methionine (SAM) through methylation reactions [4]. Given this role, a deficiency can have a profound effect on cell replication and metabolism. In humans, folate deficiency leads to megaloblastic/macrocytic anaemia in all age groups [5]. In the elderly, however, it can lead to dementia and cognitive decline [6]. However, its consequences are more pronounced in pregnancy, as folate deficiency can lead to serious consequences on embryonic and foetal development [7,8]. Chemically, folic acid consists of a pteridine derivative, 4-aminobenzoic acid and L-glutamic acid. Due to its involvement in DNA synthesis and repair, FA in topical applications has been shown to have remarkable effects in the treatment of skin ageing and photodamage [9]. In recent decades, delaying the onset of skin ageing has become increasingly important for large segments of the population. Skin ageing is the result of the interaction between endogenous and exogenous factors. About 80 per cent of the changes associated with skin ageing can be attributed to extrinsic factors such as ultraviolet (UV) radiation. Among other effects, UV-A and UV-B radiation induce cellular DNA damage, which plays a crucial role in the progression of skin ageing. Consequently, skin cells are constantly engaged in repair processes to maintain cellular

homeostasis [9]. Due to folic acid's ability to act as a cell nutrient, many topical formulations containing FA are available on the market for the treatment of photodamaged or ageing skin [10]. The very low solubility of FA makes its homogeneous dispersion in hydrophilic solvents difficult; therefore, surfactants, co-surfactants or co-solvents must be used to achieve a homogeneous formulation [11]. Many studies in the literature show that folic acid is promising in active targeting. This is possible because folic acid receptors are overexpressed on the surface of 40% of solid tumours but are negligible in healthiest tissues [12]. Therefore, folate-based delivery systems could represent a strategy to overcome the limitations associated with classical delivery systems, enabling combined and targeted therapy with the administered drug.

Material and method

Chemicals

Folic acid (FA) and all solvent were purchased by Sigma Aldrich, Milano, Italy.

Niosomal preparations

Folic acid niosomal systems were formulated using the thin-layer evaporation technique. To obtain niosomal systems consisting of FA, folic acid was salified with a KOH solution at pH 10 to form the corresponding salt, potassium folate, since FA in acid form does not allow the formation of vesicular systems. Different amounts of FA (13, 21 and 26 mg) were evaluated, but only 26 mg resulted in the formation of niosomes. Therefore, subsequent formulations were obtained from this quantity, corresponding to a concentration of 4.76×10^{-3}. Niosomal vesicles were obtained using water as the hydration solvent at various pH. Weighed quantities of FA were solubilised in ethanol in a round-bottomed flask. The solvent was then evaporated under reduced pressure and constant rotation, forming a lipid film. The film was then hydrated with 10 mL of hydration solvent for 30 min at 60°C, forming multilamellar vesicles, which then transformed into small unilamellar vesicles following sonication in an ultrasonic bath conducted after 24 h. The niosomal vesicles were then purified by exhaustive dialysis for 4 h, using Visking tubes (Spectra/Por, cut-off 12/14 kDa).

From the physical-chemical characterisation of these formulations, it was observed that the optimal experimental conditions were when the hydration solvent had pH 10.

Physical-chemical characterization

Size distribution and ξ potential

The dimensional analysis of the vesicles was conducted with a Brookhaven Instruments Corporation, New York, USA, at 25°C. The autocorrelation function was measured at 90°C and the laser beam operated at 658 nm. The polydispersion index was used to measure and evaluate the size distribution. The potential ξ of the formulations was measured with the Zetasizer ZS (Malvern Instruments Ltd., Malvern, UK), at 25.0 ± 0.1 °C. Each analysis was conducted in triplicate.

Morphology

To further verify the formation of vesicles by FA under these experimental conditions, their morphology was observed using transmission electron microscopy (TEM). Images were obtained with a Jeol 1400 Plus TEM electron microscope operating at an accelerating voltage of 80 kV. A drop of vesicle suspension was placed on a Formvar/Carbon-coated copper grid, forming a thin liquid film. Excess water was removed with a piece of filter paper, followed by air drying.

Encapsulation efficiency

The amount of Folic acid reitained in the vesicles is expressed as the percentage of surfadrug that participates in the formation of the bilayer, compared to the initial amount used. It was determined by freezing 0.1 mL of purified sample for several hours, then diluting it with 10 mL of ethanol, which allows vesicular membrane rupture and solubilisation of FA. The DL% was derived using the following equation:

$$\mathbf{DL\%} = (C_f/C_{in.}) \times 100$$

Where C_f constitutes the amount of drug retained in the bilayer after dialysis and C_{in} indicates the amount of drug initially used in the formulation. Using UV spectrophotometry, the absorbances of the samples were measured at the FA wavelength of 280 nm.

***Ex-vivo* skin permeation**

Skin permeation studies were conducted using vertical Franz diffusion cells for 24 hours at 37°C on rabbit skin obtained from a local slaughterhouse. The method is the same as previously described [art lorena]. At regular intervals, up to 24 hours, the release medium was removed, replaced with an equal volume of fresh medium and analysed by UV-Vis

spectrophotometry. The replacement of the release medium is necessary to ensure the absorption conditions and the determination of the amount of permeated drug. Each experiment was conducted in triplicate.

Skin retention studies

After the permeation experiments, the amount of FA not permeated but accumulated on the skin surface after 24 hours was assessed. The active ingredient was then extracted from the skin by placing it in 10 mL of ethanol under magnetic stirring for 1 hour. Subsequently, the solutions were filtered and the amount of retained FA was assessed by UV spectrophotometry. Each experiment was conducted in triplicate.

***In vitro* release studies**

The release of the niosomal formulations was also evaluated at different pHs to assess the release behaviour under different environmental conditions. PBS pH=7.4 for the systemic tract; PBS pH=6.8 for the intestinal tract and a 0.01 M HCl solution, pH=2 for the gastric tract were used. Release was assessed over 24 hours and 2 mL of medium was taken at fixed intervals and analysed by UV spectrophotometry. The amount of FA released was evaluated in percentage terms using the equation:

$$\%\ \boldsymbol{of\ drug\ released} = \frac{\boldsymbol{C_t}}{\boldsymbol{C_0}} \times \mathbf{100}$$

Where C_0 is the initial concentration of the drug and C_t is the concentration of the drug released over time.

Results and discussions

Upon visual observation, the different FA-based niosomal formulations were yellow and opalescent in colour, indicating the actual presence of colloidal systems. Several formulations were created starting from a concentration of 4.73 x 10^{-3} M using distilled water at various pHs as the hydration medium. The vesicular systems obtained were analysed from a chemical-physical point of view and the results are reported in **Table 1**.

Table 1. Physical-chemical characterizations of niosomal system based on FA at 25°C

Formulations	FA (mg)	Hydration solvent	Size (nm)	IP	ξ potential ± DS	DL%
Nio FA pH 8,49	26	H_2O pH 8,49	308,4 nm	0,232	- 27,3 ± 0,346	27,6%
Nio FA pH 10	26	H_2O pH 10	341,0 nm	0,204	-34,8 ± 1,04	72,65%
Nio FA pH 12	26	H_2O pH 12	304,4 nm	0,266	-31,9 ± 1,26	58,01%

Among different hydration media, distilled water at pH 10 gave vesicles with encapsulation efficiency >70%, indicating the best experimental conditions to obtain these new systems. The vesicular dimensions were not modified by the hydration medium, being predominantly around 300 nm with a polydispersity index between 0.2 and 0.26 (value indicative of a homogeneous size distribution). The ξ potential instead varied slightly as the pH of the medium varied, indicating good stability for each formulation. Nio FA b appears to be the optimal formulation as it has the highest ξ potential values, being highly stable and the highest E%, indicating that a significant amount of drug constitutes the bilayer.

The TEM images (**Figure 1**) obtained for the Nio FA b formulation showed vesicles with spherical morphology, homogeneous in shape and size, with a size range between 200 and 500 nm.

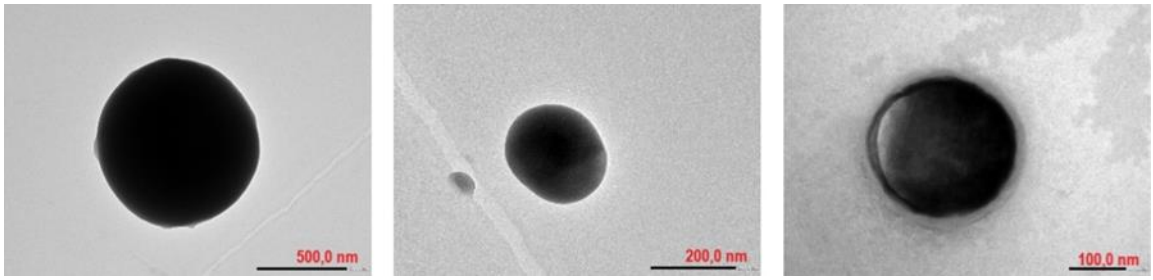

Figure 1: Microphotograpy of FA niosomal formulation

***Ex-vivo* cutaneous permeation**

To evaluate the behaviour of niosomal systems after topical administration, *ex vivo* skin permeation studies were conducted. These studies conducted using the stratum corneum of rabbit ears (which are the most comparable to human skin) allow us to evaluate the ability of colloidal systems to release the substances or drugs encapsulated within it, at a topical and transdermal level. In this case, the release profiles of the FA itself were evaluated by loading 0.3 mL of sample at 37°C (Nio FA b) into the donor compartment. **Figure 2** shows that over 24 hours, Nio FA b releases 63.36 µg/cm2 of drug, reaching a plateau phase around the eighth hour.

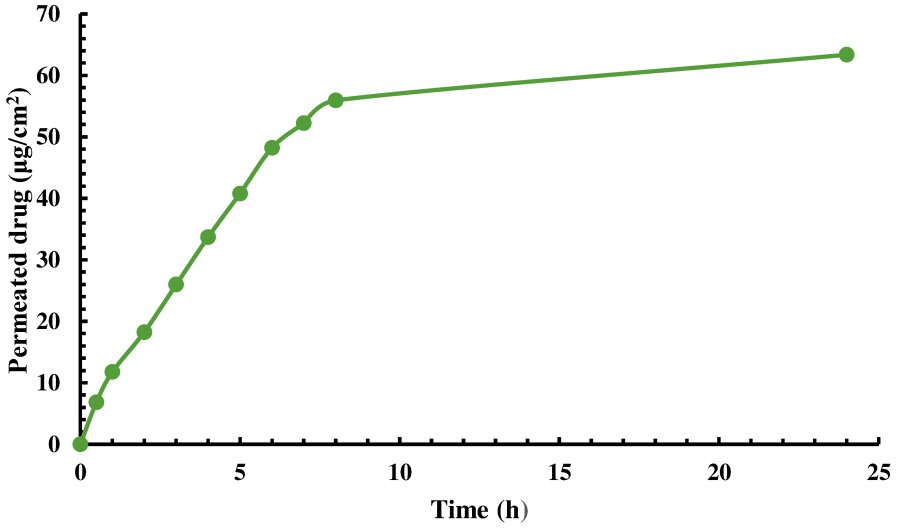

Figure 2. FA permeation through rabbit ear skin at 37°C

Typically, the value of the hydrophilic-lipophilic balance of the carrier influences the skin penetration of a drug, in fact the penetration gradually increases with the lipophilicity of the carrier, this could be due to the better interactions with the skin layers that are generated. [13]. The very structure of amphiphilic molecules alters the skin barrier [14]. The percentage of FA retained in the stratum corneum over 24 hours was also evaluated. The accumulated quantity is equal to 7.38×10^{-7} moles compared to the released quantity which is instead 1.52×10^{-7} moles.

***In vitro* release studies**

Through in vitro release studies, the possibility of proposing our niosomal systems as potential carriers to be used for the controlled release of active ingredients at a systemic level, via parenteral and gastrointestinal administration, was evaluated. The experiments were conducted using different media: PBS pH 7.4 for parenteral administration, and PBS

pH 6.8 and HCl pH 2 for gastrointestinal administration, to simulate the environments that the formulation would encounter during its systemic absorption.

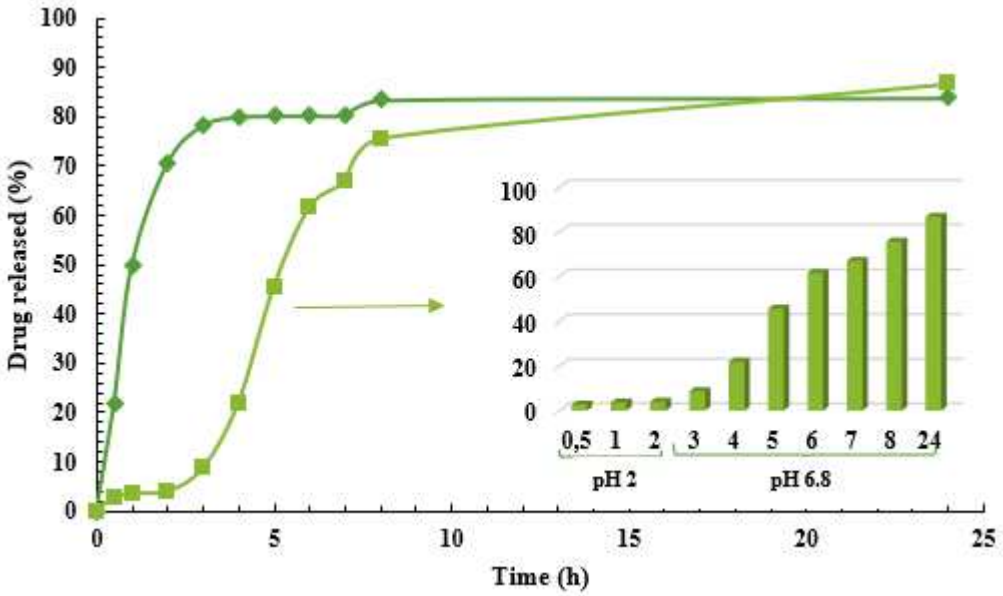

Figure 3. Diffusion release profile of Nio FA b: (♦) pH 7.4 and (■) pH 2/6.8 at 37°C

Figure 3 shows how the release trend varies depending on the release medium. In the presence of a pH 7.4 there is a more rapid release; in fact, around the fourth hour a plateaux phase is reached in which an 80% release is observed. When release is conducted in a medium that simulates the gastrointestinal tract (pH 2/6.8), a gradual release is observed over time. In an acidic environment (up to 2 hours), a considerable release of FA is not observed, but when it changes to pH 6.8 it begins to gradually release. In this case the plateaux phase is reached around the eighth hour in which approximately 80% release is reached.

Conclusions

In summary, innovative niosomal formulations based on folic acid have been developed. The innovation lies in the use of surfadrug, as using FA as a constituent of the lipid film and as a pharmaceutical molecule could improve the safety of the formulation and at the same time reduce the use of other components. FA can form small vesicles, around 300 nm, with a spherical and homogeneous shape. Permeation is slow and gradual over time, thus allowing for a delayed and controlled release. While diffusion studies at various pHs have shown that vesicles release faster under systemic conditions and more slowly under conditions simulating the gastrointestinal tract. This first study represents a first step towards the development of pharmacological systems in which FAs such as surfadrug

could allow, by conveying other pharmacologically active molecules within them, to obtain a combined or synergistic effect.

Reference

[1] Journal of Pharmacy And Experimental Medicine. Niosome: A Novel Drug Delivery System. Ms. Shubhangi V. Shekade Assistant professor, Department of pharmaceutics, Dr. D.Y. Patil Institute of Pharmaceutical Sciences and Research, Pimpri, Pune 411018. 10 May 2021

[2] Tavano, L., Mazzotta, E., & Muzzalupo, R. (2017). Nanovesicular formulations for cancer gene therapy. Current pharmaceutical design, 23(35), 5327-5335

[3] Romeo, M., Mazzotta, E., Perrotta, I. D., & Muzzalupo, R. (2022). Lidosomes: Innovative Vesicular Systems Prepared from Lidocaine Surfadrug. Pharmaceutics, 14(10), 2190.

[4] Wagner, C. (1995). Biochemical role of folate in cellar metabolism In: Folate in Health and Disease (LB Bailey ed) Marcel Dekker New York NY.

[5] Aslinia, F., Mazza, J. J., & Yale, S. H. (2006). Megaloblastic anemia and other causes of macrocytosis. Clinical medicine & research, 4(3), 236-241.

[6] Reynolds, E. H. (2014). The neurology of folic acid deficiency. Handbook of clinical neurology, 120, 927-943.

[7] MRC Vitamin Study Research Group. (1991). Prevention of neural tube defects: results of the Medical Research Council Vitamin Study. The lancet, 338(8760), 131-137.

[8] Antony, A. C. (2007). In utero physiology: role of folic acid in nutrient delivery and fetal development. The American journal of clinical nutrition, 85(2), 598S-603S.

[9] Crider, K. S., Yang, T. P., Berry, R. J., & Bailey, L. B. (2012). Folate and DNA methylation: a review of molecular mechanisms and the evidence for folate's role. Advances in nutrition, 3(1), 21-38.

[10] Off, M. K., Steindal, A. E., Porojnicu, A. C., Juzeniene, A., Vorobey, A., Johnsson, A., & Moan, J. (2005). Ultraviolet photodegradation of folic acid. Journal of Photochemistry and Photobiology B: Biology, 80(1), 47-55.

[11] Hofsäss, M. A., de Souza, J., Silva-Barcellos, N. M., Bellavinha, K. R., Abrahamsson, B., Cristofoletti, R., ... & Dressman, J. B. (2017). Biowaiver monographs for immediate-release solid oral dosage forms: Folic acid. Journal of pharmaceutical sciences, 106(12), 3421-3430.

[12] Hong, W., Guo, F., Yu, N., Ying, S., Lou, B., Wu, J., ... & Yang, G. (2021). A Novel Folic Acid Receptor-Targeted Drug Delivery System Based on Curcumin-Loaded

βCyclodextrin Nanoparticles for Cancer Treatment. Drug Design, Development and Therapy, 15, 2843.

[13] Tavano, L., Alfano, P., Muzzalupo, R., & de Cindio, B. (2011). Niosomes vs microemulsions: new carriers for topical delivery of capsaicin. Colloids and surfaces B: Biointerfaces, 87(2), 333-339.

[14] Walters, K. A., Bialik, W., & BRAIN, K. R. (1993). The effects of surfactants on penetration across the skin. International journal of cosmetic science, 15(6), 260-271.

[15] Som, I., Bhatia, K., & Yasir, M. (2012). Status of surfactants as penetration enhancers in transdermal drug delivery. Journal of pharmacy & bioallied sciences, 4(1), 2.

1.4 Antimicrobial and anesthetic niosomal formulations based on amino acid based-surfactants.

Submitted on Molecules

Introduction

Lidocaine (LID) is a local anesthetic drug widely used in clinical practice to reduce or eliminate pain, both for surgery and for the management of other acute or chronic pain. However, lidocaine, being a lipophilic compound, has poor permeation through the skin, which constitutes the main obstacle to its application in the field of transdermal administration [1, 2]. Nanotechnology has led to the production of nanomaterials as carriers of active substances that amplify their efficacy. Indeed, nanoscale engineering can overcome the limitations associated with traditional drug delivery methods. A good drug delivery system (DDS) acts as a protective shield for the payload, preventing premature decomposition in the biological environment while improving bioavailability, duration of blood circulation, cellular absorption, and therapeutic activity over longer periods. [3, 4]. Recently our group has prepared lidosomes: innovative vesicular systems prepared with lidocaine. It was found to be able to self-associate forming nanosized vesicle structures with good stability. Therefore, lidocaine can be defined as a "surfadrug", i.e. a pharmacologically active molecule with amphiphilic properties. Chemically, surfadrugs contain one or more flexible, hydrophobic aromatic nuclei, to which an ester group or a charge-carrying N atom is directly attached, or which include a pyridine-like N atom; and it is precisely the flexibility of the aromatic ring that makes these drugs resemble typical surfactants in their associative behaviour [5]. It has been observed that the use of these vesicular aggregates improves skin permeation and drug deposition in the skin of lidocaine but can act as a capsaicin transporter [6]. Capsaicin (CA) is another analgesic and anti-inflammatory drug. This compound affects the nerve cells in the skin responsible for pain. Today, infections produced by multidrug-resistant bacteria are one of the top three dangers to world health [7]. Then, the incorporation of antimicrobial compounds to the new therapeutic vesicular systems can reduce the spread of infectious illnesses. In this context, cationic amino acid-based surfactants represent promising new green and sustainable antimicrobial materials. These are structurally heterogeneous amphiphilic compounds with an amino acid hydrophilic group and an aliphatic chain as the lipophilic moiety [8]. Due to their amphiphilic nature, positive charge, and high surface activity, these cationic amphiphiles, like QACs (Quaternary

Ammonium Compounds), are expected to act via perturbation of the bacterial membrane. This mode of action hampers the development of resistant bacteria. Moreover, in contrast with QACs, they can be designed to be biodegradable in the environment and consequently, they show lower ecotoxicity.

Newly, our group has reported the synthesis of new cationic amino-acid-based surfactants based on tryptophan and phenylalanine. The synthetic approach used to prepare these compounds fits some of the green chemistry requirements: utilization of renewable starting materials and a synthetic procedure consisting of two simple chemical reactions that do not require the use of organic solvent nor protecting amino acids. The cationic charge of these compounds was situated on a protonated amine group and, consequently, their cationic character depended on the pH. It was found that these new surfactants formed unilamellar vesicles with DPPC mixtures [9]. Surfactants with C_{12}-C_{14} alkyl chain exhibited good antimicrobial activity, moreover, vesicles containing 60-80% of surfactants maintained their antimicrobial effectivity. Considering these findings, in this work, we have prepared similar phenylalanine cationic surfactants, but in this case, the cationic charge is situated in a trimethylated amine group, then the charge does not depend on the pH (**Figure 1**). We have characterized these new surfactants, and we have prepared niosomes containing lidocaine, capsaicin and the cationic surfactant in order to obtain colloidal formulation with both anesthetic and antimicrobial properties. The physical characteristics of the new formulations, vesicle size and size distribution, zeta potential, entrapment efficiency, and stability were determined. The antimicrobial effectivity of both the pure surfactants and their niosomal formulations was determined. Finally, the biocompatibility of these new formulations have been studied.

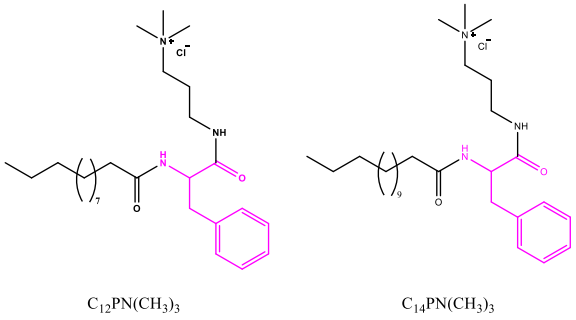

$C_{12}PN(CH_3)_3$ $C_{14}PN(CH_3)_3$

Figure 1. Chemical structure of new antimicrobial cationic surfactants based on phenylalanine. (n = 12 $C_{12}PHN(CH_3)_3Cl$ and n = 14 $C_{14}PHN(CH_3)_3$ Cl.

Materials and Metods

Lidocaine (LID), Capsaicin (CA), and Dipalmitoylphosphatidylcholine (DPPC), were purchased by Sigma-Aldrich (Milan, Italy, purity 99%), $C_{14}PNH(CH_3)_3$ Cl^- (P_{14}) and $C_{12}PHN(CH_3)_3$ CL^- (P_{12}) were synthesized in Department of Surfactants and Nanobiotechnology (IQAC-CSIC Barcelona). The organic solvents were supplied by Sigma-Aldrich (Milan, Italy). Muller-Hinton (MH) broth and agar were obtained from Difco Laboratories (Franklin Lakes, NJ, USA). Their purity was checked by High Performance Liquid Chromatography with a Waters HPLC system equipped with a Kromasil 100 C8 5 µm 25 × 2.12 column.

2.1. Synthesis of the phenylalanine based-surfactants

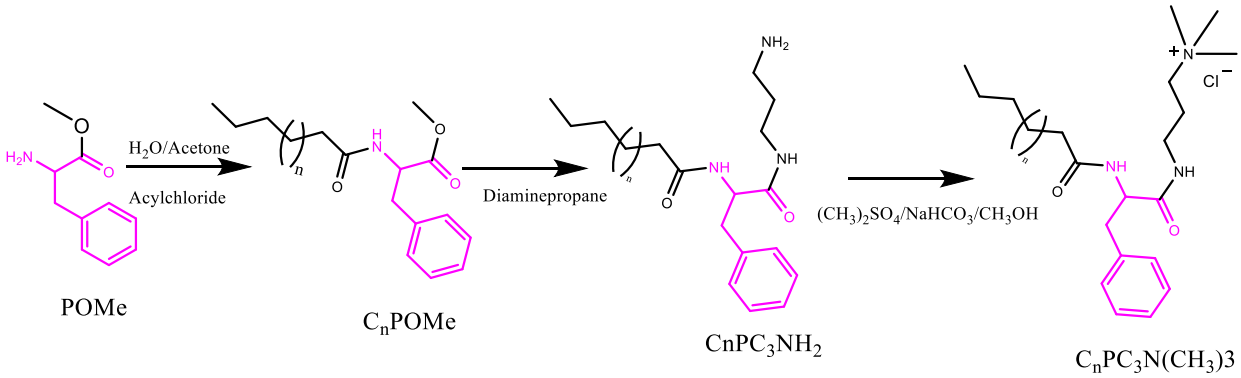

Figure 2. Synthetic pathway to obtain the phenylalanine derivatives.

The phenylalanine based-surfactants used in this work have been prepared following the synthetic procedure showed in figure 2. The $C_nPC_3NH_2$ have been synthesized using the process outline in our previous work [9]. In brief, the free amine group of the phenylalanine methyl ester was acylated with the dodecyl or tetradecyl acid chloride, then the C_nPOMe compounds were dissolved in diaminopropane at 60ºC to obtain the corresponding $C_nPC_3NH_2$. Then, 1 g of the $C_nPC_3NH_2$ was reacted with methyl iodide (CH_3I) in a DMF medium to yield the target compounds $CnPC_3NC_3I$. The reaction mixture was kept at 60°C for the required duration, with progress monitored using HPLC. After completing the reaction, excess CH_3I was removed using a rotary evaporator, and the sample was purified via preparative HPLC. The identification of the target surfactants was accomplished through HPLC, MS, and NMR analyses (refer to the Electronic Supplementary Information for details).

2.2 HPLC analysis

The reaction progress as well as the purity of all prepared molecules were monitored by HPLC (Merck-Hitachi D-2500) using a UV–vis detector (L- 4250 at 215 nm) and a Lichrospher 100 CN. The gradient elution profile used went from 25 %B to 95 %B in 24 min. Aqueous phase A was 0.1 % (vol/vol) trifluoro acetic acid (TFA) in H_2O and organic phase B was 0.085 % (v/v) of TFA in H_2O/CH_3CN (1:4).

2.3 NMR experiments

Sample solutions were prepared in deuterated methanol (20 mg/0.8 mL) using 5 mm NMR tubes.^{1}H NMR and ^{13}C NMR analyses were recorded on a Varian 400MHz spectrometer. All experiments were performed in an indirect broadband probe. Data were processed with the MestReNova (Mestrelab Research 14.1) software.

2.4 Mass spectroscopy

Surfactant solutions (in the 1×10^{-4} to 1×10^{-6} M range) were prepared in methanol. High-resolution mass spectra (HRMS) were performed on Acquity UPLC System and an LCT PremierTM XE Benchtop orthogonal acceleration time-of-flight (Waters Corporation, Milford, MA) equipped with an electrospray ionization source. All data were processed and displayed using MestReNova (Mestrelab Research 14.1) software.

2.5 Niosomes preparation

Niosomes were prepared by a thin layer evaporation. The lipid film was then hydrated with 10 mL of distilled water (pH 5.5) at 60 ◦C for 30 min. Subsequently, the vesicles were purified by exhaustive dialysis for 4 h in distilled water using Visking tubing (Spectra/Por®, cut-off 12–14 kDa), and manipulated before use according to Fenton's method [10]. After purification, formulations were stored at room temperature until the subsequent experiments. Details on vesicle compositions are reported in **Table 1**.

Table 1: Composition of niosomal formulations.

FORMULATIONS ACRONYMS	LD (mg)	DPPC (mg)	$C_{14}PC_3N(CH_3)_3$ (mg)	$C_{12}PC_3N(CH_3)_3$ (mg)	CA (mg)
L	30	-	-	-	-
L/C (9:1)	40.5	-	-	-	4.5
L/D (8:2)	24	6	-	-	-
L/C/P_{12} (7:1:2)	31.5	-	9	-	4.5
L/D/P_{12} (6:2:2)	18	6	-	6	-
L/P_{14} (9:1)	27	-	3	-	-
L/C/P_{14} (8:1:1)	24	-	3	-	3
L/C/P_{14} (7:1:2)	21	-	6	-	3
L/D/P_{14} (6:2:2)	18	6	6	-	-
L/C/D/P_{14} (6:1:2:1)	27	9	4.5	-	4.5
L/C/D/P_{14} (5:1:2:2)	22.5	9	9	-	4.5
L/C/D/P_{14} (2:1:5:2)	9	22.5	9	-	4.5

2.6 Physical-chemical characterization of vesicles

The diameter, size distribution, and ζ-potential were determined by Zetasizer ZS Malvern Instruments Ltd. (Malvern, U.K.) at 25 ± 0.1 °C. After the samples were purified by dialysis, all analyses were conducted in triplicate and expressed as mean ± standard deviation. The morphology of niosomes was determined by TEM (Transmission electron microscopy) with TEM ZEISS EM 10. Two drops of niosomal preparations placed on a copper grid with nitrocellulose and left to dry at room temperature before the microscopy observation.

2.7 Small-Angle X-ray Scattering (SAXS)

SAXS measurements were carried out using a S3-MICRO (Hecus X-ray systems GMBH Graz, Austria) coupled to a GENIX-Fox 3D X-ray source (Xenocs, Grenoble), which provides a detector focussed x-ray beam with λ = 0.1542 nm Cu K α -line with more than 97% purity and less than 0.3% K_β . Transmitted scattering was detected using a PSD 50 Hecus. Temperature was controlled by means of a Peltier TCCS-3 Hecus. The samples and background solutions were inserted in a flow-through glass capillary 1 mm diameter with 10 μm wall thickness. The SAXS scattering curves are shown as a function of the scattering vector modulus:

$$q = \frac{4\pi}{\lambda}\sin(\frac{\theta}{2}) \qquad (1)$$

where θ is the scattering angle. The q values with this setup ranged from 0.1 nm^{-1} to 6.0 nm^{-1}. The system scattering vector was calibrated by measuring a standard silver behenate sample. Because of the use of a detector focussed small beam (300 x 400 μm full width at half maximum) the scattering curves are mainly smeared by the detector width and detector depth. This smearing mainly produces a widening of the peaks without noticeable effect on the peak position in the small angle regime. The scattering curves have been background subtracted taking into account the concentration of solvent and solutes in the samples. The instrumentally smeared experimental SAXS curves were fitted to numerically smeared models for beam size, detector width and detector depth effects. A least squares routine based on the Levenberg-Marquardt scheme was used. A model of the scattering by liposomes was used with is based on the description of the bilayer electronic density profile using a Gaussian for each polar head and a Gaussian for the description of the methyl dip at the centre of the bilayer and an error function to describe the methylene contribution [11].

2.8 Determination of the Amount of LID and Efficiency Encapsulation of CA and PH in Vesicular Systems

The amount of LID retained in the niosomal formulation was carried out after sample purification by exhaustive dialysis. A total of 1 mL of purified and 1 mL of non-purified LD were diluted in 100 mL of methanol, and the LID concentration was measured by HPLC (Merck-Hitachi D-2500) using a UV–vis detector (L- 4250 at 215 nm) and a Lichrospher RP-18 (5 μm) LiChroCART® 250-4. The gradient elution profile used went from 25 %B to 95 %B in 24 min. Aqueous phase A was 0.1% (vol/vol) trifluoro acetic acid (TFA) in H_2O, and organic phase B was 0.085% (*v*/*v*) of TFA in H_2O/CH_3CN (1:4). The wavelength used for analysis was 280 nm for CA, 210 nm for LID and 215 for P_n derivatives. The LID, CA and P_n content retained in the formation of vesicle structure (E%) was calculated according to the following Equation:

$$E\ \% = C_R / C_I \times 100 \quad (2)$$

where C_R is the initial component concentration measured after purification process and C_I is the concentration used for the preparation of vesicles.

All experiments were conducted in triplicate and expressed as mean ± standard deviation (SD).

2.9 Stability Evaluation

To determine the stability of vesicles, the formulations were stored at room temperature (25 ± 2 °C) and evaluated at predetermined time intervals (0 and 30 days) in terms of visual inspection, particle size, PI, E% and ζ-potential.

2.10 Biocompatibility of the formulation: *ex-vivo* Hemolytic activity

The determination of hemolytic activity was carried out on fresh rate blood taken and used on the same day of the experiments. Rabbit blood was supplied by the Animal Experimentation Unit (Instituto de Química Avanzada de Cataluña—IQAC). We followed an adaptation of the method described by Pape et al. (1987) [12]. The red blood cells were washed three times in a phosphate buffer solution (PBS pH 7.4). The cells were then suspended at a cell density of $8x10^9$ cells per mL. A series of different volumes of niosomal solution (3760 µg/mL), ranging from 10 to 130 µL, were placed in Eppendorf, 25 µL of erythrocyte suspension and phosphate buffered saline were added to Eppendorf to a total volume of 1mL. Samples were incubated at room temperature while shaking for 10 min. Following the Eppendorf were centrifuged for 5 min at 10.000 rpm. The percentage of hemolytic activity was determined by comparing the absorbance at (575 nm) of the supernatant of the samples with that of the control hemolyzed with distilled water. Each analysis was performed in triplicate.

The therapeutic index (TI) in this context is calculated as the ratio of the concentration at which 50% of the cells are affected (HC_{50}) to the minimum inhibitory concentration (MIC) for each surfactant formulation against both microorganisms and eukaryotic cells. The equation for calculating the therapeutic index (TI) is:

$$TI = \frac{HC_{50}}{MIC} \quad (3)$$

This index provides a quantitative measure of the selectivity of the surfactant formulations against microorganisms relative to eukaryotic cells. A higher TI suggests greater selectivity and lower potential toxicity to eukaryotic cells.

2.11 *In vitro* antimicrobial activity

Antimicrobial tests were conducted using bacteria stored in our laboratory. The microorganisms were *Bacillus subtilis* (BS) ATCC 6633, *Staphylococcus epidermis* (SE) ATCC 12228, *Staphylococcus aureus* (SA) ATCC 29213, *Listeria monocytogenes* (LM) ATCC 15313, *Enterococcus faecalis* (EF) ATCC 29212, *Escherichia coli* (EC) ATCC 25922, *Acinetobacter baumanii* (AB) ATCC 19606, *Klebsiella aerogenes* (KA) ATCC

13048. The antimicrobial activity was determined in vitro to obtain the MIC value, defined as the lowest concentration of antimicrobial agents that inhibits the development of visible growth after 24 h of incubation at 37°C [13]. The MIC of our niosomes was determined using a broth microdiluition assay [14]. Serial diluition of niosomes in Mueller–Hinton broth (MHB) was dispensed, and 200 µL of these were in the corresponding wells of a 96-well polypropylene microtiter plate. Then, 10 µL of an initial culture of each bacterial strain was added to obtain a final inoculum of about 5×10^{-5} colony-forming units (CFU) per mL. The nutrient broth medium without the compound served as a growth control. The development of turbidity in an inoculated medium is a function of growth and reflects an increase in cell mass and number. To confirm the MIC observation after 24h, 20 µL of 0.015% w/v resazurin was added to each well and allowed to react for about 2 h for bacteria, al 37°C. After the incubation period, the bacterial growth indicator, which changed from blue to pink, confirmed the MIC value. To obtain the MBC, the antimicrobial concentration corresponding to at least 3-log reductions of viable cells, a 10 µL aliquot of the MIC well, and the two concentrations immediately above were seeded on MH agar and incubated for 24 h, al 37°C. MBC was determined as the lowest concentration at which no colonies were observed on the agar plates.

2.12 Statistical analysis of data

Results are expressed as the mean ± standard deviation (SD) or standard error of the mean (SEM). Data were analysed statistically by Student's t-test was used to compare the samples and *p*-values of ≤ 0.05 were considered statistically significant.

3. Results and discussion

Cationic surfactants based on quaternary ammonium groups, such as CTAB or HTAB, have been widely used as antimicrobial agents in hospitals and food industries. Nowadays, the use of these compounds is questioned because they are prepared using petrochemical feedstock and, in addition, these surfactants exhibit very low biodegradation levels in the environment [15]. In this context, there is a need to develop new antimicrobial surfactants through environmentally friendly approaches to reduce their carbon footprint. Cationic Amino acid-based surfactants may be an interesting alternative, given that they show good antimicrobial activity and can be designed to be rapidly biodegradable compounds [16]. From an economic and environmental viewpoint, single-chain surfactants with one amino-acid and one polar head, are desirable because

they can be prepared without using complicated procedures that require the use of huge quantities of organic solvents. With these considerations in mind, in this work we prepared two cationic single-chain amino acid-based surfactants. The synthesis was carried out in 3 steps: first, the free amine group of the phenylalanine methyl ester was acylated with the corresponding fatty acid chloride, second, the obtained intermediates were treated with diamine propane to obtain an amide and finally, these intermediates were reacted with CH_3I to get the target trimethylated derivative (Figure 3).

This synthetic procedure is straightforward and fits some of the green chemistry requirements for organic synthesis: use of renewable starting materials such as fatty acids and amino acids, a synthetic method consisting of three simple chemical reactions that do not require the use of protective amino acids and, moreover, two of them neither require organic solvents. Furthermore, the hydrophobic alkyl chain is linked to the α-amine group of the phenylalanine through amide bonds to ensure high biodegradability and good chemical stability. The purity of the synthesized compounds was greater than 96%, as assessed by, HPLC, ^{1}H-NMR, ^{13}C-NMR, HPLC-MS.

3.1 Physical-chemical characterization of niosomes

The incorporation of different biologically active compounds can create multifunctional nanocarriers with promising potential applications in biomedicine. Here we have created for the first time niosomes containing two different anesthetic drugs (lidocaine and capsaicin) and an antimicrobial surfactant. In recent years, great interest has been in amino acid-based surfactants, as they are biocompatible, biodegradable, and environmentally friendly compared to conventional surfactants. [17, 18, 19]. Given the different types of amino acids and their different nature, it is possible to design different amphiphilic structures with specific properties. [16]. Due to the vesicular structure of these aggregates, they can be considered drug delivery systems. To modulate the physico-chemical and biological properties of these vesicular formulations with different percentages of every component were prepared. The vesicles were always prepared using thin layer evaporation and their physico-chemical properties were evaluated by a Z-sizer instrument in terms of size distribution, polydispersion index (PI), ζ–potential and E%, parameters that may influence their biological activity (Table 2). Initially, vesicles composed of LID, $C_{14}PC_3N(CH_3)_3$ or $C_{12}PC_3N(CH_3)_3$ carriers of the CA drug were formulated. Additionally, DPPC was also incorporated to study the effect of this phospholipid on the niosome properties.

Table 2. Physico-chemical characterization of vesicular systems prepared at different concentrations in term of Hydrodynamic diameter (SIZE), polydispersion index (P.I), ζ−potential (PZ), percentage encapsulation of lidocaine (E LID%), percentage encapsulation of capsaicin (E%CA) and percentage encapsulation of cationic surfactants (E%P_n) at 25 °C.

FORMULATIONS	SIZE nm	PI	PZ	E LID%	E% P_n	E% CA
L	348.25 ± 93.7	0.381	-16.8±4.59	47.64±1.92	-	-
L/C (9:1)	294.9 ± 63.37	0.393	-9.6±1.39	28.73±5.78	-	56.13±20.3
L/D (8:2)	675.6± 31.56	0.602	-5.62± 1.54	42.30±2.65	-	-
L/C/P_{12} (7:1:2)	279.6 ± 77.45	0.446	+11.6±0.69	29.98±2.30	67.25±0.56	40.23±3.56
L/D/P_{12} (6:2:2)	194.3±15.77	0.301	+0.406±3.78	27.92±1.45	51.87±0.84	-
L/P_{14} (9:1)	289.3 ± 46.5	0.284	+15.5 ± 0.88	26.94±3.65	68.49±2.47	-
L/C/P_{14} (7:1:2)	309.6 ± 104.79	0.349	+15.7±0.42	31.30±0.31	84.18±1.28	64.34±1.52
L/D/P_{14} (6:2:2)	176.9±8.21	0.611	+15.2±1.24	23.75±2.72	86.87±2.43	-
L/C/D/P_{14}(6:1:2:1)	302.3 ± 60.52	0.564	+21±2.54	33.34±0.87	79.66±2.11	70.07±10.2
L/C/D/P_{14} (5:1:2:2)	258.6 ± 23.33	0.394	+19.6±10.25	42.86±3.87	81.49±2.48	74.69±1.27
L/C/D/P_{14} (2:1:5:2)	260.3 ± 4.10	0.583	+22.6±1.34	40.52±1.34	85.07±0.14	65.56±0.74

The L and L/C niosomes showed medium size (294-348 nm) with similar IP and negative ζ-potential values. These results agree with that observed recently by our group [6]. The incorporation of the DPPC into the LID niosomes gave rise to large aggregates with higher PI (polydispersion index). Notice that size of niosomes or vesicles is very crucial in the transdermal drug delivery systems. Ideally, the size must be below 300 nm to be able to pass through the deepest skin layer.

First, we will focus on the two niosome formulations containing the $C_{12}PC_3N(CH_3)_3$. The L/C/P_{12} niosomes had a medium size (279 nm) with a positive ζ-potential due to the presence of the positively charged surfactant. The L/D/P_{12} exhibited lower diameter size with low positive ζ-potential values, in this case, the $C_{12}PC_3N(CH_3)_3$ derivative did not offset the negative character of the LID.

For the $C_{14}PC_3N(CH_3)_3$ derivatives 7 different formulations were prepared: one with LID, two with LID and CA (L/C), another with LID and DPPC (L/D) and 3 with LID, CA and DPPC (L/C/D). The physico-chemical properties of the L/C/P_{14} and L/D/P_{14} were similar to those observed for the analogous $C_{12}PC_3N(CH_3)_3$ formulations, the only difference being that the $C_{14}PC_3N(CH_3)_3$ based-niosomes had higher positive ζ-potential values. The formulations containing all components (L/C/D/P_{14}) displayed comparable sizes (between 260-302 nm) with PI between 0.4-0.5 and large positive ζ-potential values (19.6-22.6). These parameters indicated a low degree of particle size heterogeneity and sufficiently high particle positive charges for electrostatic stabilization of the niosomes. All formulated niosomes were subjected to E% to assess the amount of CA and cationic surfactant encapsulated in the aggregates. In general, a high percentage of encapsulation

was obtained. It can be observed that the E% of CA is better for the niosomes containing the $C_{14}PC_3N(CH_3)_3$ surfactant. Moreover, this percentage increases as the Lidocaine% decreases and the DPPC% and $C_{14}PC_3N(CH_3)_3$% increases. Formulations containing the four components result in better percentages of lidocaine or capsaicin retained in the vesicles structures. It was also observed that the percentage of encapsulation of the P_{14} derivatives increased as the percentage of DPPC augmented.

The morphology of some of these formulations (L/C/P_{14}, L/C/P_{12} and L/C/D/P_{14} (5:1:2:2) and L/C/D/P_{14} (2:1:5:2) was subsequently analysed by transmission electron microscopy. Figures 4 and 5 show the photomicrographs of these niosomal formulations. The L/C formulation contains spherical vesicles (Figure 4A). Morphological analysis of Lidocaine formulations also showed that this drug forms spherical vesicles that are homogeneous in shape and size [6]. The incorporation of DPPC into the L/C formulation (Figure 4B) did not change the morphology of the aggregates. Finally, it was observed that the formulation containing all components (L/C/D/P_{14}) also showed spherical vesicles homogeneous in shape and size. Figure 5 shows the images obtained for the P_{12} derivatives. The vesicles also were spherical in shape.

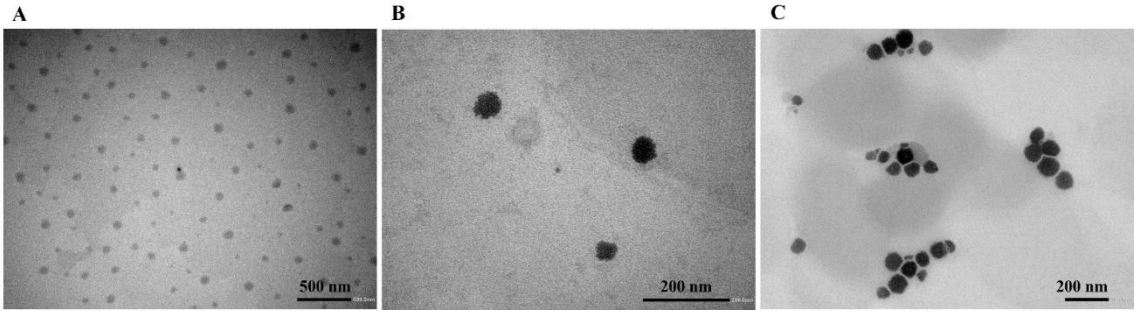

Figure 4. Typical TEM photomicrograph of lidosomes: (A) L/C/P_{14} (7:1:2) (B) L/C/D/P_{14} (5:1:2:2), and (C) L/C/D/P_{14} (2:1:5:2) formulations. Bar is 500 nm for A, and 200 nm for B and C.

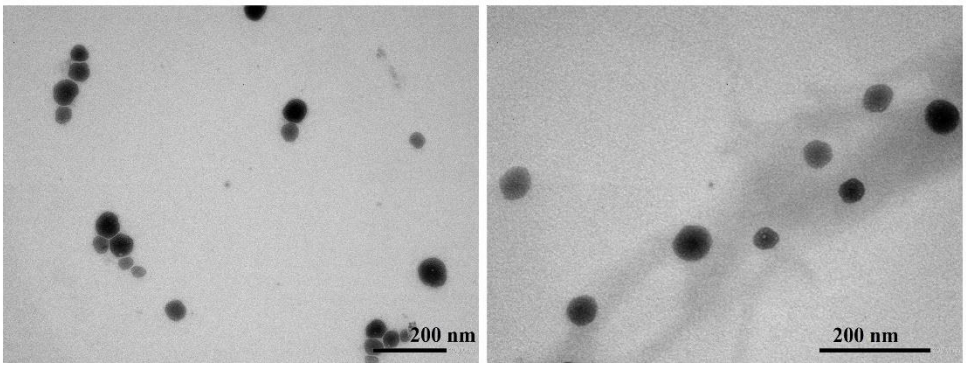

Figure 5. Typical TEM photomicrograph of lidosomes L/C/P_{12} (7:1:2) formulation. Bar is 200 nm.

3.2. Stability Evaluation

The potential use of vesicle formulations is related to their stability at different storage temperatures. The stability of these niosomal formulations was evaluated by determining average vesicle size, size distribution, and entrapment efficiency over one month of storage at 4ºC. The results, depicted in Table 3, showed that all, in general, these formulations maintained similar dimensions to the starting size. It was also observed that, for almost all preparations, the percentage of lidocaine, capsaicin, and cationic surfactant entrapped in the aggregates remains stable. However, the percentage of the E% of the P_{12} derivatives decreased significantly after one month, this behaviour can be ascribed to the lower hydrophobic character of these compounds compared with the P_{14}. It was also observed that the initial E% of this surfactant was lower than that obtained with P_{14}, it is expected that P_{12}, due to its lower alkyl chain, results in weaker hydrophobic interactions with the other components of the niosomes bilayer. For formulations without DPPC in the lipid film, vesicles polydispersion increases with time, while those containing DPPC maintain the initial values.

Table 3. Stability evaluation of LD formulations stored at 4 ◦C, expressed in diameter, P.I., ζ−potential, E% at 25°C. Data reported as mean of three independent experiments ± SD.

FORMULATIONS	TIME	SIZE	PI	PZ	E LID%	E% Pn	E% CA
L/C	0	294.9	0.393	-9.60	28.73	-	56.13
	30	1761	0.508	-6.65	36.84	-	31.32
L/C/P_{12}	0	279.6	0.446	+11.6	29	67.25	40.23
	30	183.6	0.505	+6.19	33.55	18.72	74.29
L/C/P_{14}	0	309.6	0.349	+15.7	31.30	84.18	64.34
	30	275.9	0.447	+20.6	-	-	-
L/D/P_{14}	0	176.9	0.611	+15.2	23.75	86.87	-
	30	271.5	0.430	+14.0	-	-	-
L/C/D/P_{14} (6:1:2:1)	0	302.3	0.564	+21.0	33.34	79.66	70.07
	30	122.3	0.393	+25.1	35.53	82.55	67.16
L/C/D/P_{14} (5:1:2:2)	0	258.6	0.394	+19.6	42.86	81.49	74.69
	30	162.6	0.444	+19.0	44.22	87.93	75.54
L/C/D/P_{14} (2:1:5:2)	0	260.3	0.583	+22.6	40.52	85.07	65.56
	30	102.5	0.520	+22.2	39.57	84.97	66.68

3.3 Small-Angle X-ray Scattering (SAXS)

The SAXS spectra have been scaled in absolute intensity and the water spectra subtracted. The spectra have been fitted to bilayer models consisting of two symmetric Gaussian with excess electron density representing the polar heads and a central slab with defect electron density representing hydrocarbon density [11].

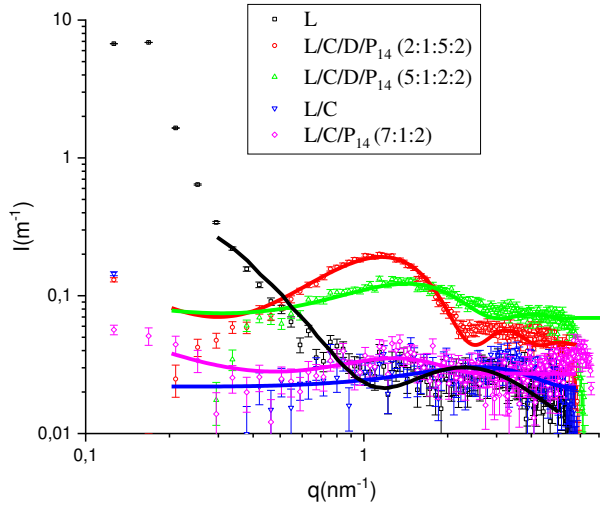

Figure 6. SAXS scattered intensity as a function of dispersion vector modulus q for all the analysed samples. The lines correspond to the best fit of bilayer models.

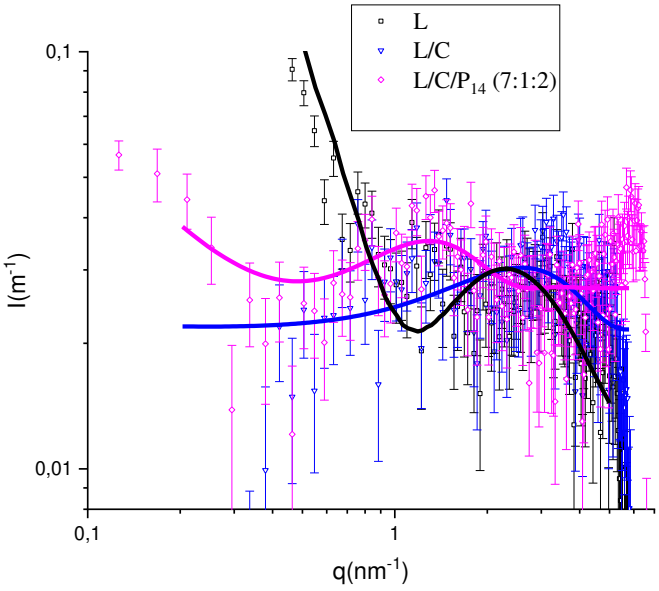

Figure 7. A zoomed-in view of SAXS scattered intensity as a function of dispersion vector modulus q for L, L/C and L/C/P_{14} 7:1:2 removed DDPC samples.

Both samples containing DPPC showed the typical band corresponding to phospholipid bilayers (with the maximum around 0.12 nm^{-1} and 0.15 nm^{-1} for L/C/D/P_{14} (2:1:5:2) and L/C/D/P_{14} (5:1:2:2) respectively, more clearly the sample with higher DPPC content. The

bilayer corresponding to the sample richer in DPPC [9] show parameter values closer to that of pure DPPC and better fitting result that the lower content one. This is expected since we can consider the bilayer as being DPPC with the introduction of some perturbation due to the additives.

The other three samples showed much lower scattered intensities and the maxima are displaced to larger q values (therefore corresponding to smaller features), as it can be appreciated in the enlarged view of these three samples (Figure 7). If we calculate the volume fraction of hydrocarbon-like moieties of the different samples, we can observe that the volume fraction of samples L/C/D/P_{14} (2:1:5:2) and L/C/D/P_{14} (5:1:2:2) are $1.6x10^{-3}$ and $1.1x10^{-3}$ respectively. While the Lidocaine sample (L) corresponds to $0.84x10^{-3}$, $0.69x10^{-3}$ for L/C/P_{14} (7:1:2) and $0.45x10^{-3}$ for L/C. In this case, the SAXS scattering is much lower and with low signal/noise ratios. Nevertheless, the sample L/C/P_{14} 7:1:2 seems to contain some significant information with a band similar to that of the two DPPC containing samples. One reason of this behaviour can be found in the reduced hydrophobic volume of both Lidocaine and Capsaicin (0.223 and 0.299 nm^3 respectively) compared to that of DDPC (0.866 nm^3) and P_{14} (0.379 nm^3). This is also congruent with the sizes fitted for bilayers, the two samples not containing DPPC or P_{14} present small bilayer thicknesses (both well below 1 nm).

We have restricted the fits to this simplified model (no depression in the center of the double layer) because of the large relative error in the measure, due to the low concentrations used. To further simplify, we have fixed the hydrophobic density to that corresponding to liquid hydrocarbon (-39 e/nm^3). The meaning of the parameters of the model are shown in figure 9 and the fitted values are shown in table 4.

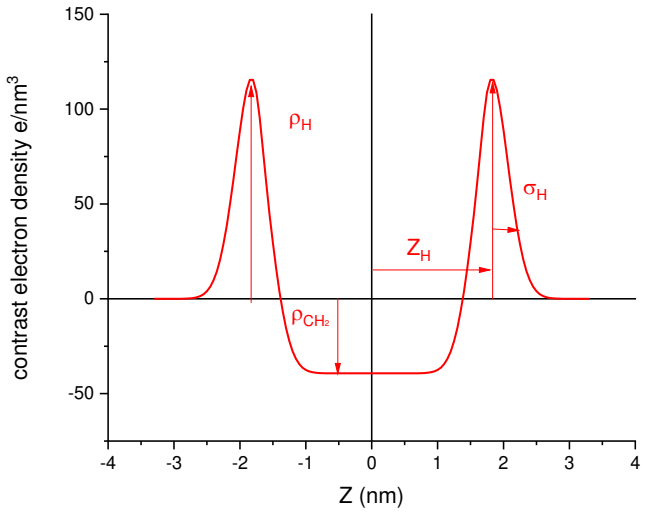

Figure 8. Gaussian based bilayer profile fitted for all the simples except for Lidocaine. In Black the bilayer profile fitted for lidocaine

Table 4. Parameters of the fits of the scattering profiles shown in figure1' The meaning of the parameters are given in Figure 6 for the Gaussian model

	L	**L/C/D/P_{14} (2:1:5:2)**	**L/C/D/P_{14} (5:1:2:2)**	**L/C**	**L/C/P_{14} (7:1:2)**
χ	3.5	1.5	1.7	1.5	1.2
σ_H	0.7±0.15	0.46±0.10	0.33±0.10	0.25±0.10	0.62±0.15
ρ_H	36±10	111±10	118±10	40±10	65±10
Z_H	0.60±0.15	1.77±0.10	1.44±0.10	0.51±0.10	1.3±0.2

The fitting of lidocaine sample to bilayers is in contrast to the findings of Shirota et al. who determined from SAXS the formation of small micelles of lidocaine hydrochloride. In their experiment on lidocaine hydrochloride they find a band present around 8 nm^{-1}, in a q range not present in our experiments However, the size of the micelles, as described by Shirota et al. [20] is far too small. They determine a hydrocarbon core radius of the micelles of just 0.3 nm which is not enough even to accommodate a single hydrophobic moiety of lidocaine. Given the high level of noise, from the point of view of the SAXS technique, the two samples containing only lidocaine (L) and lidocaine with capsaicin (L/C), are only tentatively fitted to the bilayer model. Other models would provide similar goodness of fit. What can be stated is that the structures formed are smaller in comparison with the ones in the presence of DPPC.

According to the literature, LIDHCl forms small micelles in water (Shirota et al.) [20]. At the concentrations used in the experiments here, up to 1.5 mg/mL, that is 6.3 mM, is

very well below the CMC of the ionized species (around 170 mM according to literature Efthymiu et al [21]). Using the neutral form at very low concentrations, the water acidity (more if we consider the spontaneous solubilization of CO_2) plays a role, therefore, using the neutral form at low concentrations is equivalent to having a significant amount of LID in the protonated form. In this situation, there are not enough charges in the system to form micelles but there are enough charges to stabilize vesicles. The fitting suggests that a plausible model for the observed scattering is that of vesicles with a three-slab electronic density perpendicular to the bilayer and with some polydispersity of the polar head width. However, the polydispersity of the hydrophobic slab also produced plausible scattering profiles. The noise does not allow to precise if using one or other polydispersity parameter is better, however, the electronic density distribution and overall intensity favours the polar head polydispersity.

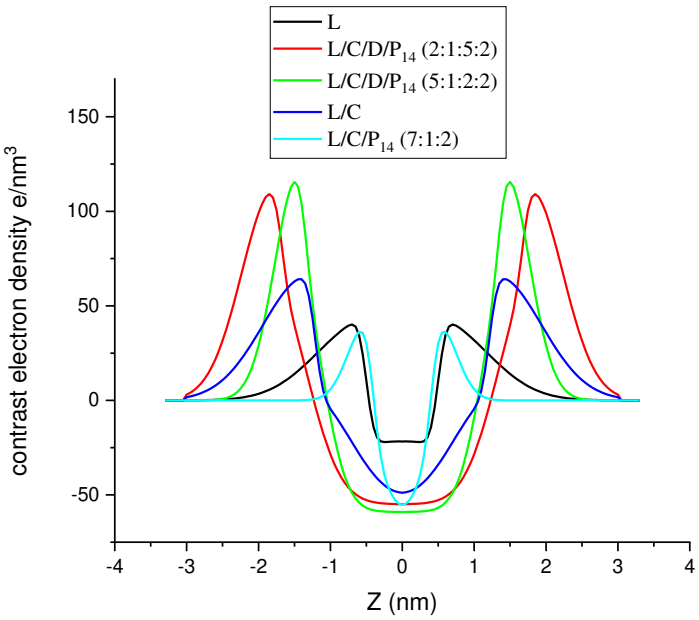

Figure 9. Electronic density profiles obtained from the fitting of the different samples

3.4 Antimicrobial activity

The growing emergence of bacterial resistance requires the development of antimicrobial systems with new modes of action that hamper the growth of resistant pathogens. Because of that, in the last years, much effort has been focused on the development of innovative, safe, and efficient antimicrobial systems. In this work, we developed new amino acid-based surfactants that have been incorporated in lidocaine-based niosomes to obtain a new anesthetic system with antibacterial activity. The antibacterial activity was tested

against some Gram-positive (Bacillus subtilis, Staphylococcus epidermidis, Staphylococcus aureus, Listeria monocytogenes, Enterococcus faecalis) and gram-negative representative bacteria strains (Escherichia coli, Acinobacter baumannii, and Klebsiella aerogenes). The obtained MIC values (concentration required to totally inhibit bacterial growth) as well as the MBC values (concentration of compounds required to kill bacteria) were determined for the pure surfactants and their niosomal formulations.

Table 5. MIC/MBC values of the pure phenylalanine-based surfactants

	$C_{12}PC_3N(CH_3)_3$ MIC (MBC) (µM)	**$C_{14}PC_3N(CH_3)_3$ MIC (MBC) (µM)**	**BAC (µM)**
Gram-positive			
BS	62 (62)	16 (16)	16
SE	32 (64)	8 (64)	16
SA	32 (128)	8 (16)	16
LM	125 (250)	16 (32)	62
EF	64 (64)	16 (16)	8
Gram-negative			
EC	125 (500)	125 (125)	62
AB	250 (250)	32 (125)	62
KA	>500 (>500)	250 (250)	62

Table 5 contains the MIC values corresponding to the pure compounds.

These two surfactants show antibacterial activity against a wide range of bacteria, the P_{14} derivatives is effective against all the microorganisms tested and P_{12} is active in 7 of the 8 bacteria assayed. It was reported that the antimicrobial activity of the cationic amphiphiles is related to the electrostatic and hydrophobic interactions with bacterial membranes and depends on the hydrophobic character and cationic charge of the surfactant. Firstly, the cationic surfactants interact with the negatively charged compounds of the bacterial membranes; subsequently, the alkyl chain interacts with the lipid bilayers of the membranes and changes their structure, ensuring transport across the cell membranes. As expected, the alkyl chain length affects the antimicrobial activity, in this case, the best effectivity was obtained for the P_{14} derivatives. The good activity of these compounds can be related to their chemical structure, which is designed to enhance interaction with lipid bilayers. By one hand, it has been reported that the presence of aromatic groups can improve the interaction of surfactants with the lipid bilayer of bacterial membranes [22].

Indeed, benzyl ammonium chloride, a widely used antiseptic agent, contains an aromatic group in the polar head. By another hand, regarding the hydrophobic group, generally, cationic amphiphiles with medium alkyl chains, usually 12/14 methylene groups, show

the best antimicrobial activity. These two surfactants showed better activity against the Gram-negative bacteria, this behaviour agrees with their mode of action, cationic surfactants activity mainly involves membrane disruption, and the Gram-negative bacteria have lower permeability of their outer membranes [23]. It should be noted that the development of antimicrobial agents with this mode of action may help to reduce the growth of resistant bacteria, given that this mechanism hampers the apparition of resistance.

Table 5 also contains the MBC values, the concentration at which >99.9% of bacteria are killed, of these phenylalanine-based surfactants. The obtained MBC/MIC ratio ranged from 1 to 2, indicating that these compounds not only impede the growth of these microorganisms but also kill them.

Comparing the antimicrobial activity of these $CnPNH(CH_3)_3$ with that of some pH-sensitive surfactants with similar chemical structure [9]. It is observed that all these cationic amphiphiles exhibit in common a broad spectrum of antibacterial activity. In this regard, the advantage of these phenylalanine derivatives is that the cationic charge does not depend on pH, so they are expected to maintain their activity in all pH mediums. Furthermore, the antimicrobial efficacy of these new cationic surfactants is comparable to that of BAC (table 5) and QACs with equivalent hydrophobic group [24].

Table 6. MIC/MBC values (μM) of formulations based on the $C_nPNH(CH_3)_3$

	L/D/P_{12} (6:2:2)	**L/C/P_{12} (7:1:2)**	**L/D/P_{14} (7:2:1)**	**L/C/P_{14} (7:1:2)**	**L/C/D/P_{14} (5:1:2:2)**
Gram-positive					
BS	161 (161)	62 (62)	41 (41)	53 (106)	12 (25)
SE	161 (161)	124 (124)	20 (20)	27 (27)	12 (12)
SA	80 (80)	62 (124)	20 (20)	54 (54)	25 (50)
LM	322 (>322)	249 (>249)	82 (82)	27 (27)	50 (50)
EF	80 (80)	124 (249)	41 (41)	54 (54)	25 (25)
Gram negative					
EC	322 (322)	249 (249)	>164 (>164)	54 (54)	100 (100)
AB	322 (322)	249 (249)	82 (82)	54 (54)	50 (50)
KA	>322 (>322)	249 (249)	>164 (>164)	106 (106)	400 (400)

Table 6 showed the MIC values obtained for some representative niosomal formulations. L/C-based niosomes did not exhibit any activity against the bacterial strains tested. Formulations based on the P_{12} derivatives did not exhibit a large difference, the MIC values for the two formulations are similar. It can be observed that the antimicrobial efficacy of this surfactant was reduced when it was incorporated into niosomal formulation. This behaviour can be ascribed to both the size and the low ζ-potential value

of these niosomes. It is well known that the cationic charge of surfactants is one of the main factors affecting their antimicrobial potency, in fact, increasing the cationic charge density of surfactants is the most common approach to improve the antimicrobial activity of cationic amphiphiles [24]. In this regard, for cationic vesicles based on amino acid surfactants, it was observed that the antimicrobial activity drastically diminished as the positive ζ-potential values decreased [25]. Given their chemical structures, it is expected that the monocatenary P_{12} derivatives forms micelles whereas its niosomes contained in the study formulations have great sizes. It was reported that large aggregates interact worst with biological membranes [26].

Interestingly, the $CnPNH(CH_3)_3$ encapsulated in these niosomes retains its antimicrobial activity. Note that the pure surfactant is more active than the P_{12} derivatives; moreover, the P_{14} based-niosomes have large positive ζ-potential values. It was observed that niosomal formulations based on this surfactant exhibited very good activity against all the Gram-negative bacteria tested and moderate activity against the Gran-negative. These results suggest that niosomes also interact with bacterial membranes, which is very interesting for reducing the growth of resistant bacteria. Niosomes containing $L/C/P_{14}$ and $L/D/P_{14}$ showed similar effectivity whereas those containing the four components exhibited better activity against the gram-positive bacteria, probably due to the better cationic charge density on the surface. It was also observed that these niosomes maintain the bactericidal activity of the cationic surfactant.

Liposomes containing antibiotics are widely reported. It has been observed that these systems can improve the stability and antimicrobial activity of these compounds [27]. In the literature works regarding the preparation of liposomes with antimicrobial activity using amino-acid based surfactants and phospholipids can be found [9, 28]. It has been also reported by our group the properties of catanionic vesicles based on arginine surfactants [25]. These systems are very interesting to be used as antimicrobial formulations. The results of this work suggest that these niosomal formulations represent a step forward in the pharmaceutical field, because of their dual pharmacological function: one related to the antimicrobial activity of the encapsulated cationic surfactant and the other related to the innate anesthetic properties of the lidocaine and capsaicin carriers.

3.5 Biocompatibility of the formulations: *ex-vivo* Hemolytic activity

To evaluate the biocompatibility of surfactants and vesicular systems, one of the most frequently used methods is the determination of hemolytic activity. Lidocaine-based systems proved to be non-hemolytic in the range of concentrations tested. Figures 7 and 8 show the HC_{50} values obtained for the pure surfactants and their formulations. The hemolytic activity of the P_{12} surfactant was very low compared to that obtained for the P_{14} derivatives. Numerous studies reported that when the hydrophobicity of the surfactant increased, stronger membrane permeabilization was achieved and the molecules became more hemolytic [29]. However, the effect of hydrophobic character on toxicity still has not been satisfactorily addressed to date, in some studies this trend has not been followed, for example, Fogt et al reported that traditionally for aliphatic chains, single-tailed cationic lipids are more toxic and less efficient than their double-tailed counterparts [30, 31], whereas Pinnaduwage et al. [32] reported that cetyltrimethylammonium bromide (CTAB) was more toxic and less efficient than DOTMA.

L L/C and LD vesicles did not showed hemolytic activity in the concentration ranged tested. Nonionic surfactant-based vesicles (niosomes) are considered non-toxic aggregates. The literature describes niosomes studies based on blood-compatible amphiphilic surfactants. Niosomes prepared with different nonionic surfactants (Brij72, Span 20,and Tween 60) exhibited very low hemolytic activity, less than 5% [33]. Ullah et al. also prepared non hemolytic niosomes with a non-ionic surfactant, atocopherol [34].

Niosomes containing the phenylalanine surfactants exhibited hemolytic activity. When niosomes interact with blood, cationic surface charge seems to be one of the most important influencing factors. The plasma membrane of erythrocytes is composed of negatively charged compounds (glycocalyx sialic acid), then, cationic niosomes exhibit higher interactions. These interactions tend to increase the surface area of the outer lipid monolayer on the erythrocytes than its inner lipid monolayer. This will eventually alter the shape of the RBC and cause the lysis. Because near-neutral charge niosomes show better biocompatibility [35]. Given the higher hemocompatibility of the P_{12} derivatives, niosomes containing this cationic surfactant also showed higher HC_{50} values. The L/D/P_{12} (6:2:2) formulation is more hemolytic than the previous formulation, reaching an HC_{50} equal to 129 Mm (Figure 10).

The hemolytic activity of cationic liposomes based on the P_{14} phenylalanine derivatives is shown in Figure 11. The L/P_{14} (9:1) and L/C/P_{14} (7:1:2) formulations showed HC_{50} values comparable to that of the cationic surfactant (around 30 μM). The addition of

DPPC led to an increase in biocompatibility, reaching HC_{50} values between 45.8 µM and 53.4 µM. The only exception is observed with the L/C/D/P_{14} (6:1:2:2) formulation, which showed an even lower hemolytic concentration than the pure surfactant solution. The hemolytic activity of cationic surfactants has been widely reported: unfortunately, very few data report on cationic niosomes surfactants. Hemolysis may be caused by the destruction of the molecular structure of the RBCs membrane, or it may be the result of the increased permeability of the membrane to external solutes. This process starts with the absorption of cationic surfactants on the erythrocyte surface and their distribution between the aqueous phase and the membrane. The presence of cationic charges on the niosomes can promote a high degree of interaction with the RBCs membrane. The characteristics of the niosomes aggregates can also affect the hemolytic activity. Vesicle aggregates of different sizes lead to significantly different hemolytic activity [36]. Small niosomes usually are more toxic than large niosomes, because they easily interact with RBCs, resulting in massive hemolysis. This premise can explain the fact that the hemolytic capacity in pure P_{14} surfactant solution is usually higher than the corresponding niosomes.

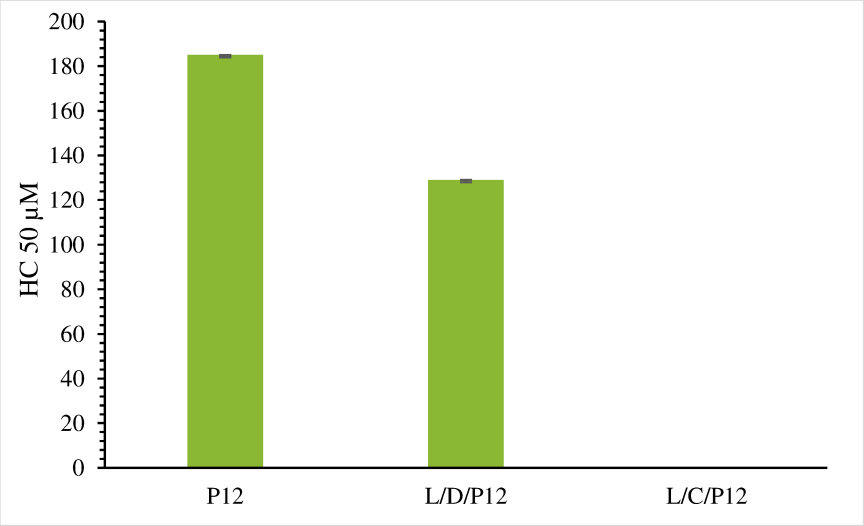

Figure 10: HC 50 of formulations based on P_{12} (mean ± S.E. of three replicates).

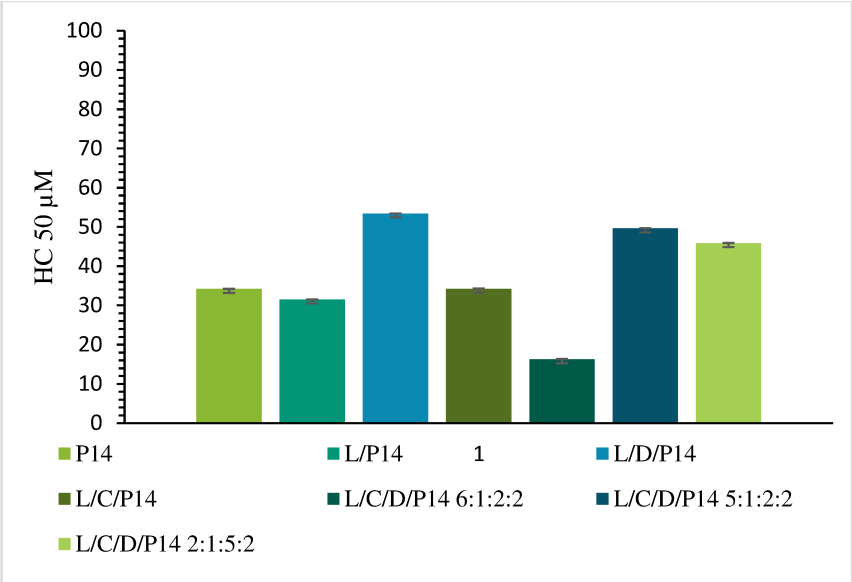

Figure 11: HC_{50} of formulations based on P_{14} (mean ± S.E. of three replicates).

The structural parameters affecting the cytotoxicity of surfactants are similar to those of antimicrobial activity. Because of that, cationic surfactants with high antimicrobial activity usually show great hemolytic activity. In this regard, it is very important to develop antimicrobial systems with selectivity against bacterial membranes. The therapeutic index (HC_{50}/MIC ratio) indicates the bacterial selectivity of them. Table 7 shows the TI for the pure surfactants and their niosomal formulations. TI values higher than 1 indicate that the compound or niosome formulation possesses antibacterial activity against the microorganism at concentrations lower than those at which they show hemolytic activity. It can be observed that pure surfactant solutions show TI higher than 1 for mall Gram-positive bacteria tested. This means that these surfactants show selectivity against Gram-positive bacteria. The better selectivity for niosomal formulations was obtained for those containing DPPC, they also show selectivity against almost Gram-positive bacteria. However, neither the pure surfactants nor their niosomal formulations exhibit selectivity against the Gram-negative microorganisms. More studies will be necessary to optimize the selectivity of this systems against these problematic bacteria.

Table 7. Therapeutic index of formulations tested

Microrganism	Therapeutic Index (TI)					
	P_{12}	P_{14}	L/D/P_{12} (6:2:2)	L/D/P_{14} (7:2:1)	L/C/P_{14} (7:1:2)	L/C/D/P_{14} (5:1:2:2)
BS ATCC 6633	2,98	2,13	0,80	1,30	0,64	4,13
SE ATCC 12228	5,78	4,27	0,80	2,67	1,27	4.13
SA ATCC 29213	5,78	4,27	1,61	2,67	0,63	1.98
LM ATCC 15313	1,48	2,13	0,40	0,65	1,27	0.99
EF ATCC 29212	2,89	2,13	1,61	1,30	0,63	1.98
EC ATCC 25922	1,48	0,27	0,40	0,32	0,63	0.49
AB ATCC 19606	0,74	1,07	0,40	0,65	0,63	0.99
KA ATCC 13048	0,37	0,14	0,40	0,32	0,32	0.12

Conclusions

The development of antimicrobial niosomes using lidocaine together with phenylalanine derivatives as primary constituents represents a significant advance in pharmaceutical formulation. Capsaicin has been used as a model drug. The niosomal systems formulated in various ratios with P12 and P14 phenylalanine derivatives and subsequently enriched with DPPC, showed sizes between 180 and 300 nm, with a uniform spherical structure. SAXS analysis showed that the DPPC-containing samples exhibited the typical band corresponding to phospholipid bilayers. The other samples showed much lower scattering intensities, however, the L/C/P14 sample (7:1:2) seems to contain significant information with a band similar to that of the two DPPC-containing samples. Surface pressure/area isotherms revealed that the presence of P12 and P14 at the interface significantly disrupts the DPPC monolayer. The phenylalanine derivatives exhibit a good antimicrobial activity against Gram-positive bacteria and moderate against the Gram-negative. The designed niosomes, particularly those containing the C14 phenylalanine homologue, retained the good bactericidal activity against Gram-negative bacteria associated with the cationic surfactants. Niosomes containing phenylalanine surfactants showed varying degrees of hemolytic activity being remarkable that some of the vesicles containing the C14 derivative and DPPC showed lower hemolytic and superior selectivity against almost all Gram-positive bacteria, probably attributed to a higher cationic charge density on the surface these results suggest an interaction between niosomes and bacterial membranes,

which is promising for combating resistant strains. This study highlights the potential of these niosomal formulations as a versatile delivery system with dual functionality. Their utilization shows promise for antimicrobial applications in pharmaceuticals by harnessing the antimicrobial properties of the encapsulated cationic surfactant, along with the intrinsic anesthetic and analgesic effects of lidocaine and capsaicin.

Reference

[1] Miwa, Y., Hamamoto, H., & Ishida, T. Lidocaine self-sacrificially improves the skin permeation of the acidic and poorly water-soluble drug etodolac via its transformation into an ionic liquid. *Eur. J. Pharm. Biopharm.*, **(2016)**, *102*, 92-100.

[2] Pathak, P., & Nagarsenker, M. Formulation and evaluation of lidocaine lipid nanosystems for dermal delivery. *Aaps PharmSciTech*, **(2009)**, *10*, 985-992.

[3] Laffleur, F., & Keckeis, V. Advances in drug delivery systems: Work in progress still needed?. *Int. J. Pharm.*, **(2020)**, *590*, 119912.[4] Khizar, S., Alrushaid, N., Khan, F. A., Zine, N., Jaffrezic-Renault, N., Errachid, A., & Elaissari, A. Nanocarriers based novel and effective drug delivery system. *Int. J. Pharm.*, **(2023)**, *632*, 122570

[5] Attwood, D. The mode of association of amphiphilic drugs in aqueous solution. *Adv. Colloid Interface Sci.* , **(1995)**, 55, 271-303.

[6] Romeo, M., Mazzotta, E., Perrotta, I. D., & Muzzalupo, R. Lidosomes: Innovative Vesicular Systems Prepared from Lidocaine Surfadrug. *Pharmaceutics*, **(2022)**, *14*(10), 2190.

[7] Serra-Burriel, M., Keys, M., Campillo-Artero, C., Agodi, A., Barchitta, M., Gikas, A., ... & López-Casasnovas, G. Impact of multi-drug resistant bacteria on economic and clinical outcomes of healthcare-associated infections in adults: Systematic review and meta-analysis. *PloS one*, **(2020)**, *15*(1), e0227139.

[8] Marqués, A. M., Pérez, L., Farfán, M., & Pinazo, A. Green surfactants: production, properties, and application in advanced medical technologies. *Biosurfactants for a sustainable future: Production and applications in the environment and biomedicine*, **(2021)**, 207-243.[9] Hafidi, Z., Pérez, L., El Achouri, M., & Pons, R. Phenylalanine and Tryptophan-Based Surfactants as New Antibacterial Agents: Characterization, Self-Aggregation Properties, and DPPC/Surfactants Vesicles Formulation. *Pharmaceutics*, **(2023)**, *15*(7), 1856.

[10] Fenton, R.R.; Easdale, W.J.; Er, H.M.; O'Mara, S.M.; McKeage, M.J.; Russell, P.J.; Hambley, T.W. Preparation, DNA binding, and in vitro cytotoxicity of a pair of

enantiomeric platinum (II) complexes, [(R)-and (S)-3-aminohexahydroazepine] dichloro-platinum (II). Crystal structure of the S enantiomer. *J. Med. Chem*. **(1997),** 40, 1090–1098.

[11] Caddeo, C., Pons, R., Carbone, C., Fernàndez-Busquets, X., Cardia, M. C., Maccioni, A. M., ... & Manconi, M. Physico-chemical characterization of succinyl chitosan-stabilized liposomes for the oral co-delivery of quercetin and resveratrol. *Carbohydr. Polym.* **(2017)**, *157*, 1853-1861.

[12]Pape, W. J.; Pfannenbecker, U.; Hoppe, U. Validation of the red blood cell test system as in vitro assay for rapid screening of irritation potencial of surfactants *Mol. Toxicol*. (**1987)**, 1, 525– 536

[13]R. N. Jones, A. L. Barry, T. L. Gavan and J. A. Washington, in *Manual of Clinical Microbiology*, ed. E. H. Lennette, A. Ballows, W. J. Hauser and H. J. Shadomy, American Society for Microbiology, Washington, DC, 4th edn, (**1985)**[14]Patel, J.B.; Tenover, F.C.; Turnidge, J.D.; Jorgensen, J.H. Book *Manual of Clinical Microbiology*. In *Susceptibility Test Methods: Dilution and Disk Diffusion Methods*, 10th ed.; Chapter 68; Versalovic, J., Carroll, K.C., Funke, G., Jorgensen, J.H., Landry, M.L., Warnock, D.W., Eds.; ASM Press: Washinton, DC, USA, (**2011)**[15] Merchel Piovesan Pereira, B., & Tagkopoulos, I. (2019). Benzalkonium chlorides: uses, regulatory status, and microbial resistance. *Appl. Environ. Microbiol.*, **2019**, *85*(13), e00377-19.

[16] Pinazo, A., Manresa, M. A., Marques, A. M., Bustelo, M., Espuny, M. J., & Pérez, L. (2016). Amino acid–based surfactants: New antimicrobial agents. *Adv. Colloid Interface Sci.*, **2016**, *228*, 17-39.[17] Tripathy, D. B., Mishra, A., Clark, J., & Farmer, T. Synthesis, chemistry, physicochemical properties and industrial applications of amino acid surfactants: A review. *C. R. Chim*, **(2018)**, *21*(2), 112-130.

[18]Brito, R. O., Marques, E. F., Silva, S. G., do Vale, M. L., Gomes, P., Araújo, M. J., ... & Mitjans, M. Physicochemical and toxicological properties of novel amino acid-based amphiphiles and their spontaneously formed catanionic vesicles. *Colloids Surf. B*, **(2009)**, *72*(1), 80-87.

[19] Bordes, R., & Holmberg, K. Amino acid-based surfactants–do they deserve more attention?. *Adv. Colloid Interface Sci.*, **(2015)**, *222*, 79-91.

[20] Shirota, H., Yanase, K., Ogura, T., & Sato, T. Intermolecular Dynamics and Structure in Aqueous Lidocaine Hydrochloride Solutions. *J. Phys. Chem.*, **2022,** *126*(8), 1787-1798.

[21] Efthymiou, C., Bergström, L. M., Pedersen, J. N., Pedersen, J. S., & Hansson, P. Self-assembling properties of ionisable amphiphilic drugs in aqueous solution. *J. Colloid Interface Sci.*, **2021**, *600*, 701-710.

[22] El Hage, S.; Lajoie, B.; Stigliani, J.-L.; Furiga-Chusseau, A.; Roques, C.; Baziard, G. Synthesis, Antimicrobial Activity and Physico-Chemical Properties of Some n-Alkyldimethylbenzylammonium Halides. *J. Appl. Biomed.*, **(2014),** 12, 245–253, doi:10.1016/j.jab.2014.02.002[23] Pérez, L., García, M. T., Pinazo, A., Pérez-Matas, E., Hafidi, Z., & Bautista, E. Cationic Surfactants Based on Arginine-Phenylalanine and Arginine-Tryptophan: Synthesis, Aggregation Behavior, Antimicrobial Activity, and Biodegradation. *Pharmaceutics*, **(2022)**, *14*(12), 2602.[24] Zhou, C., & Wang, Y. Structure–activity relationship of cationic surfactants as antimicrobial agents. *Curr. Opin. Colloid Interface,* **(2020)***, 45,* 28-43.

[25] Pinazo, A., Pons, R., Marqués, A., Farfan, M., da Silva, A., & Perez, L. Biocompatible catanionic vesicles from arginine-based surfactants: A new strategy to tune the antimicrobial activity and cytotoxicity of vesicular systems. *Pharmaceutics,* **(2020)***, 12*(9), 857.[26] Tavano, L., Infante, M. R., Riya, M. A., Pinazo, A., Vinardell, M. P., Mitjans, M., ... & Pérez, L. Role of aggregate size in the hemolytic and antimicrobial activity of colloidal solutions based on single and gemini surfactants from arginine. *Soft Matter*, **(2013)**, *9*(1), 306-319.[27] Mehrarya, M., Gharehchelou, B., Haghighi Poodeh, S., Jamshidifar, E., Karimifard, S., Farasati Far, B., ... & Seifalian, A. Niosomal formulation for antibacterial applications. *J. Drug Target.* **(2022)**, *30*(5), 476-493.

[28] Tavano, L., Pinazo, A., Abo-Riya, M., Infante, M. R., Manresa, M. A., Muzzalupo, R., & Pérez, L. Cationic vesicles based on biocompatible diacyl glycerol-arginine surfactants: physicochemical properties, antimicrobial activity, encapsulation efficiency and drug release. *Colloids Surf. B: Biointerfaces*, **(2014)**, *120*, 160-167.[29] Lukáč, M., Mojžiš, J., Mojžišová, G., Mrva, M., Ondriska, F., Valentová, J., ... & Karlovská, J. Dialkylamino and nitrogen heterocyclic analogues of hexadecylphosphocholine and cetyltrimetylammonium bromide: Effect of phosphate group and environment of the ammonium cation on their biological activity. *Eur. J. Med. Chem.*, **(2009)**, *44*(12), 4970-4977.[30] Fogt, A., Hägerstrand, H., & Isomaa, B. Effects of N, N′-bisdimethyl-1, 2-ethanediamine dichloride, a double-chain surfactant, on membrane-related functions in human erythrocytes. *Chem. Biol. Interact.*, **(1995)**, *94*(2), 147-155.[31] Lv, H., Zhang, S., Wang, B., Cui, S., & Yan, J. Toxicity of cationic lipids and cationic polymers in gene delivery. *J. Control. Release*, **(2006)**, *114*(1), 100-109.[32] Pinnaduwage, P. , Schmitt, L.

, and Huang, L. , Use of quaternary ammonium detergent in liposome mediated DNA transfection of mouse L-cells, Biochim. Biophys. Acta, **(1989)**, 985, 33.

[33] Shehata, T., Kimura, T., Higaki, K., & Ogawara, K. I. In-vivo disposition characteristics of PEG niosome and its interaction with serum proteins. *Int. J. Pharm.*, **(2016)**, *512*(1), 322-328.

[34] Ullah, S., Shah, M. R., Shoaib, M., Imran, M., Shah, S. W. A., Ahmed, F., ... & Shah, I. Hydrophilically modified self-assembling α-tocopherol derivative as niosomal nanocarrier for improving clarithromycin oral bioavailability. *Artif. Cells Nanomed.*, **(2018)**, *46*(3), 568-578.

[35] Kumar, Y., Kuche, K., Swami, R., Katiyar, S. S., Chaudhari, D., Katare, P. B., ... & Jain, S. (2020). Exploring the potential of novel pH sensitive lipoplexes for tumor targeted gene delivery with reduced toxicity. *Int. J. Pharm.*,**(2020)**, *573*, 118889.

[36] Tavano, L., Aiello, R., Ioele, G., Picci, N., & Muzzalupo, R. Niosomes from glucuronic acid-based surfactant as new carriers for cancer therapy: preparation, characterization and biological properties. *Colloids Surf. B: Biointerfaces*,**(2014)**, *118*, 7-13.

Chapter 2:

Multifunctional nanosystems for cancer therapy

2. Multifunctional nanosystems for cancer therapy

2.1 A novel hyaluronic acid-conjugated niosome for controlled and targeted delivery of Doxorubicin in cancer therapy

Introduction

Cancer is a disease with complex pathogenesis that represents a serious threat to human health. To date, chemotherapy remains the most clinically used strategy, as it is capable of blocking cell proliferation, inhibiting tumor growth, up to necrosis of the pathological tissue [1]. However, chemotherapy is an invasive treatment, as it affects all highly duplicating cells. Not only tumor tissues are targeted but also healthy tissues such as bone marrow, intestine, etc... which cause serious side effects. DDS drug delivery systems, such as niosomes, liposomes, and nanoparticles, are promising candidates to overcome the limitations of conventional chemotherapy. DDSs have attracted great attention given their excellent characteristics such as small size, biocompatibility, good stability, and solubility, sustained and targeted drug release via nanocarrier functionalization [2]. To improve the selectivity of the nanocarrier it is possible to exploit the unique characteristics of tumor tissues. In fact, in the tumor environment, there is a greater permeability of the new vessels and a deficient lymphatic system, also known as the EPR (enhanced permeation and retention) effect [3,4]. These characteristics facilitate the entry and accumulation of nanosystems at the tumor site. The tumor environment has a more acidic pH than healthy tissues [5] and presents a condition of hypoxia and hyperthermia. These attributes significantly influence the success of DDSs and, if carefully integrated into their design, could provide significant benefits in targeted cancer treatment. Another strategy is the functionalization of the nanocarrier surface with ligands, such as aptamers, antibodies, proteins, peptides, or small molecules, capable of interacting with a specific receptor. Among the most exploited receptors in tumor therapy is the CD44 receptor, a transmembrane glycoprotein, expressed in many solid tumors including V79-C13 lung cancer cells [6], breast MDA-MB 231 [7], colorectal Caco-2 [6], gastric ECL [8], cervical HeLa [9], kidney cancer [10] and Hep G2 liver cancer [11]. CD44 ligand is the extracellular matrix (HA) hyaluronate, a linear, negatively charged polysaccharide, the alternatively repeating monomers are D-glucuronic acid and N-acetyl D-glucosamine. Hyaluronic acid then binds to the extracellular domain of CD44 ensuring its activation through a conformational change of the molecule itself or a change in the distribution of CD44 molecules on the cell surface [12]. It is a biocompatible and biodegradable

hydrophilic polymer. The presence of -COOH and -OH groups allow HA to be exploited for the functionalization of nanocarriers, ensuring active targeting. This functionalization improves the internalization of the vesicular systems and increases the intracellular concentration of the drug delivered to the tumor environment [13]. Among DDS, particular importance has been given to cationic niosomes, which have a positive surface charge thanks to the presence, in the lipid film, of cationic surfactants (CTAB, DODAB, or DDAB). The presence of quaternary N in the structure allows these surfactants to mimic the effects of vitamins, enzymes, phosphatidylcholine, and acetylcholine and to exhibit antimicrobial and antifungal activity. Doxorubicin is an anticancer drug, that acts as a DNA intercalator, inhibiting topoisomerase II, generating single and double interruptions that form the basis of mutated fragments, such as to induce cellular apoptosis [1]. However, the clinical use of this drug is limited by acute and chronic side effects, including marrow wasting, vomiting, alopecia, and cardiotoxicity when used at high doses [14]. To date, DOX-based liposomal formulations are present commercially, such as Doxil ® used for the treatment of cancer. Liposomes present limitations due to rapid elimination from the blood circulation by macrophages and the endothelial reticulum [15, 16], physical and chemical instability (fusion, degradation, hydrolysis, and oxidation of phospholipids), as well as high production costs [17]. For these reasons, we thought about designing smart niosomes to improve the direction of an anticancer drug like DOX. Cationic liposomal systems were formulated, and subsequently functionalized with HA, by cross-linking. If HA were to bind to the surface of cationic nanocarriers containing anticancer agents such as Doxorubicin, thanks to CD44-mediated endocytosis, it would allow its internalization into the cell and the subsequent release of the anticancer agent. The specific administration of DOX in the tumor environment would therefore allow to reduce the administered dose and improve patient compliance.

Materials and methods

Materials

Span 80 (S80), cholesterol (CHOL), dioctadecyl-dimethylammonium bromide (DODAB), Hyaluronic acid (HA), doxorubicin (DOX), buffer, and all solvents used were bought by Sigma-Aldrich (Milan, Italy).

Cationic niosomal preparation

To formulate the cationic niosomal systems, the two surfactants S80 and DODAB were mixed with cholesterol in different molar ratios. Once mixed, the components were

dissolved in chloroform in a single-neck flask, and subsequently evaporated under reduced pressure. To eliminate residual traces of solvent, a vacuum pump was used for 8 hours. The lipid film was then hydrated with 10 mL of distilled water for 30 minutes at 60°C and for the formulations were loaded with a doxorubicin solution ($5x10^{-4}$ M). The formulation was left to rest overnight at room temperature and after 24 hours subjected to a sonication bath for 30 min, to ensure the flaking of the vesicles. Each formulation was then dialyzed using synthetic cellulose membranes (molecular mass Spectra/Por, cut-off 12/14 kDa), previously treated with the Fenton method [18]. The samples were stored in the dark at 4°C until further use. Four different formulations (S1, S2, S3 and S4) were obtained maintaining a ratio of total surfactants to cholesterols of 1:1 and characterized in term of size and ζ-potential.

Conjugation of vesicles with hyaluronic acid

HA conjugation is based on ionic cross-linking between empty niosomes or positively charged DOX-loaded niosomes and negatively charged HA. HA solution was added to 1 mL of niosome suspension, under magnetic stirring, to promote complete conjugation.

Niosomal characterization

All vesicular formulations were characterized in terms of size (nm), polydispersion index (PI), ζ-potential, and morphology. Dynamic Light Scattering (DLS) was used for dimensional analysis using the 90 Plus Particle Analyzer (Brookhaven Instrument Corportion, New York, USA) at a temperature of 25.0 ± 0.1 °C. The scattering angle is 90°C and the incident light beam has a wavelength of 658 nm. The ζ potential was assessed using a Zetasizer ZS (Malvern Instrument Ltd, Malvern, UK). All analyses were performed on purified samples, in triplicate. Finally, the morphology was observed by transmission electron microscopy (TEM), using a ZEISS EM 10 TEM, operating with an accelerating voltage of 80 kV. Sample preparation was carried out by pouring a drop of colloidal suspension onto a Formvar/Carbon copper screen, until a thin liquid film was formed, and excess water was removed using filter paper.

Encapsulation efficiency

The amount of drug encapsulated in the vesicular systems was expressed as a percentage (EE%), using the initial amount for the formulation as a reference. EE% was determined by breaking 0.2 mL of each purified and non-purified sample by freezing. Subsequently, aliquots were diluted in 10 mL of ethanol and analysed using a JASCO V-530

spectrophotometer. The absorbances, relating to the amount of drug present in the samples, were measured at a wavelength of 495 nm, at which the characteristic DOX peak is observed. The equation used to derive the encapsulation efficiency is the following:

$$\boldsymbol{EE}\ \% = \frac{C_{fin}}{C_{in}} \times 100$$

Where C_{fin} represents encapsulated drug concentration in purified suspension and C_{in} represents the initial drug concentration used for the preparation.

***In vitro* release studies**

Release studies allow the ability of vesicular systems to release their pharmacological contents to be evaluated. Release studies were conducted in two environmental conditions, in phosphate buffer pH 7.4 (PBS) and in acetate buffer pH 5.5, to evaluate the release capacity both in a physiological environment and in a tumor environment. 1 mL of each sample was placed in a dialysis bag and placed under continuous stirring in 25 mL of medium. The amount of drug released from niosomal systems was determined indirectly, to do this the release profile required a separate vials for each time point. At regular intervals, over 48 hours, samples were taken and diluited in ethanol to evaluate the amount of drug remaining in the vesicles and the corresponding drug released. The aliquots taken were analysed by UV-Vis spectrophotometry. The experiments were conducted on systems loaded with conjugated DOX and not with HA in triplicate, to ensure data reproducibility.

Hemolytic assay

For the determination of hemolytic activity, fresh blood was used, collected, and processed on the same day, following the method described by Pape et al. [19]. The red blood cells are washed with PBS (pH 7.4) 3 times, after which they are used to prepare a suspension with a density of $8x10^9$ cells/mL. Different volumes of niosomal solution, ranging from 10 to 100 µL, were collected and placed in Eppendorf tubes. Phosphate buffer and 25 µL of erythrocytes were subsequently added to reach a total volume of 1 mL. The Eppendorf's are then incubated with shaking for 10 minutes and then centrifuged at 10,000 rpm for 5 minutes at room temperature. Hemolytic activity is determined by comparing the absorbance value of the supernatant at 575 nm with that of the control. The control represents the total cellular hemolysis obtained by bringing the erythrocytes and distilled water into contact. Analyses were conducted in triplicate on all selected samples.

Cell culture

HeLa and NIH-3T3 cells from the American Type Culture Collection (ATCC, Manassas, VA, USA) were grown in Dulbecco's modified Eagle's medium (DMEM) (Thermo-Fischer Scientific, Waltham, MA, USA) supplemented with 10% (*v*/*v*) fetal bovine serum (FBS), 2 Mm l-glutamine, 100 UI/mL penicillin, and 100 µg/mL streptomycin at 37 °C in a humidified incubator with 5% CO_2. The cells in 25-cm^2 flasks were passed into 96-multiwell plates, using trypsin ethylenediaminetetraacetic acid (EDTA), when they reached approximately 80% confluence.

MTT assay

Cytotoxicity of niosomal systems was evaluated by MTT assay. Briefly, HeLa and NIH-3T3 cells were incubated for 24 h at 37 °C and 5% CO_2. Quantities equal to 0.1, 1 and 10 g/mL of free Doxorubicin, coated and uncoated empty niosomes, uncoated and coated niosomes with the encapsulated drug are then added. Untreated HeLa and NIH-3T3 cells are used as a control. After 4 hours of incubation, the cells are washed and incubated with a fresh medium for 72 hours. At this point, 10 µL of MTT (5 ng/mL) dissolved in Dulbecco's phosphate-buffered saline at pH 7.4 is added to each well; after another 4 hours of incubation at 37 °C and 5% CO_2, the medium is discarded and 100 µl of a solubilizing solution (16% SDS in 40% DMF at pH 4.7) is added to dissolve the formazan crystal. The amount of formazan produced is assessed using an ELX800 microplate reader (Bio-Tek Instruments, Inc., Winooski, VT, USA), in triplicate [20]. The percentage of viable cells is given by the average of two different experiments ± SD, and is calculated with the following equation:

$$\boldsymbol{Cell\ viability} = \frac{AT}{AU}\ x\ 100$$

where AT is the absorbance of treated cells, AU is the absorbance of untreated cells.

Cellular uptake studies

For cellular uptake studies, HeLa and NIH-3T3 cells were seeded onto six-well plates and incubated; then, they were exposed to doxorubicin-free and doxorubicin-encapsulated niosomes, both uncoated and HA-coated. After 4 hours, the medium was refreshed, and the cells were incubated for 24 hours at 37°C; they were subsequently washed 3 times with PBS at pH 7.4 and fixed with 4% paraformaldehyde in PBS for 10 minutes at room temperature. All coverslips were mounted on clean slides with UltraCruz, a mounting medium containing 4,6-diamidino-2-phenylindole DAPI0 (Santa Cruz Biotechnology,

TX, USA), and examined on a Nikon Microphot-FX conventional fluorescence microscope. Doxorubicin can be excited with an argon laser (488 nm) [21].

Results

Cationic vesicles for targeted DOX delivery were prepared with increasing amounts of cationic surfactant to identify the minimum amount to give a positive surface charge. The ratios used generated vesicles ranging in size from 431 to 575 nm with good size distribution. The ζ potential, when minimal amounts of DODAB were used, was negative, so the S80 hydroxylic group prevailed. By progressively increasing amount of DODAB, the ζ potential inversion from -39 to +39 mV was observed, as reported in **Table 1**. The vesicles were stable and homogeneous, without undergoing agglomeration, precipitation, and flocculation phenomena.

Table 1. Physical-chemical characterization of cationic niosomes stored at 4°C in term of size (nm), PI and ζ -potential at 25°C

FORMULATION	Size (nm)	PI	ζ-potential (mV)
S1	479.5	0.262	-39.3±0.98
S2	575.7	0.194	-13.2±1.33
S3	431.1	0.224	+39.2±0.78
S4	452.1	0.188	+40.0±1.04

Stability of colloidal suspensions depends on both electrostatic repulsions and Wan der Walls attractive forces between the particles. Over time, vesicles prepared according to this new ratio were observed. The colloidal system-maintained stability characteristics over time (**Table 2**), with a ζ potential value of approximately +40 mV. This high value of the ζ potential allows repulsive interactions between particles such as to prevent the formation of agglomerates. The size and PI have also not changed significantly over time.

Table 2. Stability analysis of niosome stored at 4 ◦C evaluated by measuring diameter, P.I., ζ−potential, and DL%. Data was collected at specific time points, up to 3 months, and expressed as mean of three independent experiments ± SD.

	Time (days)	Size (nm)	PI	ζ-potential (mV)
S4	0	452.1	0.192	+40.0±1.04
	30	477.5	0.198	+41.0±0.56
	60	559.6	0.239	+39.2±0.78
	90	487.6	0.223	+42.1±1.56
	120	475.7	0.154	+39.0±1.33

Given the good results obtained, this formulation was used for the subsequent experiments, loading DOX, and using it for the HA coating. The empty and filled formulations appeared visually opalescent, a typical characteristic of colloidal systems, and in the presence of DOX they took on a red color, characteristic of this drug (**Fig. 1**).

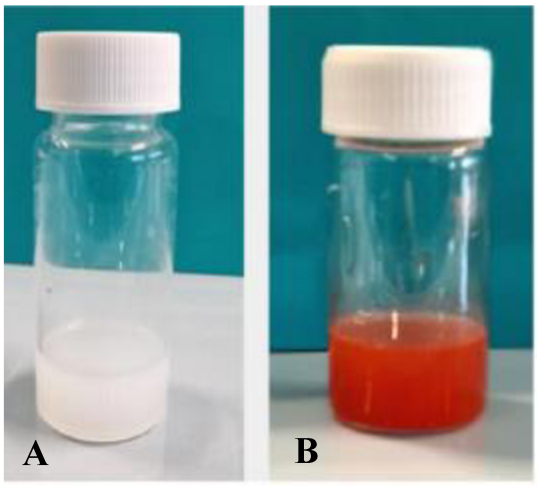

Figure 1. Visual appearance of cationic niosomes **(A)** S4, **(B)** S4-DOX

Table 3 reports the results of the chemical-physical characteristics of cross-linked and non-cross-linked formulations with hyaluronic acid. As can be seen, the cross-linking of the empty niosomes with HA has led to an increase in size from approximately 450 to 550 nm. The cross-linking of colloidal systems also determines a notable inversion of the ζ potential, which varies from +40 mV to -37 Mv. When the systems carry DOX, no notable changes in size and ζ potential are observed, appearing like the corresponding blank formulation. In agreement with what has been reported in other studies, this nanodevice also has an excellent drug encapsulation capacity; in fact, the encapsulation percentage (expressed as EE%) is equal to 80%.

Table 3. Physical-chemical characterization of cationic niosomes stored at 4°C in term of size (nm), PI and ζ -potential at 25°C and expressed as mean of three independent experiments ± SD.

FORMULATION	Size (nm)	PI	ζ -Potential (mV)
S4	452.1±4.31	0.192	+43.9±0.65
S4-HA	546.2±16.26	0.206	-37.7±0.61
S4-DOX	473.1±51.68	0.239	+45.5±1.46
S4-DOX-HA	584.1±50.91	0.232	-24.4±0.36

Morphology of developed nanosystems was evaluated by electronic transmission microscopy (TEM) and the frames are shown in **Figure 2.** Cationic vesicles showed a spherical morphology with regular and well-defined outline (**Figure 2A**), with dimensions slightly smaller than those detected by DLS.

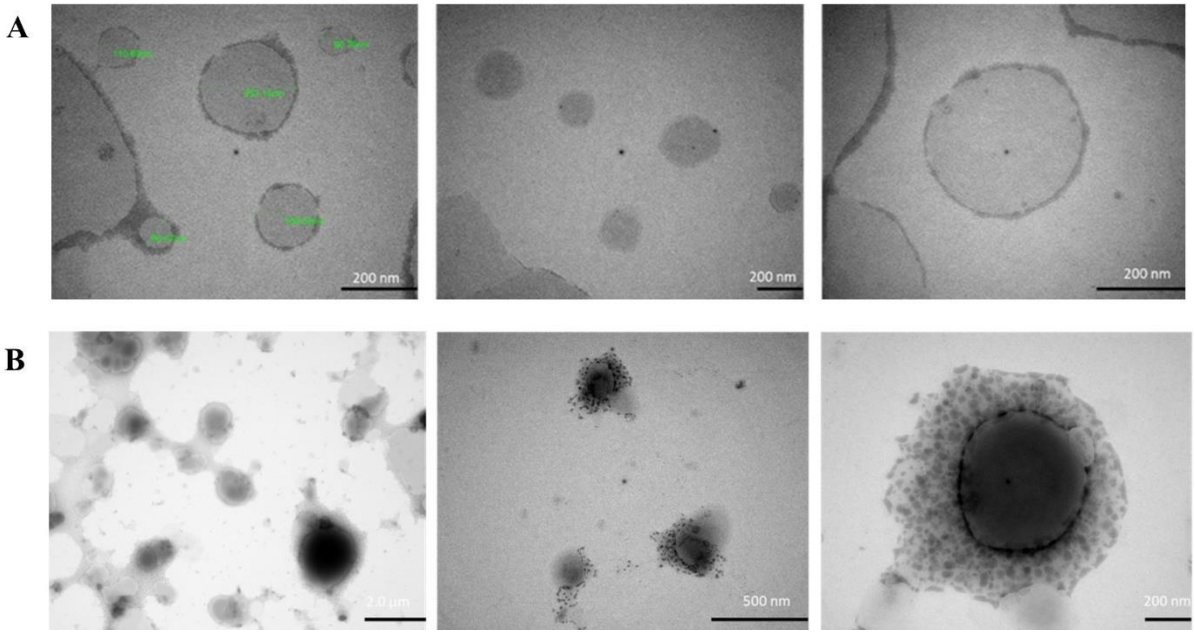

Figure 2. Typical TEM photomicrograph of cationic niosome: **(A)** S4; **(B)** S4-HA. Bar is 1 µm

TEM obtained for the HA cross-linked formulation confirmed the effective coating of the vesicles with hyaluronic acid. From the photograms (**Figure 2 B**) we observe the presence of a jagged coating around the vesicles and a corresponding increase in the average size.

In vitro release studies

It is important that in the tumor environment delivery systems maintain good stability in the blood circulation and the ability to release the drug rapidly and completely. The ability of nanocarriers to gradually release administered drugs was evaluated in various fluids using passive diffusion studies. The experiments were conducted in phosphate buffer (pH 7.4) and acetate buffer (pH 5.5), to respectively simulate the physiological environment

and the acidotic conditions typical of the tumor microenvironment. As seen in **Figures 3A** and **B**, encapsulation of the drug in niosomal systems slows release compared to the free form. Free DOX is completely released in 5 hours at pH 5.5, compared to when it is encapsulated. This trend is observed for both coated and uncoated systems, where the amount of drug released after 48 hours is 59.63% and 26%, respectively. The slowed release is probably due to the presence of cholesterol which increases the rigidity of the bilayer, slowing the escape of the drug from the nanocarrier. Another factor that could influence the slow release of DOX is the presence of the cationic surfactant in the lipid film. In the literature [22] it is reported that charged lipids are necessary to tighten the molecular packing of the vesicle bilayer, resulting in a decrease in the release of transported drugs. However, having a prolonged release over time is advantageous, as it limits the premature release of the drug into the systemic circulation, reducing toxic effects on healthy cells.

A faster release profile was observed in the coated nanocarriers compared to the uncoated ones, in both environments. The surface charge inversion that occurs in the coated niosomes could generate an electrostatic attraction between the drug and the carboxyl

groups of the HA chains. This results in a greater presence of DOX molecules near the niosomal surface, resulting in increased release

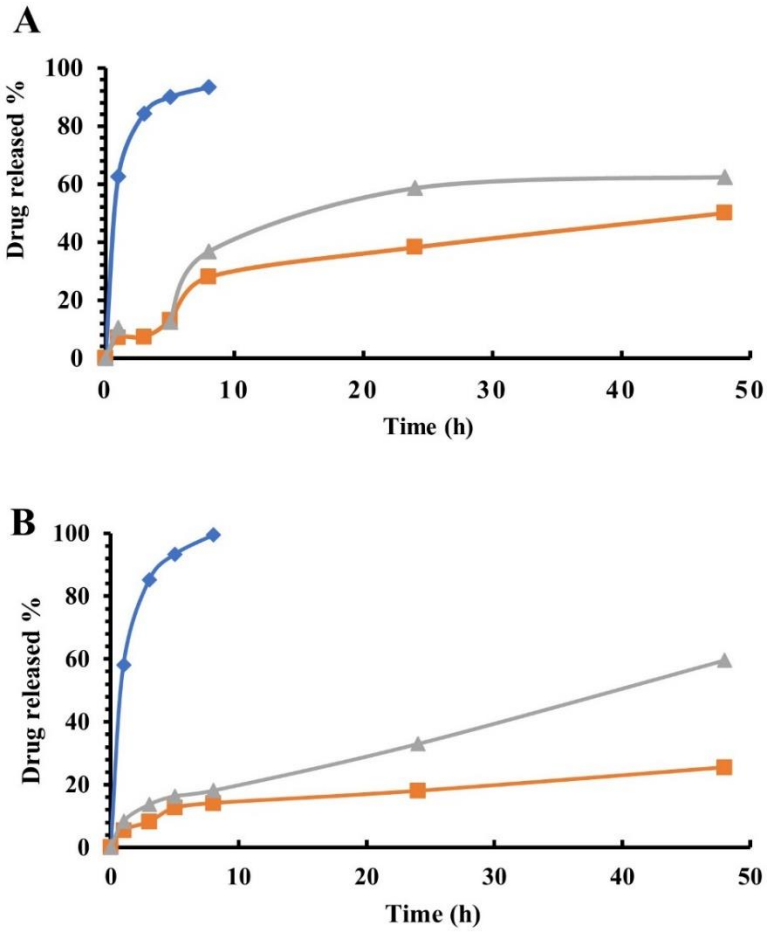

Figure 3. *In vitro* release of: **(A)** (♦) DOX solution; (■) S4-DOX; (▲) S4-DOX-HA in buffer pH 7.4 and **(B)** (♦) DOX solution; (■) S4-DOX; (▲) S4-DOX-HA in buffer pH 5.5.

Hemolytic assay

Like all surfactants, anionic and cationic, non-ionic, and zwitterionic, even those used in the design of the niosomal systems proposed in this work, can alter the bilayer of cell membranes and be potentially toxic [23]. For this reason, the analysis of hemolytic activity conducted on mammalian erythrocytes, the blood cells on which the interaction between surfactant and membrane is commonly tested, may be of particular importance. The experiments were carried out *in vitro* on erythrocytes using a concentration of the cationic surfactant between 12 and 126 μM (**Table 4**). From the data obtained, it can be observed that the non-cross-linked systems are not hemolytic at the concentrations tested, while loaded with DOX the percentage of hemolysis increases, reaching 10%. In comparison, HA cross-linked 27 systems, whether empty or loaded, maintain a hemolysis rate of approximately 4%, which in both cases is negligible.

Table 4. Percentage of hemolytic activity of niosomal systems tested

CONC. µM	% S4	% S4-HA	% S4-DOX	% S4-DOX-HA
12,68	0,24	0,14	0,52	0,17
25,36	0,65	0,46	0,89	0,83
38,04	0,45	0,67	1,67	1,10
50,72	0,48	1,31	2,41	1,64
63,39	0,72	1,55	3,48	2,15
76,07	0,88	2,05	4,48	2,55
88,75	0,83	2,81	6,22	3,01
101,37	1,02	2,81	7,66	3,55
114,11	1,08	2,98	8,73	4,06
126,79	1,24	3,49	10,44	4,81

In vitro cytotoxicity

To evaluate the toxicity of coated and uncoated niosomes, both in the presence and absence of DOX, the MTT assay on HeLa cells and NIH-3T3 cells were used. Data reported in **Figure 4** showed that cells treated with the empty systems had a good viability after 72 hours. However, HA coating increased the toxicity of the systems toward HeLa cells. This could be due to greater internalization of the nanocarrier within the tumor cell given the overexpression of the CD44 receptor. As regards, however, the niosomes loaded with DOX, at the low concentrations tested (0.1 and 1 µM) when coated with HA showed greater toxicity compared to the uncoated systems. Cell viability was found to be 59% and 41% respectively for cells treated with the uncoated and coated systems at a concentration of 0.1 µM. At this concentration, the cytotoxic effect of DOX when encapsulated in the coated niosomes was significantly greater than in the free form, after 72 hours the cell viability of cells treated with the free drug was 82.4%. These results highlight the target effect of hyaluronic acid which appears to promote the internalization of nanosystems in tumor cells. At the maximum concentration used (10 µM), a sort of plateau in the cytotoxic activity was observed, probably related to a saturation of the HA receptors.

py

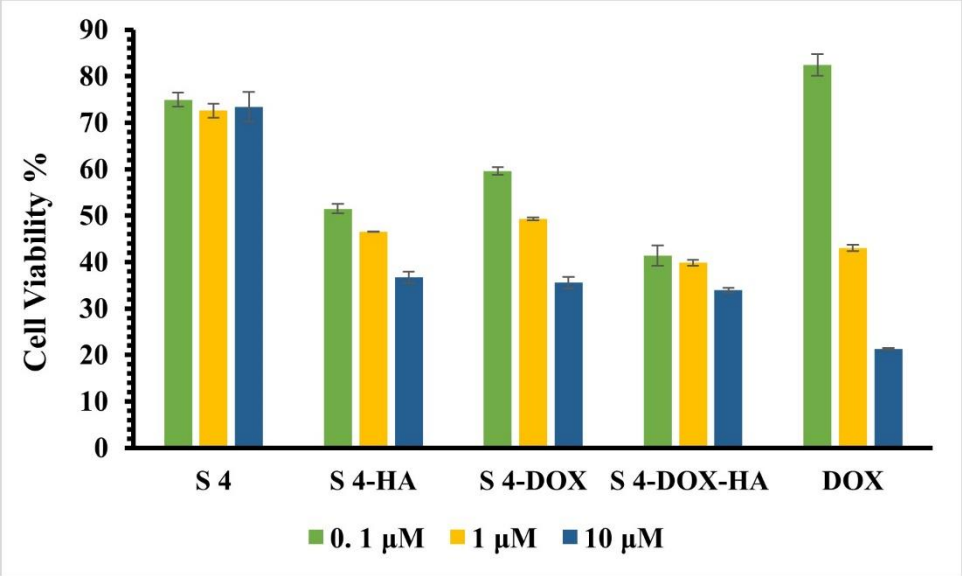

Figure 4. *In vitro* cytotoxicity assay: HeLa cell viability after 72 h incubation with DOX and S4, S4-HA, S4-DOX e S4-DOX-HA at concentrations of 0.1, 1 and 10 µM. Each value represents the mean ± SD of experiments conducted in triplicate.

To confirm the selectivity of these vesicular systems for tumor cells, we evaluated cell viability on cells lacking the hyaluronic acid receptor (NIH-3T3 cells). As depicted in **Figure 5**, the results indicate robust viability for cells treated with all niosomal systems after 72 hours. Interestingly, the HA-cross-linked systems, known for their toxicity towards HeLa cells, exhibited no adverse effects on NIH-3T3 cells, underscoring the cell-selective nature of these systems. For doxorubicin-loaded niosomes, both cross-linked and non-cross-linked, the viability remained high at 92% and 83%, respectively, at the lowest concentration tested (0.1 µM). At the highest concentration (10 µM), the cell viability dropped to 75% and 56%, respectively. Notably, this reduction in viability is significantly less than that observed with free DOX solution, which, at a concentration of 10 µM, resulted in a substantial decrease in cell viability to 41%. These findings highlight the specific targeting capability of our functionalized systems, by the presence of hyaluronic acid (HA), and emphasize the considerable reduction in systemic toxicity associated with DOX when delivered through our designed vesicular systems.

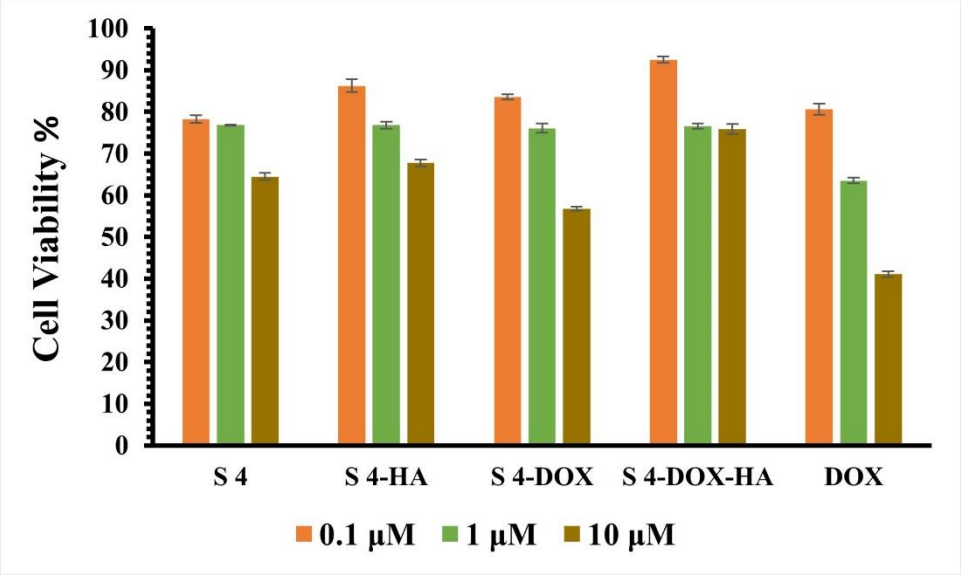

Figure 5. *In vitro* cytotoxicity assay: NIH-3T3 cell viability after 72 h incubation with DOX and S4, S4-HA, S4-DOX e S4-DOX-HA at concentrations of 0.1, 1 and 10 µM. Each value represents the mean ± SD of experiments conducted in triplicate.

In vitro cellular uptake

To evaluate the intracellular distribution of the encapsulated Doxorubicin, HeLa cells were placed in contact with the different prepared devices and incubated at 37 °C. The images obtained showed that the free drug, having a lipophilic portion in its structure, could be internalized in HeLa cells and localize at the nuclear level. A similar situation was observed for DOX-loaded cationic niosomes which from the images obtained appear to be localized in the same cellular pattern (**Figure 6**). In fact, positively charged systems have an intrinsic capacity to be internalized by cells given the ability to interact with negatively charged cell membranes. An important observation concerns the coated niosomes containing the drug; from the images shown in Figure 6 we can see a punctiform fluorescence concentrated at the cytoplasmic level. This could indicate a localization of doxorubicin no longer only in the nucleus, but also in other cellular organelles such as mitochondria, lysosomes, and the Golgi apparatus [24]. This suggests that coated niosomes are taken up by HeLa cells by a different mechanism than free, uncoated drug niosomes and which appears to involve the CD44 receptor.

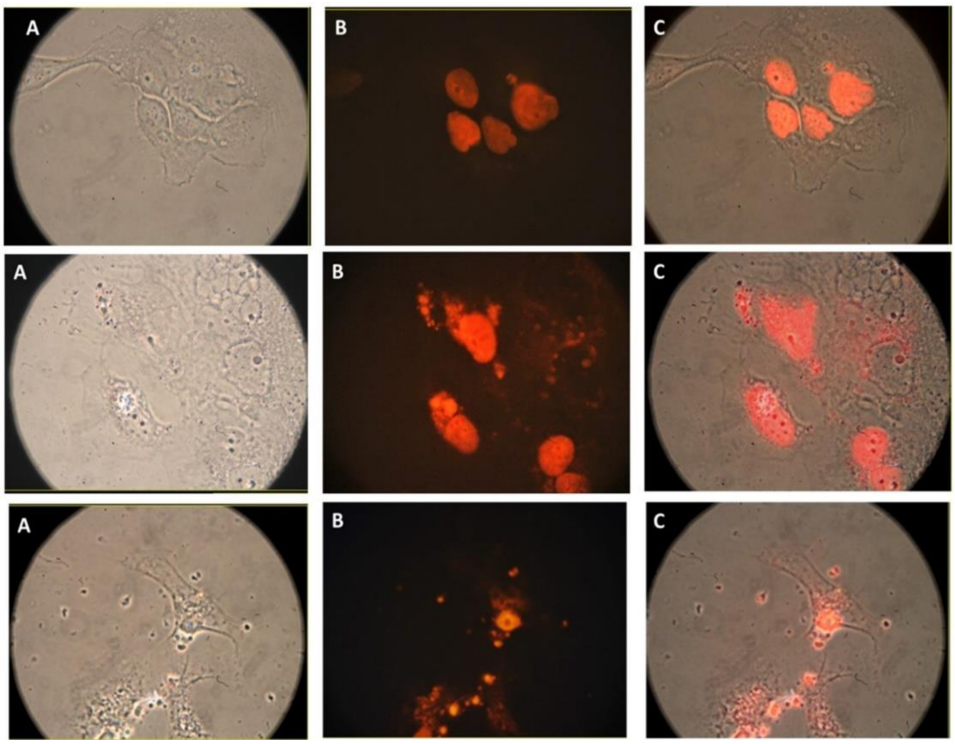

1. DOX

2. S4-DOX

3. S4-DOX-HA

Figure 6. Fluorescence microscopy analysis after incubation for 4 hours with [1] DOX, [2] S4-DOX, [3] S4-DOX-HA. Images: [A] in phase contrast, [B] fluorescence detected at 488 nm and [C] superposition of the previous ones

Conclusions

In this study, cationic niosomes with tumor-targeting properties were developed as systems for intracellular delivery of DOX. The formulated systems were successful as they showed selective toxicity towards tumor cells compared to healthy cells. Surface functionalization of the vesicles was achieved by cross-linking with HA, which conferred selectivity to the systems. The coated nanocarriers showed faster release in acidic environments compared to the corresponding uncoated nanocarriers. While in a physiological environment the slower release showed good physiological stability. *In vitro* studies have demonstrated that these new coated cationic systems are non-hemolytic over the range of concentrations tested. Cross-linking with HA appears to promote internalization of the nanosystems into tumor cells, leading to even greater toxicity on tumor cells compared to the free drug solution. Toxicity to healthy cells, however, is lower when cross-linking is present, thus demonstrating the selectivity of conjugated systems. Cellular uptake studies have also demonstrated the ability of the formulated niosomes to be internalized by tumor cells, but with a different localization based on the presence or absence of HA. Consequently, the designed nanodevices represent promising delivery

systems for targeted cancer therapy, which will be further studied to demonstrate their efficacy and safety.

Reference

[1] Gmeiner, W. H., & Ghosh, S. (2014). Nanotechnology for cancer treatment. *Nanotechnology reviews*, *3*(2), 111-122.

[2] Chamundeeswari, M., Jeslin, J., & Verma, M. L. (2019). Nanocarriers for drug delivery applications. *Environmental Chemistry Letters*,*17*, 849-865.

[3] Din, F. U., Aman, W., Ullah, I., Qureshi, O. S., Mustapha, O., Shafique, S., & Zeb, A. (2017). Effective use of nanocarriers as drug delivery systems for the treatment of selected tumors. *International journal of nanomedicine*, 7291-7309.

[4] Kalyane, D., Raval, N., Maheshwari, R., Tambe, V., Kalia, K., & Tekade, R. K. (2019). Employment of enhanced permeability and retention effect (EPR): Nanoparticle-based precision tools for targeting of therapeutic and diagnostic agent in cancer. *Materials Science and Engineering: C*, *98*, 1252-1276.

[5] Vander Heiden, M. G., Cantley, L. C., & Thompson, C. B. (2009). Understanding the Warburg effect: the metabolic requirements of cell proliferation. *science*, *324*(5930), 1029-1033.

[6] Michele A. Floriano e Marco Russo. ―I modelli nelle Scienze‖. Quaderni di Ricerca in Didattica, numero speciale 6 (pag 4-12). 2019

[7] Lee, H. S., Seo, E. Y., Kang, N. E., & Kim, W. K. (2008). [6]-Gingerol inhibits metastasis of MDA-MB-231 human breast cancer cells. *The Journal of nutritional biochemistry*, *19*(5), 313-319.

[8] Torretta, A., De Berardis, B., Cicconi, M., Marinelli, S., Romanelli, P., Cacciatore, G., ... & Lucantoni, R. (2006). CASI CLINICI Gastric carcinoid: Case report and review of the literature *Ann. Ital. Chir*, *77*(3), 253.

[9] Lucey, B. P., Nelson-Rees, W. A., & Hutchins, G. M. (2009). Henrietta Lacks, HeLa cells, and cell culture contamination. *Archives of pathology & laboratory medicine*, *133*(9), 1463-1467.

[10] Ebert, T. B. N. H., Bander, N. H., Finstad, C. L., Ramsawak, R. D., & Old, L. J. (1990). Establishment and characterization of human renal cancer and normal kidney cell lines. *Cancer research*, *50*(17), 5531-5536.

[11] Miret, S., De Groene, E. M., & Klaffke, W. (2006). Comparison of in vitro assays of cellular toxicity in the human hepatic cell line HepG2. *SLAS Discovery*, *11*(2), 184-193.

[12] Lesley, J., He, Q., Miyake, K., Hamann, A., Hyman, R., & Kincade, P. W. (1992). Requirements for hyaluronic acid binding by CD44: a role for the cytoplasmic domain and activation by antibody. *The Journal of experimental medicine*, *175*(1), 257-266.

[13] Song, L., Pan, Z., Zhang, H., Li, Y., Zhang, Y., Lin, J., ... & Hou, Z. (2017). Dually folate/CD44 receptor-targeted self-assembled hyaluronic acid nanoparticles for dual-drug delivery and combination cancer therapy. *Journal of Materials Chemistry B*, *5*(33), 6835-6846.

[14] Alyane, M., Barratt, G., & Lahouel, M. (2016). Remote loading of doxorubicin into liposomes by transmembrane pH gradient to reduce toxicity toward H9c2 cells. *Saudi pharmaceutical journal*, *24*(2), 165-175

[15] La-Beck, N. M., Zamboni, B. A., Gabizon, A., Schmeeda, H., Amantea, M., Gehrig, P. A., & Zamboni, W. C. (2012). Factors affecting the pharmacokinetics of pegylated liposomal doxorubicin in patients. *Cancer chemotherapy and pharmacology*, *69*, 43-50.

[16] Even-Or, O., Joseph, A., Itskovitz-Cooper, N., Samira, S., Rochlin, E., Eliyahu,H., Goldwaser, I., Balasingam, S., Mann, A.J., Lambkin-Williams, R., Kedar, E., Barenholz, Y. A new intranasal influenza vaccine based on a novel polycationic lipid-ceramide carbamoyl -spermine (CCS). II. Studies in mice and ferrets and mechanism of adjuvanticity, Vaccine. 2011, 29,2474–2486.

[17] Tantisripreecha, C., Jaturanpinyo, M., Panyarachun, B., Sarisuta, N. Development of delayed-release proliposomes tablets for oral protein drug delivery. Drug Dev. Ind. Pharm.2012, 38, 718–727.

[18] Fenton, R. R., Easdale, W. J., Er, H. M., O'Mara, S. M., McKeage, M. J., Russell, P. J., & Hambley, T. W. (1997). Preparation, DNA binding, and in vitro cytotoxicity of a pair of enantiomeric platinum (II) complexes,[(R)-and (S)-3-aminohexahydroazepine] dichloro-platinum (II). Crystal structure of the S enantiomer. *Journal of medicinal chemistry*, *40*(7), 1090-1098.

[19] Pape, W. J., Pfannenbecker, U., & Hoppe, U. (1987). Validation of the red blood cell test system as in vitro assay for the rapid screening of irritation potential of surfactants. *Molecular toxicology*, *1*(4), 525-536.

[20] Mazzotta, E., De Benedittis, S., Qualtieri, A., & Muzzalupo, R. (2019). Actively targeted and redox responsive delivery of anticancer drug by chitosan nanoparticles. *Pharmaceutics*, *12*(1), 26.

[21] Alyane, M., Barratt, G., & Lahouel, M. (2016). Remote loading of doxorubicin into liposomes by transmembrane pH gradient to reduce toxicity toward H9c2 cells. *Saudi pharmaceutical journal*, *24*(2), 165-175.

[22] Hasan, A. A., Madkor, H., & Wageh, S. (2013). Formulation and evaluation of metformin hydrochloride-loaded niosomes as controlled release drug delivery system. *Drug delivery*, *20*(3-4), 120-126.

[23] Salarpour, S., Rajaee, M., Mohajeri, E., Hobab, M., Ohadi, M., Banat, I. M., & Dehghannoudeh, G. (2021). A Thermodynamic Micellization and Hemolysis Evaluation of Polysorbate Surfactants in Combination with Short-Chain Alcohols. *Journal of Cluster Science*, 1-9.

[24] Gillies, E. R., & Fréchet, J. M. (2005). pH-responsive copolymer assemblies for controlled release of doxorubicin. *Bioconjugate chemistry*, *16*(2), 361-368.

2.2 Multifunctional chitosan nanoparticles for mitochondrial target in cancer therapy

Introduction

Mitochondrial dysfunction contributes to a wide variety of human disorders, ranging from neurodegenerative and neuromuscular diseases to obesity and diabetes, to ischemia-reperfusion injury and cancer. The identification of molecular targets of mitochondrial drugs together with the development of methods necessary to selectively deliver biologically active molecules to mitochondria have laid the foundation for new therapies for the treatment of mitochondria-related pathologies. Polymeric nanoparticles are among the most promising DDSs given their effectiveness in improving the pharmacokinetic and biodistribution profiles of drugs with high selectivity and specificity. The advantages of NPs include prolonged systemic circulation, high preferential accumulation at tumor sites by enhancing the EPR effect, and the ability to overcome P-glycoprotein-mediated multidrug resistance [1]. Our focus has been on chitosan-based NPs, since this polysaccharide provides an advantageous tool for the creation of administration systems given its biocompatibility, biodegradability, mucoadhesive and non-toxicity [2]. The presence of reactive functional groups offers the possibility of chemically modifying the molecule and therefore making it target-specific. Furthermore, the cationic nature of this polymer allows its use as a drug delivery system, thanks to electrostatic interactions with the negatively charged cell surface. Various methods have been developed to selectively target mitochondria, including the use of targeting ligands such as peptides and chemical compounds such as triphenylphosphonium. TPB (4-carboxybutyl triphenylphosphonium bromide) is a molecule composed of three phenyl groups, it is a cation with a delocalized positive charge and sufficient lipophilicity to facilitate transport and crossing of the mitochondrial barrier. Folic acid, on the other hand, is one of the most widely used ligands for active targeting, due to its advantages such as low cost, high stability, and wide range of conjugation reactions. In fact, FA can selectively bind to folate FR receptors, overexpressed by various tumor cells, ensuring its use as a pharmacological target in anti-tumor therapy [3,4]. Emerging research in cancer therapy focuses on exploiting the selective targeting and accumulation of mitochondria-targeted cations (MTCs) and their ability to alter ROS-mediated redox signaling and antiproliferative pathways in tumor cells [5,6,7]. Therefore, our goal was to synthesize multifunctional chitosan nanoparticles. They have been bifunctionalized using TPB, to ensure the mitochondrial

target and FA, to ensure the target to the FR receptors overexpressed in the tumor environment.

Materials

Chitosan (low molecular weight), TPB (4-carboxybutyl triphenylphosphonium bromide), Folic acid (FA), EDC (1-Ethyl-3-(3-dimethylaminopropyl) carbodiimide)), Rhodamine B, Fluorescein sodium salt and FITC (Fluorescein isothiocyanate) were purchased by Sigma Aldrich Milan, Italy, purity 99%). All organic solvents were supplied from Sigma-Aldrich (Milan, Italy).

Preparation of bi-functionalized chitosan

Chitosan-folic-TPB was synthesized by conjugation of TPB and folic acid to the chitosan backbone, either separately or in a two-step process. Initially, a polymer solution of 1% (w/v) chitosan in 1% (v/v) acetic acid was prepared. The carboxyl group of TPB was activated with EDC in distilled water for 1 hour and subsequently added drop by drop to the polymer solution, previously obtained, under magnetic stirring. The pH of the mixture was then adjusted to 5.5 by adding 1 M NaOH. The solution was then left under stirring for 4 hours in the dark at room temperature. Subsequently, the mixture was dialyzed using dialysis tubing (Spectra/Por®, cut-off 12–14 kDa), manipulated before use according to the Fenton method [6], for three days, first in HCl 5 mM, then twice with HCl containing 1% NaCl and finally with 1 mM HCl. Finally, the polymer was freeze-dried and stored at 4°C until further use.

Folic acid conjugation was achieved by adding EDC (0.04 mmol) to a solution of folic acid (0.02 mmol) in DMSO and stirring at room temperature for one hour. At this point, chitosan (100 mg/mL) was solubilized in 1% (v/v) acetic acid and added to the above solution. The solution was left under magnetic stirring at room temperature for 16 hours. at the end the solution was precipitated by adding NaOH reaching a pH of 9. The precipitate was then collected and dialyzed against an excess quantity of 0.1 M phosphate buffer (PBS) pH 7.4 for three days, and then with distilled water for another three days. Finally, the polymer was freeze-dried. The same procedure described initially was used for the synthesis of the CHIT/FOL/TPB derivative, adding the chitosan already functionalized with TPB to the folic acid solution, in the reaction described previously. Finally, we functionalized the chitosan with FITC to impart surface fluorescence to the polymer. A polymer solution of 1% (w/v) chitosan in 1% (v/v) acetic acid was added with solution of FITC (0.064 mmol), 25 mL of methanol anhydrous and stirring at room

temperature in the dark for 4 hours. The mixture was precipitated by adding NaOH 0.2 M at 2500 Rpm for30 min. The precipitate obtained was separated from the supernatant and then washed with ethanol to remove the unreacted drug. the last wash was conducted in distilled water and finally the polymer was lyophilized.

Nanoparticle preparations.

Multifunctional nanoparticles were prepared by ionic gelation. This technique involves the complexation of a cationic polymer (chitosan) with an anionic cross-linking agent, sodium triphosphate (TPP). Briefly, the functionalized chitosan derivatives were solubilized in 1% (v/v) acetic acid. As a model drug to evaluate the efficacy of mitochondrial targeting, three fluorescent molecules, rhodamine B (RHD), fluorescein sodium salt (FL), and FITC (fluorescein isothiocyanate), were used as molecules capable of emitting fluorescence. Corresponding concentrations of RHD ($1.36x10^{-4}$), FL ($1.36x10^{-2}$) were then added and the pH was adjusted to 5.5. Nanoparticles with FITC were obtained by functionalization of chitosan with this fluorescent molecule. Nanoparticles formed spontaneously after dropwise addition of TPP solution (2 mg/mL) under constant stirring. Finally, the NPs were purified by ultracentrifuge at 20,000 rpm for 90 min**.**

Physico-chemical characterization

The Np formulations were analysed for size and polydispersity determined by Zetasizer ZS Malvern Instruments Ltd. (Malvern, UK) at 25 ± 0.1 ◦C, 24 h after preparation. The Z potential analysis was also carried out with the same instrument, after dilution 1/50 in distilled water. All results are reported as the average of three independent experiments.

Drug encapsulation efficiency

The drug encapsulation efficiency was determined by UV-Vis spectrophotometry. the NPs were centrifuged, and the supernatant was separated. Therefore, an indirect method was used that involved evaluating the concentration of free drug in the supernatant at the specific length of the drug used. In particular, the wavelengths relating to the three drugs are: nm for FL, nm for RHD and nm for FITC. The drug encapsulation efficiency was calculated using the following equation:

$$E\% = \frac{Drug_{\text{tot}} - Drug_{\text{free}}}{Drug_{\text{tot}}} x\ 100$$

Results and discussions

Physical-chemical characterization

The multifunctional nanoparticle systems were analysed in terms of size, polydispersity index, Z-potential and encapsulation efficiency. The data obtained are reported in **Table 1.**

Table 1. Physical-chemical characterization of multifunctional nanoparticles in terms of size (nm), PI, Z-potential and drug loading at 25°C.

FORMULATIONS	SIZE (nm)	I.P.	Z POTENTIAL	E %
NP CHIT/TPB/FL	246.5	0.282	24.0 ± 2.16	93.80%
NP CHIT/FA/FL	263.3	0.282	20.2 ± 0.404	95.63%
NP CHIT/TPB/FA/FL	262.1	0.192	22.2 ± 0.606	97.67%
NP CHIT/CHIT-FA/CHIT-TPB/FL	276.5	0.155	21.3 ± 1.42	96.17%
NP CHIT-FA/CHIT-TPB/FL 50:50	249.3	0.275	46.4 ± 1.69	97.45%
NP CHIT/TPB/RDH	206.7	0.260	25.2 ± 1.66	56.20%
NP CHIT/FA/RDH	203.5	0.214	19.9 ± 0.265	59.00%

The results obtained showed that the NP formulations in each case have an optimal size between 200 and 270 nm. The polydispersity index, always lower than 0.3, shows monodispersed and homogeneous nanoparticle populations. The encapsulation efficiency of FL was found to be very high, for all the formulations that contained it, in particular with values above 90%. RDH, on the other hand, shows an EE% much lower than fluorescein but still above 50%, making it suitable for evaluating cellular uptake. FITC also showed rather high encapsulation efficiencies in formulations containing it. All formulations were therefore optimal for subsequent studies.

Conclusions

The aim of our study was to synthesize chitosan nanoparticles functionalized in such a way as to ensure a double target, mitochondrial and folate. Therefore, chitosan was functionalized with both TPB and FA. The formulations were prepared starting from the conjugated polymers and the nanoparticles were obtained by ionotropic gelation. The chemical-physical characterization studies have shown adequate results for biomedical applications, therefore subsequent studies will be carried out to evaluate the effective site-specific action of the nanoparticles.

Reference

[1] Bertrand, N.; Wu, J.; Xu, X.; Kamaly, N.; Farokhzad, O.C. Cancer nanotechnology: The impact of passive and active targeting in the era of modern cancer biology. *Adv. Drug Deliv. Rev.* 2014, *66*, 2–25.

[2] Kim, S. Competitive Biological Activities of Chitosan and Its Derivatives: Antimicrobial, Antioxidant, Anticancer, and Anti-Inflammatory Activities. *Inter. J. Polym. Sci* 2018, *1708172*, 13.

[3] Kelemen, L.E. The role of folate receptor α in cancer development, progression and treatment: Cause, consequence or innocent bystander? *Int. J. Cancer* 2006, *119*, 243–250.

[4] McGuire, J.J. Anticancer antifolates: Current status and future directions.*Curr. Pharm. Des.*2003,*9*, 2593–2613.

[5] Cheng, G.; Zielonka, J.; McAllister, D.; Hardy, M.; Ouari, O.; Joseph, J.; Dwinell, M. B.; Kalyanaraman, B. Antiproliferative Effects of Mitochondria-Targeted Cationic Antioxidants and Analogs: Role of Mitochondrial Bioenergetics and Energy-Sensing Mechanism. Cancer Lett. 2015, 365, 96−106.

[6] Rao, V. A.; Klein, S. R.; Bonar, S. J.; Zielonka, J.; Mizuno, N.; Dickey, J. S.; Keller, P. W.; Joseph, J.; Kalyanaraman, B.; Shacter, E. The Antioxidant Transcription Factor Nrf2 Negatively Regulates Autophagy and Growth Arrest Induced by the Anticancer Redox Agent Mitoquinone. J. Biol. Chem. 2010, 285, 34447−34459.

[7] Sassi, N.; Mattarei, A.; Azzolini, M.; Szabo, I.; Paradisi, C.; Zoratti, M.; Biasutto, L. Cytotoxicity of Mitochondria-Targeted Resveratrol Derivatives: Interactions with Respiratory Chain Complexes and ATP Synthase. Biochim. Biophys. Acta, Bioenerg. 2014, 1837, 1781−1789.

[6] Fenton, R.R.; Easdale, W.J.; Er, H.M.; O'Mara, S.M.; McKeage, M.J.; Russell, P.J.; Hambley, T.W. Preparation, DNA binding, and in vitro cytotoxicity of a pair of enantiomeric platinum (II) complexes, [(R)-and (S)-3-aminohexahydroazepine] dichloro-platinum (II). Crystal structure of the S enantiomer. *J. Med. Chem.* 1997, *40*, 1090–1098.

Chapter 3:

Nanosystems for topical and transdermal drug delivery

3.1 Pluronic 123 liquid lyotropic crystals for transdermal delivery of caffeic acid - insights from structural studies and release profiles.

Martina Romeo[1], Elisabetta Mazzotta[1], Francesca Lovati[1], Michele Porto[2], Cesare Oliverio Rossi[2], Rita Muzzalupo[1*]

[1] Department of Pharmacy, Health and Nutritional Sciences, University of Calabria, via P. Bucci, 87036 Arcavacata di Rende (CS), Italy;
[2] Department of Chemistry and Chemical Technologies, Cubo 14/D, University of Calabria, via P. Bucci, 87036 Arcavacata di Rende (CS), Italy.

Published to *Gels*. 2024;10(3):181.

GRAPHICAL ABSTRACT

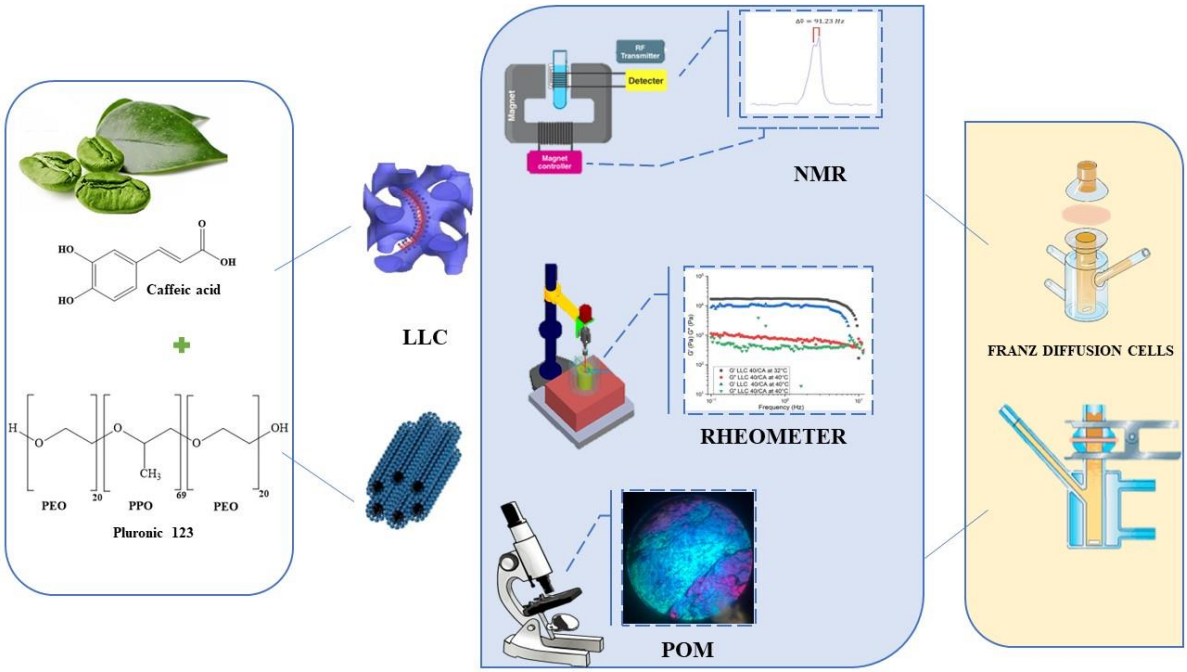

ABSTRACT

Background: This study aims to evaluate the percutaneous permeation profiles of caffeic acid (CA) from cubic and hexagonal liquid crystalline phases of Pluronic P123/water mixtures.

Method: The resulting drug-loaded mesophases were subjected to characterization through deuterium nuclear magnetic resonance spectroscopy and polarized optical microscopy observations. These analyses aimed to evaluate the structural changes that occurred in the mesophases loading with CA. Additionally, steady and dynamic rheology studies were conducted to further explore their mechanical properties and correlate them to the supramolecular structure. Finally, CA release experiments were carried out at two

different temperatures to examine the behaviour of the structured systems in a physiological or hyperthermic state.

Results: As the concentration of the polymer increases, an increase in the viscosity of the gel is noted; however, the addition of caffeic acid increases microstructure fluidity. It is observed that the temperature effect conforms to expectations. The increase in temperature causes a decrease in viscosity and, consequently, an increase in the rate of permeation of caffeic acid.

Conclusions: The CA permeation profile from the prepared formulations is mostly dependent on the structural organization and temperature. Cubic mesophase LLC 30/CA showed greater skin permeation with good accumulation in the skin at both tested temperatures.

1. Introduction

In recent years, antioxidants have gained increasing interest in the pharmaceutical, cosmetic, medical, and food sectors due to their many benefits. These prophylactic molecules play a crucial role in the prevention and management of pathologies associated with oxidative stress, such as cancer [1], atherosclerosis [2], diabetes [3], ocular diseases [4], and Alzheimer's disease [5]. Their action involves inhibiting or reducing the effects caused by free radicals and oxidizing compounds. Due to regulatory restrictions on the use of synthetic antioxidants, driven by potential risks associated with in vivo administration, there is a growing interest in natural antioxidants [6]. Among these, phenolic antioxidants act as scavengers of reactive species, including free radicals, actively participating in metal chelation during the oxidative process. The donation of an electron or hydrogen atoms stabilizes free radicals, imparting antioxidant activity [7]. An example of a phenolic antioxidant is caffeic acid (CA), also known as 3,4-dihydroxycinnamic acid, found in blueberries, apples, cider, coffee, and propolis. In addition to its antioxidant properties, CA exhibits antimicrobial activity, antiinflammatory activity, is known as a cancer inhibitor, and contributes to the prevention of heart diseases and atherosclerosis. Several studies have indeed demonstrated the ability of CA to counteract inflammation evident in various diseases, such as skin conditions like atopic dermatitis [8, 9], and intestinal disorders like ulcerative colitis and Crohn's disease [10]. CA has gained considerable attention in the pharmaceutical field as a promising photoprotective agent and for skincare. However, the poor water solubility and low chemical stability of CA require the use of suitable delivery

systems to ensure solubilization, protection from degradation, and pharmaceutical efficacy [11,12]. The field of nanotechnology has indeed focused extensively on antioxidant molecules due to their numerous benefits, despite their low bioavailability and improper release into undesired cellular compartments. Consequently, this has led to the development of antioxidant nanosystems [13, 14] aimed at enhancing the effectiveness of conventional antioxidants, improving stability, increasing bioavailability, and ensuring a controlled and targeted release. In recent years, research on transdermal delivery systems has undergone considerable development, focusing on a wide range of drug carriers, such as liposomes, niosomes, microemulsions, transdermal patches, microneedles, etc... The first approved transdermal delivery system was the scopolamine patch for motion sickness in 1979. Since then, drugs, such as non-steroidal anti-inflammatory [15], antimicrobials [16], antioxidants [17] and anti-cancer [18], have been successfully formulated as transdermal drug delivery systems (TDDS). Transdermal drug delivery systems, such as lyotropic liquid crystals (LLC), are considered promising alternatives to improve pharmacological effectiveness, safety, and patient compliance [19]. The LLC are soft materials that combine their anisotropic order with the mechanical stability of a gel. A significant advantage of LLCs is their ability to act as a barrier that controls the rate of release of encapsulated drugs [20,21]. This allows a prolonged drug release while maintaining effective concentrations in the desired region. Lyotropic liquid crystals (LLC) or self-assembling materials are typically formed from water and surfactants in well-defined ratios. The structure-forming surfactants can absorb a certain amount of water and then spontaneously form gel-like phases with unique internal structures. They self-assemble into cubic, hexagonal (H_2), and lamellar (Lα) mesophases, depending on the concentration of constituents and temperature [22]. Among the surfactants most used for LLC formulation are Pluronic surfactants, which are block copolymers consisting of repeating units of ethylene oxide (EO) and propylene oxide (PO), represented by the general formula $(PEO)_n(PPO)_m(PEO)_n$. Pluronic P123 ($EO_{20}PO_{70}EO_{20}$), depending on temperature and concentration, is capable of making various structures in water [23,24], as observed in the phase diagram of the P123-water system determined by Wanka et al.[25].

The purpose of this article is to evaluate the percutaneous permeation profile of CA from cubic and hexagonal liquid crystalline phases of Pluronic P123/water mixtures, and identify how transdermal drug delivery was affected by the gel- like microstructure at different bodily functions. In detail, permeation and diffusion studies were performed at

32°and 40°C, to highlight any differences between physiological conditions while, the data on the characterization were carried out also at 25°C to point out our formulations storage temperature. Mesophases obtained, with or without CA, were analysed by deuterium nuclear magnetic resonance spectroscopy (^{2}H-NMR), polarised optical microscopy (POM) observations and by dynamic rheology experiments, to identify the influence of CA in the mesophases structures

2. Results and discussion

2.1 LLC physical-chemical characterization

Pluronic P123 (EO20PO70EO20), belonging to the PEO-PPO-PEO block copolymer series, has been widely used in cosmetics, pharmaceuticals, the food industry, etc. [26] The phase behaviour in water was studied by Wanka et al. [25] and shown in Figure 1.

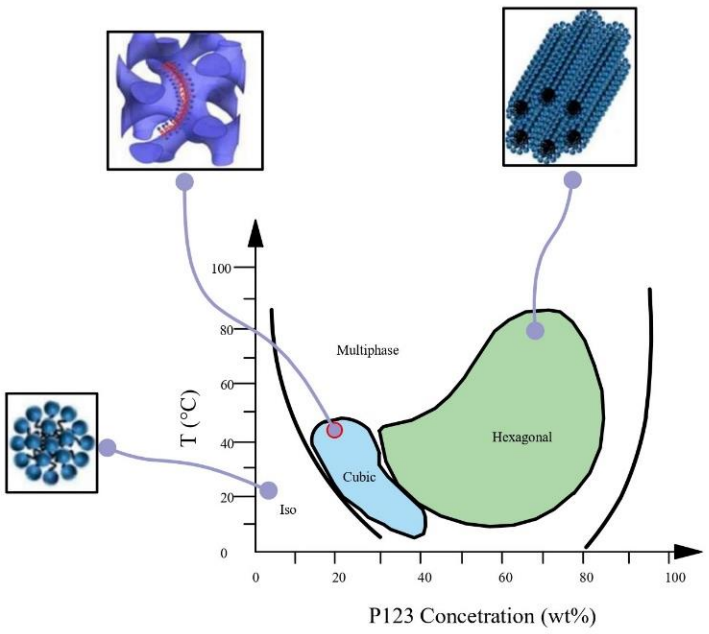

Figure 1. Phase diagram of the Pluronic P123 redrawn from [25].

Different mesophases such as isotropic, cubic, and hexagonal are formed by increasing the copolymer concentration increases and changing the temperature. Based on this phase diagram, samples were made with three different concentrations of P123: 30 wt% (LLC30), 40 wt% (LLC40) and 45 wt% (LLC45). At these concentrations and in the temperature range 32-40°C, the cubic and hexagonal phases in the P123/water binary system are reported. Typically, the hexagonal phase consists of rod-shaped micelles arranged in a three-dimensional hexagonal lattice [27]. While the cubic phase is characterised by a spherical arrangement, with the polar segment of the molecule positioned on the surface of the sphere and the non-polar segment residing in the center

of the sphere [28]. The incorporation of drugs into the mesophase composition could induce structural changes, so it was decided to test two hexagonal structures at 40% and 45%. The 40% P123/water hexagonal structure was identified as the system most affected by the introduction of a third component, as it is closest to the boundary phase between the cubic and hexagonal phases. Therefore, CA was added to P123, to assess its effect on the structural organization of the LLC and the possible improvement of drug penetration into the skin. The amount of CA in the LLC was always 0.5 wt%. Visually, LLC 40 and LLC 45 had a gel-like consistency, high viscosity and birefringence, while LLC 30 was less viscous and isotropic.

The characterization of liquid crystalline phases was carried out using the polarizing optical microscope (POM). Indeed, hexagonal mesophase are anisotropic and birefringent as, having mostly two refractive index, they can split the polarised light ray into two radiations that oscillate at different frequencies, while cubic mesophases are isotropic and they appeared as solutions. POM observation allowed us to identify hexagonal phases (LLC 40, LLC 45) because they are birefringent, but not cubic phase (LLC 30) which is isotropic. Figure 2 shows the typical hexagonal texture of LLC 45 formulations at different temperature.

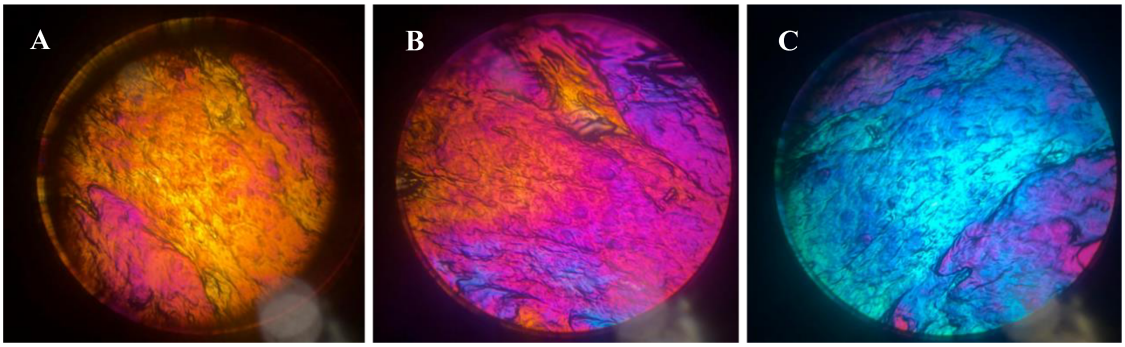

Figure 2. POM images of mesophase LLC45 at (A) 25°C, (B) 32°C and (C) 40°C.

LLC were analysed by magnetic nuclear resonance ^{2}H-NMR. Empty LLC and CA-loaded LLC were evaluated at three temperatures (25°C, 35°C and 40°C). LLC 30 showed a typical spectrum of cubic phase at each temperature, confirming the POM observation. While, LLC 40, was shown an indicative biaxial spectrum typical of hexagonal phase at each temperature, LLC 45 appears to show a uniaxial spectrum at all the recorded temperature, as shown in Figure 3, but the same formulation both under the microscope and observation in polarised light shows birefringence (Figure 2). This could be related to the lack of long-range order in the gel microstructure, or even to the fact that it takes a much longer time (as opposed to a few weeks) to reach homogeneity, as reported in the

literature. [29]. Therefore, the spectra obtained could be due to the presence of very small domains, which do not reveal the structure at NMR times. By introducing caffeic acid, even in a small percentage, disorder is generated in all structured phases as can be seen in Figure 4. The division of the quadrupolar peak or the width at half-height of the recorded spectrum becomes smaller as the drug is introduced.

25°C	35°C	40°C	LLC
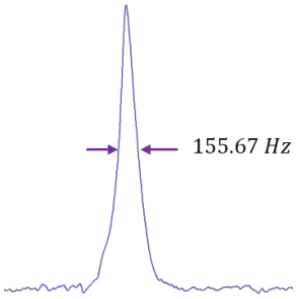	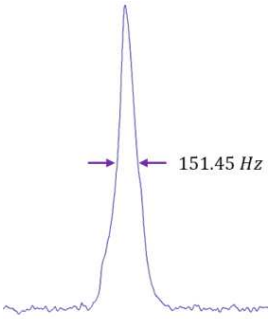	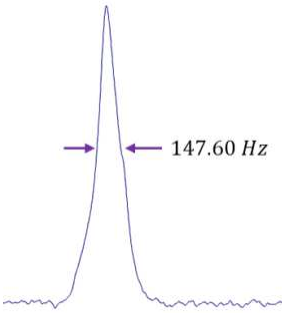	**30**
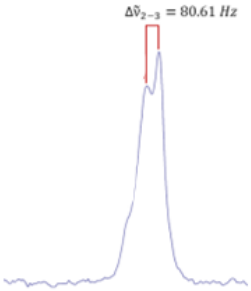	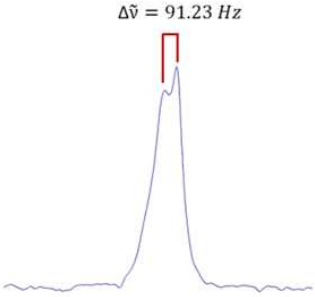	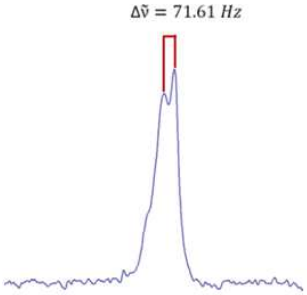	**40**
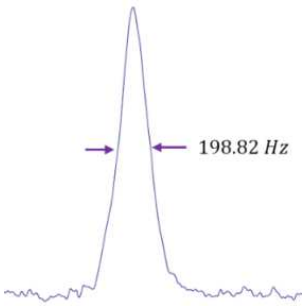	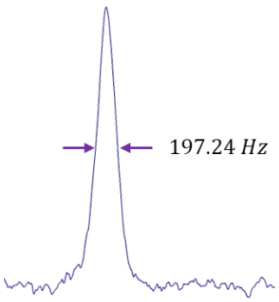	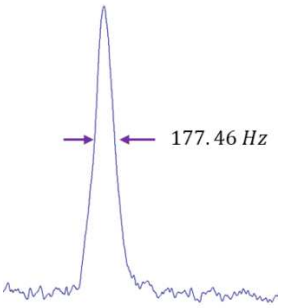	**45**

Figure 3. ^{2}H-NMR spectra of LLC 30, LLC 40 and LLC 45 at 25°C, 35°C and 40°C.

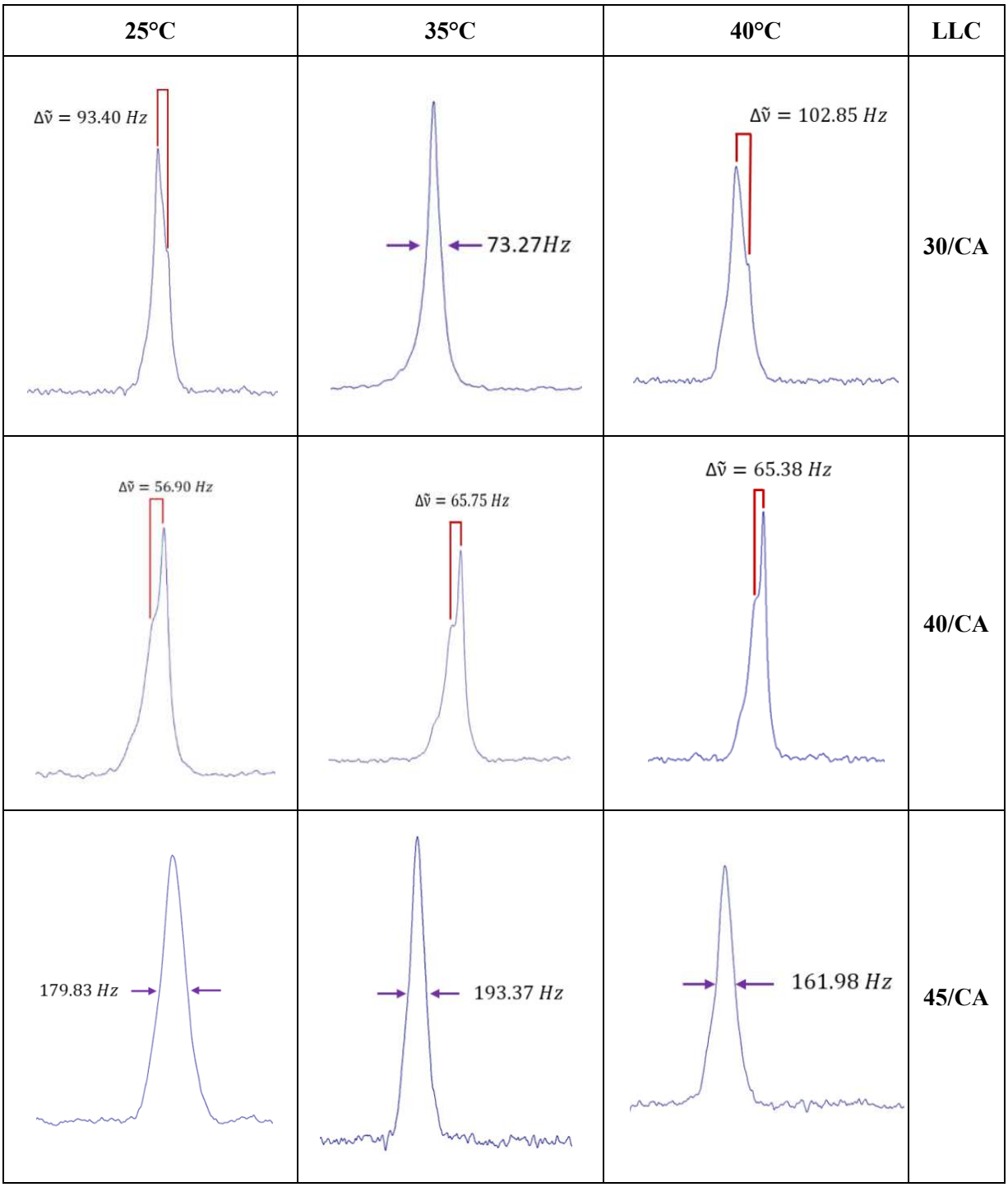

Figure 4. ^{2}H-NMR spectra of LLC 30/CA, LLC 40/CA and LLC 45/CA at 25°C, 35°C and 40°C.

2.2 Rheological characterisation

For the steady flow experiments, the temperature and concentration dependence of the viscosity are reported in Table 1. The data suggest the presence of a low-viscous gel at lower concentration, while the system becomes more viscous with increasing the concentration of P123 polymer. It is worthy note the fluidifying effect of the addition of CA in the systems, marked by the decreasing of viscosity. The effect of the temperature is expected. The viscosity decreases with increasing temperature, and this is due to kinetic effects. The LLC40/CA shows a higher viscosity value at 40°C. This data suggests a structural modification along this isopletal line.

Table 1. Formulations viscosity values at 25 °C, 32°C and 40°C at 100 Pa of stress. Error percentage is about 3%.

Formulations	Eta Pa s 25 °C	Eta Pa s 32°C	Eta Pa s (40°C)
LLC 30	3x 10^5	0.3	0.25
LLC 30/CA	3x 10^5	0.2	0.18
LLC 40	8x 10^5	3x 10^5	2x10^5
LLC 40/CA	8x 10^5	1x10^4	2x10^5
LLC 45	1x 10^6	1x10^6	7x 10^5
LLC 45/CA	1x 10^6	4x10^5	6 x10^5

At low temperature (25°C), the viscosity is higher and at this temperature it is not possible to appreciate the effect of CA on the structure since the changes are within the experimental error. Typical strong gel spectra, consisting of two nearly horizontal straight lines on G' and G'', were recorded. In Figure 5 the dynamic spectra for the 40% sample are shown. G' is typically one order of magnitude greater than G'', quite apart from the temperature considered. However, it must be mentioned that while the mechanical profile for all mixtures appears similar, differences can be observed in the value of the elastic and viscous moduli. They are lower with CA addition and at higher temperatures.

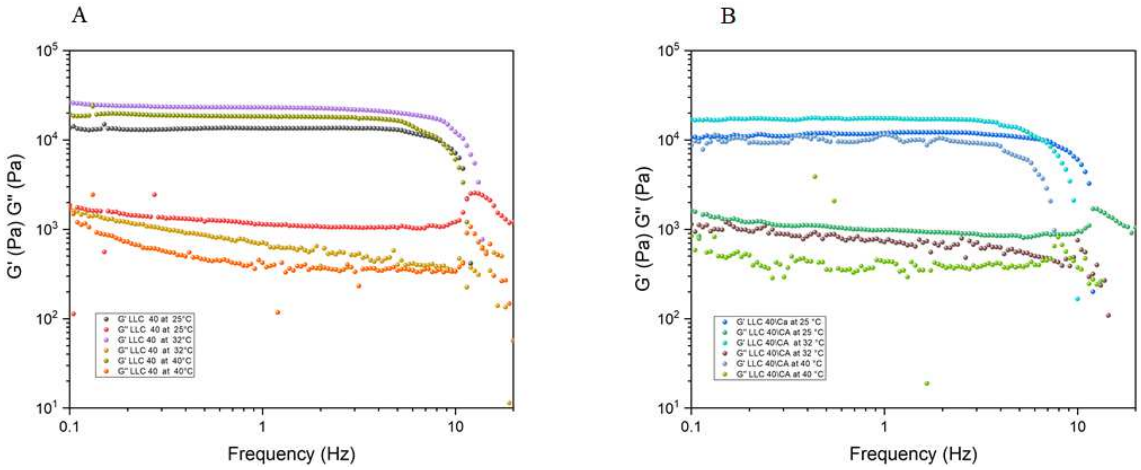

Figure 5. G' and G''Representation of (**A**) LLC 40 at 25°C, 32°C and 40°C and (**B**) LLC 40/CA at 25°C, 32°C and 40°C.

Dynamic shear experiments (Figure 6) show the composition and temperature dependence of the model parameters of the weak gel, z and A, obtained by fitting the viscoelastic data to Eq. 5. The system exhibits a high flow coordination number, z, and high interaction strength values, A, in the hexagonal phase. Additionally, these data confirm the presence of the gel that becomes stronger with increasing polymer concentration. The flow coordination number jumps from a value close to 10 (cubic phase) up to about 90 for mixtures at 45 wt% when a hexagonal phase is formed. This means a hardening of the gel network and a different structural organization in the hexagonal phase, characterized by the increasing of A and z respectively.

Once again, the effect of adding CA is evident for the LLC 30 and LLC 45 mixtures, where the A and z parameters decrease in presence of the CA and with the increasing of the temperature. The LLC 40/CA mixture, although weaker in terms of gel interactions (A), shows a higher coordination number than the mixture without CA at 32°C, additionally, it keeps constant in temperature. This trend is reversed for all other investigated mixtures. The A and z decrease both with the addition of CA and with increasing temperature. It appears that CA induces a more coordinated tridimensional structure, which not modified by temperature.

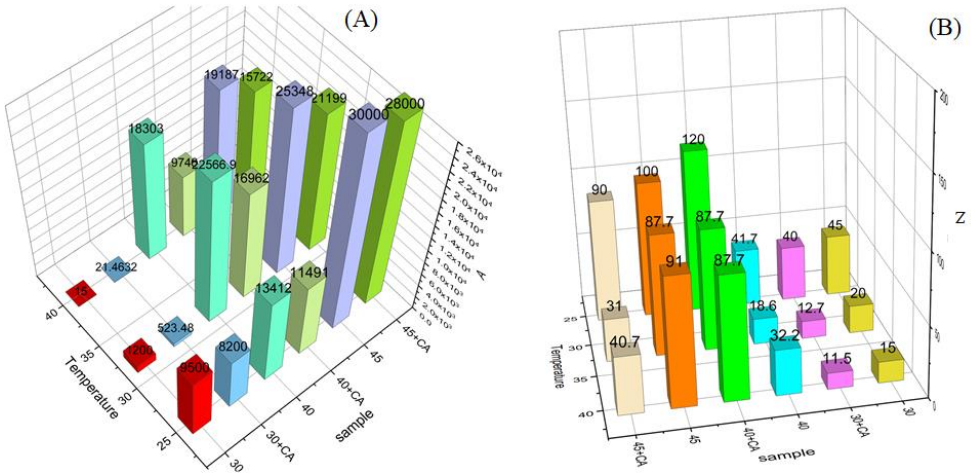

Figure 6. Weak-gel model parameters for the investigated formulations. The "gel strength", A (**A**) and the "flow coordination number", z, (**B**) are shown at different temperatures.

2.3 *In vitro* diffusion and *ex vivo* permeation studies

Diffusion studies (Figure 7) were performed using cellulose membranes for 24 h. LLC 30/CA was the formulation capable of releasing the highest amount of CA, corresponding to 625.67 µg/cm^2 at 32°C and 714.38 µg/cm^2 at 40°C. The other two structured phases showed a similar release profile at both temperatures.

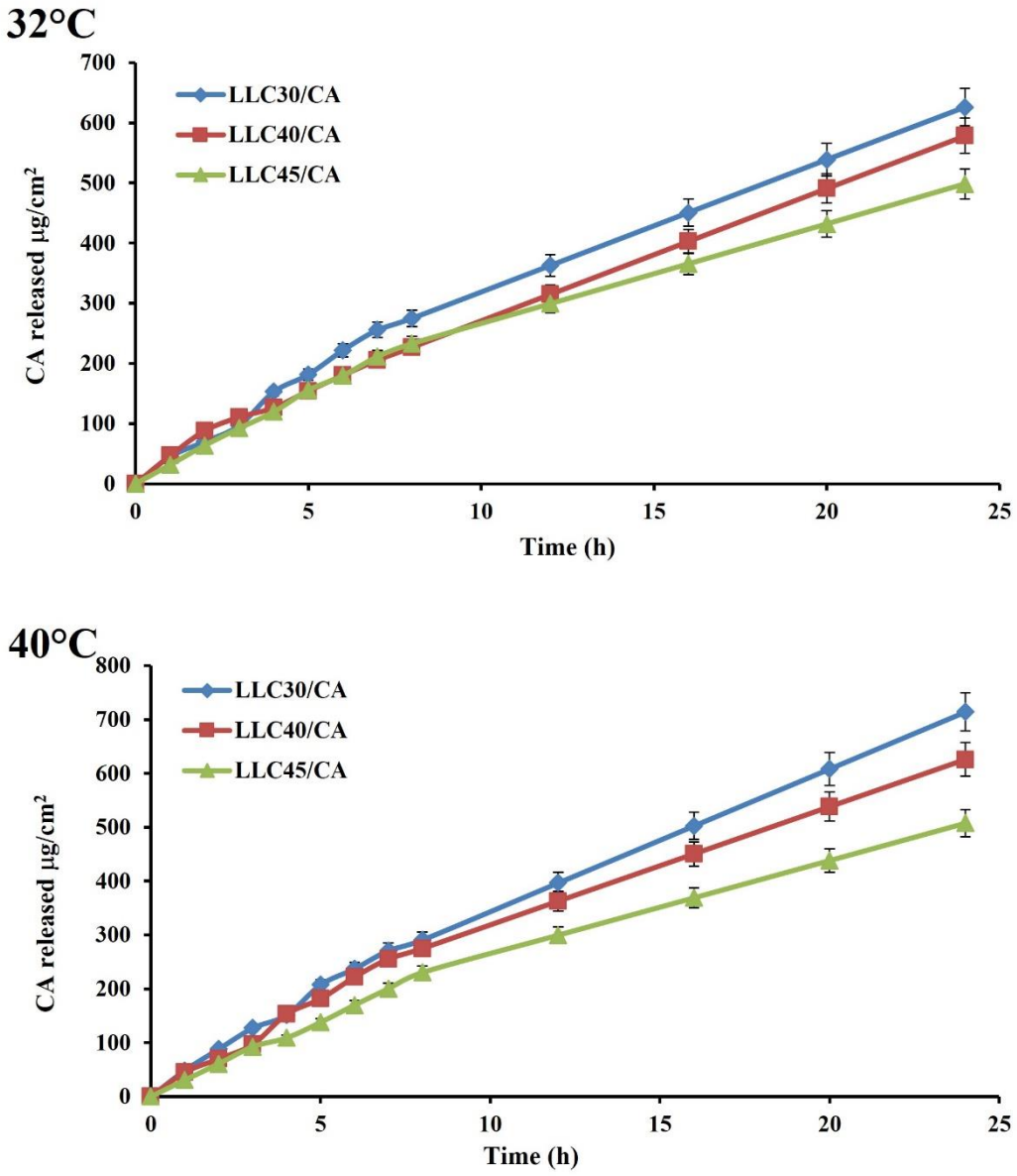

Figure 7. Diffusion profiles: **A** at 32°*C;* **B** at 40°C.

The diffusion coefficient (D, cm^2/s) for formulations investigated in diffusion studies at both 32°C and 40°C, were determined using Higuchi's equation (Eq. 1) [30]:

$$\frac{Q}{C_0} = 2\sqrt{\frac{D}{\pi}}\sqrt{t} \quad (1)$$

Where Q is the molar flow of the drug across the surface, C_0 is the drug concentration and t is the release time.

The diffusion of drugs loaded in LLC phases is influenced by both structural factors and external factors such as temperature. Normally the diffusion of drugs from cubic phases is faster than from hexagonal ones and the increase in temperature causes an increase in the diffusion of the loaded drug [31].

For our LLC formulations, diffusion coefficients (Table 2) were higher in cubic (LLC 30/CA) than hexagonal phase (LLC 40/CA and LLC 45/CA), while were affected little by temperature in the LLC 40 and LLC45 formulations while in the LLC 30 formulation, the diffusion was more affected by increasing temperature, also shown by the rheological data.

Table 2. Diffusion coefficient (D)and R^2 value of formulations tested. ***p* value< 0.05 32°C vs. 40°C.

T (°C)	LLC 30/CA	LLC 40/CA	LLC 45/CA
32°C	$D= 5.82x10^{-15}$	$D= 3.86x10^{-15}$	$D= 2.19x10^{-15}$
	$R^2= 0.9882$	$R^2= 0.9881$	$R^2= 0.9940$
40°C	$^{*}D= 7.38x10^{-15}$	$D= 3.29x10^{-15}$	$D= 2.29x10^{-15}$
	$R^2= 0.9817$	$R^2= 0.9662$	$R^2= 0.9869$

The statistical analysis confirmed that increasing temperature a significant difference in drug release was observed (p value <0.05) for LLC 30/CA, while LLC 40/CA and LLC 45/CA did not show no significant difference at either temperature.

Permeation profiles of P123 lyotropic liquid crystals with CA were performing using rabbit ear skin, with vertical Franz diffusion cells for 24h at 32°C and 40°C and the amount of released CA was assessed with UV spectroscopy at 286 nm. For LLCs, the release profile is strongly influenced by the phase taken up by microstructure, e.g. the cubic phase releases encapsulated drugs faster than the hexagonal phase [32,33]. At both temperatures, a faster and higher release can be seen for LLC 30/CA, 42.78 μg/cm^{2,} and 89.70 μg/cm^2 respectively. Furthermore, at 40°C, LLC 45/CA released faster than LLC 40/CA, in contrast to 32°C (Figure 8).

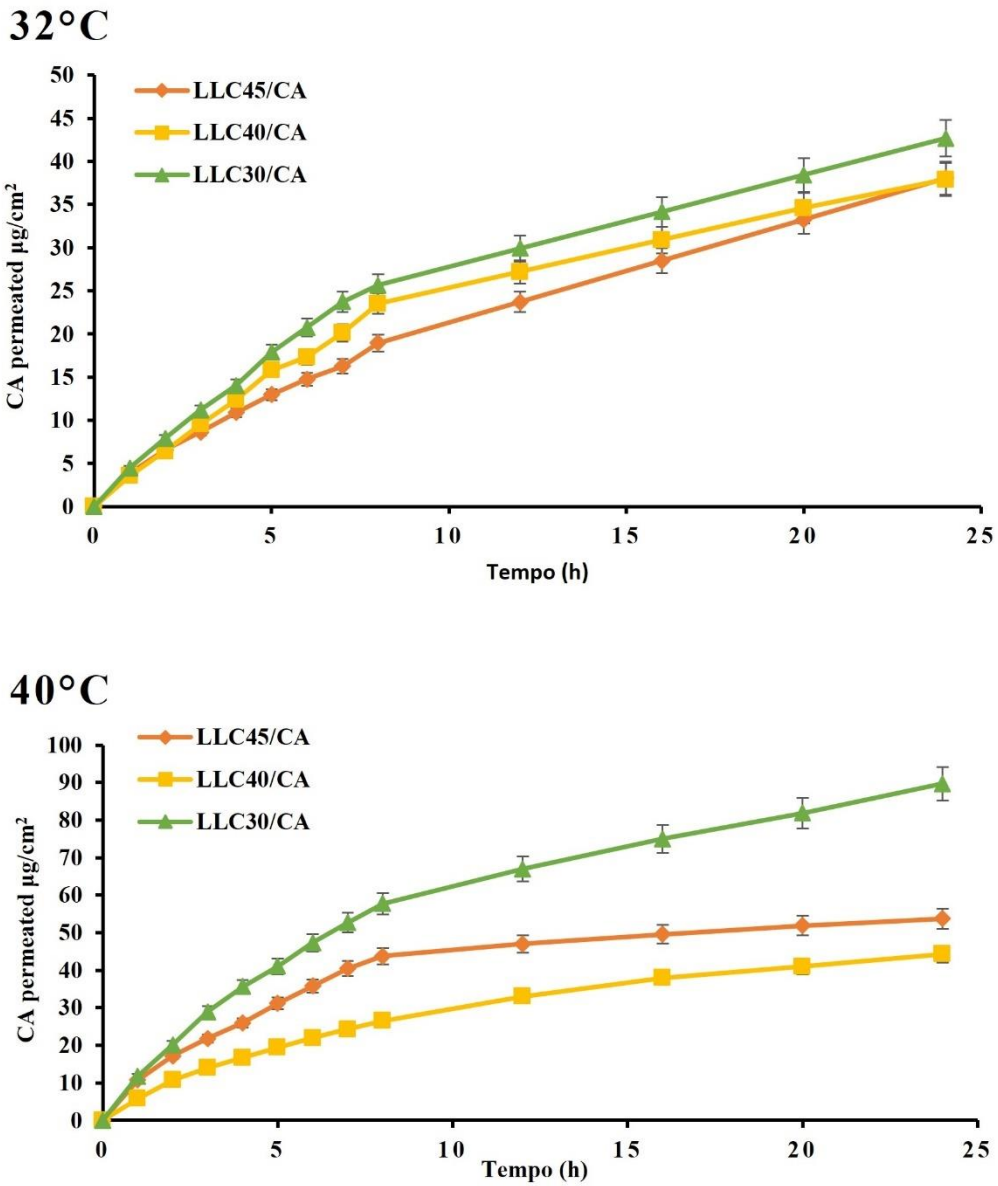

Figure 8. Permeation profiles through rabbit ear skin:**A** at 32°*C;* **B** at 40°C.

In skin permeation studies, two parameters are crucial: the permeability coefficient (*Kp*) and the steady-state flux (J_{ss}). The permeability coefficient is calculated from the flux and initial concentration (*Ci*) of polyphenols in the donor compartment, while the steady-state flux measures the amount of permeant crossing the membrane at a constant rate (Eq. 2) and reported in table 3:

$$Kp = \frac{J}{Ci} \tag{2}$$

Table 3. Permeation coefficient (Kp) and steady-state flux(Jss) values of formulations tested.

T (°C)	LLC 30	LLC 40	LLC 45
32°C	*Jss*=3.2196 *Kp*=4.50x10^{-4}	*Jss*=3.0448 *Kp*=3.65x10^{-4}	*Jss*=1.9829 *Kp*=2.18x10^{-4}
40°C	*Jss*=5.7526 *Kp*=8.05x10^{-4}	*Jss*=2.516 *Kp*=3.02x10^{-4}	*Jss*=4.7164 *Kp*=5.19x10^{-4}

All formulations increase the permeation rate of caffeic acid with increasing temperature, but only LLC 30/CA and LLC 45/CA double the amount of permeated drug. LLC 40/CA also has an anomalous behaviour: although the amount of permeated drug increases slightly, the flux and permeation coefficient decrease with increasing temperature.

2.4 Caffeic acid skin retention studies

Intracutaneous accumulation of the drug is a possibility to prolong its duration of action and improve drug treatment. For this reason, the amount retained in the skin after 24 hours of release was evaluated. Results were compared at both temperatures and reported in table 4. At 32°C, the LLC45/CA formulation showed a higher accumulation in the skin 267.58 µg/cm^2, but slower drug release. At 40°C, in contrast, the LLC40/CA formulation showed a higher affinity for the skin layer (201.47 µg/cm^2) than LLC45/CA (90.35 µg/cm^2), but the amount of drug released over 24hours was comparable. These results confirm those obtained in the skin permeation study with LLC.

Table 4. Amount of CA retained into skin at 32°C and 40°C for all formulations tested.

Formulations	CA Retained into Skin (µg/cm^2) at 32°C	CA Retained into Skin (µg/cm^2) at 40°C
LLC 30/CA	215.33	169.36
LLC 40/CA	163.38	201.47
LLC 45/CA	267.58	90.35

The data obtained seem to justify the reported flux and *Kp* values. In fact, the hexagonal structure of the LLC 40/CA sample presents a greater accumulation in the skin as the temperature increases, while the LLC 45/CA sample, although presenting the same hexagonal phase, reduces its accumulation in the skin by almost three times by increasing the amount permeated. The LLC 40/CA mixture appears to be affected in both diffusion

and permeation by the increased coordination found in the dynamic rheology and viscosity studies.

LLC 30/CA showed a higher amount of drug permeated and a good CA retained in the skin, about 215 μg/cm^2 and 169 μg/cm^2, at different temperature tested.

3. Materials and methods

3.1 Materials

Caffeic acid (CA), pluronic 123 (P123), cellulose membranes and all solvents were purchased from Sigma Aldrich (Milan, Italy). Deionized water with 5 wt% deuterium oxide (Aldrich, Milan) was used in order to perform ^{2}H-NMR measurements. Rabbit ear skin was provided by local farm that killed rabbits for slaughter purposes, where slaughter is defined as killing for human consumption. Therefore, these are waste materials from farms for which no ethical regulations are foreseen.

3.1 Liquid lyotropic crystals gel preparations

For preparations of Pluronic 123 LLC gels a fixed drug percentage of CA (0.5% wt) and various ratios of Pluronic to water were used to obtain the different P123 lyotropic liquid phases [34]. Briefly, 25 mg of CA was mixed with an appropriate amount of water and block copolymer, details on sample preparations are given in Table 5. Subsequently, samples were centrifuged several times and stored at room temperature, or 4°C, to ensure complete homogenization. As some of samples exhibit negative thermoreological behaviour, they were liquid at low T, but LLC at room temperature [35]. Samples were evaluated and analysed after two weeks.

Table 5. LLC composition

Formulation	P123 wt%	H_2O wt%	CA wt%
LLC 30	30	70	-
LLC 40	40	60	-
LLC 45	45	55	-
LLC 30/CA	29.85	69.65	0.5
LLC 40/CA	39.80	59.70	0.5
LLC 45/CA	44.78	54.72	0.5

3.2 Optical microscopy observations

Leica 12 Pol optical polarizing microscope equipped with a heating unit, was used for the phase characterization of the samples. Indeed, the lyotropic liquid phases (except cubic phases) can be identified by comparing the typical textures of each liquid lyotropic phase with those reported in liquid crystal texture handbook [36].

3.3 ^{2}H-NMR theory and experiments

^{2}H-NMR is employed in the examination of liquid crystals due to their manifestation of a distinctive NMR line contingent upon the anisotropy, geometry, and domain size of the liquid crystal aggregates, along with the motion of deuterated water molecules. When subjected to a magnetic field, liquid crystalline phases align in a manner influenced by the molecular diamagnetic susceptibility. ^{2}H-NMR are predicated on quadrupolar interactions, determining the spectral frequency as follows (Eq. 3):

$$\Delta\nu = \pm\frac{3}{8}\nu_q(3\cos^2\theta - \eta\sin^2\theta\cos 2\varphi) \quad (3)$$

Where ν_q is the partially averaged quadrupole coupling constant, θ and φ are the polar and azimuthal angles defining the direction of the external magnetic field in the aggregate frame and η is the asymmetry parameter. The theoretical ^{2}H-NMR spectra, illustrated in Figure 9 exhibit distinct characteristics for different phases of a liquid lyotropic crystal—lamellar, hexagonal, and cubic. The lamellar structure displays a lineshape characterized by two shoulders separated by a value of 3/2 ν_q, along with two edge singularities separated by a value of 3/4 ν_q. The hexagonal phases exhibit a lineshape like the lamellar phase but with a smaller separation between the shoulders and singularities. In the case of an isotropic sample, such as a cubic phase, a singlet is observed.

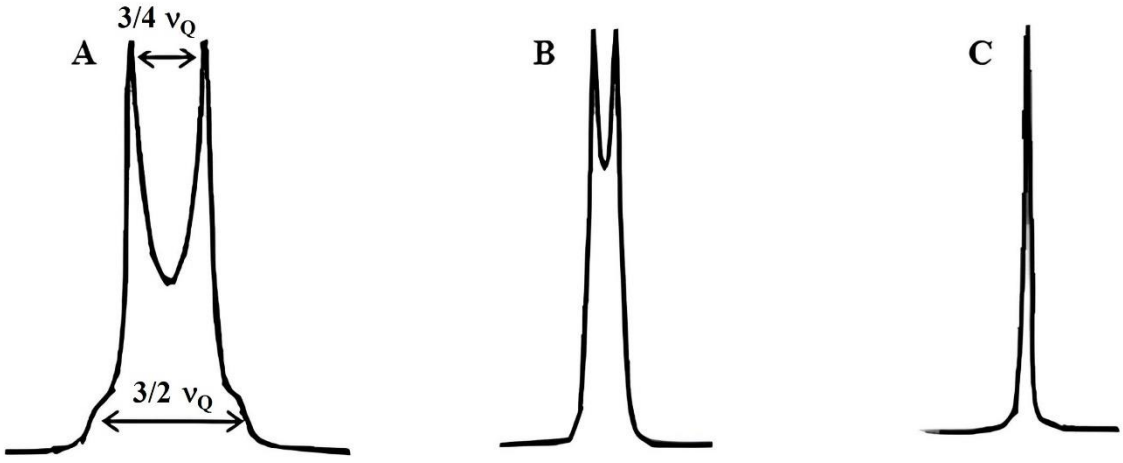

Figure 9. Typical^{2}H-NMR spectra of lamellar (A), hexagonal (B) and cubic (C) phase.

For the ^{2}H-NMR experiments, a quadrupole echo sequence with a $\pi/2$ pulse width of 3.5 μsec was employed. The delay between the two $\pi/2$ pulses was 40 μsec and repetition was 1 sec. Spectra were recorded 30 minutes after each temperature setting to allow samples

to reach thermal equilibrium. The experiments were conducted using a Bruker AVANCE 300 pulsed superconducting spectrometer operating in Fourier Transform mode, at a resonance frequency of 46.53 MHz. The sample temperature was controlled by passing air through the sample holder at three different temperatures (25±1°C, 35±1°C and 40±1°C).

3.4 Rheological characterisation

Rheological characterization of P123 crystalline mesophases were conducted using a shear stress-controlled rheometer SR5000 (Rheometrics, USA) equipped with a plate-plate geometry (gap 1.00 mm, diameter 25). The temperature was controlled by a Peltier apparatus (±0.1°C). All measurements were performed in triplicate. The error was calculated and it is around 3%. To prevent errors due to evaporation, measuring geometries were surrounded by a solvent trap containing water. Two different kinds of experiments were carried out: a) Steady flow experiments; b) Dynamic shear experiments were performed in a frequency range between 0.1 and 15.9 Hz. The small amplitude dynamic tests provided information on the linear viscoelastic behaviour of materials through the determination of the complex shear modulus (Eq. 4).

$$G^*(\omega) = G'(\omega) + iG''(\omega) \tag{4}$$

where $G'(\omega)$ is the in phase (or storage) component and $G''(\omega)$ is the out-of-phase (or loss) component. $G'(\omega)$ is a measure of the reversible, elastic energy, while $G''(\omega)$ represents the irreversible viscous dissipation of the mechanical energy. The dependence of these quantities on the oscillating frequency gives rise to the so-called mechanical spectrum, allowing the quantitative rheological characterization of studied materials. All dynamic rheological measurements were performed within the linear viscoelastic region. Weak Gel Model [37] was also applied to oscillatory spectra (Eq. 5):

$$\left|G^*(\omega)\right| = \sqrt{G'(\omega)^2 + G''(\omega)^2} = A\omega^{\frac{1}{Z}} \tag{5}$$

where "A" is interpreted as the interaction strength between the rheological units: a sort of amplitude of cooperative interactions, and "z" as the coordination number, which corresponds to the number of flow units interacting with each other to give the observed flow response [38].

3.5 Percutaneous permeation and diffusion release studies

Permeation and diffusion release were performed using Franz's vertical diffusion cells for 24 hours at two different temperatures: 32°C and 40°C. For permeation studies, full-thickness rabbit ear skin from a local slaughterhouse was used, previously frozen at -18°C and 2 hours before the experiments pre-equilibrated in saline at room temperature. A portion of this skin was placed between the receptor and donor compartments, with the epidermal side exposed to environmental conditions and the dermal side facing the receptor solution. Portions of cellulose membranes (Spectra/Por®, cut-off 12-14 kDa), were used for the diffusion studies. For all formulated mesophases, 0.4 g of CA-LLC gel was loaded and covered with parafilm to prevent water loss. The receptor compartment was filled with 5.5 mL of distilled water. At regular intervals and up to 24 hours, the medium was taken for analysis and filled with an equal volume of fresh water. The amount of drug in the samples was assessed by UV-VIS spectrometry. The experiments were repeated three times and expressed as mean ± SD.

3.6 Caffeic acid skin retention studies

To assess the amount of caffeic acid retained into the skin, after permeation studies, the skin was removed to Franz diffusion cells and placed in ethanol. The solution was filtered with 0.22 μm and evaluated by UV-Vis spectroscopy Millipore membrane filters and analysed. All experiments were conducted in triplicate and expressed as mean ± SD.

3.7 Statistical analysis

All experiments were performed three times, and the results were expressed as mean ± SD. Statistical analysis was performed using a Student’s t-test and p-values of ≤ 0.05 were considered statistically significant.

4. Conclusions

Caffeic acid loading in lyotropic liquid crystal based on the P123/water microstructures showed a good permeation profile and retention in the skin ensuring sustained drug release. The addition of CA did not so much lead to changes in the LLC microstructure of binary system P123/water, as reported by the ^{2}H-NMR spectra and POM observations, but rather modified its fluidity as showed the dynamic rheological measurements. All experiments were carried out at 32°C and 40°C to reproduce the physiological and hyperthermic condition typical of inflammatory-based diseases. The permeation profile of all formulations showed an increased steady-state flux (J_{ss}), and a decreased skin drug retained at highest temperature tested. Only LLC 40/CA formulation showed a different behaviour, in terms of NMR spectra, results of the rheology studies, and diffusion and permeation profiles, if compared to the similar hexagonal phase obtained by increasing the polymer concentration (LLC 45/CA). This may have been attributed to the greater coordination that caffeic acid establishes in this structure with the polymer chains, which determined an increase the CA skin retained at 40°C.

The liquid crystalline mesophases obtained from pluronic P123 could represent a good strategy for the skin treatment of a lipophilic drug such as caffeic acid.

In particular, the cubic phase LLC 30/CA shows a higher permeation profile and good accumulation in the skin at both temperatures tested.

Reference

[1] Tamimi, R. M., Hankinson, S. E., Campos, H., Spiegelman, D., Zhang, S., Colditz, G. A., ... & Hunter, D. J. Plasma carotenoids, retinol, and tocopherols and risk of breast cancer. *Am. J. Epidemiol.* **(2005)**, *161*(2), 153-160.

[2] Bagchi, K., & Puri, S. Free radicals and antioxidants in health and disease: a review. *EMHJ- East Mediterr Health J* **(1998),** 4 (2), 350-360, 1998.

[3] Davì, G., Falco, A., & Patrono, C. Lipid peroxidation in diabetes mellitus. *Antioxid Redox Signal* **(2005)**, *7*(1-2), 256-268.

[4] Hoffman, F. Antioxidant vitamins newsletter. *Nutr Rev*, **(1997)**, *14*, 234-236.

[5] Nunomura, A., Castellani, R. J., Zhu, X., Moreira, P. I., Perry, G., & Smith, M. A. Involvement of oxidative stress in Alzheimer disease. *J Neuropathol Exp Neurol* **(2006)**, *65*(7), 631-641.

[6] Laguerre, M., Lecomte, J., & Villeneuve, P. Evaluation of the ability of antioxidants to counteract lipid oxidation: Existing methods, new trends and challenges. *Prog. Lipid*

Res. **(2007)**,*46*(5), 244-282.[7] Spagnol, C. M., Assis, R. P., Brunetti, I. L., Isaac, V. L. B., Salgado, H. R. N., & Corrêa, M. A. In vitro methods to determine the antioxidant activity of caffeic acid. *Spectrochim Acta A Mol Biomol Spectrosc* **(2019)**, *219*, 358-366.

[8] Song, H. S., Park, T. W., Sohn, U. D., Shin, Y. K., Choi, B. C., Kim, C. J., & Sim, S. S. The effect of caffeic acid on wound healing in skin-incised mice. *Korean J Physiol Pharmacol* **(2008)**, *12*(6), 343-347.

[9] Zhang, M., Zhou, J., Wang, L., Li, B., Guo, J., Guan, X., ... & Zhang, H. Caffeic acid reduces cutaneous tumor necrosis factor alpha (TNF-α), IL-6 and IL-1β levels and ameliorates skin edema in acute and chronic model of cutaneous inflammation in mice. *Biol Pharm Bull* **(2014)**, *37*(3), 347-354.

[10] Zielińska, D., Zieliński, H., Laparra-Llopis, J. M., Szawara-Nowak, D., Honke, J., & Giménez-Bastida, J. A. Caffeic acid modulates processes associated with intestinal inflammation. *Nutrients* **(2021)**, *13*(2), 554.

[11] Razborsek, M. I., Ivanovic, M., & Kolar, M. Validated stability-indicating GS-MS method for characterization of forced degradation products of trans-caffeic acid and trans-ferulic acid. *Molecules* **(2021)**, *26*(9), 2475.

[12] Andueza, S., Manzocco, L., De Pena, M. P., Cid, C., & Nicoli, C. Caffeic acid decomposition products: Antioxidants or pro-oxidants? *Food Res Int* **(2009)**, *42*(1), 51-55.

[13] Khalil, I., Yehye, W. A., Etxeberria, A. E., Alhadi, A. A., Dezfooli, S. M., Julkapli, N. B. M., ... & Seyfoddin, A. Nanoantioxidants: Recent trends in antioxidant delivery applications. *Antioxidants* **(2019)**, *9*(1), 24.

[14] Deligiannakis, Y., Sotiriou, G. A., & Pratsinis, S. E, Antioxidant and antiradical SiO2 nanoparticles covalently functionalized with gallic acid. *ACS Appl Mater Interfaces* **(2012)**, *4*(12), 6609-6617.

[15] Kumar, L., Verma, S., Singh, M., Chalotra, T., & Utreja, P. Advanced drug delivery systems for transdermal delivery of non-steroidal anti-inflammatory drugs: A review. *Curr. Drug Deliv.*, **(2018)**, *15*(8), 1087-1099.

[16] Zaid Alkilani, A., Hamed, R., Musleh, B., & Sharaire, Z. Breaking boundaries: the advancements in transdermal delivery of antibiotics. *Drug Deliv.*, **(2024)**, *31*(1), 2304251.

[17] Hatem, S., Nasr, M., Elkheshen, S. A., & Geneidi, A. S. Recent advances in antioxidant cosmeceutical topical delivery. *Curr. Drug Deliv.*, **(2018)**, *15*(7), 953-964.

[18] Kriplani, P., & Guarve, K. Transdermal drug delivery: A step towards treatment of

cancer. *Recent Pat. Anti-Cancer Drug Discov.*, **(2022)**, *17*(3), 253-267.

[19] Hmingthansanga, V., Singh, N., Banerjee, S., Manickam, S., Velayutham, R., & Natesan, S. Improved topical drug delivery: Role of permeation enhancers and advanced approaches. *Pharmaceutics* **(2022)**, *14*(12), 2818.

[20] Kim, D. H., Jahn, A., Cho, S. J., Kim, J. S., Ki, M. H., & Kim, D. D. Lyotropic liquid crystal systems in drug delivery: a review. *J. Pharm. Investig*., **(2015)**, 45, 1-11.

[21] Silvestrini, A. V. P., Caron, A. L., Viegas, J., Praca, F. G., & Bentley, M. V. L. B. Advances in lyotropic liquid crystal systems for skin drug delivery. *Expert Opin.Drug Deliv*., **(2020)**, 17(12), 1781-1805.

[22] Rajabalaya, R., Musa, M. N., Kifli, N., & David, S. R. Oral and transdermal drug delivery systems: role of lipid-based lyotropic liquid crystals. *Drug Des. Devel. Ther*., **(2017)**, 393-406.

[23] Chen, Z., Greaves, T. L., Fong, C., Caruso, R. A., & Drummond, C. J. Lyotropic liquid crystalline phase behaviour in amphiphile–protic ionic liquid systems. *Phys. Chem. Chem. Phys*., **(2012)**, 14(11), 3825-3836.

[24] Zhao, L. Y., & Zhang, W. M. Recent progress in drug delivery of pluronic P123: pharmaceutical perspectives. *J. Drug Target*., **(2017)**, 25(6), 471-484.

[25] Wanka, G., Hoffmann, H., & Ulbricht, W. Phase diagrams and aggregation behavior of poly (oxyethylene)-poly (oxypropylene)-poly (oxyethylene) triblock copolymers in aqueous solutions. *Macromolecules* **(1994)**, *27*(15), 4145-4159.

[26] Tavano, L., Muzzalupo, R., Cassano, R., Trombino, S., Ferrarelli, T., & Picci, N. New sucrose cocoate based vesicles: preparation characterization and skin permeation studies. *Colloids Surf B Biointerfaces* **(2010),** *75*(1), 319-322.

[27] Neto, A. M. F., & Salinas, S. R. The physics of lyotropic liquid crystals: phase transitions and structural properties **(2005)** OUP Oxford, 62.

[28] Rajak, P., Nath, L. K., & Bhuyan, B. Liquid Crystals: An Approach in Drug Delivery. *Indian J Pharm Sci* **(2019)**, *81*(1).

[29] Malmsten, M., & Lindman, B. Self-assembly in aqueous block copolymer solutions. *Macromolecules* **(1992)**, *25*(20), 5440-5445.

[30] Martiel, I., Baumann, N., Vallooran, J. J., Bergfreund, J., Sagalowicz, L., & Mezzenga, R. Oil and drug control the release rate from lyotropic liquid crystals. *J Control Release* **(2015)**, *204*, 78-84.

[31] Huang, Y., & Gui, S. Factors affecting the structure of lyotropic liquid crystals and the correlation between structure and drug diffusion. *RSC Adv.*,**(2018)**, *8*(13), 6978-

6987.

[32] Zabara, A., & Mezzenga, R. Controlling molecular transport and sustained drug release in lipid-based liquid crystalline mesophases. *J.Control. Release* **(2014)**,*188*, 31-43.

[33] Negrini, R., & Mezzenga, R. pH-responsive lyotropic liquid crystals for controlled drug delivery. *Langmuir* **(2011)**, *27*(9), 5296-5303.

[34] Galarneau, A., Cambon, H., Di Renzo, F., Ryoo, R., Choi, M., & Fajula, F. Microporosity and connections between pores in SBA-15 mesostructured silicas as a function of the temperature of synthesis. *New J Chem* **(2003)**, *27*(1), 73-79.

[35] Juhasz,J., Lenaerts, V., Raymond, P., & Ong, H. Diffusion of rat atrial natriuretic factor in thermoreversible poloxamer gels. *Biomaterials* **(1989)**, *10*(4), 265-268.

[36] Demus, D. Textures of liquid crystals **(1979)**.

[37] Gabriele, D., de Cindio, B., & D'Antona, P. A weak gel model for foods. *Rheol. Acta* **(2001)**, *40*(2), 120-127.

[38] Coppola, L., Gianferri, R., Nicotera, I., Oliviero, C., & Ranieri, G. A. Structural changes in CTAB/H2O mixtures using a rheological approach. *Phys. Chem. Chem. Phys.* **(2004)**, *6*(9), 2364-2372.

3.2 Liposomal, niosomal and nanoparticle encapsulation of an olive leaf extract: physical-chemical characterisation, release studies and evaluation of antioxidant activity

Introduction

The scientific community is paying increasing interest to plant extracts as active ingredients in pharmaceutical formulations due to their countless benefits. The pharmaceutical applications of these extracts are certainly related to beauty and health, as they exhibit antioxidant, antibacterial, healing, photoprotective, anti-inflammatory and anti-cancer activities. Among these, particular attention has been paid to the bioactive compounds of olive (Olea europea) leaves. The olive oil industry generates a significant volume of by-products, including crude pomace, vegetation water, twigs and leaves, which account for about 10% of the total weight of olives [1]. Although olive leaves and panels are commonly used as animal feed, opportunities for use in higher value-added sectors, such as the cosmetic, therapeutic and food industries, can be explored, as the phenolic fractions oleuropein and hydroxytyrosol are potent antioxidant, anti-inflammatory and anti-cancer agents [2, 3].

However, factors such as exposure to light, temperature variations, the presence of oxygen, pH changes and the presence of metal ions during processing, storage and gastrointestinal digestion may compromise the stability of these compounds. Furthermore, the poor water solubility of hydrophobic compounds hinders their complete dissolution and absorption. Likewise, the limited diffusion and permeability of these compounds through the cells of the intestinal epithelium significantly affects their bioavailability [4]. To overcome these limitations, the use of nanotechnology emerges as an attractive strategy. The design and production of drug delivery systems, particularly nanometric ones with dimensions between 50 and 300 nm, are now an integral part of clinical use. These systems represent an advanced approach to optimise the therapeutic efficacy of extracts and essential oils. A successful drug delivery system should have optimal loading and payload release properties, ensuring a long shelf life and increase therapeutic efficacy, resulting in reduced side effects. Different types of transporters have been used in recent decades, including organic components such as lipids (such as fatty acids and phospholipids), proteins (including caseins, whey proteins and gelatin), carbohydrates (such as starch, cellulose, chitosan and pectin) and inorganic transporters such as silver, gold and mesoporous silica. This range of transporters has been used to

develop different delivery systems, including nano- and microparticles, liposomes, hydrogel niosomes, etc. This development was made possible using various encapsulation techniques, such as coacervation, emulsion and others [5,6,7,8]. Therefore, our attention was turned to the development of different vesicular systems for the delivery of olive leaf extract, with the aim of examining the release profile and the corresponding antioxidant activity. Liposomal, cationic niosomal and chitosan nanoparticle systems were designed. These systems were carefully characterised from a physicochemical point of view and, subsequently, the optimal formulations were subjected to in vitro release studies, followed by the evaluation of antioxidant activity.

Materials and methods

Materials

Lecithin (LEC), cholesterol (CHOL), Span 80 (S80), dioctadecyldimethylammonium bromide (DODAB), chitosan (CHIT), sodium tripolyphosphate (TPP), NHS (N-Hydroxysuccinimide), EDC (N-(3-Dimethylaminopropyl)-N-ethylcarbodiimide hydrochloride)), were purchased by Sigma Aldrich (Milan, Italy). All solvents used bought by VWR International.

Polyphenol extraction from olive leaves

Polyphenols extraction was performed on micronised olive leaves, and the method used is described in Muzzalupo et al. 2011 [9]. Approximately 20 g of micronised olive leaves were solubilised in 100 mL of ethanol and shaken magnetically overnight. Subsequently, the product was sonicated with a pulse sonicator for twenty minutes on ice. It was centrifuged at 9000 rpm for ten minutes and separated from the olive leaves by vacuum filtration. The filtrate obtained was brought to dryness by evaporation under reduced pressure.

Characterization of extract

HPLC conditions

HPLC analysis was conducted using an Agilent 1100 series chromatograph equipped with a Mod. G1312A binary pump, a Mod. G1315B DAD detector and a Mod. G1328B injection system. Chromatographic separation was performed on a Phenomenex GEMINI reverse phase C18 110A column, 25.00 x 0.46 cm, packed with 5.00 μm particles, at a temperature of 40°C. The solvents used were always degassed by filtration through a nylon membrane, porosity 0.45 mm, under vacuum. Elution was performed in gradient

mode using a binary solvent mixture consisting of water acidified with 0.2% phosphoric acid (solvent A) and methanol/acetonitrile 50/50 (solvent B). A linear gradient was performed from 96% (A) and 4% (B) to 50% (A) and 50% (B) for 40 minutes; this was switched to 40% (A) and 60% (B) for 5 minutes; during 15 minutes this was switched to 0% (A) and 100% (B), after rebalancing the initial composition for 12 minutes. The flow rate of the mobile phase was 1 ml/min and the injection volume of each sample was 20 µL. All phenolic compounds were identified by comparing their retention times with those of the standards.

Folin-Ciocalteu assay

The quantification of total phenols in the formulations was conducted by spectrophotometric analysis at a wavelength of 750 nm, using the Folin-Ciocalteau method as outlined by Fuentes et al. (2012) [10]. The extract, solubilised in water at a concentration of 10 mg/mL, was subjected to a reaction in which 0.5 mL of sample was combined with an equal volume of Folin-Ciocalteau reagent. This mixture was then incubated in the dark for 5 minutes. Next, 3 mL of 20% Na_2CO_3 and 5 mL of distilled water were added. After a further 20-minute incubation in the dark, the samples were subjected to centrifugation at 3500 rpm for 10 minutes and analysed at uv-spectrometer.

ABTS Assay

The antioxidant activity of olive leaves extract was assessed by measuring their ability to scavenge the free radical ABTS•. A stock solution containing 7 mM ABTS was combined with 2.45 mM potassium persulfate and stirred in the dark for 12 hours to generate the ABTS• free radical. Prior to use, the solution was diluted with ethanol until an absorbance of 0.7 was achieved. Subsequently, 1 mL of the samples was added to 3 mL of the ABTS•+ solution, and after 6 minutes, the absorbance was measured at 734 nm using a UV spectrophotometer. The ABTS scavenging activity was then calculated using the following equation:

$$\%\ inhibition = \left(\frac{A_0 - A_s}{A_0}\right) x\ 100$$

Where, A_s is the absorbance of the sample at 734 nm and A0 is the control. All tests were realised in triplicate and the results expressed as means ± SD.

Liposomes and niosomes preparations

Thin-layer evaporation was used to formulate the liposomes. Appropriately weighed amounts of lecithin and cholesterol were solubilised in dichloromethane and evaporated

under reduced pressure. The resulting film was then hydrated with 10 mL of distilled water or extract solution for 30 minutes at 40°C. After 24 hours at room temperature, the formulation was subjected to pulse sonication for 15 minutes to obtain unilamellar vesicles. To remove unincorporated material, all formulations were purified by dialysis using previously treated synthetic cellulose membranes (Spectra/Por molecular mass, cut-off 12/14 kDa). The same procedure was performed for the niosomal systems, weighing appropriate amounts of S80, CHOL and DODAB. The amounts of the components used for each formulation are shown in **Table 1**.

Chitosan nanoparticles preparation

Chitosan nanoparticles (NPs) were synthesized using the ionotropic gelation method, following the procedure outlined by Rampino et al. (2013) [11]. Low molecular weight chitosan was dissolved in 5 mL of 1% (v/v) acetic acid, reaching a final concentration of 1 mg/mL, and allowed to stir for one hour. The pH of the solution was adjusted to 5.5 using 0.5 M NaOH, and 1 mL of TPP (pentasodium tripolyphosphate) at a concentration of 2 mg/mL was added dropwise. The entire solution was stirred for 30 minutes at room temperature.

Preparation of olive leaves-conjugated nanoparticles.

Briefly, EDC (15 mg) and NHS (9 mg) were dissolved in 1 mL of polyphenol extract solution and shaken magnetically for about 90 minutes in the dark. Subsequently, 1 mL of chitosan nanoparticles was added to this solution and left to shake magnetically in the dark overnight.

Nanosystem characterization

All nanosystem formulations were analysed in terms of size, size distribution and potential ζ and TEM. For size analysis, the 90 Plus particle analyser (Brookhaven Instrument Corporation, New York, USA) was used, maintaining a constant temperature of 25.0 ± 0.1 °C. The ζ potential was assessed with a Zetasizer ZS (Malvern Instrument Ltd, Malvern, U.K.). All analyses were conducted on purified samples and repeated in triplicate. Morphological analysis was conducted by transmission electron microscopy (TEM) using a ZEISS EM 10 TEM, operating at an accelerating voltage of 80 kV.

Drug Loaded Efficiency

For vesicular systems (niosomes and liposomes), the amount of encapsulated drug was expressed as a percentage (E%). This parameter was determined by freezing-broken 0.2

mL of each sample, both purified and unpurified. Subsequently, the resulting portions were diluted in 10 mL of ethanol and analysed with a JASCO V-530 spectrophotometer. The absorbances, which correlated with the amount of polyphenolic extract in the samples, were measured at a wavelength of 276 nm, at the characteristic peak. The equation used to calculate the encapsulation efficiency is as follows:

$$E\% = \frac{Cpurified}{Cinitial} x\ 100$$

where $C_{purified}$ is the concentration of the polyphenols contained in the dialysed nanoparticle dispersion, while C_{intial} is the initial polyphenols concentration including both the encapsulated drug and the polyphenols remaining outside the vesicles.

For nanoparticles, E% was determined by indirect method. The nanoparticles were first filtered through syringe filters with a porosity of 0.2 μm (Millipore, Italy). Subsequently, 1 mL of filtrate was taken and brought to a final volume of 7 mL with distilled water to obtain the same conditions as the solution without chitosan and TPP. The absorbance of the sample was measured with a UV spectrophotometer at 276 nm. The equation used was:

$$EE\% = \frac{total\ amount\ of\ polyphenols\ -\ free\ polyphenols}{total\ amount\ of\ polyphenols} x\ 100$$

Stability studies

The stability of the vesicular systems was evaluated by storing the formulation at 4 °C for three months and monitoring diameter, PI and ζ-potential initially after 4 days, and then every month. Each analysis was carried out in triplicate.

***In vitro* release studies**

The release of phenolic compound from nanoparticles was estimated using diffusion Franz cells for 24 hours at 37°C. Visking dialysis membrane, 20/30 cut-off: 12.000-14000 Da, were placed between the donor and receptor compartment and 0.5 mL of different nanosystems was added in donor compartment. The acceptor compartment was filled with 5.5 mL of distilled water, after, was removed at pre-determined time intervals and spectrophotometrically analysed.

Antioxidant activity

To determine the antioxidant activity of phenolic nanoparticles, the DPPH assay was used, following method describe by Yen and Hsieh [12]. Antioxidant activity was

evaluated on the drug quantity release from medium corresponding to different concentration of antioxidant. Three dilutions (500 µL, 1000 µL and 1500 µL) were performed at set time intervals.

Hemolytic activity

Fresh blood, collected and processed the same day, was used for the determination of hemolytic activity. The red blood cells were washed three times with PBS (pH 7.4) and then used to prepare a suspension with a density of 8 x 10^9 cells per mL. Several volumes (10 to 100 µL) of aqueous solution of extract or liposomal systems were taken and placed in eppendorf tubes. Appropriate amounts of phosphate buffer and 25 µL of blood were added to the eppendorf tubes, until a volume of 1 mL was reached. The tubes were incubated under agitation for ten minutes and centrifuged at 10000 Rpm for five minutes at room temperature. Hemolytic activity was determined by comparing the absorbance value of the supernatant at 575 nm with the control value. The test was conducted in triplicate on all selected samples.

Results

HPLC analysis of olive leaves extract

HPLC analysis made it possible to determine the chemical composition of olive leaf extract. As shown in Figure 1, the chromatogram shows several peaks, the retention times of which were compared with certain standards, thus enabling their identification. The most representative peak appears to be that of oleuropein, which represents a percentage equal to 27.84% of the polyphenols identified. The other polyphenols identified are tyrosol (8.06%) and quercetin (10.5%).

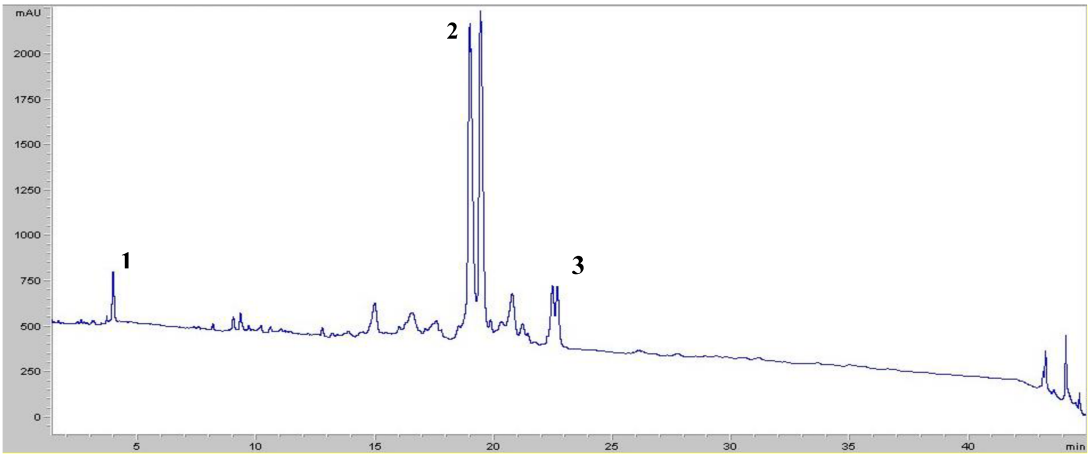

Figure 1. Chromatogram obtained from olive leaf extract in which tyrosol (1), oleuropein (2) and quercetin (3) are highlighted.

Polyphenol quantifications

The determination of polyphenol content in the extract was carried out using the Folin Ciocalteu assay. Using a spectrophotometer, this method made it possible to confirm both the presence of polyphenols and to define their concentration expressed in mg oleuropein equivalent/g extract, which was 631.84 mg/g.

Antioxidant activity: ABTS Assay

To assess the antioxidant activity of the leaf extract, the ABTS assay was conducted. Starting from an initial concentration of 0.054 mg/mL, serial dilutions (0.0036 to 0.0216 mg/mL) were performed. The concentration range tested showed a dose-dependence in antioxidant activity, reaching 90% inhibitory activity of the ABTS radical.

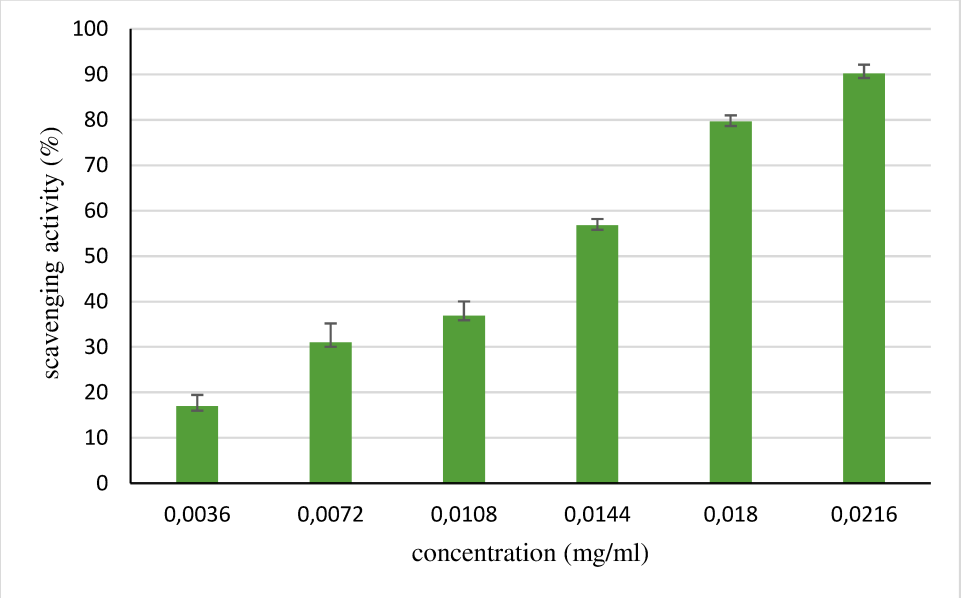

Nanosystems characterization

Three different antioxidant nanosystems were realised: liposomes, niosomes and nanoparticles. All systems were characterised in terms of size, IP, ζ-potential and E%; the results are shown in **Table 2**. Specifically, empty liposomal formulations were created with solutions with increasing concentrations of polyphenolic extract (10, 20 and 30 mg/mL), previously treated to eliminate cellulose. The empty lecithin-based liposomes had quite small dimensions, around 150 nm with good polydispersity (around 0.2). By encapsulating the extract, it was observed that all three liposomal formulations were similar, with an average diameter between 199 and 237 nm and a PI of about 0.2, indicating a good and homogenous size distribution. The ζ–potential between -20 and -24 mV indicates that the vesicular systems are quite stable. The main difference observed was the encapsulation efficiency: the LIP/EF 2 formulation had a lower encapsulation efficiency of 52% compared to LIP/EF 1, which achieved an encapsulation efficiency of about 70%.

Table 2. Physico-chemical characterization of DDS prepared with different concentrations of polyphenol extract: size (nm), P.I, ζ–potential, and E% at 25 °.

Formulations	EF mg/mL	Size (nm)	IP	ζ–potential	E%	EF encapsulated (mg/ml)
LIP/EF 1	5.6	199.1	0.255	-20 ± 0.781	76%	2.13
LIP/EF 2	10.45	214.4	0.214	-24.8 ± 0.772	52.16%	5.43
LIP/EF 3	17.94	236.9	0.271	-23.4 ± 0.560	58%	10.41
NIO/EF 1	6.15	245.1	0.189	24.1 ± 1.66	59.52%	3.66
NIO/EF 3	18.36	511.1	0.269	30 ±1,89	40%	7.34
NP CHIT/EF 3	14.17	234.6	0.179	16 ± 0.557	26.76 %	0.60
NP CHIT-EF 4	15.86	424.8	0.292	13.3 ± 0.569	30.80%	1.40

The cationic niosomal formulations, on the other hand, showed a significant increase in size as the polyphenolic extract concentration increased. Indeed, a diameter of 245 nm was observed in the presence of the extract with a concentration of 3.66 mg/mL, while a diameter of about 500 nm was observed in the presence of the polyphenolic extract concentration of 7.34 mg/mL. Although this size variation was observed, PI values <0.3 indicate good homogeneity and ζ–potential values > 30 mV good colloidal stability. A good encapsulation efficiency of 59.52 % for the NIO/EF 1 formulation and 40% for NIO/EF 2 was also observed. Finally, the chitosan nanoparticles were made from the most concentrated polyphenolic extract solution of 15 mg/mL. The extract carrier nanoparticles (NP CHIT/EF 3) showed a smaller diameter and lower polydispersion than the corresponding functionalised nanoparticles (NP CHIT-EF 4). The ζ–potential values were

similar, with values >13 mV, and no significant variations were also observed for E%, reaching around 30% efficiency.

Stability studies

The stability of the designed nanosystems was evaluated by monitoring the physico-chemical characteristics of the formulations stored at 4°C for a period of three months. First, the stability of the liposomal systems was assessed for 120 days (**Table 3**). The size of the vesicular systems remained similar for 90 days, increasing slightly after 120 days. The PI and ζ–potential values remain almost unchanged throughout the 120 days, thus demonstrating the good stability of these vesicular systems. Subsequently, the stability of the formulations containing the polyphenolic extract was monitored (**Table 4**). These results shows that even when transporting the polyphenolic extract, the liposomal systems retain their chemical-physical properties, while the E% decreases slightly after 30 days in all three formulations tested. The niosomal systems NIO/EF 1 and NIO/EF 3 show stability, as no significant changes in their properties are observed after 60 days.

Table 3. Stability analysis of liposomes based on lecithin and cholesterol, stored at 4 °C evaluated by monitoring diameter, P.I. and ζ−potential. Data was collected at specific time points, up to 3 months, and expressed as mean of three independent experiments ± SD.

Time (days)	Size (nm)	I.P	ζ potential
0	166,6	0,257	-24,4 ± 0,493
4	183,1	0,230	-18,8 ± 1,85
8	189,7	0,231	-19,9 ± 0,757
30	218,7	0,234	-20,7 ± 1,54
60	194,4	0,255	-20,1 ± 0,208
90	208,4	0,258	-20,5 ± 0,221
120	281,7	0,264	-24,4 ±0,321

Table 4. Stability analysis of DDS stored at 4 °C evaluated by monitoring diameter, P.I., ζ−potential, and E%. Data was collected at specific time points, up to 3 months.

FORMULATIONS	Time (days)	Size (nm)	PI	ζ potential	E %
LIP/EF1	0	199.1	0.255	-20 ± 0.781	76%
	15	180.7	0.287	-23.4 ±0.485	40.17 %
	30	195.5	0.287	-21.1 ± 0.357	38.80 %
	60	218.2	0.289	-22.8 ± 0.45	41.85 %
LIP/EF2	0	214.4	0.214	-24.8 ± 0.722	50.35 %
	15	247.2	0.259	-27.2 ± 1.92	48.17 %
	30	226.5	0.266	-23.6 ± 1.30	43.87%
	60	230.4	0.263	-24.7 ± 0,57	39.92%
LIP/EF3	0	236.9	0.271	-23.4 ± 0.560	58%
	15	195.3	0.212	-19.3 ± 0.58	64.50 %
	30	198.6	0.242	-20.4 ± 0.456	63.43 %
	60	215.3	0.251	-21.0 ± 0,350	55.20 %
NIO/EF1	0	245.1	0.189	24.1 ± 1.66	59.52%
	30	161.4	0.227	36.7 ± 1.89	50.50 %
	60	172.0	0.190	40.2 ± 2.21	49.50 %
NIO/EF3	0	511.1	0.269	30 ±1,89	40%
	30	650.8	0.260	28.2 ± 0.88	38.24%
	60	670.2	0.243	30.4± 2.45	35.87%
NANO/CHIT/ EF2	0	234.6	0.179	16.6 ±0.557	26.76 %
	30	266.6	0.213	20.1 ± 0.51	23.50 %
	60	300.1	0.220	17.9 ± 0.487	20.80 %
NANO/CHIT-EF4	0	424.8	0.292	13.3 ± 0.569	30.80%
	30	400.9	0.184	18.4 ± 1.45	17.30 %
	60	403.8	0.178	17.5 ± 1.89	15.80%

In vitro release studies and antioxidant activity

The ability of nanosystems to release the encapsulated polyphenols was evaluated using Franz diffusion cells for 24 hours and compared with the release profiles of olive leaves extract solutions. As shown in **Figure 2,** the LIP/EF 1 formulation showed a slower and more prolonged release of the phenolic extract than the free solution. In particular, a release of 66% was recorded after 24 hours, in contrast to the 84% obtained with the phenolic extract solution. NIO/EF 1 initially (in the first 5 hours) showed a rapid release comparable to that of the phenolic extract solution. From the sixth hour onwards, the niosomal systems show a slower and more prolonged course, reaching a release of 65%. The antioxidant activity of the tested samples shows, in each case, a concentration dependency. The scavenging power of the liposomal systems, however, is significantly lower than that of the leaf extract solution, in line with the prolonged release due to liposome delivery. Although the antioxidant activity remained relatively constant from the third to the sixth hour for all three samples, a significant increase was observed at the

highest concentration tested for the niosomal systems, reaching 50% inhibition compared to the solution (32%).

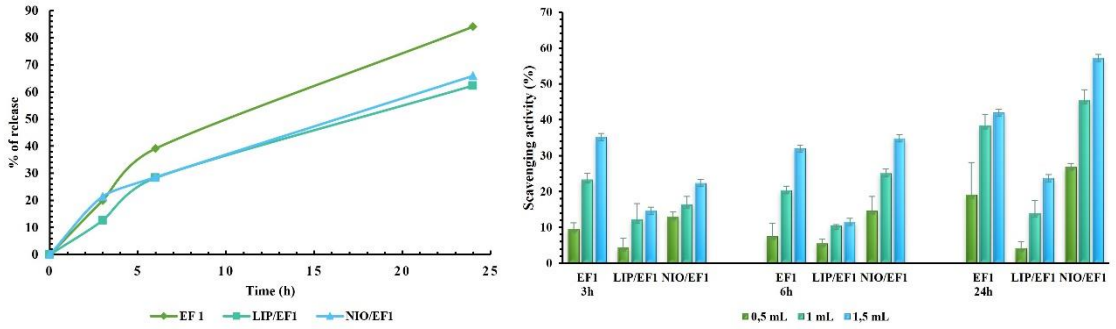

Figure 2. Release profile of (♦) olive leave extract (■) olive leave extract liposomes and (▲) olive leave extract niosomes correspondingly, and evaluation of antioxidant activity with DPPH assay at 3h, 6h and 24h of release.

A similar dynamic emerges in Figure 3. The liposomal system shows slower release, reaching 67% release in 24h. A more sustained and rapid release is manifested by the niosomal systems reaching 92% in 24h, similar to the release observed petr the free extract, which reaches 98%. Analysis of antioxidant activity again shows a concentration-dependent inhibitory action. In particular, in the first 6 hours, higher inhibition values are recorded for the liposomal and niosomal systems (ranging from 50 to 70%) than for the free solution (about 40%) when tested at the highest concentration. After 24 hours, however, all three systems maintain a correlation with concentration, maintaining comparable antioxidant power. For the extract at the highest concentration tested (EF3), it is observed that the antioxidant efficacy is affected by both dose and time.

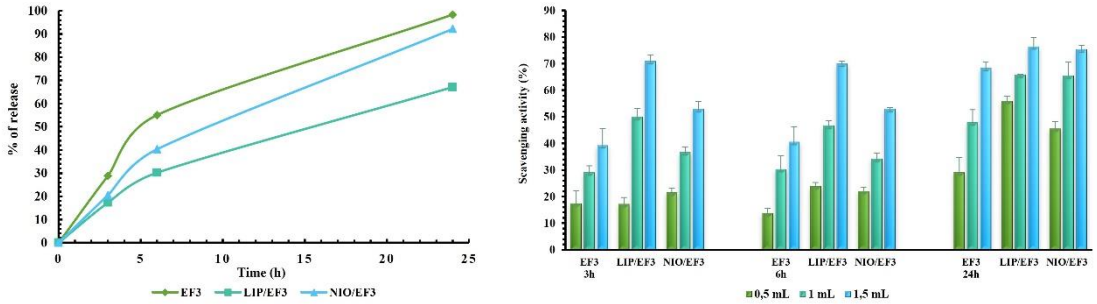

Figure 3. Release profile of (♦) olive leave extract (■) olive leave extract liposomes and (▲) olive leave extract niosomes correspondingly, and evaluation of antioxidant activity with DPPH assay at 3h, 6h and 24h of release.

Hemolytic activity

Emphasis is placed on the analysis of hemolytic activity on mammalian erythrocytes, the blood cells commonly used to assess surfactant-membrane interaction. The experiments

were performed *in vitro* on erythrocytes, using a phospholipid concentration between 38 and 380 µg/mL (**Table 6**). Analysis of the data obtained shows that the liposomal systems do not exhibit hemolytic activity in the range of concentrations tested. Similarly, the niosomal systems based on cationic surfactants also show no signs of hemolytic activity in the range explored (**Table 7**).

Table 6. % of hemolysis for liposomal formulation

Concentrations (µg/mL)	% of hemolysis
38	1,50
76	1,60
114	2,16
152	3,91
190	3,95
228	5,23
266	5,67
304	7,52
345	8,75
380	11,35

Table 7. % of hemolysis for niosomal formulation

Concentrations (µg/mL)	% of hemolysis
8	0,24
16	0,65
24	0,45
32	0,48
40	0,72
48	0,88
56	0,83
63	1,01
72	1,08
80	1,24

Conclusions

Nanosystems bearing olive leaf extract were obtained by means of the thin-layer evaporation technique. Chemical-physical analysis showed that the particles have a size of around 200 nm in the case of liposomes and between 200 and 500 nm in cationic niosomes. Both systems show a high encapsulation capacity, with liposomes achieving an E% of 70%, while niosomes are around 50%. The polydispersity index, with values of 0.2 in all cases, indicates a remarkable homogeneity of the system. Stability studies conducted for three months showed good chemical-physical stability, maintaining

parameters similar to the initial ones. *In vitro* release studies were conducted for both systems, followed by evaluation of antioxidant activity. The vesicular formulations with the lowest amount of leaf extract showed a longer and slower release profile than the corresponding extract solution. The antioxidant activity, although lower than that of the extract, showed a dose dependence, but only slightly influenced by time. Similar results were found for the vesicular formulations with the highest amount of extract, although a more significant release was observed when the extract was administered compared to the solution. This is reflected in the antioxidant activity, which is comparable between the free extract and the vehicle extract. Consequently, these systems could be an excellent solution for the administration of extracts with antioxidant properties, as well as offering the opportunity to explore further activity over time.

Reference

[1] Guinda, Á., Pérez-Camino, M. C., & Lanzón, A. (2004). Supplementation of oils with oleanolic acid from the olive leaf (Olea europaea). *European journal of lipid science and technology*, *106*(1), 22-26.

[2] González, E., Gómez-Caravaca, A. M., Giménez, B., Cebrián, R., Maqueda, M., Martínez-Férez, A., ... & Robert, P. (2019). Evolution of the phenolic compounds profile of olive leaf extract encapsulated by spray-drying during in vitro gastrointestinal digestion. *Food chemistry*, *279*, 40-48.

[3] Moudache, M., Colon, M., Nerín, C., & Zaidi, F. (2016). Phenolic content and antioxidant activity of olive by-products and antioxidant film containing olive leaf extract. *Food Chemistry*, *212*, 521-527.

[4] Bao, C.; Jiang, P.; Chai, J.; Jiang, Y.; Li, D.; Bao, W.; Liu, B.; Liu, B.; Norde, W.; Li, Y. The delivery of sensitive food bioactive ingredients: Absorption mechanisms, influencing factors, encapsulation techniques and evaluation models. *Food Res. Int.* **2019**, *120*, 130–140.

[5] Zuidam, N.J.; Nedovic, V.A. *Encapsulation Technologies for Active Food Ingredients and Food Processing*; Springer: New York, NY, USA, 2010; ISBN 9781441910073.

[6] Martínez-Ballesta, M.; Gil-Izquierdo, Á.; García-Viguera, C.; Domínguez-Perles, R. Nanoparticles and controlled delivery for bioactive compounds: Outlining challenges for new “smart-foods” for health. *Foods* **2018**, *7*, 72.

[7] McClements, D.J. Advances in nanoparticle and microparticle delivery systems for increasing the dispersibility, stability, and bioactivity of phytochemicals. *Biotechnol. Adv.* **2020**, *38*, 107287.

[8] Ahmad, R.; Srivastava, S.; Ghosh, S.; Khare, S.K. Phytochemical delivery through nanocarriers: A review. *Coll. Surf. B Biointerfaces* **2021**,*197*, 111389.

[9] Muzzalupo, I., Badolati, G., Chiappetta, A., Picci, N., & Muzzalupo, R. (2020). In vitro antifungal activity of olive (Olea europaea) leaf extracts loaded in chitosan nanoparticles. *Frontiers in bioengineering and biotechnology*, *8*, 151.

[10] Pimentel-Moral, S., Teixeira, M. C., Fernandes, A. R., Arráez-Román, D., Martínez-Férez, A., Segura-Carretero, A., & Souto, E. B. (2018). Lipid nanocarriers for the loading of polyphenols–A comprehensive review. Advances in colloid and interface science, 260, 85-94.

[11] Rampino A., Borgogna M., Blasi P: (2013). Chitosan nanoparticles: preparation, size evolution and stability. International Journal of Pharmaceutics; 455: 219-228.

[12] Yen and Hsieh (1995). Antioxidative activity and scavenging effects on active oxygen of xylose-lysine Maillard reaction products. J SciFood Agric; 67: 415-420.

3.3 Exploring the antioxidant efficacy of Caffeic acid solution and micellar dispersions through photostability investigations.

Introduction

Caffeic acid (CA), (3,4-dihydroxycinnamic acid) is a naturally occurring polyphenol with low molecular weight isolated from various plants such as coffee, tea, thyme, oregano, sage, berry, apple and potato [1] In addition to widely reported antioxidant activity [2], CA also exhibits various pharmacological properties such as anticancer, antibacterial, hepatoprotective, anti-inflammatory and antiglycemic [3, 4, 5, 6] . Recently, it has been also reported the therapeutic potential of CA in preventing and treating Alzheimer disease by reducing the production and aggregation, and promoting the clearance of amyloid β peptide [7]. Despite, the pharmaceutical potential of this molecule, its application is limited by the high hydrophobicity, poor bioavailability and high instability to environmental stress [8,9]. It is known that CA has poor photostability and is readily converted into cis stereoisomers degradation product upon exposure to light [10]. Aqueous CA solution resulted also be sensitive to oxygen, light, and high temperature leading to a complete degradation after 30 days of storage [11]. In this contest, encapsulation in nanoscale delivery systems could represent a useful strategy to improve solubility and control chemical stability. Among the various nano delivery systems, polymeric micelles are interesting devices for delivery of hydrophobic compounds. Polymeric micelles have a shell-core structures formed by the spontaneous self-assemble of amphiphilic polymers in water. Other than improving solubility, the encapsulation of hydrophobic drug in polymeric micelles have been studied for the ability to protect photosensitive drug from light. Various research groups reported, indeed, the reduced photodegradation of chemicals when incorporated in polymeric micelles [12,13,14]. Moreover, polymeric micelles are widely used for their ability to enhance skin permeation of a wide range of poorly water soluble molecules [15,16,17]. Polymeric micelles could enhance drug solubilization into the skin, increase partitioning into the skin deeper layers and form a depot into the skin by slow and sustained drug release from intact polymeric micelles [17]. Among the polymeric micelles, pluronic copolymers have been widely used in the fields of nanomedicine. Pluronics (PEO-PPO-PEO or PPO-PEO-PPO) are the first family of synthetic non-ionic surfactants, designed and manufactures by BASF, recognized as safe and biocompatible materials in pharmaceutical field and widely used for their capacity to solubilize lipophilic drugs [18]. Thank their amphiphilic nature, they

form, in fact, micelles above the critical micellar concentration. The hydrophobic PPO segments were assembled in the core of the micelle, while the hydrophilic PEO chain forms a corona shell owing to its high hydrophilicity. Pluronic micelles are widely employed as drug delivery systems since their good biocompatibility, biodegradability and ability to increase solubility, improve circulation time, and release drugs at the target sites [19]. P123 is a hydrophobic pluronic widely used for the drug delivery in brain and cancer therapy [20,21]. P123 results very interesting since exhibits a temperature dependent aggregation behaviour: at low temperatures, polymer is well-soluble in water and appear as independent polymer chains, while with the temperature increase P123 solubility decreases and the chains start to aggregate and form micelles with spherical, worm-like and lamellar structures [22,23]. The aim of the present study was to develop P123 micelle to enhance aqueous solubility, topical bioavailability and light stability of CA. Micelles were prepared using various polymer concentrations and loading several drug amount. CA encapsulation was carried out using direct dissolution method and was confirmed using UV–visible spectroscopy followed by the physico-chemical characterization of micelle formulations and *in-vitro* drug release studies. Specifically, release experiments and rheological characterization was performed at two different temperatures considering the variety of different temperature dependent P123 micelle morphologies. Moreover, stability experiments to light and temperature were carried on CA free and loaded in micelles. All the prepared formulations were subjected to forced degradation tests, according to the International Conference on Harmonization (ICH) rules [24]. Along with the degradation experiments, the antioxidant activity of the CA free and loaded in micelle before and after stress stability test was investigated.

Materials and methods

Chemicals

Caffeic acid (CA) 2,2-Diphenyl-1-picrylhydrazyl (DPPH), was purchased by Sigma Aldrich, Milan, Italy. Water and ethanol of absolute grade were purchased by J.T. Baker (Amsterdam, The Netherlands). Pluronic P123 having molar mass of 5800 $gmol^{-1}$ with average composition of $(PEO)_{20}(PPO)_{70}(PEO)_{20}$ was purchased from Merck.

Instruments and software

UV spectra were registered in the range of 200–450 nm using a Perkin-Elmer Lambda 850+ UV/Vis Spectrophotometer (PerkinElmer, Boston, MA, USA) under the following conditions: scan rate: 1 nm s −1, time response:1 s, and spectral band: 1 nm. The software

UV Winlab® 7.3.0.340 (PerkinElmer, Boston, MA, USA) was used for spectral acquisition and elaboration. According to the ICH rules, photodegradation experiments were made by means of a light cabinet, Suntest XLS+ (Heraeus, Milan, Italy), equipped with a Xenon lamp (Atlas Material Testing Technology, Mt Prospect, IL, USA). The apparatus closely simulate sunlight and allow to select a spectral region between 300 and 800 nm. A cooling system connected to the irradiation chamber allows temperature control inside the box. Thermal stability tests were performed in a thermostatically controlled ovens (2100 High Performance Oven, produced by Fratelli Galli, Via dell'Artigianato, 12, 20072 Pieve Emanuele, Milano – Italy). Kinetic profiles of CA formulations during all degradation experiments were calculated by applying the Multivariate Curve Resolutions (MCR) algorithm to the spectral data by using the Matlab® computer environment software (Mathwork Inc., version 7, Natick, MA, USA).

Standard solutions

Standard solutions of CA were prepared in water and in ethanol in the concentration range of 5.0 – 30.0 mg mL^{-1}.

Preparation and characterization of micelles

Empty and CA-loaded micelles were prepared by direct dissolution method using amount of P123 equal to 5%, 10% and 20 % (w/w) according to the phase diagram of P123 in aqueous solution [25]. Accurately weighted amount of P123 and CA ranging from 0.1% to 5%(w/w) were solubilized in water and stirred at room temperature overnight to reach thermodynamic equilibrium. The average particle hydrodynamic diameter, the polydispersity index (PI) and the surface charge of the resulting micelles were determined by light scattering techniques using Zetasizer Nano ZS 90 (Malvern Instrument, Worcestershire, UK). CA-loaded micelles were filtered through a 0.22 μm pore-size syringe filter to remove CA excess. The structure of the micelles was destroyed by dilution with ethanol and the concentration of CA solubilized in the final solution was evaluated using UV-Vis spectroscopy at 285 nm (absorbance maximum of CA) using the standard curve method. The encapsulation efficiency (EE%) was calculated using the following Eq 1:

$$EE\% = \frac{CA\ concentration\ in\ micelle}{Initial\ CA\ concentration}\ x\ 100 \quad (1)$$

All samples were analysed in triplicate.

Rheological characterization

The rheological properties of P123 micelles were studied by Dynamic Shear Rheological (DSR) measurements. The rheological measurements were conducted using a shear strain-controlled rheometer RFS III (Rheometrics, USA) equipped with concentric cylinder geometry (inner radius 17 mm, gap 1.06 mm). The temperature is controlled directly via the rheometer software by a fluid circulator (error ±0.1). To prevent errors due to evaporation, the measuring geometries were surrounded by a solvent trap containing water. The fresh surfactant solutions were submitted to shearing rates during experiments, were fully transparent and free from foam and air bubbles.

Steady flow experiments (flow curves) were performed in a shear rate range of 0.02–1700 s^{-1}. Sometimes it was not possible to coverall shear rate range due to the instrumental limits imposed by the viscosity of the samples.

***In vitro* hemolysis assay**

Red blood cells were separated from heparinized blood by centrifugation at 3000 rpm for 10 min. Then, the plasma was removed, and the red blood cells were redispersed in PBS and washed three times. For the hemolysis assay, erythrocytes suspension was diluted in PBS to $8x10^9$ cells/ml. An aliquot of 25 mL of erythrocyte suspension was mixed with various volume of micelle in microtube and the final volume was completed to 1 mL with PBS pH 7.4. The mixtures were incubated under shaking at room temperature for 10 min. At the end of the incubation, the samples were centrifuged at 10000 rpm for 5 min. Absorbance of the hemoglobin release in supernatants was measured at 540 nm using a UV-vis spectrophotometer and the percentages of hemolysis were determined by comparison with the positive control samples completely hemolyzed.

Experimental conditions in the stability studies

Five aqueous solutions of CA were prepared at the following concentration values: 5.0, 10.0, 15.0, 20.0 and 30.0 mg mL^{-1}. Each solution was directly light irradiated in the Suntest cabinet by applying the following experimental conditions: irradiation range between 320 and 800 nm; irradiance power fixed to 350 W m^{-2}, corresponding to a light dose of 21 kJ min^{-1} m^{-2}; temperature of 25 °C. The UV spectra were recorded just after the preparation and at the following interval times of light exposure: 1, 2, 3, 4, 5, 6, 7, 8, 10, 15, 20, 30, 60, 90 and 120 min. Three aqueous solutions were exposed to thermal tests in the thermostatic bath at 60 and 80 °C, respectively. The UV spectrum was acquired for each experiment just after the preparation and at the same interval time used for

photodegradation experiments until a total time of 120 min. The data matrix obtained from the collected spectra for each experiment was analysed by MCR-ALS to define the number of the involved components (number of degradation products), their absorbance spectra, and the kinetic rate of the degradation process (k values).

Radical scavenging activity

Stock dispersions of CA free and loaded in micelles were diluted in order to obtain different concentrations 1.5 mL of the sample were incubated with 1.5 mL of ethanol DPPH solution 0.25 mM at room temperature in the dark. After 30 min, absorbance measurements were taken at 517 nm with UV-vis spectrophotometer. The DPPH radical scavenging activity was calculated according to the following equation:

$$DPPH\ Scavenging\ activity\ (\%) = \frac{(A_0 - A_1)}{A_0} x100 \quad (4)$$

where A_0 is the absorbance of control and A_1 is the absorbance in presence of CA free and loaded in micelle formulations. Moreover, the antioxidant activity of degradation products of caffeic acid was estimated after photodegradation process. Each experiment was carried out in triplicate and the results expresses as means ± SD.

***In vitro* diffusion and skin permeation studies**

In vitro CA diffusion and skin permeation from P123 micelles has been evaluated by Franz cells at two different temperatures, 32 and 40 °C. Particularly, the diffusion barrier was Visking tubing (Spectra/Por®, cut-off 12–14 kDa), while for permeation studies rabbit ear skin was used. The artificial membrane and skin was clamped between the donor and the receptor compartment of the Franz diffusion cell. The effective penetration area was 0.416 cm^2, and the receptor compartment capacity was 5.5 mL. The receptor compartment was filled with medium and at various time points the medium in the receptor compartment was collected and replenished immediately with an equal amount to maintain sink conditions. Then, the CA concentration released were quantified using UV-vis spectroscopy. The cumulative amount of CA permeated per unit area was calculated, and the permeation profile was plotted as a function of time. In order to determine the amount of CA retained in the skin, the skin was carefully separated from the diffusion cell at the end of skin permeation experiments (24 h) and rinsed with deionized water to remove any residual formulation. Then the retained CA in skin was extracted by soaking in 10 mL of ethanol for 1 h with constant stirring in the dark. The

solution was then filtered by a membrane (0.22 μm), and the content of CA was analysed by UV-vis spectroscopy.

Results and discussions

Micelles characterization

In this manuscript, attempts were made to solubilize CA in P123 micelle to increase the bioavailability, stability and antioxidant activity. Micellar aggregates were prepared using three different surfactant concentrations (5%, 10% and 20%). The maximum solubilized concentration of CA in 10% and 20 % (w/w) P123 micelle solution was 0.5 (w/w) %. Instead, micelles made up of 5 % of surfactant were able to solubilize only the 0.2(w/w) % of CA. For this reason, the micellar solution prepared with 5 % of surfactant was eliminated from the subsequent study. The average size for empty micelles and drug-loaded micelles are reported in Table. The mean diameter of empty P123 micelles and drug-incorporated micelles was in the range between 11.7 and 15.9 nm with rather narrow size distribution (PI lower than 0.218). Loading micelles with CA did not visibly affect their size

Table 1. Physicochemical characterization of empty and CA loaded mixed micelles**.**

Sample	P123 %(w/w)	CA %(w/w)	Size (nm)	PI	Z Potential (mV)	EE %
MC5	5	-	17.7	0.029	-5.45±0.225	-
MC5CA0.1	5	0.1	15.86±0.16	0.087	-5.27±1.07	77.68
MC5CA0.2	5	0.2	15.85±0.02	0.103	-7.78±2.11	82.59
MC10	10	-	15.9	0.149	-7.31±1.66	-
MC10CA0.5	10	0.5	13.53±0.92	0.097	-1.08 ±0.18	78.73
MC20	20	-	11.7	0.214	-0.59±0.35	-
MC20CA0.5	20	0.5	12.83±1.12	0.218	-1.62±0.42	80.55

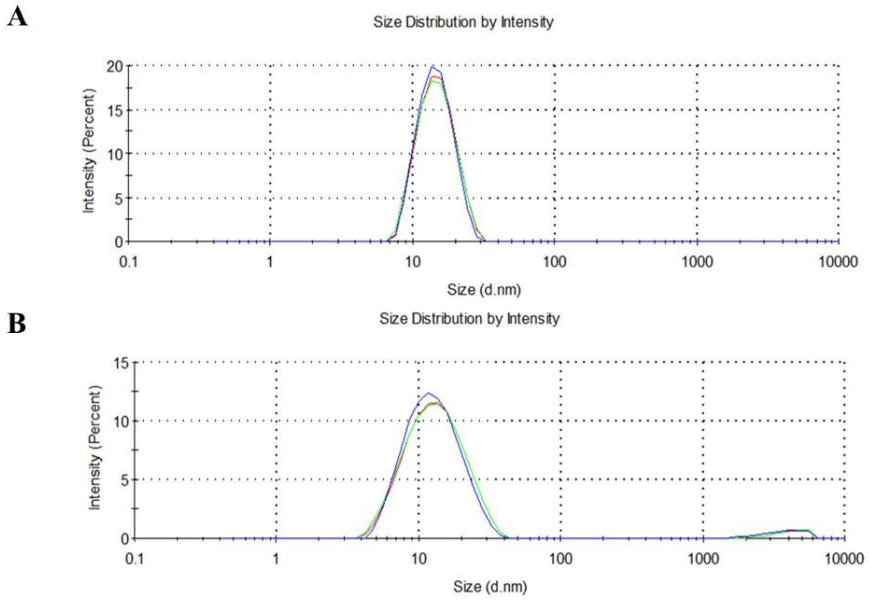

Figure 1. Intensity size distribution of MC10CA0.5 (A) and MC20CA0.5 (B) determined by DLS.

Rheological studies

Rheological characterization was carried out on MC10 and MC20 micellar formulations, both empty and CA-loaded. The experiments were conducted at 3 different temperatures: 25°C, 32°C and 40°C. These studies show that for the empty micelles solutions (Figure 2), in both cases (10%wt and 20%wt), the viscosity decreases with increasing temperature. It is worthy to note the initial shear thinning and low viscosity values. It means the micelles are small and lightly oblate. The effect of the temperature is expected. The viscosity decreases in temperature to kinetics reasons. This thinning behaviour is slightly more pronounced with increasing of the P123 content and the viscosity is higher. The micelles are more oblate at higher percentage of P123.

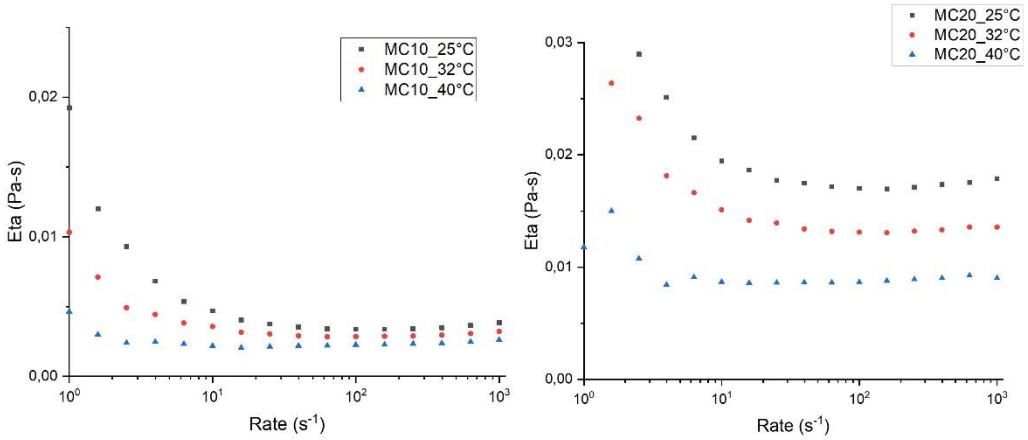

Figure 2. Rheological characterization of (A) MC10 (B) MC20 at 25°C (■), 32°C (●) e 40°C (▲)

When the CA-is loaded in micelles (Figure 3), the viscosity decreases at 32°C and after it increases at 40°C. However, this behaviour can be observed in both micelle solutions, but at 20 %wt: this effect is dominant, in fact the flow curves of the MC20CA0.5 solution is higher than that one measured at 25°C. This means that at 40°C the CA induces the "gel formation". In presence of CA the micelles grow and the shape becomes more asymmetrical.

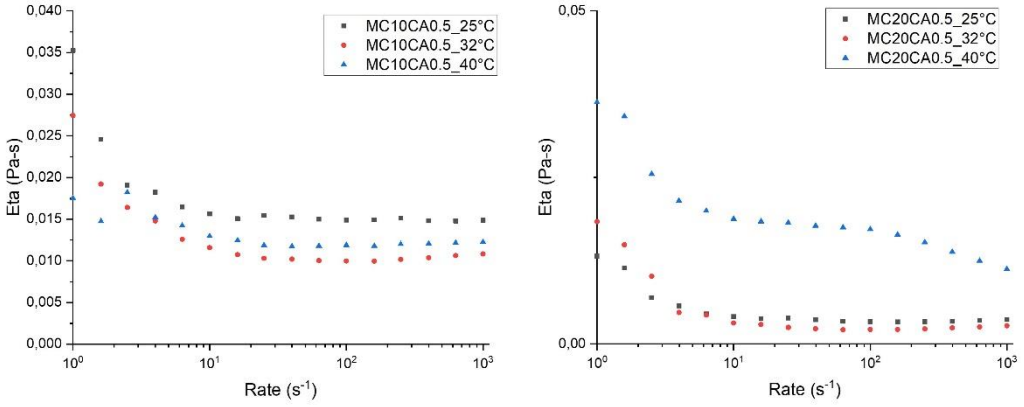

Figure 3. Rheological characterization of (A) MC10CA0.5 (B) MC20CA0.5 *at* 25°C (■), 32°C (●) e 40°C (▲).

From this behaviour, it can be assumed that the micelles have an oblate and not completely spherical shape. In addition, a characterisation of the size of MC20CA0.5 was conducted by means of dynamic light-scattering analysis at different temperatures. Table

2 shows the values obtained, from which it can be seen that as the temperature increases, the average micelle diameter also increases.

***In vitro* diffusion and permeation studies**

In vitro diffusion and permeation studies were performed at two different temperatures, 32 and 42 °C, to evaluate the relation of CA release from these micelles with respect to increase in the temperature.

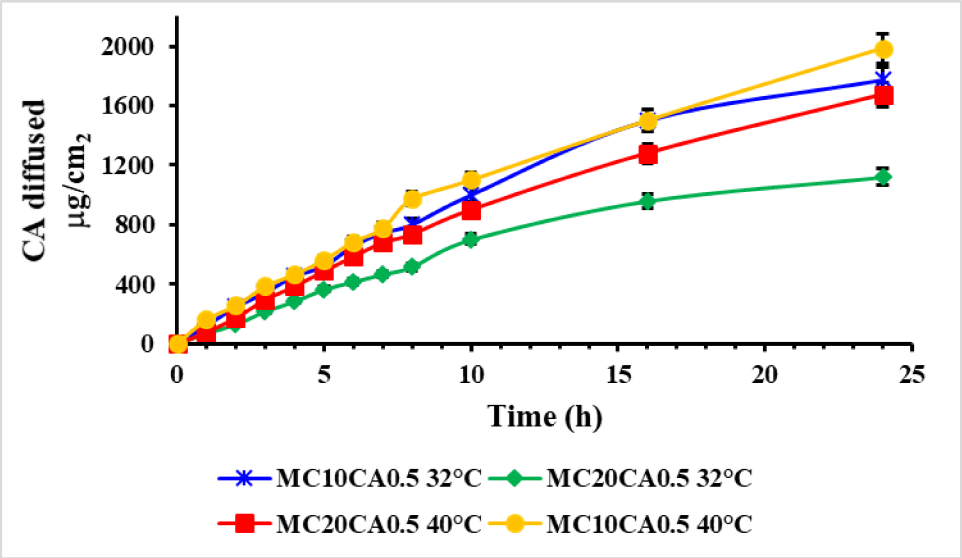

Figure 4. *In vitro* skin diffusion profiles of CA from MC10 and MC20 at 32°C and 40 °C. Results were presented as mean ± SD

In vitro diffusion profile of CA micelles was investigated using Franz diffusion cells at 37 °C for 24 h. As shown in Figure 4 it was concluded that the diffusion clearly decreases with increasing the polymer concentration. In fact, the micelle made up of 10 % of P123 exhibited higher amount of diffused drug compared to MC20. This means that as the micelle microstructure gets stronger by polymer addition, the drug diffusion is slower and can be used for prolonged release. The temperature increase led to an increase of CA diffusion for both formulations.

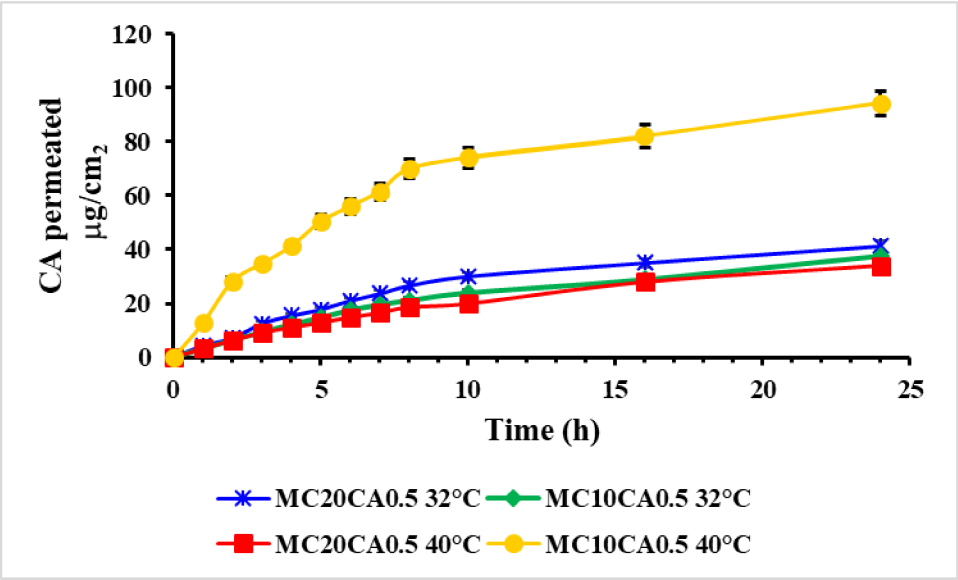

Figure 5. *In vitro* skin permeation profiles of CA from MC10 and MC20 at 32°C and 40 °C. Results were presented as mean ± SD

Franz skin permeation study was also performed to evaluate the permeability of CA from various formulations at 32 °C and 40 °C (Figure 5). At 32 °C permeation profile of CA from MC10 and MC 20 was similar, on the contrary a significant higher permeation was observed for MC10 at 40 °C. Moreover, the temperature increase led to a higher permeation for MC10 sample: in fact, the amount of CA permeated at 40 °C equal to 94.18 µg/cm^2 resulted to be 2.47 times higher respect the amount permeated at 32 °C equal to 37.76 µg/cm^2. This trend was not observed for MC20 formulation. CA permeation profile from MC20 was very similar at both temperatures achieving an amount of drug permeated after 24 h equal to 41.19 and 34.02 µg/cm^2 respectively at 32 and 40 °C. To better understand the mechanism of the different behaviour of the micelle in permeation study with the temperature increase, studies focused on the effect of temperature on micelle size and rheological properties were carried out. DLS experiments were performed to find the hydrodynamic diameter of micelles as a function of temperature increase as depicted in **Table 2**.

Table 2. DLS analysis of micelle formulation with temperature increases from 25°C to 44 °C

	MC10CA0.5		**MC20CA0.5**	
	Size (nm)	*PI*	*Size (nm)*	*PI*
25°C	16.04	0.180	12.16	0.217
29°C	16.80	0.195	12.41	0.210
32°C	22.78	0.340	13.82	0.271
35°C	30.36	0.393	19.13	0.458
38°C	35.40	0.369	19.13	0.558
41°C	37.75	0.367	26.54	0.529
44°C	41.58	0.373	27.52	0.470

The micellar size was observed to increase with temperature grow, which revealed that temperature alters the thermodynamics of micellization and the structure of Pluronic assemblies as also reported in literature [26]. At low temperature, water molecules predominantly form hydrogen bonds with the PEO blocks, while the PPO micelle core is mostly dehydrated. With the temperature increase, the hydration of the polymer chains decreases, and the block units undergo conformational changes, which result in lower polarity and in micelle assemble and anisotropic grow in size and change in morphology [27]. Moreover, this effect result be dependent also by polymer concentration [28].

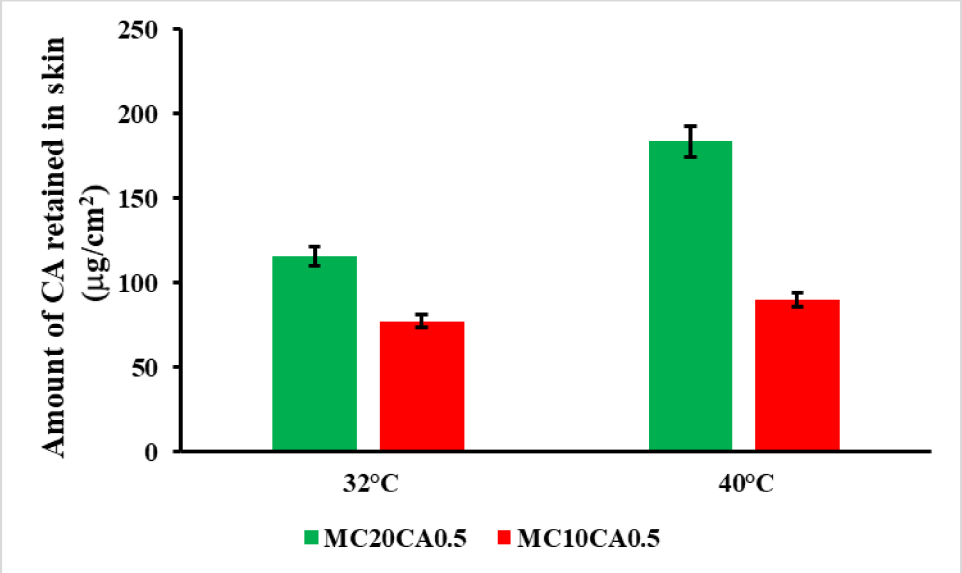

Figure 6. CA retention in rabbit ear skin after exposure to MC10CA0.5 and MC20CA0.5 for 24 h. Results were presented as mean ± SD.

The amount of CA that accumulated in the skin delivered by MC20 within 24 h was 1.5 and 2 times higher than that delivered by MC10 respectively at 32 °C and 40 °C indicating the ability of micelle made up of 20 % of P123 to form a drug depot in skin layers.

Stability studies

Stability profile of CA was assessed in aqueous solution. Abebe Belay in 2011 described the self-association of CA in water solution depending on the concentration. [29] When the concentration of CA is greater than 53.1 µM, the peak intensity at ~319 nm is greater than that of two-peak band, but for concentrations less than 53.1 µM the peak intensity at ~215 nm is greater than that of the doublet. Accordingly, we prepared five solutions in the concentration range of 5 – 30 mg mL^{-1} subdued to the spectrophotometric measurement. The behaviour of CA and the shift of the maximum absorbance is depicted in Figure 7. This shift of absorbance, intensity variation, and isosbestic points clearly suggests the self-association of caffeic acid, occurring via hydrogen bonding due to catechol or carboxylic groups.

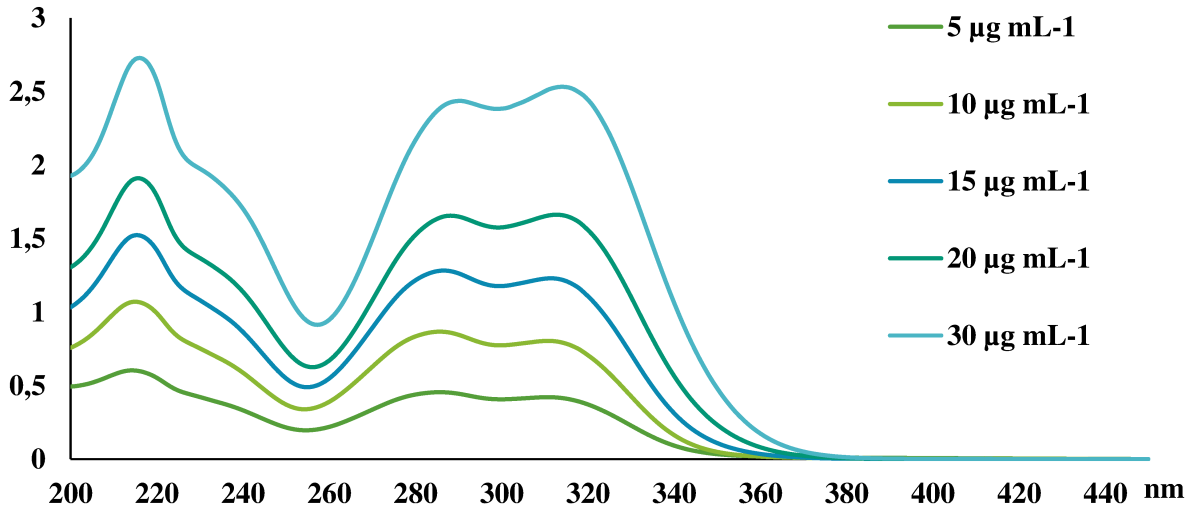

Figure 7. Absorbance spectra of CA aqueous solutions at different concentration values.

The effects of the temperature and light were verified on the prepared solutions. The applied experimental conditions are described in section 3.6 for both experiments. At this aim, five aqueous solutions of CA at the concentration values of 5.0, 10.0, 15.0, 20.0, and 30.0 mg mL^{-1} were exposed to light. Moreover, three aqueous solutions at the concentration values of 5.0, 20.0, and 30.0 mg mL^{-1} were exposed to thermal tests in the thermostatic bath at 60 and 80 °C, respectively. The UV spectra were recorded just after

the preparation and at different interval times of stressed exposure until to a total time of 120 min. The data matrix obtained from the collected spectra for each experiment was analysed by Multivariate Curve Resolution- Alternating Least Squares (MCR-ALS) to define the number of the involved components (number of degradation products), their absorbance spectra and the kinetic rate of the degradation process (k values). This chemometric procedure aims to resolve the chemical contributions to the outcome of an experiment as described through a data matrix. The MCR method decomposes the experimental data matrix (D) into a reduced set of contributions of chemical species (in our study, CA and its degradation products) using a bilinear model. The number of components involved in the matrix D (chemical rank) can be estimated by Principal Component Analysis (PCA) algorithms. The chemical rank assumes that the species contributing to the measured spectra have singular values larger than the other signal contributions, such as experimental or instrumental noise. Once the number of components is known, the ALS algorithm uses a series of constraints to optimize the MCR model. The application of constraints such as non-negativity, unimodality, and concentration closure allows one to optimize the results according to a chemical meaning. The quality and reliability of the multivariate resolution can be assessed using the explained variance (%R^2) and the lack of fit (%). Wavelengths below 215 nm were discarded as preliminary selection, due to their high variability or instrumental noise. Therefore, the MCR processing was applied to spectral data between 215 and 450 in all experiments.

When CA is exposed to light, data processing shows the formation of a single photoproduct (CA-Ph) for all the tested concentration values. As an example, figures 8 showed the spectral sequence (part A) recorded during the photodegradation experiment on the CA solution at a concentration value of 20.0 mg mL^{-1}, concentration profiles (part B), and the UV spectra of the pure compound and the relative photoproducts (part C).

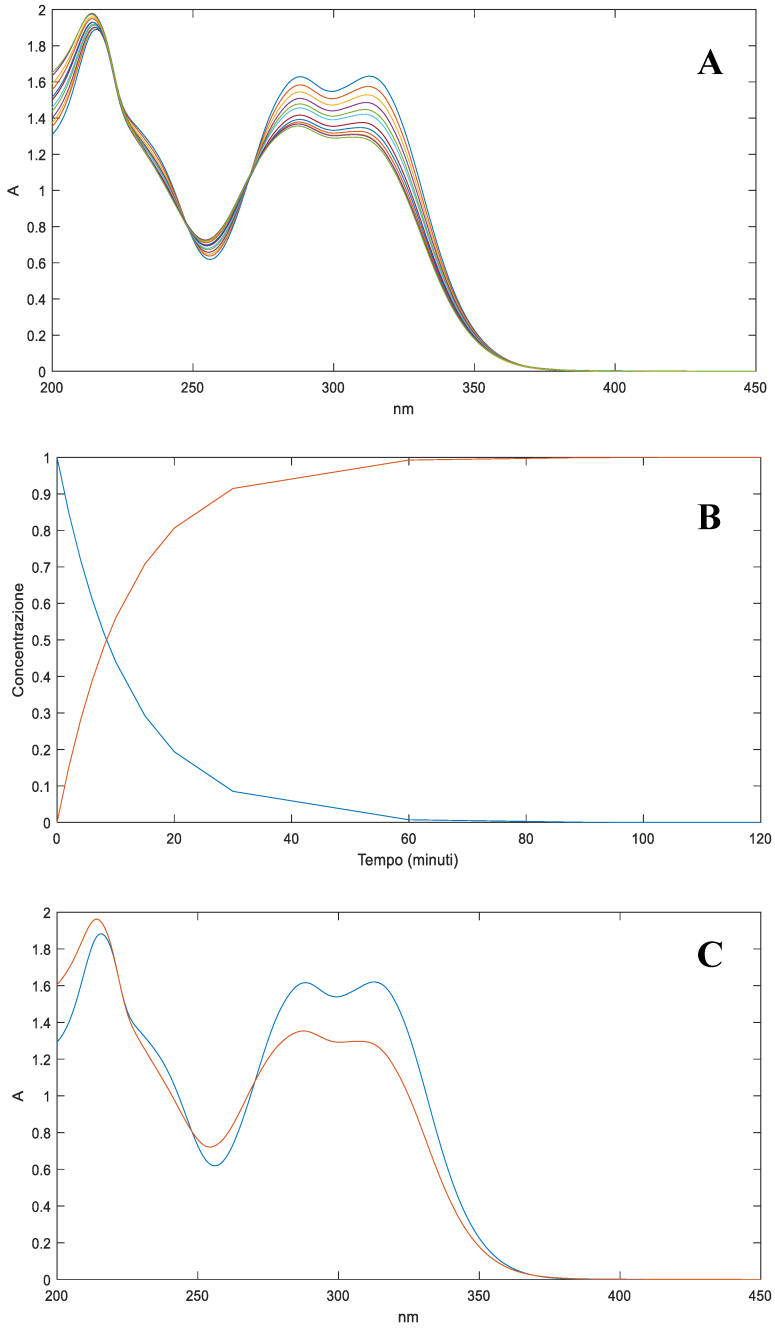

Figure 8. Photodegradation experiments of CA at a concentration of 20.0 μg mL^{-1}. **(A)** Spectral sequences and **(B, C)** concentration profiles and relative absorbance spectra, respectively, of the pure compounds (blue line) and the photoproduct (red lines) obtained from MCR elaboration.

A first-order kinetic equation was calculated in all photodegradation experiments as follows:

$$\ln(\%CA) = -k\ x\ t + 4.67 \quad (5)$$

where %CA is the percentage of residual absorbance, k is the photodegradation rate, t is the time (s), and 4.67 is the logarithm of initial absorbance (100%). In all experiments,

the parameter lack of fit (% lof), which indicates the quality of the MCR results, was less than 5%, and the R^2 was higher than 99.5%. Table 3 summarizes the kinetic parameters calculated for CA in the different exposure conditions. The data were collected from three replicate analyses for each sample, and very low variance was measured in all the cases.

Table 3. Kinetic parameter calculated for CA solutions exposed to light

Samples	k	lof %	R^2
Light exposure			
[CA] 5 µg mL^{-1}	0,0013835	4,0707	99,8343
[CA] 10 µg mL^{-1}	0,0017097	1,0425	99,9891
[CA] 15 µg mL^{-1}	0,0014513	0,87917	99,9923
[CA] 20 µg mL^{-1}	0,0013682	0,65749	99,9957
[CA] 30 µg mL^{-1}	0,0015067	0,35465	99,9987
MC10CA0.5	-	-	-
MC20CA0.5	-	-	-

When CA solutions are exposed to rising temperatures, no formation of degradation product was observed. Furthermore, a complete protection was observed for CA when loaded in micelle formulations (Figure 9).

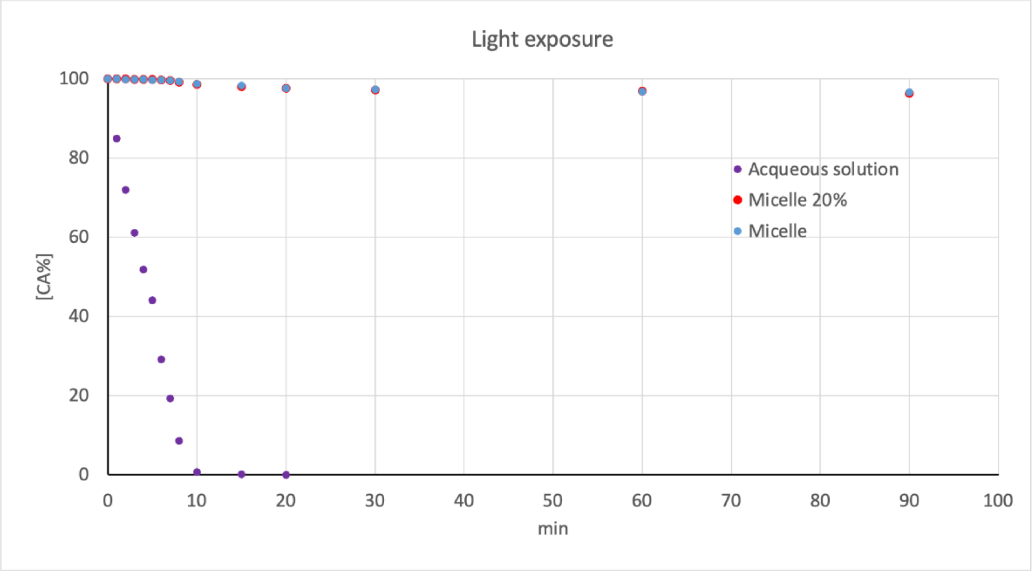

Figure 9. Light exposure of micelle formulations and aqueous solution of caffeic acid

Antioxidant properties

To investigate, whether CA retains its antioxidant properties when loaded in micelle systems, the DPPH scavenging activity of the formulations were evaluated and compared to free CA (Figure 10).

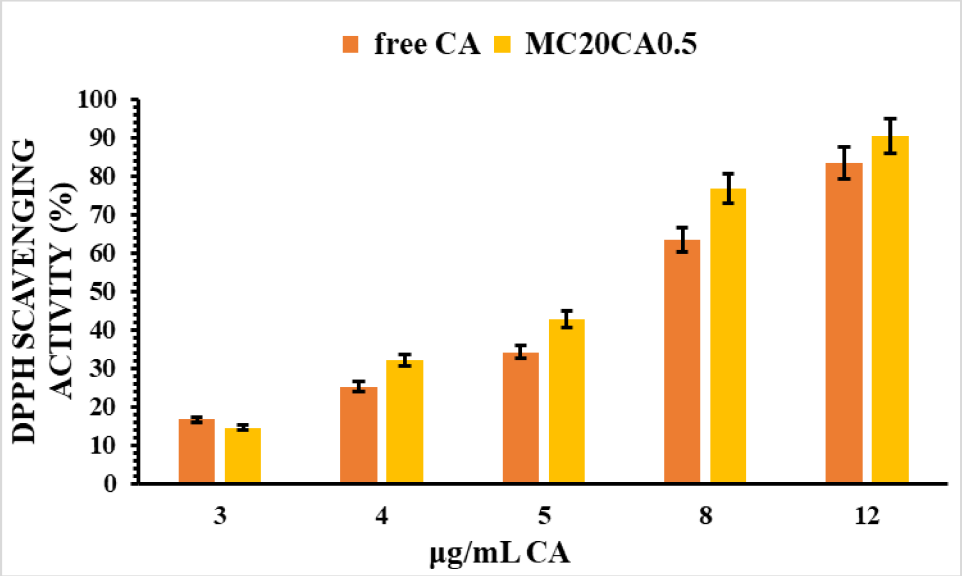

Figure 10. Antioxidant activity by DPPH radical scavenging assay of CA free and loaded in MC20. Data is represented as Mean ± SD, n=3.

CA both free and loaded in micelle formulations displayed a significant concentration-dependent free radical scavenging activity (Figure 10). Moreover, no significant differences were observed for the antioxidant activity of free CA and loaded in micelles that showed an amount required for 50% inhibition of DPPH activity equal to 7.05 and 6.19, respectively. So, our results showed that the loading of CA in micellar systems preserved its antioxidant activity. Moreover, the antioxidant activity of CA both as free and as loaded in micellar formulations after stressed degradation experiment was also evaluated and compared with that before degradation tests. As shown in Figure 11 and 12, the thermal stressed test carried out at 60 and 80 °C did not affect antioxidant activity of free CA according to degradation studies that demonstrated that free CA was stable in these conditions. On the contrary, antioxidant activity of free Ca after photodegradation experiments changed at the various time points (Figure 13). This is probably related to the drug instability to light that transform it in new photoproduct with different antioxidant activity. Anyway, antioxidant activity of CA loaded in micelle was similar at each time points investigated during photodegradation test, indicating the increased light stability of the drug when loaded in micellar formulations (Figure 14 and 15).

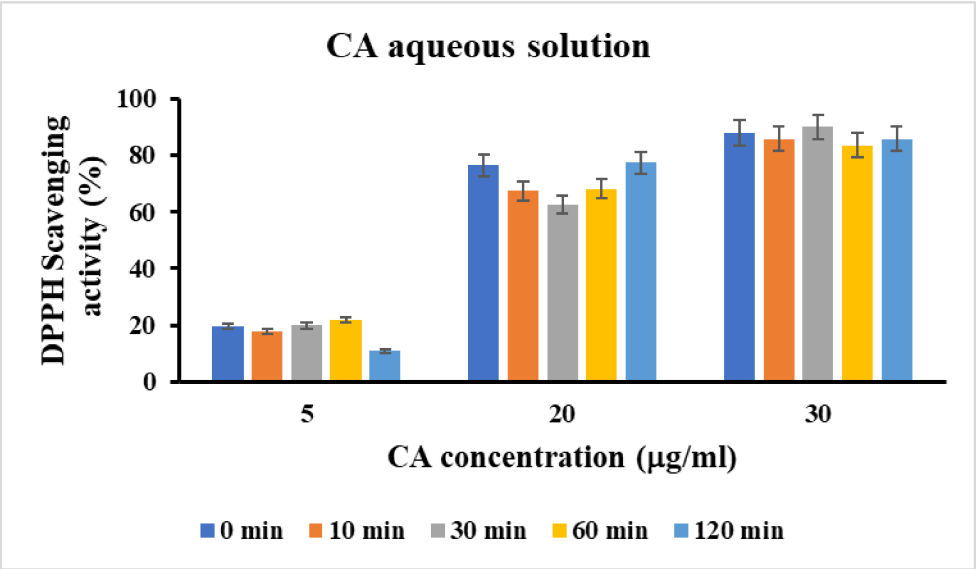

Figure11. DPPH scavenging activity of CA aqueous solutions after thermal degradation experiment carried out at 60°C

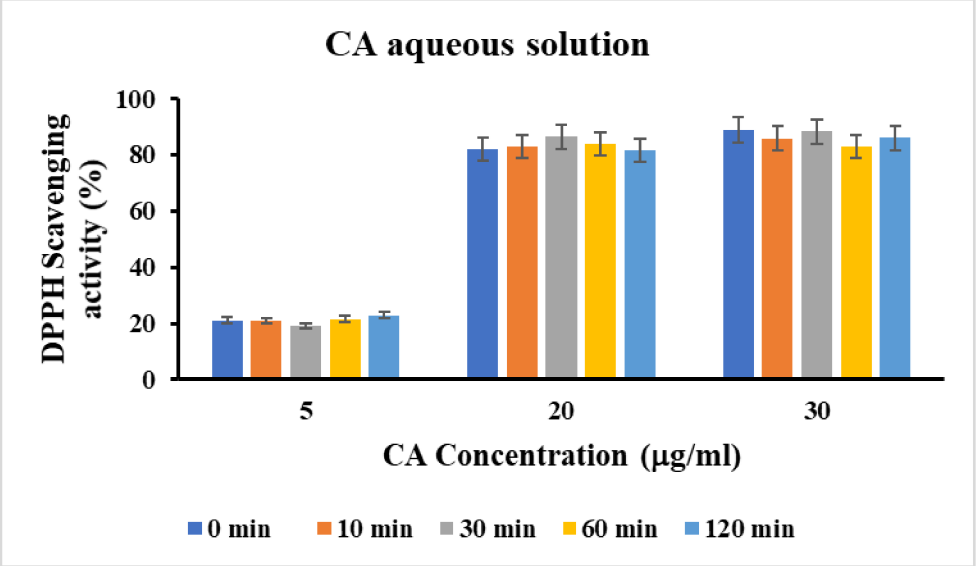

Figure 12. DPPH scavenging activity of CA aqueous solutions after thermal degradation experiment carried out at 80°C

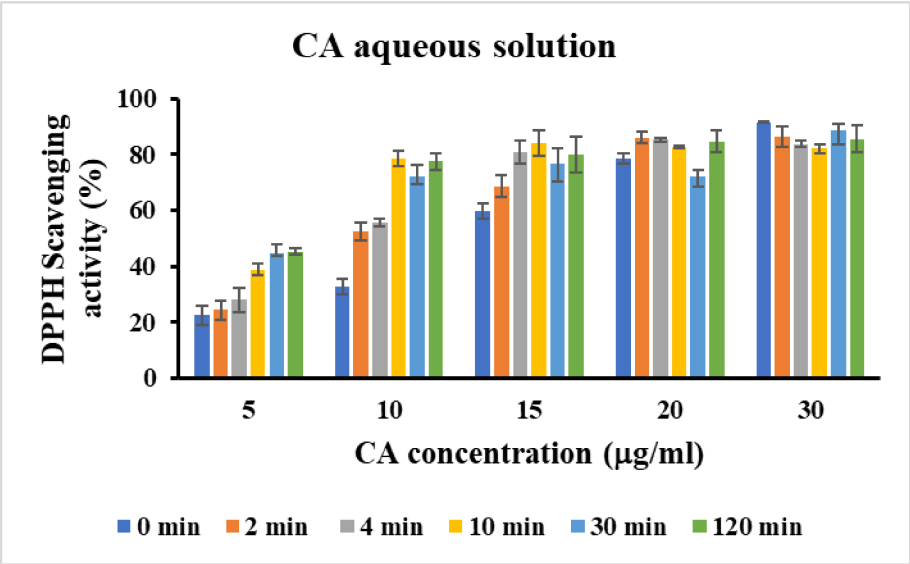

Figure 13. DPPH scavenging activity of CA aqueous solutions after photodegradation experiment. . Data is represented as Mean ± SD, n=3.

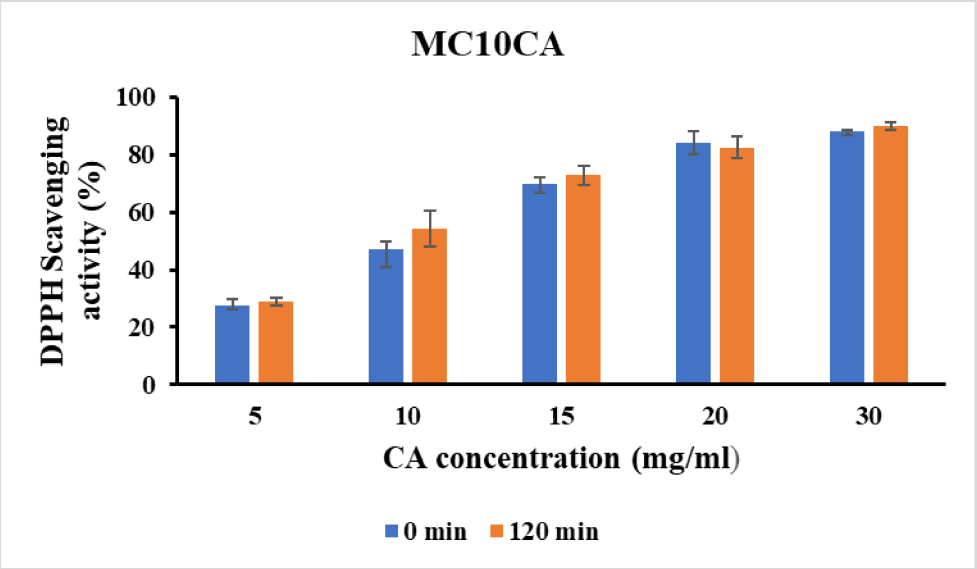

Figure 14. DPPH scavenging activity of MC10 formulations after photodegradation experiment. . Data is represented as Mean ± SD, n=3.

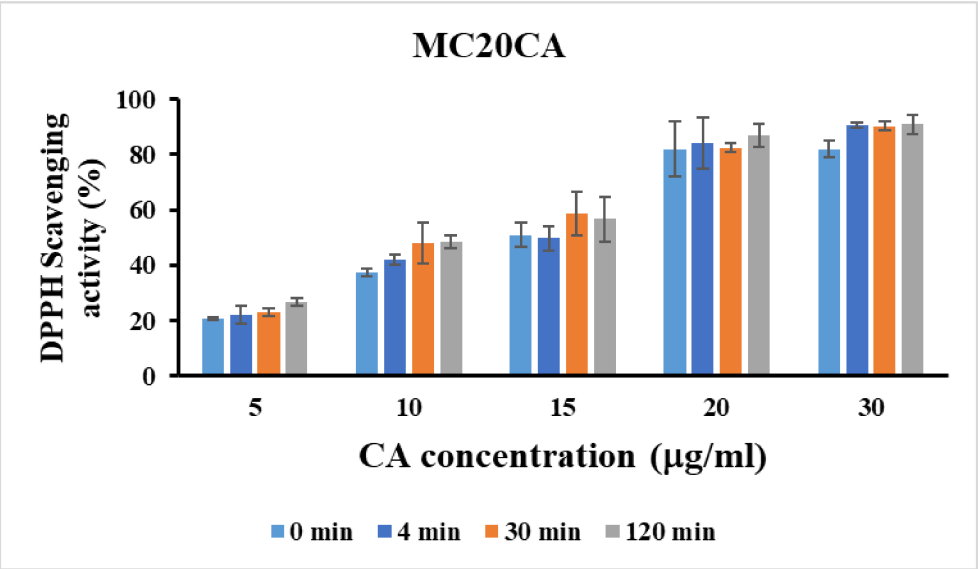

Figure 15. DPPH scavenging activity of MC20 formulations after photodegradation experiment. . Data is represented as Mean ± SD, n=3.

Conclusions

In summary, polymeric micelles of caffeic acid were prepared using Pluronic P123 at two different concentrations to enhance its solubility, bioavailability and stability. Loading CA within the micelles increased significantly its water solubility, resulting in formulations with high colloid stability suitable for various routes of application. More importantly, micelles developed effectively protect CA from degradation when exposed to UV light, offering significant benefits for various biomedical applications. Overall, the use of Pluronic P123 micelles as carriers for caffeic acid encapsulation represents a promising approach to address issues of poor solubility and stability, paving the way for the development of safer, cost-effective delivery systems with enhanced therapeutic potential.

REFERENCE

[1]Anantharaju, P. G., Gowda, P. C., Vimalambike, M. G., & Madhunapantula, S. V. An overview on the role of dietary phenolics for the treatment of cancers. *Nutr. J.*, **2016**, *15*(1), 99–114. https://doi.org/10.1186/s12937-016-0217-2 [2] Khan, F. A., Maalik, A., & Murtaza, G. Inhibitory mechanism against oxidative stress of caffeic acid. *J. Food Drug Anal.*, **2016**, *24*(4), 695–702. https://doi. org/10.1016/j.jfda.2016.05.003.

[3] Silva, T., Oliveira, C., & Borges, F. (2014). Caffeic acid derivatives, analogs and applications: A patent review (2009–2013). *Expert Opin. Ther. Pat .*, **2014**, *24*(11), 1257-1270. https://doi.org/10.1517/13543776.2014.959492

[4] Mishra, M., Panta, R., & Miyares, M. Influence of coffee and its components on breast cancer: A review. *Asian Pac. J. Trop. Dis.*, **2016**, *6*(10), 827-831. https://doi.org/10.1016/S2222-1808(16)61140-4

[5] Magnani, C., Isaac, V. L. B., Correa, M. A., & Salgado, H. R. N. Caffeic acid: a review of its potential use in medications and cosmetics. *Anal. Methods*, **2014**, *6*(10), 3203-3210. https://doi.org/10.1039/C3AY41807C

[6] Pinho, E., Soares, G., & Henriques, M. Evaluation of antibacterial activity of caffeic acid encapsulated by β-cyclodextrins. *J. Microencapsul.,* **2015**, *32*(8), 804-810. https://doi.org/10.3109/02652048.2015.1094531

[7] Andrade, S., Loureiro, J. A., & Pereira, M. C. Caffeic acid for the prevention and treatment of Alzheimer's disease: The effect of lipid membranes on the inhibition of aggregation and disruption of Aβ fibrils. *Int. J. Biol. Macromol.*, **2021**, *190*, 853-861. https://doi.org/10.1016/j.ijbiomac.2021.08.198

[8] Mota, F.L.; Queimada, A.J.; Pinho, S.P.; Macedo, E.A. Aqueous Solubility of Some Natural Phenolic Compounds. *Ind. Eng. Chem. Res.* **2008**, *47*, 5182–5189. https://doi.org/10.1021/ie071452o

[9] Jung, U.J.; Lee, M.-K.; Park, Y.B.; Jeon, S.-M.; Choi, M.-S. Antihyperglycemic and antioxidant properties of caffeic acid in db/db mice. *J. Pharmacol. Exp. Ther.* **2006**, *318*, 476–483. https://doi.org/10.1124/jpet.106.105163

[10] Razboršek, M. I., Ivanović, M., & Kolar, M. Validated stability-indicating GC-MS method for characterization of forced degradation products of trans-caffeic acid and trans-ferulic acid. *Molecules*, **2021**, *26*(9), 2475. https://doi.org/10.3390/molecules26092475

[11] Hallan, S. S., Sguizzato, M., Mariani, P., Cortesi, R., Huang, N., Simelière, F., ... & Esposito, E. Design and characterization of ethosomes for transdermal delivery of caffeic acid. *Pharmaceutics*, **2020**, *12*(8), 740. https://doi.org/10.3390/pharmaceutics12080740

[12] Opanasopit, P., Ngawhirunpat, T., Rojanarata, T., Choochottiros, C., & Chirachanchai, S. N-Phthaloylchitosan-g-mPEG design for all-trans retinoic acid-loaded polymeric micelles. *Eur. J. Pharm. Sci*, **2007,** *30*(5), 424-431. https://doi.org/10.1016/j.ejps.2007.01.002

[13] Valero, M., Levin, P. P., Sultimova, N. B., & Houston, J. E. Photochemistry of nabumetone in aqueous solution of sodium dodecyl sulfate (SDS) micelles. J. Mol. Liq., **2020,** *319*, 114093. https://doi.org/10.1016/j.molliq.2020.114093

[14] Ioele, G., Muzzalupo, R., Gündüz, M. G., De Luca, M., Mazzotta, E., Grande, F., ... & Ragno, G. Use of Pluronic Surfactants in Gel Formulations of Photosensitive 1, 4-

Dihydropyridine Derivatives: A Potential Approach in the Treatment of Neuropathic Pain. Pharmaceutics, **2021**, *13*(4), 527. https://doi.org/10.3390/pharmaceutics13040527

[15] Lapteva, M., Mignot, M., Mondon, K., Möller, M., Gurny, R., & Kalia, Y. N. Self-assembled mPEG-hexPLA polymeric nanocarriers for the targeted cutaneous delivery of imiquimod. *Eur. J. Pharm. Biopharm.* **2019**, *142*, 553-562. https://doi.org/10.1016/j.ejpb.2019.01.008

[16] Wang, Z., Xue, Y., Chen, T., Du, Q., Zhu, Z., Wang, Y., ... & Liu, Q. (2021). Glycyrrhiza acid micelles loaded with licochalcone A for topical delivery: Co-penetration and anti-melanogenic effect. *Eur. J. Pharm. Sci*, **2021**, *167*, 106029. https://doi.org/10.1016/j.ejps.2021.106029

[17] Makhmalzade, B. S., & Chavoshy, F. (2018). Polymeric micelles as cutaneous drug delivery system in normal skin and dermatological disorders. *J. Adv. Pharm. Technol. Res.*, **2018**, *9*(1), 2. https://doi.org/ 10.4103/japtr.JAPTR_314_17

[18] Javan, R. *Biological Structures*; Elsevier Ltd.: Richmond, VA, USA, **2005**.

[19] Batrakova, E. V., & Kabanov, A. V. Pluronic block copolymers: evolution of drug delivery concept from inert nanocarriers to biological response modifiers. *J. Control. Release.*, **2008**, *130*(2), 98-106. https://doi.org/10.1016/j.jconrel.2008.04.013

[20] Zhao, L. Y., & Zhang, W. M. Recent progress in drug delivery of pluronic P123: pharmaceutical perspectives. *J. Drug Target.*, **2017**, *25*(6), 471-484. https://doi.org/10.1080/1061186X.2017.1289538

[21] Zhang, X., Chen, W., Bai, J., Jin, L., Kang, X., Zhang, H., & Wang, Z. Pluronic P123 modified nano micelles loaded with doxorubicin enhanced tumor-suppressing effect on drug-resistant breast cancer cells. *Aging (Albany NY)*, **2020**, *12*(9), 8289. https://doi.org/10.18632/aging.103138

[22] Guo, C., Liu, H. Z., & Chen, J. Y. (1999). A Fourier transform infrared study of the phase transition in aqueous solutions of ethylene oxide–propylene oxide triblock copolymer. *Colloid Polym. Sci*, **1999**, *277*, 376-381. https://doi.org/10.1007/s003960050395

[23] Guo, C., Wang, J., Liu, H. Z., & Chen, J. Y. Hydration and conformation of temperature-dependent micellization of PEO− PPO− PEO block copolymers in aqueous solutions by FT-Raman. *Langmuir*, **1999**, *15*(8), 2703-2708. https://doi.org/10.1021/la981036w

[24] ICH. Photostability testing of new drug substance and products. In ICH Harmonized Tripartite Guideline, Federal Register; ICH: Geneva, Switzerland, **1997**; Volume 62.

[25] Alexandridis P., Holzwarth J. F., Hatton T. A. "Micellizzation of poly(ethylene oxide)-poly(propilene oxide)-poly(ethylene oxide) triblock copolymers in aqueous solutions: thermodynamics of copolymer association". Macromolecules, 27 (**1994**): 2414-2425.

[26] Singla, P., Singh, O., Sharma, S., Betlem, K., Aswal, V. K., Peeters, M., & Mahajan, R. K. Temperature-dependent solubilization of the hydrophobic antiepileptic drug lamotrigine in different pluronic micelles—A spectroscopic, heat transfer method, small-angle neutron scattering, dynamic light scattering, and in vitro release study. *ACS omega*, **2019**, *4*(6), 11251-11262. https://doi.org/10.1021/acsomega.9b00939

[27] Mortensen, K. Structural studies of aqueous solutions of PEO-PPO-PEO triblock copolymers, their micellar aggregates and mesophases; a small-angle neutron scattering study. *J. Condens. Matter Phys.*, **1996**, *8*(25A), A103. https://doi.org/10.1088/0953-8984/8/25A/008

[28] Mukherjee, K., Barman, A., & Biswas, R. Hydration dynamics in aqueous Pluronic P123 solution: Concentration and temperature dependence. *J. Chem. Phys.*, **2019**, *151*(18). https://doi.org/10.1063/1.5124526

[29] Belay, A. Self-association, sodium ion complexation and optical transition probabilities of caffeic acid determined spectrophotometrically. *Infection*, **(2012)**, *1*, 3.

Chapter 4:

Intelligent stimulus-responsive nanosystems for drug delivery

4. Intelligent stimulus-responsive nanosystems for drug delivery

4.1 Vesicular drug delivery systems: a novel approach in current nanomedicine

Elisabetta Mazzotta, Martina Romeo and Rita Muzzalupo

Department of Pharmacy, Health and Nutritional Sciences, University of Calabria, Rende, Italy

Pubblished on Molecular Pharmaceutics and Nano Drug Delivery Fundamentals and Challenges 2024, Pages 135-159

1 Introduction

The last century has witnessed unprecedented growth of nanotechnology applications in medicine with the aims to advance medical treatments, both for diagnostics and therapy, and improve health care quality. The design at the nanoscale range allows for the development of scaffolding systems able to overcome the limitations of conventional drug delivery. The reasons why nanoscale particles are attractive for medical purposes are their important and unique features, such as the small size and large functional surface that can be engineered to bind, adsorb, and carry compounds with targeting, imaging, and/or therapeutic properties. Various types of nanostructure materials have been developed by researchers for pharmaceutical applications. Among them, vesicular systems have caught increasing attention. Vesicular systems are core-shell structures consisting of one or more concentric bilayers formed as a result of self-assembling of amphiphilic molecules in aqueous environments. In aqueous media, indeed, amphiphilic molecule polar groups line up to form a water-attracting surface, while their lipophilic chains form a water-free zone (Fig. 1).

Their architecture makes them a versatile platform for the delivery of both hydrophilic and hydrophobic therapeutic agents. Hydrophilic drugs can be included in the core, whereas the lipid bilayer offers space for integration of hydrophobic drugs. They have been largely used, indeed, as a carrier of anticancer, antimicrobial drug, protein, gene, and imaging agents [1]. Many studies have demonstrated that vesicular systems improve drug pharmacokinetics and protect it against dilution and degradation or inactivation in the bloodstream. Interestingly, targeted delivery of drugs at the desired pathological tissue can also be achieved, thereby lowering its concentration at the other sites in the body and reducing toxic side effects [2]. Key advantages of vesicular delivery systems are

versatility and plasticity. Vesicle com- position is, indeed, an important parameter affecting physicochemical characteristics including particle size,

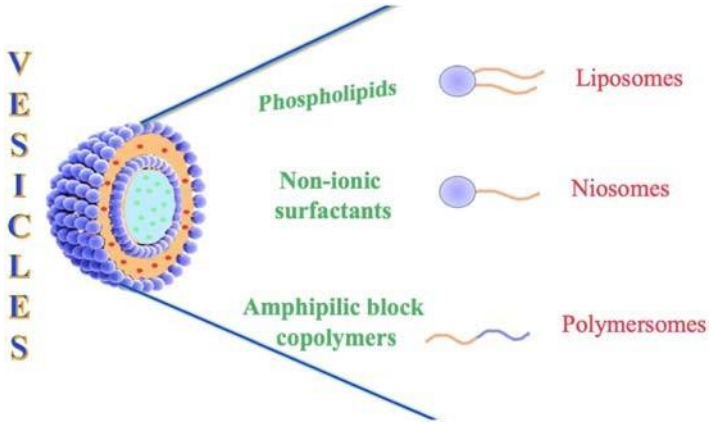

Figure 1. Sketch of different types of vesicular nanocarriers

surface charge, bilayer fluidity and permeability, stability and drug loading, and release rate [3]. Therefore, composition may vary and be chosen depending on the desired application. Source materials may be natural compounds such as phospholipids and polymers or have a "chemical" origin such as nonionic surfactants. Some of the most used amphiphilic molecules employed in the design of a vesicle structure are reported in Fig. 2. In addition, some drugs may be formulated as nanoscale vesicles and then function as their own "carrier." In addition, some drugs can be formulated as nanoscale vesicles and act as vectors of themselves. These types of drugs, known as surfadrug, have in their structure one or more flexible and hydrophobic aromatic nuclei, to which an ester group or a charge-bearing N atom is directly linked, or which include a pyridine-like N atom [4]. The direct use of drugs for vesicle preparation offers the possibility to bypass the use of additional excipients, improve formulation safety, and increase the amount of loaded drugs.

The pioneer formulations of vesicles made up of a drug, known as diclosomes, were developed by Tavano and coworkers [5]. The authors proposed the use of antiflammatory drug, diclofenac sodium, as the main component of the vesicular bilayer and it was observed that diclosomes exhibit the best performance with respect to traditional niosomes loaded with the diclofenac sodium aqueous core.

2. Type of vesicles

Vesicles for drug delivery purposes are categorized based on the amphiphilic component of the bilayer in liposome, niosomes, and polymersomes (Fig. 1). The nature of the amphiphilic molecule affects vesicle properties, and some of the main differences are summarized in Table 1. In the next paragraph, we will describe in detail the most interesting advantages and application of every vesicular aggregate.

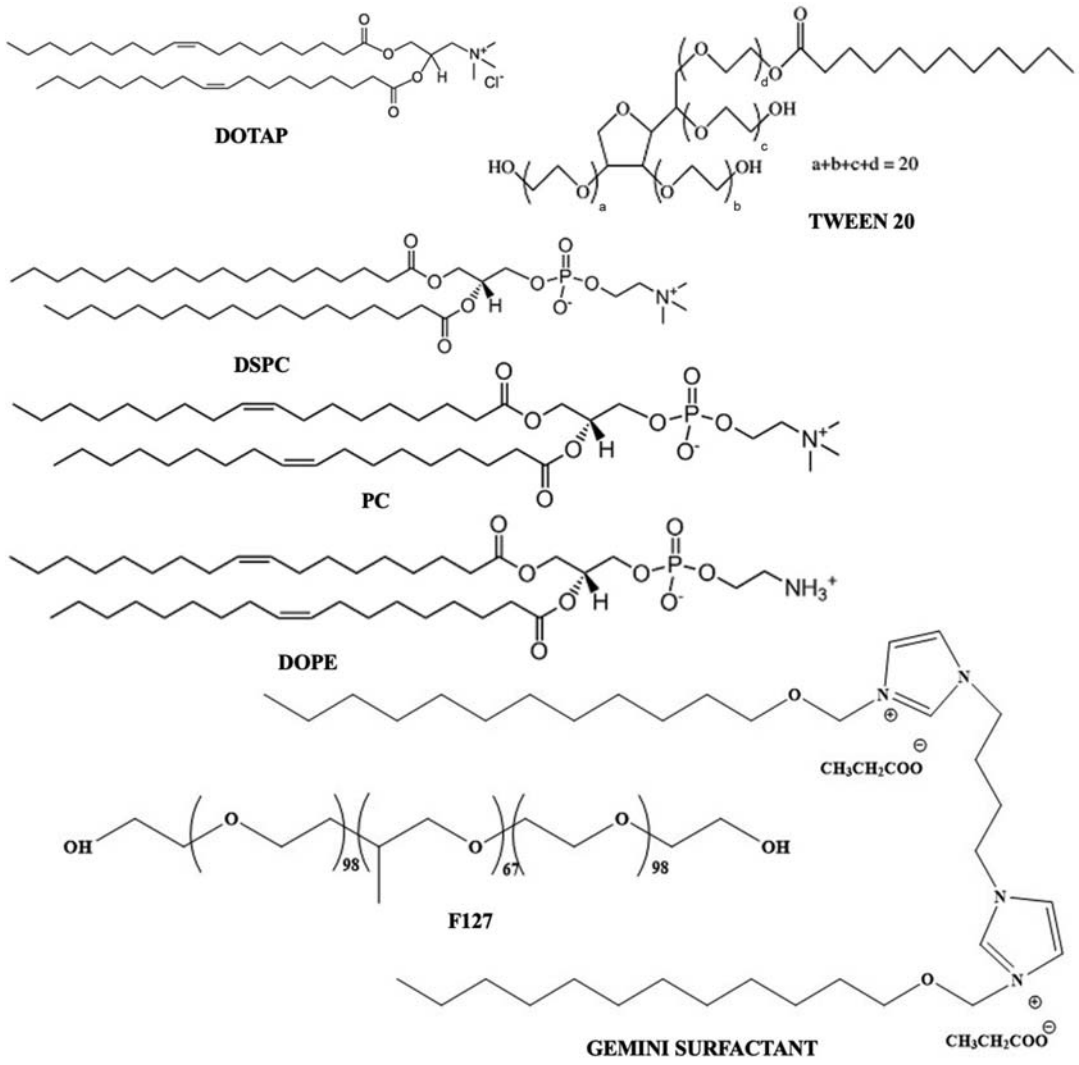

Figure 2. Common amphiphilic molecules employed in the design of vesicular drug delivery systems.

2.1 Liposomes

Liposomes are the oldest vesicles used as drug carriers and depict the first example of a clinically approved nanomedicine [6,7]. Actually, there are, indeed, more than 40 liposomal products either on the market or in various phases of clinical trials (Doxil, AmBisome, and Myocet) [8]. The main reasons of their wide translation in clinical therapy are their low immunogenicity, toxicity, and better therapeutic efficacy [9].

Liposomes are concentric bilayer vesicles composed of natural or synthetic lipids. A large variety of lipids with different head groups, chain saturation, chain lengths, and charge are available for their synthesis.

Table 1 Comparative features of liposomes, niosomes, and polymersomes.

Liposomes	Niosomes	Polymersomes
Phospholipids	Nonionic surfactants	Amphiphilic block copolymer
Chemically unstable	Chemically stable	Chemically stable
High permeability	Tunable permeability	Low permeability
Special storage condition	No special storage conditions	No special storage conditions
Expensive	Inexpensive	Inexpensive
Limited versatility	Wide chemical versatility	Wide chemical versatility

Common phospholipids used are phosphatidylcholines, phosphatidylethanolamines, phosphatidylserines, and phosphatidylglycerols [10]. From their first description in 1960, several improvements of liposome technology have been pursued evolving various formulations with distinctive characteristics such as conventional liposomes, sterically stabilized liposomes, ligand-targeted liposomes, and multi- functional liposomes [11].

Conventional liposomes are composed of anionic, cationic, or neutral phospholipids. Despite their ability to improve drug pharmacokinetics, conventional liposomes exhibit many problems such as fast macrophage uptake, chemical instability, and high membrane permeability, resulting in poor retention efficiency and drug leakage during blood circulation. Many approaches have been addressed to enhance in vivo performance, and one of them was the surface modification with hydrophilic polymers such as polyethylene glycol (PEG) developing stealth liposomes.

The hydrophilic polymer is able to establish a steric barrier reducing rapid recognition and uptake by reticuloendothelial system (RES) and in vivo opsonization remaining, there- fore, in circulation longer than conventional liposomes [12]. Anyway, the stealth strategy shows several drawbacks such as poor targeting efficiency. To overcome this limitation, liposomes conjugated on their surface with molecules selectively overexpressed at the dis- ease target site such as antibodies, peptides, and carbohydrates, glycoproteins or specific receptors ligands have been developed. Ligand-targeted liposomes increase drug selectivity, achieving a narrow distribution and accumulation at the site of interest with minimal deposition in healthy tissues. Finally, a new generation

of liposomes, which incorporate multiple complementary targeting strategies, have been developed to further improve liposomal targeting and maximize therapeutic outcomes.

2.2 Niosomes

Niosomes are structurally similar to liposomes and have attracted increasing interest as a better alternative to liposomes, thanks to their higher stability and lower production cost. Niosomes and liposomes display almost similar behaviour in sustained and targeted drug delivery. The only difference is their composition and chemical properties related to the material used in their preparation. Nonionic surfactants are the main constituent of niosomes and show better chemical stability with respect to phospholipids. Moreover, niosomes do not require a special storage condition, handling, and purification, which are necessary for liposome preparation. A variety of nonionic surfactants, such as polysorbates, alkyl esters, and alkyl ethers, are typically used for niosome preparation. In the last few years, attention has been focused on the development of newer classes of surface- active agents such as gemini surfactants to prepare innovative devices.

Gemini surfactants are composed of two hydrophobic chains and two polar head groups covalently connected by a covalently spacer group at the level of the head groups. Compared to corresponding single-chain surfactants, gemini surfactants exhibit superior aggregation capacity and, thus, lower CMC value [13]. Gemini surfactants based on amino acid have attracted increasing interest for the ability to combine the advantages of gemini surfactants in terms of efficiency with the higher biodegradability and lower toxicity of amino acids [14]. Specifically, gemini surfactants derived from lysine and arginine are very interesting since in addition to their better physicochemical properties, they showed an important antibacterial activity against a broad spectrum of gram-positive and gram- negative microorganisms [15].

2.3 Polymersomes

Polymersomes are artificial vesicles based on the self-assembly of amphiphilic copolymers. Block copolymers are macromolecules similar to lipids composed of a combination of hydrophilic and hydrophobic portions, which tend to self-assemble into various supramolecular structures. Amphiphilic block copolymers can be composed of two and three types of monomers with different structures like ABA, BAB, or ABC formats, where A and C are hydrophilic blocks with diverse chemical composition and B

is the hydrophobic block and also complex multiblock copolymers with linear or grafted blocks [16].

Typical hydrophilic blocks are nonionic polyethylene oxide or PEG, anionic polymethylacrylic acid or polyacrylic acid (PAA), cationic poly(2-vinyl pyridine) or poly(4-vinyl pyridine), and so forth. Instead, common hydrophobic blocks are polystyrene, polypropylene oxide, polybutadiene, and polylactic acid. Molecular composition and length of the hydro- phobic and hydrophilic blocks, indeed, influence different physicochemical properties such as membrane rigidity, size, and stability.

Owing to the material used to prepare them, polymersomes present countless advantages such a high stability [17], extended blood circulation, drug loading capacity, and membrane versatility due to the great variability of the starting materials. Compared to liposomes, polymersomes exhibit a greater life span and are generally more stable due to low membrane permeability; therefore, they can retain drugs with greater efficiency.

An interesting feature of these type of vesicles is the large versatility of polymer chemistry. Unlike phospholipids that exhibit a large limitation of functionalization, polymers can be functionalized in countless ways, and so, they are easily tunable for the desired therapeutic application [18]. This capability allows to design a variety of polymersomes with adjustable fluidity, permeability, stability, responsiveness, and targeting and imaging properties.

3 Engineered vesicles for therapeutic purposes.

The main goal of nanoscale vesicles as delivery agents is to deliver drugs with high selectivity to target tissues. Various approaches have been explored by researchers to develop smarter, safer, and more effective therapeutic nanovesicles systems. Advances in nanomedicine to achieve personalized therapy include targeted drug delivery, responsiveness to specific stimuli, and multifunctional approaches. The main goal of nanomedicine is to enable nanosystems to deliver the cargo (drugs, genes, radioisotopes, etc.) in a specific manner to avoid systemic toxicity and accurately measure the therapeutic efficacy delivered.

3.3 Transformable drug delivery vesicles

One strategy to improve the therapeutic index of nanoparticles is to engineer them to be transformable in response to the given stimuli. Nanovesicles, indeed, can be engineered to be sensitive and release their cargo under the action of specific stimuli. Taking advantage of the abnormal environment of pathological site, nanosized vesicles can be

tailor-made by making their structure moieties sensitive to a specific environmental stimulus. These smart vesicles may selectively localize drug release in a specific disease tis- sue and represent good tools to achieve controlled or on-demand release [19]. Two main strategies are widely exploited in the design of nanodevices with personalized release kinetics. In one approach, internal stimuli related to the intrinsic difference between healthy and pathological tissue may be used to trigger drug release. Changes in pH, enzymatic expression, and concentration of the redox agent are common internal triggers used to provide an intrinsic, autonomous, and targeted drug release pattern [20]. Conversely, the second approach used to improve drug selectivity relies on the use of physical stimuli externally applied. These include temperature, light, ultrasound, and electric or magnetic fields (Fig. 6.3). The use of external stimuli allows to achieve a pulsatile drug release profile and provide also a high control over temporal and spatial drug release into the targeted site [21-23].

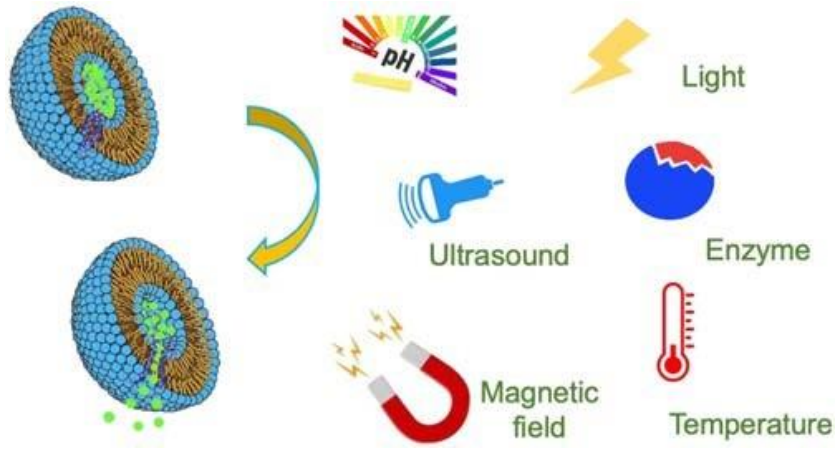

Figure 3. Schematic representation of main exogenous and endogenous stimuli involved in the design of transformable vesicles

3.4 Actively targeted vesicles

A further approach applied to improve drug selectivity is the active strategy that relies on the covalent attachment on the nanocarrier surface of ligands highly specific for target cells. These devices, so engineered, recognize and bind to receptors overexpressed on the pathological targeting site, inducing their internalization via receptor-mediated endocytosis. This specific molecular recognition offers the opportunity to address and deliver drugs to a specific site and to decrease cytotoxicity and side effects of drugs on healthy cells and organs, which are common drawbacks of traditional therapy. Various receptors have been recognized as a potential target for treatment of several diseases, and

a large number of ligands such as antibodies aptamers, peptide, polysaccharide, and small molecules have been studied to promote binding to themselves [24] (Table 2). Folic acid [41], epidermal growth factor [42], and transferrin [27] are common target moieties widely employed in the design of a target drug delivery system for cancer therapy. In the last few years, particularly appealing results have led to the employment of antibodies, aptamers, and peptides in the design of tumor-targeting nanoparticles for their low immunogenicity and high specificity and affinity to their biomarker [43]. Moreover, the simultaneous conjugation of more than one targeting moiety on the nanocarrier surface has been proposed to prevent receptor saturation and allows for a sufficient concentration of nanocarriers in the intracellular environment of pathological cells [44]. The high surface-area-to-volume ratio of nano- sized vesicles allows, indeed, to achieve high ligand density on the surface and to bypass the activity of multidrug resistance transporter cells. To achieve better clinical outcomes, one of the last challenges of nanomedicine is the targeting of subcellular organelles such as nucleus or mitochondria [45]. Common drugs act, in fact, at the nucleus or mitochondria level, and so, the direct release at the subcellular site/organelle is necessary to enhance therapeutic efficacy. The simultaneous conjugation on the nanocarrier surface of cellular and subcellular targeting allows for nanovesicle internalization via endocytosis in disease cells and then nanoparticle delivery to a specific intracellular compartment by organelle-targeting moieties on their surface. Typical moieties widely used to mediate nuclear and mitochondrial targeting are, respectively, transactivator of transcription (TAT) peptide [46] and triphenylphosphonium (TPP) moiety [47].

3.5 Multifunctional vesicles

A further advance of nanotechnology relies on the development of vesicles that integrate multiple complementary targeting approaches in the same systems to optimally per- form delivery functions and so improve drug efficacy.

The ability to engineer nanoscale vesicles to possess multiple functions represents the greatest remaining challenges in the field of drug delivery, opening a new avenue in clinical therapy. The design of the drug delivery platforms by combining passive, active, and stimuli-responsive targeting enhances their safety and efficacy resulting tools able to inter- act with a high degree of specificity with a specific cell or tissue [48].

Various combinations of targeting strategies have been investigated in the design of smart functional vesicles and have shown exciting results in preclinical studies, demonstrating their potential as therapeutics carriers [49]. Vesicles engineered to exhibit multifunctionality and smart release provide better control of cargo release and reduced toxicity on normal tissue [50]. Moreover, nanovesicles that integrate various functionalities may perform imaging, drug monitoring, targeted delivery, and controlled release simultaneously, enhancing accurate disease diagnosis and prognosis.

Table 2 Diverse targeting ligands used for active and specific cell recognition of nanovesicles for cancer therapy.

	Ligand	Target	Formulation	Drug	Cells	References
Small molecules	Folic acid	FR	Span 80 niosomes	Curcumin	MCF-7, MDA-MB 231	[25]
	Folic acid	FR	FA-PEG-DSPE liposomes	5-Fluorouracil	CT26	[26]
	Transferrin	Tf-R	L64ox/Cho lniosomes	Doxorubicin	MCF-7, MDA-MB-231	[27]
Peptides	ApoE	LDLR	ApoE-PS-DOX	Doxorubicin	U-87 MG	[28]
	Stearyl-H16 peptide	Lysosome	H16-Liposomes DOPC, CHOL	α-GAL (lysosomal enzyme)	HT1080	[29]
	Peptide R8	Brain	EPC, CHOL, DSPE-PEG2000 liposomes	Doxorubicin	U87-MG	[30]
	MPP Peptide	Cytochrome C reductase	CHOL, DOPE Liposomes	Antimycin A	A549	[31]
Antibodies	Anti-ER-antibody	ER	SPC, CHOL, DSPE-PEG2000 liposomes	Doxorubicin	MCF-7	[32]
	Cetuximab	EGFR	DPPC, CHOL, DSPE-PEG2000 liposomes	Doxorubicin	A431-A549	[33]
	Anti-CD123 antibodies	IL3R	Span-80, cholesterol niosomes	Daunorubicin hydrochloride	NB4, THP-1	[34]
Aptamers	TLS1c	Biotin	BioTL-Cab/ liposomes	Cabazitaxel	Caco-2, HepG2, MEAR cell lines	[35]
	AS1411	Nucleolin	Aptamer-Doxorubici nLiposomes	Doxorubicin	MCF-7	[36]
	AS1411	MMP2	PEG-Peptide-PLA polymersomes	SN38	CHO, C26	[37]
	AS1411	Nucleolin	Tween-80 niosomes	Nucleolipidic Ru(III)-complex HoThyRu	HeLa, HTB-38,HCC2998, HEK-293T	[38]
Carbohydrates	Hyaluroni cacid	CD44	HA-PEG-BMLs liposomes	Doxorubicin	MEF, LLC1, U87	[39]
	Hyaluroni cacid	CD44	Egg yolk lecithin, DOPE, Chol liposome	Paclitaxel	A549, MCF-7	[40]

4 Pharmaceutical application of vesicles

4.3 Cancer Therapy

Exploiting the unique characteristics of the tumor microenvironment, vesicular systems can be smartly designed to be high selective to cancer cells. To this purpose, several

strategies are used, such as active and passive targeting and stimuli-responsiveness. Passive targeting relies on the spontaneous nanodevice accumulation to the tumor site by the enhanced permeability and retention effect. Vesicles with a diameter range of 60—500 nm commonly extravasate the leaky vessels of tumor vasculature [51,52]. Anyway, this tendency is significantly limited by RES uptake in liver and spleen. To bypass this problem and extent vesicle half-life, long-circulating vesicles by surface coating with PEG have been developed [53].

Active targeting consists of covalent attachment to the vesicle surface of targeted ligands, the receptors of which are overexpressed in tumor tissue [54]. This approach pro- motes specific binding and cellular uptake, achieving high targeting specificity and drug delivery efficiency, avoiding the nonspecific toxic effect on healthy tissue. A large variety of molecules have been employed in the design of cancer-targeted vesicles (Table 6.2). Specific targets include growth factor receptors, G protein-coupled receptors, and integrin receptors (αvβ3 and αvβ5) [55]. Sometimes, vesicle constituents may possess intrinsic targeting properties as with sugar-based surfactants that exhibit glycan moieties able to address insulin-independent glucose transporter, being widely overexpressed in human tumors enhancing targeted delivery of anticancer drugs [56]. More interesting biological moieties for target drug delivery are antibodies and peptides, which exhibit improved selectivity and specificity toward overexpressed cell membrane receptors [57]. Many novel peptides have been discovered to act as ligands with high affinity of various receptors such as transferrin, epidermal growth factor (EGFR/HER1 and HER2), gastrin-releasing peptide, aminopeptidase N, vascular endothelial growth factor 2, and integrin receptors overexpressed in many tumor phenotypes [58]. In 2021, Ouyang et al. [28] demonstrated that the functionalization of polymersomes with apolipoprotein E derived peptide results in eightfold higher enrichment of doxorubicin intratumoral concentration, effectively inhibiting glioblastoma and representing a safe chemotherapy. A further advance in drug targeting was carried out by researchers developing the concept of dual targeting based on the simultaneous conjugation of various targeting ligands exploiting the synergist effect and reducing receptor saturation [59]. Folic acid was widely used for the design of dual ligand-endowed vesicles: promising results consisting of an improved cellular uptake and enhanced tumor killing effect have been observed when combined with transferrin [60], glutamic hexapeptide [61], and TAT peptide [62].

After internalization in cancer cells, it may be ideal that the nanocarrier undergoes transformation, releasing entrapped drugs in response to a given local stimulus. In light

of this, smart stimulus-sensitive vesicles have been designed to achieve a specific controlled release, avoiding drug leakage in healthy tissue and subsequent toxic effects [63]. Typically, tumors have a lower pH than healthy tissues, so labile bonds based on diorthoesters, vinyl esters, cisterine-cleavable lipopolymers, double esters, and hydrazones have been proposed for the design of pH-sensitive vesicles [64]. In addition, some molecules with pH-titratable groups such as phospholipids, cholesterol derivative, and polymers [64—66] are also employed for constructing pH-sensitive tools. A further stimulus largely investigated to achieve target cancer therapy is redox potential, which takes advantage of the higher GSH intracellular concentration in tumor cells, which are able to cleave redox- cleavable groups and trigger drug release. In light of this, introduction of disulfide bonds (—S—S—), diselenide bonds (—Se—Se—), thioether bonds (—C—S—S—C—), and thioketal linkers have been actively pursued [67,68].

The use of multifunctional vectors that simultaneously possess more than one useful targeting property in the same system has been proposed as a further evolution in the field of nanomedicine [69]. Multifunctional nanoparticle systems can integrate imaging, targeting, and treatment modalities for simultaneous delivery of multiple treatment agents, applying effective combinatorial therapeutic regimens against cancer. It has been reported that stealth vesicles equipped with the targeting part possess several pharmacokinetic advantages over traditional ligand-targeted vesicles [70,71]. In 2021, Peng et al. [72] designed multitarget redox-sensitive liposomes comodified with glucose and TPP to ensure effective delivery of doxorubicin and lonidine for antiglioma therapy. Antiglioma evaluation showed that the two drugs have a synergistic effect and their delivery into liposomes could enhance their cooperation. In vitro antiglioma efficacy showed that multi- functional liposomes can inhibit tumor cell proliferation and induce apoptosis. In addition, the devices have significant interference on mitochondria, such as reducing intracellular ATP production, inducing ROS generation, and promoting depolarization of mitochondrial membrane potential. Moreover, the introduction of PEGylation through glutathione- sensitive disulfide bonds confers to the vesicle-favorable in vivo pharmacokinetic proper- ties, brain targeting ability, low toxicity, and high antiglioma efficacy. A fascinating attempt was carried out by Baradan et al. [73], who coated liposomes encapsulating 5- fluoruracil using hyaluronic acid having not only pH sensitivity but also targeting proper- ties to colorectal cancer cells expressing CD44 receptors. These modified liposomes showed optimal targeted delivery and drug release

into colorectal cancer cells, rendering them susceptible to apoptosis, cell cycle arrest, and decreased colony formation.

A revolutionary method to fight cancer has recently emerged and is focused on the use of immune vesicles to boost immune response against tumor cells. This approach is the main strategy pursued in cancer treatment and is discussed in the paragraph below.

4.4 Diagnostic

Early diagnosis is a crucial factor influencing disease survival and clinical outcome [74]. Conventional diagnostics systems carry several disadvantages, such as untargeted biodistribution, low bioavailability, and delayed detection [75]. Nanoparticles hold great promise as diagnostic tools since they may be engineered to achieve high specificity toward a target, delivering a large payload amount in a single dose and simultaneously delivering both imaging agents and therapeutics, resulting in nanosystems that can simultaneously diagnose, treat, and monitor therapeutic response (nanotheranostic) [76]. Fluorescent molecules or contrast agents like gadolinium chelates and superparamagnetic iron oxide nanoparticles (SPIONs) are typically loaded in vesicles to improve their half-life and stability [77], developing nanosensors for detecting and grading diseases at the early stage. The spatial orientation of molecular cargos such as magnetic resonance imaging (MRI) contrast agents, fluorescent dyes, and drug molecules is influenced by the physico-chemical properties of vesicles. Consequently, physicochemical properties could be engineered to increase the diagnostic and therapeutic efficacy of molecular cargos [78]. For example, gadolinium relaxivity depends on the ability to interact with water protons. Liposomes are not suitable devices for the gadolinium derivative due to the slower water diffusion across the lipid bilayers [79]. Polymersomes with a porous structure were prepared using a chemical initiator and phospholipids that were subsequently extracted with a surfactant, generating a highly porous outer membrane, which showed an R1 relaxivity that is threefold higher than that of nonporous polymersomes [80]. Another strategy relies on the immobilization of the chelated gadolinium on the polymersome surface that decreases the distance between the gadolinium ions and the surrounding water [81].

A niosomal formulation of methyl aminolevulinate was developed for the encapsulation of radionuclides to achieve an improved PDD/PDT (photodynamic diagnosis/therapy) system [82]. To do so, the surface of these liposomes was decorated with folate and the resulting devices demonstrated superior activities compared to the free compound. In another study, folate-targeted and radiolabeled liposomes were used for the codelivery of

paclitaxel (PTX) and vinorelbine, aiming to design a theranostic system. Data obtained highlighted higher uptake in the tumor tissue, stronger antitumoral effect, and imaging potential, suggesting their promising role as a nanotheranostic agent [83].

Peptides are also employed to selectively address diagnostic nanovesicles [84]. Song et al.

[85] proposed the simultaneous functionalization with two peptides targeted for angiogenesis of liposomes for the delivery of a gadolinium derivative. From the results obtained, it can be found that the simultaneous presence of two targeting moieties exerts a synergistic effect in delivering the contrast agent to the tumor site with specificity, enhancing the signal rate in in vivo MRI and resulting in a good system for molecular imaging of tumors. A pH- responsive peptide able to produce targeting activity at low pH such as that of tumor tissue was proposed for the design of theranostic devices based on liposomal formulation containing PTX and SPIONPs. The resulting nanovesicles showed effective antitumor activity with an MRI effect by producing dual functionality with a single therapeutic dosage form [86]. Demir and coworkers [87] encapsulated gold nanoparticles and a photosensitizer, protoporphyrine IX, in FA-modified targeted Tween 80/Chol niosomes to develop a theranostic tool for cancer therapy. The resulting nanovesicles, thanks to their targeting capability, exhibited therapeutic efficacy in HeLa and A549 cell lines for radiotherapy and photodynamic therapy as well as for combined therapy (PDT 1 RT) and cell imaging applications. An innovative tool to support COVID-19 diagnosis was developed by Hu and coworkers [88] combining two different technologies: antibody-mediated capture and liposome-mediated delivery. In the assay, extracellular vesicles directly captured from plasma through the interaction of an antibody with the surface protein CD81 were then fused with reagent-loaded liposomes to sensitively amplify and detect a SARS-CoV-2 gene target. This approach accurately identified patients with COVID-19, and its major utility is the ability to detect plasma extracellular vesicles-derived SARS-CoV-2 RNA as an early and durable sign of systemic infection and could be used as a secondary test for suspected COVID-19 cases that are negative with quantitative polymerase chain reaction with reverse transcription.

4.5 Gene delivery

The delivery of nucleic acids to mammalian cells (transfection) has emerged as a new frontier of molecular medicine for the genetic treatment of hereditary diseases, cancers, and some viral infections [89—92]. Although naked nucleic acid administration is

considered the safest way to transfect cells, such a process is sadly ineffective. To overcome this limitation, researchers have focused on developing and using vectors as a vehicle for safe and effective gene delivery, such as nanovesicles. In 2018, the first gene nanomedicine based on lipo- somes (Patisiran, ONPATTRO) has been approved by the US Food and Drug Administration for the treatment of the polyneuropathy of hereditary TTR-mediated amyloidosis, enhancing the translation of gene therapy from concept to clinical application [93]. More recently, liposome technology to formulate mRNA vaccines to treat the devastating COVID-19 disease has received the approval by regulatory agencies. The main feature vesicles used to develop efficient gene delivery systems must have is the presence of a positive charge on the vesicle surface. In fact, the presence in the vesicle bilayer of cationic polymers (e.g., poly-l-lysine, polyethylenimine, poly(starchamine), and chitosan) [94] or lipids [95—97] enhances the formation of complexes with anionic nucleic acids through simple electrostatic interactions improving intracellular transfer [98]. Moreover, several studies have suggested that the type and amount of cationic lipid or surfactant significantly affects the transfection efficiency. Specifically, some helper and neutral lipids such as 1, 2-dioleoyl-sn-glycero-3-phosphoethanolamine (DOPE), dioleoylphosphatidylcholine (DOPC), monoolein (MO), and cholesterol are commonly employed in the design of gene delivery vesicles for their ability to significantly improve transfection efficiency [99]. Nonionic surfactants such as Span and Tween have been also recognized to act as a helper component, improving transfection efficiency and the stability and bilayer fluidity [100,101]. Recently, chloroquine and sphingolipids have been proposed as an interesting material for gene delivery due to their ability to act as a biophysical properties enhancer and to improve deoxyribonucleic acid (DNA) binding affinity and so transfection efficiency of niosomal formulations [102,103]. Acyl chain length and saturation influence also the efficacy of gene therapy. Abumanhal Masarweh et al. [104] found that liposomes with longer acyl chains and monounsaturated phospholipid performed much better than shorter tails and saturated phospholipid on cellular uptake.

Transfection efficiency resulted in dependence on vesicle size and surface charge. Sakai-Kato et al. [105] investigated the effect of particle size (100—200 nm) on transfection efficiency that enhanced with the increase of particle size, which was due to the strong electrostatic interaction between cationic liposomes and plasma membrane. Conversely, fusion efficiency was reduced as the size of lipoplexes increased because larger lipoplexes were more stable than their smaller counterparts during the process of endosomal mem-

brane fusion [106]. For efficient and targeted gene delivery to brain cells, Singhs et al. [107] developed surface-modified liposomes with a cell-penetrating peptide and transferrin loaded with chitosan-complexed plasmid DNA. Transfection efficiency in neuronal cells has been reported to be higher using bifunctional liposomes (PenTf-liposomes) compared to Plain-, Tf-, and Pen-liposomes. The efficient cellular internalization and endosomal escape properties resulted in transfection enhancement, suggesting the potentiality of the dual-targeting liposome gene delivery system to provide better brain targeting ability and therapeutic efficacy for treatment of neurodegenerative disease. More advanced approaches to augment effectiveness of gene therapy are based on the codelivery of biotherapeutic molecules along with traditional drugs in smart vesicles [108]. Saad et al.

[109] formulated cationic liposomes loaded with doxorubicin complexed with siRNA for the treatment of multiresistant lung cancer cells that revealed a higher apoptosis index than each of the therapeutics when used individually. Similar results were manifested by Shim et al. [110], in whose study trilysinoyl oleylamide-based cationic liposomes were pre- pared for systemic codelivery of siRNA and an anticancer drug. The advantages of chemo- therapeutic and biological drugs were also combined in a pH-sensitive liposome-based platform by Swami et al. [111], achieving a notably elevated tumor cell toxicity compared to individual counterparts. Maurer and coworkers [112] designed magnetic cation niosomes for siRNA delivery in combination with either erlotinib or trastuzumab against BT- 474 cells. The niosome mediated downregulation of the antiapoptotic LFG gene in BT-474 cells, increasing the activity of the targeted antineoplastic agents more profoundly as com- pared to their combination with free siRNA.

4.6 Immunotherapy and vaccines

Nowadays, immunotherapy and vaccines, both aiming to boost the human immune system, represent the mainstream and efficacious strategies for the prevention and treatment of a variety of diseases, including infectious and cancer.

The first vaccines based on killed microorganisms or viruses, live attenuated organisms, and inactivated toxins drastically reduced the morbidity and mortality of numerous diseases over the past two centuries [113]. Despite the progress and wide use of these conventional vaccines, they still have the risk that attenuated antigens may revert to full virulence and there will be limited immune response [114]. Recent advances in vaccinology have led to the development of nanovaccines that have advantages of lymph

node accumulation and antigen presentation compared with conventional vaccines. One of the main advantages of using nanovesicles for antigen delivery is the ability to protect it from nonspecific degradation, to control the delivery profile, and to codeliver other chemotherapeutics for a potential synergic therapy [115]

Strategies employed to design vesicles for immunotherapy application involve mainly the activation of antigen-presenting cells (APCs) or the amelioration of the cell microenvironment from immunosuppressive to immunoactive [116].

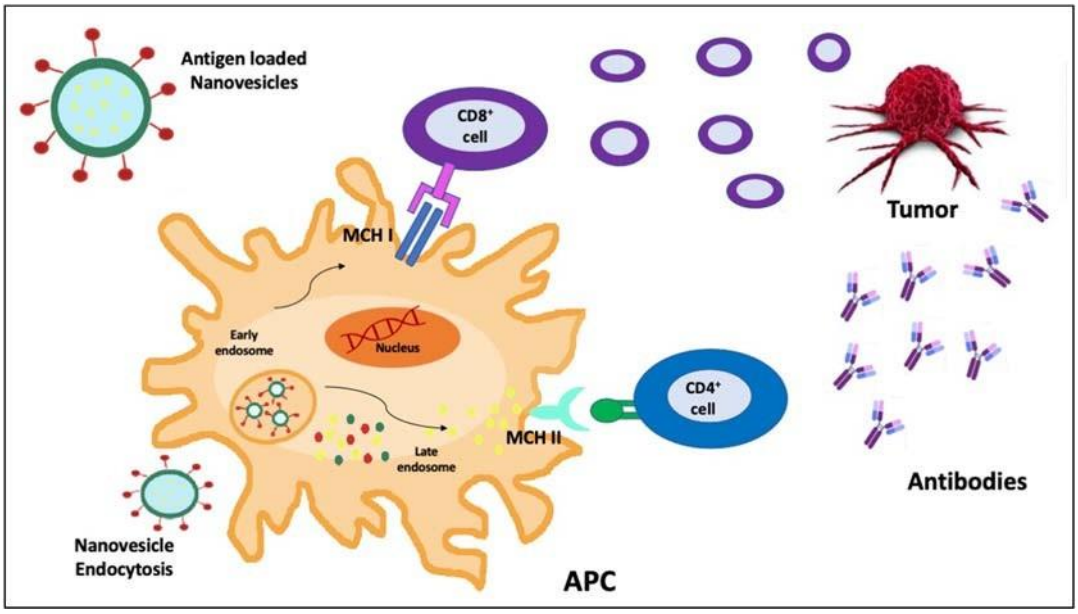

Figure 4. Schematic representation of cancer immunotherapy mediated by nanovesicles. Nanovesicles loaded with antigens or mRNA-encoding antigen proteins are recognized by APC-inducing antigen presentation by two major pathways. In the first, the exogenous antigen is degraded via the endosome pathway and is loaded onto major histocompatibility complex (MHC) class II, activating the helper ($CD4^1$) cell and thus inducing humoral immunity. This interaction promotes the activation of B cells that produce proinflammatory cytokines and antibodies that trigger tumor apoptosis. In the second pathway, the endogenous antigen is degraded in proteasomes and is loaded onto MHC class I molecules, thereby inducing the activation of $CD8^1$ lymphocytes that subsequently attack tumor cell inducing cytotoxicity.

To this goal, nanovesicles can be loaded with several immune modulators (cytokines, interleukins, chemokines, antibodies, and toll-like receptor (TLR) agonists) or antigens (proteins, peptides, DNA, etc.). In the first strategy, vesicles loaded with antigens are recognized and uptaken by APCs that present the captured antigens on major histocompatibility complex (MHC) molecules to T cells by two different pathways. In the first, the exogenous antigen is degraded via the endosome pathway and is loaded onto MHC class II molecules, activating B cells and thus inducing humoral immunity. In the second pathway, the endogenous antigen is degraded in proteasomes and is loaded onto MHC class I molecules, thereby inducing cel- lular immunity via the proliferation and

differentiation into specific cytotoxic T cells, thus more effectively exerting the cell killing effect (Fig. 4).

Liposomes represent ideal devices for the cytosolic pathway for their intrinsic membrane fusion ability [117]. Furthermore, different studies highlight the ability of the cation lipid to increase the deposition of antigen at the injection site and prolong the presence of antigen depot in the draining lymph nodes, resulting in sustained antigen uptake and APC activation [118].

It has been shown that surface charge is the crucial factor affecting immune response activation and that positively charged (cationic) liposomes are more effective as vaccine adjuvants than negatively charged (anionic) and zwitterionic (neutral) liposomes [119,120] This superiority is due to the ability of cationic liposomes to promote the effective uptake by APCs due to the electrostatic interaction between the cationic liposomal parts and the negatively charged molecules on the surface of APCs [121]. This facilitates fusion with APCs, with subsequent intracellular localization of the liposomes and release of their anti- gen payload.

For instance, in 2018, Sailor and coworkers [122] used positively charged fusogenic siRNA-loaded liposomes to enhance immune responses to Staphylococcus aureus infection, resulting in the knock down of proinflammatory marker IRF5 in macrophages and increased elimination capacity and accelerate healing.

The immunostimulatory effect of cationic liposomes depends on the composition of the phospholipid used, including the type of lipid head groups, hydrophobic acyl tails, and their degree of saturation. Cationic liposomes based on ethylphosphocholine derivatives (1,2-dioleoyl-sn-glycero-3-ethylphosphocholine) are more effective in stimulating the maturation of DCs than those prepared using 1,2-dioleoyl-3-trimethylammonium-propane (DOTAP) lipids. A variety of cationic liposomes have been shown to mediate immunostimulatory effects. The most commonly used cationic liposomes are those prepared with dimethyl dioctadecylammonium, 3β-[N-(N^0, N^0-dimethylaminoethane)-carbamoyl] cholesterol, and DOTAP [123].

To increase antigen cross-presentation, nanovesicles have been rationally designed in multiple ways. One strategy relies on surface modifications using pH-responsive or fusogenic materials that lead to cross-presentation of exogenous antigens via the cytosolic pathway. Conversely, the targeting of receptors on APCs has been pursued to selectively release exogenous antigen in early endosomes, activating the vacuolar pathway.

In the cytosolic pathway, surface conjugation with a pH-sensitive polymer or fusogenic peptide has been proposed to induce a vesicular destabilization in the acidic cytosol environment, resulting in the cytosolic delivery of encapsulated immunostimulating agents and enhanced therapeutic effect. Cell-penetrating peptides such as octaarginine (R8) and fusogenic peptides (e.g., GALA and KALA) are commonly use to achieve them [124]. Similarly, synthetic polymers based on poly(carboxyl acid) having pH-responsive mem- brane-disruptive ability such as poly(ethyl acrilic acid) and poly(propyl acrylic acid), and carboxyl group-introduced poly(glycidol)s that are able to induce membrane fusion after protonation of their carboxyl groups are also employed [125]. Innovative tools for cancer immunotherapy were developed by Pithchamaini et al. [126] that synthetize fusogenic NKsome made up of activated natural killer membranes fused with the cationic liposome capable of directly target tumor cells, thanks to the abnormal expression of NK-92 cell membrane receptors. The engineered NKsome loaded with doxorubicin can recognize tumor cells with the help of NK cell markers and fused with the tumor cells more efficiently than normal cells, thereby showing its antitumor potential by releasing the chemo- therapeutic drug. NKsome shows a higher affinity toward cancer than normal cells and exhibits enhanced tumor homing efficiency in vivo with an extended circulation half-life. Moreover, liposomes showed excellent antitumor potential against human breast cancer cells and MCF-7 in vitro and *in vivo.*

As already cited, another strategy used in immunotherapy is the targeting of APCs by conjugation on the vesicle surface of the molecule that is able to specifically target receptors overexpressed on APCs. In light of this, glycan molecules that exhibit a high specificity toward C-type lectin receptors (CLRs) are widely used, which enhance loading and presentation of antigen through MHC class I and II, induce antigen-specific $CD4^1$ and $CD8^1$ T-cell proliferation, and skew T-helper cells [127]. In 2019, Liu et al. [128] designed drug-free mannosylated liposomes that can target macrophage phenotypes, enhancing tumor growth inhibition compared to bare liposomes. An interesting result was achieved using glycoliposomes obtained by coating liposomes with glycan Lewis(Le)X, which is highly specific for CLR. The obtained liposomes when loaded with the adjuvant monophosphoryl lipid A induced dendritic cell maturation and a potent antitumor response [129].

Inclusion of methoxypoly(ethyleneglycol), mPEG-phospholipid, into the liposomal bilayer successfully enhanced lymph node accumulation [130]. In a recent study, Truong

et al. [131] investigated the effect of Tween 80 and Tween 20 incorporation in the lipid bilayer on size, charge, stability, DNA encapsulation, and in vivo transfection efficiency. Tweens belong to a family of PEG surfactants with branched PEG chains attached to lipid tails with different lengths, and so, this difference could affect immune response. Indeed, in vivo transfection studies demonstrated that particles with the shorter Tween 20 were able to target the lymph nodes more efficiently and achieved highly specific transfection better than the longer Tween 80.

The second strategy used in the development of immunovesicles is turning the immunosuppressive environment immunoactive by upregulation of immunoactive signaling pathways (e.g., the stimulator of interferon genes [STING] pathway), inhibition of immune checkpoints (e.g., PD-1, PD-L1, and cytotoxic T-lymphocyte antigen 4 [CTLA-4]), and polarization of M2 TAMs to M1 macrophages.

A cytosolic pattern recognition receptor utilized for spontaneous induction of antitumor T-cell immunity is used to activate STING. Wilson J. T. et al. [132]. designed pH-sensitive polymersomes for efficient cytosolic delivery of 2^0,5—3^05^0 cyclic guanosine monophosphate—adenosine monophosphate, agonists of STING. The incorporation of pH-sensitive, cat- ionic 2-(diethylamino) ethyl methacrylate groups in the polymersome structure mediates the intracellular release of GAMP via an endosomal escape mechanism enhancing its immunomodulatory potency and therapeutic efficacy, resulting in tumor growth inhibition and inducing a immunological memory that protects against tumor rechallenge. In 2020, Chang H. C. et al. [133]. constructed pH-induced transformable nanovesicles based on poly(e-caprolactone)-hydrazone-PEG for the codelivery of tumor endogenous antigens HCP and immunological adjuvants CpG ODNs. Nanovesicles were also modified with CD80 antibody for APC targeting, and after APC-targeted delivery inside immune organs (spleen and lymph nodes), they remarkably are degraded in the acidic environment of endosome/lysosome, resulting in a stronger cargo release. Subsequently, CpG ODNs activate TLR9 signaling, while HCPs were presented by MHC I and II molecules, and these two routes induce a synergistic T cell-mediated antitumor immune response.

Another strategy to enhance antitumor immunoresponse involves the use of antibodies or inhibitor that block programmed death ligand-1 (PD-L1)/PD-1 pathways. In light of this, the research group of Guo [134] developed pH-sensitive liposome coloaded with docetaxel and PD-L1 antibody to kill tumor cell directly, while switching off immunosuppression. This smart platform exhibited effective tumor inhibition and

prolonged survival time due to activation of the tumor-specific $CD8^1$ T cell, highly selective tumor killing, and decreased systemic toxicity. Another checkpoint inhibitor widely used to enhance nanoparticle immune response is CD47. For instance, Zhou and coworkers

[135] designed MMP-2/pH dual-activable prodrug vesicle for cancer immunotherapy combining CD induction and CD47 blockade via the loading with a photosensitizer and oxaliplatin. The obtained nanoplatform efficiently suppressed the growth of both primary tumors and distant metastasis. Moreover, a specific antitumor immune memory effect to prevent autologous tumor recurrence was also observed. Using monoclonal antibodies is also one of the main ongoing clinical approaches to enhance immune responses against cancer cells. For instance, Irvine et al. [136] engineered, with anti-CD137 and an IL-2Fc fusion protein, the surfaces of PEGylated liposomes to activate tumor-specific T lymphocytes and tumor-draining lymph nodes and, thus, antitumor immune response. PEGylated liposomes containing CTLA-4-blocking monoclonal antibodies were prepared and their therapeutic effect and biodistribution were evaluated in mice bearing colon carcinoma tumors. PEGylated liposomes had prolonged blood half-lives and higher accumulation at the tumor site than non-PEGylated liposomes and free CTLA-4 blockade antibody. According to these results, improved therapeutic response consisting of lowest tumor volume and highest survival time were also observed, suggesting their great potentiality to be translated to clinical trials [137].

In the last few years, using nucleic acid vaccines has become an innovative and interesting strategy for combatting infectious diseases and cancers. Compared with traditional vaccines, nucleic acid-based vaccines have the advantages of being safe, easy to produce, scalable, modifiable, and inexpensive and exhibiting a shorter production cycle [138]. Notably, the application of mRNA as vaccine has long been hampered by instability, innate immunogenicity, and low delivery efficiency in vivo. To overcome these hurdles, appropriate delivery systems have been studied and the emerging of SARS-COV-2 infection in 2019 accelerated the development of mRNA vaccines [139]. In December 2020, FDA approved the first mRNA drugs (Pfizer/BioNTech COVID-19 vaccines) for use in humans. Nucleic acid loaded in nanocarriers contain instructions to guide the host cells to produce antigenic proteins, which, subsequently, stimulate specific immune responses. Vaccines are cationic nanoparticles, consisting of a cholesterol, an ionizable cationic lipid, a PEGylated lipid, a phospholipid (distearoylphosphatidylcholine) helper lipid, and entrapped mRNA coding for the protein spike of the coronavirus. The mRNA

will then be expressed as the spike protein, in turn promoting an immune response to it that will kill or inactivate the invading virus. The mechanism by which liposomes act as an immunological adjuvant to augment the immune response to the spike protein is not clear at present.

Richner et al. [140] developed mRNA nanovesicles vaccine encoding Zika structural genes to protect against Zika virus infection for intramuscular delivery to induce high levels of protein expression in vivo. The results showed that it conferred protection and sterilized immunity in several strains of immunocompetent mice and the protective response was durable; even 14 weeks after boosting, challenged mice showed no morbidity or mortality. In one of the first proof-of-concept study, researchers compared the efficacy to boost mice's immune response of mRNA vaccine based on liposomes consisting of ionizable amino lipid, phospholipid, cholesterol, and PEG containing lipid and commercial vaccines by inactivated virus against rabies and influenza [141]. A strong immune response in mice were achieved, which was like or even higher than that achieved after a single intramuscular injection of nonreplicating mRNA vaccines, which induced functional antibody titers comparable to vaccination with a full human dose of licensed vaccines based on inactivated virus. The efficacy remained stable during an observation period of up to 1 year after one single booster dose, opening new avenues for accelerated vaccine development in the field of infectious diseases. More recently [142], a first-in-human study focused on mRNA vaccine encapsulated in liposomes using as anti- gen rabies virus glycoprotein was carried out to assess the safety, reactogenicity, and immunogenicity potential of this new vaccine model in comparison with a licensed rabies vaccine formulation in adult human volunteers. The authors observed a high reactogenicity at the initial tested doses of 5 μg, while when tested at 1 and 2 μg doses, no vaccine- related serious adverse events or withdrawals occurred. Moreover, liposomal formulation had functional antibody responses after two doses that were comparable with three doses of licensed rabies vaccine up to 4 weeks after the second dose.

To date, in clinical trials of tumor immunotherapy applications, many studies have evaluated the antitumor effect of mRNA vaccines and indicated that it is feasible to use mRNA vaccines for the prevention and treatment of tumors.

In 2018, Guan et al. [143] developed immunostimulatory spherical nucleic acids consisting of liposomal cores functionalized with a dense shell of RNA inserted into the wall of the lipid core via hydrophobic cholesterol moieties. The resulting device was able to selectively target toll-like receptors TLRs and triggered an NF-κB pathway to activate

dendritic cells greater than that of free or cationic lipid-transfected RNA of the same sequence selective for them.

In another work, Markov et al. [144] proposed the use of mannosilated liposomes for the delivery of plasmid DNA encoding EGFP and total tumor RNA to DC. The resulting device enhanced the antitumor response in a murine melanoma model reducing five- to sixfold the number of melanoma lung metastases.

Sayour and coworkers [145] designed RNA cancer vaccine based on nanoliposomes encapsulated with personalized tumor-derived mRNA (representing a tumor-specific transcriptome). The developed vaccine was shown to significantly increase percent expression of MHC class I/II, costimulatory molecules, and activation markers on tumor APCs and potentiate antitumor T cell immunity through endogenous host T-cell responses.

A promising vaccine platform for cancer treatment based on DPPP:Chol liposomes coencapsulating the pore-forming protein sticholysin II (StII) with ovalbumin (OVA) has been developed by Lanio et al. [146]. Resulting devices were able to induce OVA-specific cytotoxic T lymphocyte (CTL) activation and an antitumor response in vivo. Specifically, the study highlighted that liposomes were encapsulated by a phagocytic mechanism resulting in the cross-presentation of the encapsulated OVA by the vacuolar pathways, suggesting the vital role of macrophages in antigen cross presentation and inducing of immune response.

5 Conclusions and outlooks

Overall, vesicular systems are some of the best new delivery entities that have great potential for targeted drug delivery. Smart vesicles have already enhanced anticancer therapy and the delivery of vaccines, proteins, and DNA, and further benefits could be achieved soon, allowing for their translation in clinical practice. In addition to their biocompatibility and biodegradability, they provide an ideal opportunity for the development of versatile drug delivery platforms owing to possibility of using several kinds of material in the vesicular membrane, such as polymers, lipids, and nonionic surfactants. An accurate selection of different components could lead to the construction of tailor- made devices with desirable properties for the desired therapeutic purpose. Some liposome-based formulations are currently in clinical use, but despite extensive studies, there are still many hurdles to overcome before the full therapeutic potential of vesicular systems can be achieved. Reliable and reproducible fabrication processes and

good scale-up properties must be developed. Moreover, the in vivo behaviour of vesicle systems in terms of biodistribution, biological fate, and acute and subacute toxicity needs to be intensively investigated. We can hope to know more about it in the coming years.

References

[1] Kapoor B, Gupta R, Gulati M, Singh SK, Khursheed R, Gupta M. The why, where, who, how, and what of the vesicular delivery systems. *Adv Colloid Interface Sci,* 271. **2019**. p. 101985.

[2] Kamboj S, Saini V, Magon N, Bala S, Jhawat V. Vesicular drug delivery systems: a novel approach for drug targeting. *Int J Drug Deliv* **2013**;5(2):121—30.

[3] Liang CH, Chou TH. Effect of chain length on physicochemical properties and cytotoxicity of cationic vesicles composed of phosphatidylcholines and dialkyldimethylammonium bromides. *Chem Phys Lipids* **2009**;158(2):81—90.

[4] Attwood D. The mode of association of amphiphilic drugs in aqueous solution. *Adv Colloid Interface Sci* **1995**; 55:271—303.

[5] Tavano L, Mazzotta E, Muzzalupo R. Innovative topical formulations from diclofenac sodium used as surfadrug: the birth of diclosomes. *Colloids Surf B: Biointerfaces* **2018**;164:177—84.

[6] Bangham AD, Horne RW. *Nature* **1962**; 196:952—3.

[7] Alibolandi M, Abnous K, Mohammadi M, Hadizadeh F, Sadeghi F, Taghavi S, et al. *J Contr Rel* **2017**;264:228.

[8] Mathiyazhakan M, Wiraja C, Xu C. A concise review of gold nanoparticles-based photo-responsive liposomes for controlled drug delivery. *Nano-micro Lett* **2018**;10(1):1—10.

[9] Mohammadi M, Shaegh SAM, Alibolandi M, Ebrahimzadeh MH, Tamayol A, Jaafari MR, et al. *J Contr Rel* **2018**;274:35.

[10] Barenholz Y. Liposome application: problems and prospects. *Curr Opcol interface Sci* **2001**;6(1):66—77.

[11] Sercombe L, Veerati T, Moheimani F, Wu SY, Sood AK, Hua S. Advances and challenges of liposome assisted drug delivery. *Front Pharmacol* **2015**;6:286.

[12] Moghimi SM, Szebeni J. Stealth liposomes and long circulating nanoparticles: critical issues in pharmacokinetics, opsonization and protein-binding properties. *Prog Lipid Res* **2003**;42:463—78.

[13] Mahale NB, Thakkar PD, Mali RG, Walunj DR, Chaudhari SR. Niosomes: novel sustained release nonionic stable vesicular systems—an overview. *Adv Colloid Interface Sci* **2012**;183:46—54.

[14] Perez L, Pinazo A, Pons R, Infante M. Gemini surfactants from natural amino acids. *Adv Colloid Interface Sci* **2014**;205:134—55.

[15] Pinazo A, Manresa MA, Marques AM, Bustelo M, Espuny MJ, Perez L. Amino acid—based surfactants: new antimicrobial agents. *Adv Colloid Interface Sci* **2016**;228:17—39.

[16] Kita-Tokarczyk K, Grumelard J, Haefele T, Meier W. Block copolymer vesicles—using concepts from polymer chemistry to mimic biomembranes. *Polymer* **2005**;46(11):3540—63.

[17] Jang WS, Park SC, Kim M, Doh J, Lee D, Hammer DA. The effect of stabilizer on the mechanical response of double-emulsion-templated polymersomes. *Macromol Rapid Commun* **2015**;36(4):378—84.

[18] Egli S, Schlaad H, Bruns N, Meier W. Functionalization of block copolymer vesicle surfaces. *Polymers* **2011**;3 (1):252—80.

[19] Wang S, Hu X, Wei W, Ma G. Transformable vesicles for cancer immunotherapy. *Adv Drug Deliv Rev* **2021**;179:113905.

[20] El-Sawy HS, Al-Abd AM, Ahmed TA, El-Say KM, Torchilin VP. Stimuli-responsive nano-architecture drugdelivery systems to solid tumor micromilieu: past, present, and future perspectives. *ACS Nano* **2018**;12 (11):10636—64.

[21] Wang Y, Kohane DS. External triggering and triggered targeting strategies for drug delivery. *Nat Rev Mater* **2017**;2(6):1—14.

[22] Kauscher U, Holme MN, Bjornmalm M, Stevens MM. Physical stimuli-responsive vesicles in drug delivery: Beyond liposomes and polymersomes. *Adv Drug Deliv Rev* **2019**;138:259—75.

[23] Thambi T, Lee DS. Stimuli-responsive polymersomes for cancer therapy. Stimuli responsive polymeric nanocarriers for drug delivery applications. *Woodhead Publishing*; **2019**. p. 413—38.

[24] Kim JW, Cochran JR. Targeting ligand—receptor interactions for development of cancer therapeutics. *Curr OpChem Biol* **2017**;38:62—9.

[25] Akbarzadeh I, Yaraki MT, Ahmadi S, Chiani M, Nourouzian D. Folic acid-functionalized niosomal nanoparticles for selective dual-drug delivery into breast cancer cells: an in-vitro investigation. *Adv Powder Technol* **2020**;31(9):4064—71.

[26] Moghimipour E, Rezaei M, Ramezani Z, Kouchak M, Amini M, Angali KA, et al. Folic acid-modified liposomal drug delivery strategy for tumor targeting of 5-fluorouracil. *Eur J Pharm Sci* **2018**;114:166—74.

[27] Tavano L, Muzzalupo R, Mauro L, Pellegrino M, Ando S, Picci N. Transferrin-conjugated pluronic niosomes as a new drug delivery system for anticancer therapy. *Langmuir* **2013**;29(41):12638—46.

[28] Ouyang J, Jiang Y, Deng C, Zhong Z, Lan Q. Doxorubicin delivered via ApoE-directed reduction-sensitive polymersomes potently inhibit orthotopic human glioblastoma xenografts in nude mice. *Int J Nanomed* **2021**;16:4105.

[29] Hayashi T, Shinagawa M, Kawano T, Iwasaki T. Drug delivery using polyhistidine peptide-modified liposomes that target endogenous lysosome. *Biochem Biophys Res Commun* **2018**;501(3):648—53.

[30] Yuan BO, Zhao Y, Dong S, Sun Y, Hao F, Xie J, et al. Cell-penetrating peptide-coated liposomes for drug delivery across the blood—brain barrier. *Anticancer Res* **2019**;39(1):237—43.

[31] Mallick S, Lee S, Park JI, Choi JS. Liposomes containing cholesterol and mitochondria-penetrating peptide (MPP) for targeted delivery of antimycin A to A549 cells. *Colloids Surf B: Biointerfaces* **2018**;161:356—64.

[32] Wang Y, Wang Z, Qian Y, Fan L, Yue C, Jia F, et al. Synergetic estrogen receptor-targeting liposome nanocarriers with anti-phagocytic properties for enhanced tumor theranostics. *J Mater Chem B* **2019**;7(7):1056—63.

[33] Liu KC, Arivajiagane A, Wu SJ, Tzou SC, Chen CY, Wang YM. Development of a novel thermal-sensitive multifunctional liposome with antibody conjugation to target EGFR-expressing tumors. *Nanomed Nanotechnol Biol Med* **2019**;15(1):285—94.

[34] Liu FR, Jin H, Wang Y, Chen C, Li M, Mao SJ, et al. Anti-CD123 antibody-modified niosomes for targeted delivery of daunorubicin against acute myeloid leukemia. *Drug Deliv* **2017**;24(1):882—90.

[35] Cheng Y, Ou Z, Li Q, Yang J, Hu M, Zhou Y, et al. Cabazitaxel liposomes with aptamer modification enhance tumor-targeting efficacy in nude mice. *Mol Med Rep* **2019**;19(1):490—8.

[36] Xing H, Tang L, Yang X, Hwang K, Wang W, Yin Q, et al. Selective delivery of an anticancer drug with aptamer-functionalized liposomes to breast cancer cells in vitro and in vivo. *J Mater Chem B* **2013**;1 (39):5288—97.

[37] Ramezani P, Abnous K, Taghdisi SM, Zahiri M, Ramezani M, Alibolandi M. Targeted MMP-2 responsive chimeric polymersomes for therapy against colorectal cancer. *Colloids Surf B: Biointerfaces* **2020**;193:111135.

[38] Riccardi C, Fabrega C, Grijalvo S, Vitiello G, D'Errico G, Eritja R, et al. AS1411-decorated niosomes as effective nanocarriers for Ru (III)-based drugs in anticancer strategies. *J Mater Chem B* **2018**;6(33):5368—84.

[39] Jose G, Lu YJ, Chen HA, Hsu HL, Hung JT, Anilkumar TS, et al. Hyaluronic acid modified bubblegenerating magnetic liposomes for targeted delivery of doxorubicin. *J Magnetism Magnetic Mater* **2019**;474:355—64.

[40] Tian Y, Zhang H, Qin Y, Li D, Liu Y, Wang H, et al. Overcoming drug-resistant lung cancer by paclitaxel loaded hyaluronic acid-coated liposomes targeted to mitochondria. *Drug Dev Ind Pharm* **2018**;44(12):2071—82.

[41] Narmani A, Rezvani M, Farhood B, Darkhor P, Mohammadnejad J, Amini B, et al. Folic acid functionalized nanoparticles as pharmaceutical carriers in drug delivery systems. *Drug Dev Res* **2019**;80(4):404—24.

[42] Grapa CM, Mocan T, Gonciar D, Zdrehus C, Mosteanu O, Pop T, et al. Epidermal growth factor receptor and its role in pancreatic cancer treatment mediated by nanoparticles. *Int J Nanomed* **2019**;14:9693.

[43] Bazak R, Houri M, El Achy S, Kamel S, Refaat T. Cancer active targeting by nanoparticles: a comprehensive review of literature. *J Cancer Res Clin Oncol* **2015**;141(5):769—84.

[44] Peiris PM, He F, Covarrubias G, Raghunathan S, Turan O, Lorkowski M, et al. Precise targeting of cancer metastasis using multi-ligand nanoparticles incorporating four different ligands. *Nanoscale* **2018**;10 (15):6861—71.

[45] Chen WH, Luo GF, Zhang XZ. Recent advances in subcellular targeted cancer therapy based on functional materials. *Adv Mater* **2019**;31(3):1802725.

[46] Pan L, He Q, Liu J, Chen Y, Ma M, Zhang L, et al. Nuclear-targeted drug delivery of TAT peptide- conjugated monodisperse mesoporous silica nanoparticles. *J Am Chem Soc* **2012**;134(13):5722—5.

[47] Battogtokh G, Choi YS, Kang DS, Park SJ, Shim MS, Huh KM, et al. Mitochondria-targeting drug conjugates for cytotoxic, anti-oxidizing and sensing purposes: current strategies and future perspectives. *Acta Pharm Sin B* **2018**;8(6):862—80.

[48] Choudhury H, Gorain B, Pandey M, Nirmal J, Kesharwani P. Surface engineering of nanoparticles for imparting multifunctionality. Nanoparticle therapeutics. *Academic Press*; **2022**. p. 181—210.

[49] Tavano L, Muzzalupo R. Multi-functional vesicles for cancer therapy: the ultimate magic bullet. *Colloids Surf B: Biointerfaces* **2016**;147:161—71.

[50] Meng S, Su B, Li W, Ding Y, Tang L, Zhou W, et al. Enhanced antitumor effect of novel dual-targeted paclitaxel liposomes. *Nanotechnology* **2010**;21(41):415103.

[51] Maeda H, Nakamura H, Fang J. The EPR effect for macromolecular drug delivery to solid tumors: improvement of tumor uptake, lowering of systemic toxicity, and distinct tumor imaging in vivo. *Adv Drug Deliv Rev* **2013**;65(1):71—9.

[52] Fang J, Nakamura H, Maeda H. The EPR effect: unique features of tumor blood vessels for drug delivery, factors involved, and limitations and augmentation of the effect. *Adv Drug Deliv Rev* **2011**;63(3):136—51.

[53] Gabizon A, Catane R, Uziely B, Kaufman B, Safra T, Cohen R, et al. Prolonged circulation time and enhanced accumulation in malignant exudates of doxorubicin encapsulated in polyethylene glycol coated liposomes. *Cancer Res* **1994**;54(4):987—92.

[54] Frisch B, Hassane FS, Schuber F. Conjugation of ligands to the surface of preformed liposomes by click chemistry. *Liposomes. Humana Press*; **2010**. p. 267—77.

[55] Vhora I, Patil S, Bhatt P, Gandhi R, Baradia D, Misra A. Receptor-targeted drug delivery: current perspective and challenges. *Ther Deliv* **2014**;5(9):1007—24.

[56] Muzzalupo R, Tavano L, La Mesa C. Alkyl glucopyranoside-based niosomes containing methotrexate for pharmaceutical applications: evaluation of physico-chemical and biological properties. *Int J Pharm* **2013**;458 (1):224—9.

[57] Mojarad-Jabali S, Farshbaf M, Walker PR, Hemmati S, Fatahi Y, Zakeri-Milani P, et al. An update on actively targeted liposomes in advanced drug delivery to glioma. *Int J Pharm* **2021**;602:120645.

[58] Aronson MR, Medina SH, Mitchell MJ. Peptide functionalized liposomes for receptor targeted cancer therapy. *APL Bioeng* **2021**;5(1):011501.

[59] Hare JI, Moase EH, Allen TM. Targeting combinations of liposomal drugs to both tumor vasculature cells and tumor cells for the treatment of HER2-positive breast cancer. *J Drug Target **2013***;21(1):87—96.

[60] Tavano L, Mauro L, Naimo GD, Bruno L, Picci N, Ando` S, et al. Further evolution of multifunctional niosomes based on pluronic surfactant: dual active targeting and drug combination properties. *Langmuir* **2016**;32(35):8926—33.

[61] Yang Y, Zhao Z, Xie C, Zhao Y. Dual-targeting liposome modified by glutamic hexapeptide and folic acid for bone metastatic breast cancer. *Chem Phys Lipids* **2020**;228:104882.

[62] Zhao P, Wang H, Yu M, Cao S, Zhang F, Chang J, et al. Paclitaxel-loaded, folic-acid-targeted and TATpeptide-conjugated polymeric liposomes: in vitro and in vivo evaluation. *Pharm Res* **2010**;27(9):1914—26.

[63] Mura S, Nicolas J, Couvreur P. Stimuli-responsive nanocarriers for drug delivery. *Nat Mater* **2013**;12 (11):991—1003.

[64] Ferreira DDS, Lopes SCDA, Franco MS, Oliveira MC. pH-sensitive liposomes for drug delivery in cancer treatment. *Ther Deliv* **2013**;4(9):1099—123.

[65] Baranei M, Taheri RA, Tirgar M, Saeidi A, Oroojalian F, Uzun L, et al. Anticancer effect of green tea extract (GTE)-Loaded pH-responsive niosome Coated with PEG against different cell lines. *Mater Today Commun* **2021**;26:101751.

[66] Kocak G, Tuncer C, Butun V. pH-responsive polymers. Polym Chem 2017;8:144—76.

[67] Scott EA, Stano A, Gillard M, Maio-Liu AC, Swartz MA, Hubbell JA. Dendritic cell activation and T cell priming with adjuvant and antigenloaded oxidation-sensitive polymersomes. *Biomaterials* **2012**;33:6211—19.

[68] Ong W, Yang Y, Cruciano AC, McCarley RL. Redox-triggered contents release from liposomes. *J Am Chem Soc* **2008**;130(44):14739—44.

[69] Singh A, Talekar M, Tran TH, Samanta A, Sundaram R, Amiji M. Combinatorial approach in the design of multifunctional polymeric nano-delivery systems for cancer therapy. *J Mater Chem B* **2014**;2(46):8069—84.

[70] Noble GT, Stefanick JF, Ashley JD, Kiziltepe T, Bilgicer B. Ligand-targeted liposome design: challenges and fundamental considerations. *Trends Biotechnol* **2014**;32(1):32—45.

[71] Sapra P, Allen TM. Ligand-targeted liposomal anticancer drugs. *Prog Lipid Res* **2003**;42(5):439—62.

[72] Peng Y, Lu J, Li R, Zhao Y, Hai L, Guo L, et al. Glucose and triphenylphosphonium co-modified redox-sensitive liposomes to synergistically treat glioma with doxorubicin and lonidamine. *ACS Appl Mater Interfaces* **2021**;13(23):26682—93.

[73] Mansoori B, Mohammadi A, Abedi-Gaballu F, Abbaspour S, Ghasabi M, Yekta R, et al. Hyaluronic acid-decorated liposomal nanoparticles for targeted delivery of 5-fluorouracil into HT-29 colorectal cancer cells. *J Cell Physiol* **2020**;235(10):6817—30.

[74] Stephen BJ, Suchanti S, Mishra R, Singh A. Cancer nanotechnology in medicine: a promising approach for cancer detection and diagnosis. *Crit Rev Ther Drug Carr Syst* **2020**;37:375—405.

[75] Siegmund KD, Marjoram P, Woo YJ, Tavare S, Shibata D. Inferring clonal expansion and cancer stem cell dynamics from DNA methylation patterns in colorectal cancers. *Proc Natl Acad Sci USA* **2009**;106:4828—33.

[76] Indoria S, Singh V, Hsieh MF. Recent advances in theranostic polymeric nanoparticles for cancer treatment: a review. *Int J Pharm* **2020**;582:119314.

[77] Ahmad J, Ahmad MZ, Akhter H. Surface-engineered cancer nanomedicine: rational design and recent progress. *Curr Pharm Des* **2020**;26:1181—90.

[78] Leong J, Teo JY, Aakalu VK, Yang YY, Kong H. Engineering polymersomes for diagnostics and therapy. *Adv Healthc Mater* **2018**;7(8):1701276.

[79] Smith CE, Shkumatov A, Withers SG, Yang B, Glockner JF, Misra S, et al. *ACS Nano* **2013**;7:9599.

[80] Cheng Z, Tsourkas A. *Langmuir* **2008**;24:8169.

[81] Turner JL, Pan D, Plummer R, Chen Z, Whittaker AK, Wooley KL. *Adv Funct Mater* **2005**;15:1248.

[82] Haran G, Cohen R, Bar LK, Barenholz Y. Transmembrane ammonium sulfate gradients in liposomes produce efficient and stable entrapment of amphipathic weak bases. *Biochim Biophys Acta* **1993**;1151(2):201—15.

[83] Karpuz M, Silindir-Gunay M, Ozer AY, Ozturk SC, Yanik H, Tuncel M, et al. Diagnostic and therapeutic evaluation of folate-targeted paclitaxel and vinorelbine encapsulating theranostic liposomes for non-small cell lung cancer. *Eur J Pharm Sci* **2021**;156:105576.

[84] Wang SH, Lee ACL, Chen IJ, Chang NC, Wu HC, Yu HM, et al. Structure-based optimization of GRP78-binding peptides that enhances efficacy in cancer imaging and therapy. *Biomaterials* **2016**;94:31 44.

[85] Song Y, Li W, Meng S, Zhou W, Su B, Tang L, et al. Dual integrin αvβ 3 and NRP-1-targeting paramagnetic liposome for tumor early detection in magnetic resonance imaging. *Nanoscale Res Lett* **2018**;13(1):1—9.

[86] Zheng XC, Ren W, Zhang S, Zhong T, Duan XC, Yin YF, et al. The theranostic efficiency of tumor-specific, pH-responsive, peptide-modified, liposome-containing paclitaxel and superparamagnetic iron oxide nanoparticles. *Int J Nanomed* **2018**;13:1495.

[87] Demir B, Barlas F, Gumus ZP, U¨ nak P, Timur S. Theranostic niosomes as a promising tool for combined therapy and diagnosis: “All-in-One” approach. *ACS Appl Nano Mater* **2018**;1(6):2827—35.

[88] Ning B, Huang Z, Youngquist BM, Scott JW, Niu A, Bojanowski CM, et al. Liposome-mediated detection of SARS-CoV-2 RNA-positive extracellular vesicles in plasma. *Nat Nanotechnol* **2021**;16(9):1039—44.

[89] Lostale´-Seijo I, Montenegro J. Synthetic materials at the forefront of gene delivery. *Nat Rev Chem* **2018**;2(10):258—77.

[90] Wirth T, Parker N, Yla-Herttuala S. History of gene therapy. *Gene* **2013**;525(2):162—9.

[91] Pan JJ, Zhang SW, Chen CB, Xiao SW, Sun Y, Liu CQ, et al. Effect of recombinant adenovirus-p53 combined with radiotherapy on long-term prognosis of advanced nasopharyngeal carcinoma. *J Clin Oncol* **2009**;27 (5):799—804.

[92] Aied A, Greiser U, Pandit A, Wang W. Polymer gene delivery: overcoming the obstacles. Drug *Discov Today* **2013**;18(21—22):1090—8.

[93] Hoy SM. Patisiran: first global approval. *Drugs* **2018**;78:1625—31.

[94] Barua S, Ramos J, Potta T, Taylor D, Huang HC, Montanez G, et al. Discovery of cationic polymers for non- viral gene delivery using combinatorial approaches. *Comb Chem High Throughput Screen* **2011**;14 (10):908—24.

[95] Hoekstra D, Rejman J, Wasungu L, Shi F, Zuhorn I. Gene delivery by cationic lipids: in and out of an endosome. *Biochem Soc Trans* **2007**;35(1):68—71.

[96] Alvarez-Lorenzo C, Barreiro-Iglesias R, Concheiro A, Iourtchenko L, Alakhov V, Bromberg L, et al. Biophysical characterization of complexation of DNA with block copolymers of poly (2-dimethylaminoethyl) methacrylate, poly (ethylene oxide), and poly (propylene oxide). *Langmuir* **2005**;21(11):5142—8.

[97] Simoes S, Filipe A, Faneca H, Mano M, Penacho N, Duzgunes N, et al. Cationic liposomes for gene delivery. *Expert Opin drug Deliv* **2005**;2(2):237—54.

[98] Ojeda E, Agirre M, Villate-Beitia I, Mashal M, Puras G, Zarate J, et al. Elaboration and physicochemical characterization of niosome-based nioplexes for gene delivery purposes. In Non-viral gene delivery vectors. New York, *NY: Humana Press*; **2016**. p. 63—75.

[99] Tavano L, Mazzotta E, Muzzalupo R. Nanovesicular formulations for cancer gene therapy. *Curr Pharm Des* **2017**;23(35):5327—35.

[100] Huang YZ, Gao JQ, Chen JL, et al. Cationic liposomes modified with non-ionic surfactants as effective non-viral carrier for gene transfer. *Colloids Surf B: Biointerfaces* **2006**;49:158—64.

[101] Huang Y, Rao Y, Chen J, et al. Polysorbate cationic synthetic vesicle for gene delivery. *J Biomed Mat Res **2011***;96:513—19.

[102] Sainz-Ramos M, Villate-Beitia I, Gallego I, Al Qtaish N, Menendez M, Lagartera L, et al. Correlation between biophysical properties of niosomes elaborated with chloroquine and different tensioactives and their transfection efficiency. *Pharmaceutics* **2021**;13(11):1787.

[103] Qtaish NA, Gallego I, Villate-Beitia I, Sainz-Ramos M, Martınez-Navarrete G, Soto-Sanchez C, et al. Sphingolipid extracts enhance gene delivery of cationic lipid vesicles into retina and brain. *Eur J Pharm Biopharm* **2021**;169:103—12.

[104] Abumanhal-Masarweh H, da Silva D, Poley M, Zinger A, Goldman E, Krinsky N, et al. Tailoring the lipid composition of nanoparticles modulates their cellular uptake and affects the viability of triple negative breast cancer cells. *J Control Rel* **2019**;307:331—41.

[105] Sakai-Kato CK, Yoshida K, Izutsu KI. Effect of surface charge on the size-dependent cellular internalization of liposomes. *Chem Phys Lipids **2019***; 224:104726—32.

[106] Bruininks BMH, Souza PCT, Ingolfsson H, Marrink S-JJ. A molecular view on the escape of lipoplexed DNA from the endosome. *eLife* **2020**;9:52012—28.

[107] Dos Santos Rodrigues B, Banerjee A, Kanekiyo T, Singh J. Functionalized liposomal nanoparticles for efficient gene delivery system to neuronal cell transfection. Int J Pharm 2019;566:717—30.

[108] Abtahi NA, Naghib SM, Ghalekohneh SJ, Mohammadpour Z, Nazari H, Mosavi SM, et al. Multifunctional stimuli-responsive niosomal nanoparticles for co-delivery and co-administration of gene and bioactive compound: in vitro and in vivo studies. *Chem Eng J* **2022**;429:132090.

[109] Saad M., Garbuzenko O.B., Minko T. Co-delivery of siRNA and an anticancer drug for treatment of multidrug-resistant cancer; **2008**.

[110] Shim G, Han SE, Yu YH, Lee S, Lee HY, Kim K, et al. Trilysinoyl oleylamide-based cationic liposomes for systemic co-delivery of siRNA and an anticancer drug. *J Contr Rel* **2011**;155(1):60—6.

[111] Swami R, Kumar Y, Chaudhari D, Katiyar SS, Kuche K, Katare PB, et al. pH sensitive liposomes assisted specific and improved breast cancer therapy using co-delivery of SIRT1 shRNA and Docetaxel. *Mater Sci Eng C* **2021**;120:111664.

[112] Maurer V, Altin S, Ag Seleci D, Zarinwall A, Temel B, Vogt PM, et al. In-vitro application of magnetic hybrid niosomes: targeted siRNAdelivery for enhanced breast cancer therapy. *Pharmaceutics* **2021**;13:394.

[113] De Gregorio E, Rappuoli R. From empiricism to rational design: a personal perspective of the evolution of vaccine development. *Nat Rev Immunol* **2014**;14(7):505—14.

[114] Appay V, Douek DC, Price DA. CD8 1 T cell efficacy in vaccination and disease. *Nat Med* **2008**;14(6):623—8.

[115] Sahdev P, Ochyl LJ, Moon JJ. Biomaterials for nanoparticle vaccine delivery systems. *Pharm Res* **2014**;31:2563—82.

[116] Shi Y. Clinical translation of nanomedicine and biomaterials for cancer immunotherapy: progress and perspectives. *Adv Ther* **2020**;3(9):1900215.

[117] Yuba E. Design of pH-sensitive polymer-modified liposomes for antigen delivery and their application in cancer immunotherapy. *Polym J* **2016**;48(7):761—71.

[118] Henriksen-Lacey M, Christensen D, Bramwell VW, Lindenstrøm T, Agger EM, Andersen P, et al. Liposomal cationic charge and antigen adsorption are important properties for the efficient deposition of antigen at the injection site and ability of the vaccine to induce a CMI response. *J Contr Rel* **2010**;145:102—8.

[119] Smith DM, Simon JK, Baker Jr JR. Applications of nanotechnology for immunology. *Nat Rev Immunol* **2013**;13(8):592—605.

[120] Latin N, Bachhawat BK. The effect of liposome surface charges in immunopotentiation. *Biosci Rep* **1984**;4:99—107.

[121] Nakanishi T, Kunisawa J, Hayashi A, Tsutsumi Y, Kubo K, Nakagawa S, et al. The positively charged liposome functions as an efficient immune adjuvant in inducing immune responses to soluble proteins. *Biochem Biofis res Common* **1997**;240:793—7.

[122] Kim B, Pang HB, Kang J, Park JH, Ruoslahti E, Sailor MJ. Immunogene therapy with fusogenic nanoparticles modulates macrophage response to Staphylococcus aureus. *Nat Commun* **2018**;9(1):1—13.

[123] Inglut CT, Sorrin AJ, Kuruppu T, Vig S, Cicada J, Ahmad H, et al. Immunological and toxicological considerations for the design of liposomes. *Nanomaterials* **2020**;10:190.

[124] Yang Z, Ma Y, Zhao H, Yuan Y, Kim BY. Nanotechnology platforms for cancer immunotherapy. Wiley *Interdiscip Rev Nanomed Nanobiotechnol* ***2020***;12(2):e1590.

[125] Yuba E. Liposome-based immunity-inducing systems for cancer immunotherapy. *Mol Immunol* **2018**;98:8—12.

[126] Pitchaimani A, Nguyen TDT, Aryal S. Natural killer cell membrane infused biomimetic liposomes for targeted tumor therapy. *Biomaterials*. **2018**;160:124—37.

[127] Streng-Ouwehand I, Unger WW, Van Kooyk Y. C-type lectin receptors for tumor eradication: future directions. *Cancers* **2011**;3(3):3169—88.

[128] Ye J, Yang Y, Dong W, Gao Y, Meng Y, Wang H, et al. Drug-free mannosylated liposomes inhibit tumor growth by promoting the polarization of tumor-associated macrophages. *Int J Nanomed* ***2019***;14:3203.

[129] Boks MA, Ambrosini M, Bruijns SC, Kalay H, van Bloois L, Storm G, et al. MPLA incorporation into DC-targeting glycoliposomes favours anti-tumour T cell responses. *J Control Rel* **2015**;216:37—46.

[130] Moghimi SM. The effect of methoxy-PEG chain length and molecular architecture on lymphnode targeting of immuno-PEG liposomes. *Biomaterials* **2006**;27:136—44.

[131] Zukancic D, Suys EJA, Pilkington EH, Algarni A, Al-Wassiti H, Truong NP. The importance of poly(ethylene glycol) and lipid structure in targeted gene delivery to lymph nodes by lipid nanoparticles. *Pharmaceutics* **2020**;12:68.

[132] Shae D, Becker KW, Christov P, Yun DS, Lytton-Jean AKR, Sevimli S, et al. Endosomolytic polymersomes increase the activity of cyclic dinucleotide STING agonists to enhance cancer immunotherapy. *Nat Nanotechnol* **2019**;14:269—78.

[133] Chang HC, Zou ZZ, Wang QH, Li J, Jin H, Yin QX, et al. Targeting and specific activation of antigen presenting cells by endogenous antigen-loaded nanoparticles elicits tumor-specific immunity. *Adv Sci* **2020**;7:1900069.

[134] Gu Z, Wang Q, Shi Y, Huang Y, Zhang J, Zhang X, et al. Nanotechnology-mediated immunochemotherapy combined with docetaxel and PD-L1 antibody increase therapeutic effects and decrease systemic toxicity. *J Contr Rel* **2018**;286:369—80.

[135] Zhou F, Feng B, Yu H, Wang D, Wang T, Ma Y, et al. Tumor microenvironment-activatable prodrug vesicles for nanoenabled cancer chemoimmunotherapy combining immunogenic cell death induction and CD47 blockade. *Adv Mater* **2019**;31(14):1805888.

[136] Kwong B, Gai SA, Elkhader J, Wittrup KD, Irvine DJ. Localized immunotherapy via liposome-anchored Anti-CD137 1 IL-2 prevents lethal toxicity and elicits local and systemic antitumor immunity. *Cancer Res* **2013**;73(5):1547—58.

[137] Nikpoor AR, Tavakkol-Afshari J, Sadri K, Jalali SA, Jaafari MR. Improved tumor accumulation and therapeutic efficacy of CTLA-4-blocking antibody using liposome-encapsulated antibody: in vitro and in vivo studies. *Nanomedicine* **2017**;13:2671—82.

[138] Azad N, Rojanasakul Y. Vaccine delivery-current trends and future. *Curr drug Deliv* **2006**;3(2):137—46.

[139] Wang Y, Zhang R, Tang L, Yang L. Nonviral delivery systems of mRNA vaccines for cancer gene therapy. *Pharmaceutics* **2022**;14(3):512.

[140] Richner JM, Himansu S, Dowd KA, Butler SL, Salazar V, Fox JM, et al. Modified mRNA vaccines protect against zika virus infection. *Cell* **2017**;168:1114—25.

[141] Lutz J, Lazzaro S, Habbeddine M, Schmidt KE, Baumhof P, Mui BL, et al. Unmodified mRNA in LNPs constitutes a competitive technology for prophylactic vaccines. *NPJ Vaccines* **2017**;2(1):1—9.

[142] Aldrich C, Leroux-Roels I, Huang KB, Bica MA, Loeliger E, Schoenborn-Kellenberger O, et al. Proof-of concept of a low-dose unmodified mRNA-based rabies vaccine formulated with lipid nanoparticles in human volunteers: a phase 1 trial. *Vaccine* **2021**;39:1310—18.

[143] Guan C, Chernyak N, Dominguez D, Cole L, Zhang B, Mirkin CA. RNA-based immunostimulatory liposomal spherical nucleic acids as potent TLR7/8 modulators. *Small* **2018**;14(49):1803284.

[144] Markov OV, Mironova NL, Shmendel EV, Serikov RN, Morozova NG, Maslov MA, et al. Multicomponent mannose-containing liposomes efficiently deliver RNA in murine immature dendritic cells and provide productive anti-tumour response in murine melanoma model. *J Contr Rel* **2015**;213:45—56.

[145] Sayour EJ, De Leon G, Pham C, Grippin A, Kemeny H, Chua J, et al. Systemic activation of antigen presenting cells via RNA-loaded nanoparticles. *Oncoimmunology* **2017**;6(1):e1256527.

[146] Cruz-Leal Y, Grubaugh D, Nogueira CV, Lopetegui-Gonzalez I, Del Valle A, Escalona F, et al. The vacuolar pathway in macrophages plays a major role in antigen cross-presentation induced by the pore-forming protein sticholysin II encapsulated into liposomes. *Front Immunol* **2018**;2473.

4.2 Controlled release and antibacterial activity of thermosensitive niosomes based on eutectic mixture of natural fatty acids.

Elisabetta Mazzotta[1*], Martina Romeo[1], Zakaria Hafidi[2], Lourdes Perez[2], Rita Muzzalupo[1]

1 Department of Pharmacy, Health and Nutritional Sciences, University of Calabria, via P. Bucci, 87036 Arcavacata di Rende (CS), Italy;

2 Department of Surfactants and Nanobiotechnology, Institute for Advanced Chemistry of Catalonia (IQAC-CSIC), 08034 Barcelona, Spain

Submitted to Journal of Molecular Liquid

Abstract

In the current study, a smart release systems responsive to temperature was developed to improve tetracycline (TC) efficacy in antibacterial therapy. The nanovesicles designed consists of non-ionic surfactant, SPAN60, cholesterol and a phase change material (PCM), as a thermo-responsive gating material. Niosomes were prepared using increasing amount of PCM and characterized in term of size, Zeta potential, colloidal stability and thermoresponsive properties. The vesicles developed were homogenous in size, had good biocompatibility and stability up to 3 months and owned thermo-responsive behaviour. A low drug leakage was observed at 37°C, while a rapid release occurred at 42°C due to the faster diffusion rate of the drug trough the melted PCM. This controllable drug release capacity allows to avoid premature drug release minimizing unwanted and toxic effects and ensuring a long retention time in the nanodevice so that it reaches the infected sites. In addition, TC-loaded niosomes were screened for investigating their antibacterial activity against various Gram-positive and Gram-negative bacteria by minimum inhibitory concentration (MIC) and minimum bactericidal concentration (MBC) assays. An interesting temperature-dependent antibacterial activity was observed against some bacterial strains: the niosomes activity against S. Epidermis, for example, was improved by the temperature increase as suggested by reduction in MIC values from 112.81 to 14.10 μM observed at 37 and 42 °C, respectively. Taken together, the thermoresponsive platform developed allows to use lower antibiotic amount while ensuring therapeutic efficacy and, so, which will advance the development of a novel antibacterial agent in clinic.

Keywords: Phase change materials, natural fatty acids, niosomes, thermoresponsive release, antibacterial activity

Introduction

Nowdays, infectious diseases are a serious and critical threat for global health representing the major cause of morbidity and mortality. Several factors contribute to the ineffectiveness of existing antibiotics such as low water solubility, low bioavailability and stability, low patient compliance as a result of frequent administration and the rise of adverse side effects [1]. Furthermore, the excessive and improper use of conventional antibiotics has led to the emergence and rapid spread of multidrug-resistant (MDR) bacteria such as *Escherichia coli*, *Klebsiella pneumoniae* and *Staphylococcus aureus* that do not respond to standard treatments [2]. The development of new effective and safe antibacterial agents is a complex and expensive process that require long time. Consequently, new strategies have been developed to enhance the effectiveness of existing antibiotics. Recently, nanotechnology represents an attractive way to improve therapeutic effect of common antibiotics. Nano-size structures can act as antibacterial agents by themselves or as carriers of existent antimicrobials to promote bioavailability and effectiveness [3].

Nanocarriers result able to improve solubility of hydrophobic antibiotics, enhance cell membranes permeability, sustain antibiotic release and intracellular concentrations [4,5]. Notably, a few formulations based on liposomes (AmBisome® , Abelcet®, Amphotec®) have been already approved by regulatory agencies for use in human patients and exhibited better pharmacokinetics than conventional formulations, including prolonged systemic-circulation half-life, enhanced therapeutic efficacy and, most importantly, reduce side effects [6]. Various factors such as chemistry, particle size and shape, surface-to-volume ratio and zeta potential affect antimicrobial activity [2]. However, the short shelf-life and stability, encapsulation efficacy and the rapid clearance from the blood stream limits the efficacy of liposomes for antimicrobial treatment.

Recently, stimuli-responsive antimicrobial nanoparticles have gained considerable importance as they have overcome some important challenges in the treatment of infections. This is because they recognize and respond dynamically to specific internal stimuli associated with the pathological infection microenvironment or to external physical stimuli obtained by applying an external source [7]. Targeted drug release allows to increase the local concentration of the active substance at the infection site minimizing the accumulation in healthy tissue and reduces the risk of systemic side effects [8]. Both chemical and physical stimuli can be used to induce conformational changes of these smart antibiotic devices that deliver antibiotics to the infection site in a controlled way

[9]. Nanocarriers, indeed, can be tailor-made designed to possess a wide range of chemical functionalities that easily undergo hydrolysis, enzymatic degradation or conformational changes in response to pH, redox status, temperature, light, ultrasound and proteolytic enzymes. Among them, temperature is the most widely used external stimulus to induce drug release from smart nanocarriers. Typically, these formulations contain in their structure molecules that change their physical properties in response to temperature alterations [10]. Therefore, drug release could be tailored to be slow and steady under physiological conditions, whereas fast when the temperature increase.

Various molecules can be used to achieve temperature-controlled release such polymers, surfactant, phospholipid, and phase change material [11, 12]. Specifically, phase change materials (PCM) are materials with a high latent heat of fusion that undergo to solid-liquid or liquid-solid transition in response to narrow temperature change [13]. PCM are promising tools to construct smart delivery systems for the release control as at transition temperature melt and release drug quickly [14]. Consequently, this responsivity to specific temperatures allows to control the release of drugs at the target site avoiding premature drug leakage improving therapeutic efficacy and reducing harmful side effects. Among the various type of PCM available, very interesting are natural fatty acids for their low toxicity, easy biodegradation and low cost [15, 16].

Due to the limited types of natural fatty acids, it is difficult to achieve PCM with melting points close to the physiological temperature from a single component [13]. Therefore, researchers proposed to employ two or more kinds of fatty acids in several ratios to overcome these drawbacks and to achieve controllable melting temperature [17]. In this light, this study has been conceived to design smart thermo-responsive niosomes based on eutectic mixtures of natural fatty acids for antibiotic delivery. For this purpose, a eutectic mixture of natural fatty acids composed of lauric acid and stearic acid was used as thermoresponsive gate in vesicle bilayer. In fact, the eutectic mixture at weight ratio of lauric acid (mp = 44 °C) and stearic acid (mp = 69 °C) 4:1, exhibit a sharp melting point at 39 °C and can be used for thermoresponsive targeting. This PCM was incorporated in niosomes bilayer based on Span 60 and cholesterol in order to control the release of a broad-spectrum antibiotic, Tetracycline hydrochloride (TC), active against both gram-positive and gram-negative bacteria. Commonly, TC efficacy is seriously limited by its low bioavailability, side effects and the emergence of resistance [18, 19]. Consequently, its encapsulation in a smart nanodevice as proposed in this work could be a potential solution to improve its clinical efficacy.

Materials

Lauric acid, stearic acid, cholesterol, sorbitan monostearate (Span® 60), tetracycline hydrochloride (TC) were purchased from Sigma-Aldrich (Milan, Italy). Mueller-Hinton Broth was purchased from Difco Laboratories (Detroit, MI, USA). All solvents were of analytical grade and used without further purification.

Preparation of thermo-responsive niosomes.

First, lauric acid and stearic acid (4:1 by weight), were dissolved in chloroform to prepare PCM. Various niosomes formulations were developed by modulating molar ratio of Span60, Ch and PCM using the thin-film hydration method (Table 2). For this purpose, Span60 and Ch were solubilized in ethanol and chloroform mixed solvents (v/v 4:1). PCM were added directly to the solubilized surfactant and the final solution was then dried in a rotary evaporator at 40 °C to obtain thin lipid film. The lipid film was then hydrated with 10 ml TC aqueous solution (8.31 x 10^{-4} M) for 20 min at 60°C. After that, the dispersions obtained were firstly cooled at room temperature for 5 min and then at 4 °C in an ice water bath for 10 min accompanied by mechanical stirring to rapidly solidify the fatty acid eutectic mixture and promote the encapsulation of drug.

Characterization of thermoresponsive niosomes

The size and zeta potential of thermoresponsive niosomes were evaluated by dynamic light scattering (Malvern, Zetasizer Nano ZS) at a scatting angle of 90°. The morphology was characterized by transmission electron microscopy (HITACHI, Ht-7700). Encapsulation efficiency (EE %) of TC in nanovesicles were evaluated after purification by dialysis method. Purified niosomes were diluted 1:100 (v/v) using ethanol in order to break the niosomal bilayers and release the encapsulated compounds. The concentration of TC was measured using a UV−vis spectrometer at 271 nm and calculated according to a standard curve. The EE was calculated using **eq 1:**

$$\boldsymbol{EE}\ \% = (\boldsymbol{TC\ in\ purified\ niosomes})/(\boldsymbol{TC\ c\ in\ \ non\ purified\ niosomes}) \times \mathbf{100}$$

The stability of thermosensitive vesicles were evaluated by determining the sizes and zeta potentials at specific time points up to 3 months. Each measure was repeated three times, and the results were recorded as the mean ± standard deviation. Moreover, we sought to examine *in vitro* stability of niosomes in PBS, NaCl 0.9% and MH medium since these conditions would affect particle size and consequently the stability, uptake and

antibacterial efficacy. To perform this preliminary biological evaluation, 0.5 ml of niosomes were diluted up to 5 ml and the average size, polydispersity index, and ζ-potential were evaluated by DLS maintaining samples at 37 °C and performing measurements at different time points (0, 0.5, 2, 5, 24,48 and 120 h). Thermograms of the physical mixture of Span60, CH and PCM mixtures were recorded using differential scanning calorimetry (DSC SETARAM 131). Samples were placed in an aluminum pan and scanned at a rate of 3 °C/min over a temperature range of 20–85 °C under a purge of nitrogen.

***In vitro* thermo-responsive drug release.**

To evaluate the thermo-responsivity of developed niosomes, antibiotic release experiments were investigated by dialysis method at two different temperatures (37 and 42 ◦ C). Typically, 1 mL of TC niosomes solution was poured into a dialysis bag (MWCO = 12-14 kDa), which was immersed in 25 mL of distilled water in a thermostat bath. At certain time intervals, 2 mL of solution was taken out and replaced with 2 mL fresh buffer. The absorbance value of the release solution was recorded at 271 nm by UV–vis spectrophotometer and the drug concentration was calculated according to the standard curve of TC. The results are reported as cumulative release (%) using **eq**:

$$\boldsymbol{TC\ Release}\ \% = (\boldsymbol{TC\ release\ from\ niosomes})/(\boldsymbol{initial\ TC\ in\ niosomes})\ \times \mathbf{100}$$

Analysis of drug release kinetics.

The mechanism of TC release for each formulation was exploited fitting release data to different kinetic models including first order, Korsmeyer-Peppas, Peppas-Sahlin and Weibull model [20] using the mathematical equation reported in Table 1:

Table 1. Kinetic model used to analyze the data of TC release from the developed thermosensitive niosomes.

Release Kinetic Model	Mathematical equation
First order	$Q/Q_0 = 1- e^{kt}$
Korsmeyer-Peppas	$Q/Q_0 = k\ t^n$
Peppas-Sahlin	$Q/Q_0 = K_1t^m+k_2\ t^{2m}$
Weibull	$Q / Q_0 = 1-e^{(-b * t\hat{}a)}$

where Q represents the amount of drug released at time t; Q0 is the initial amount of drug; k is the release constant. The applicability of the release kinetics models was evaluated considering the regression coefficient of correlation (r2), Adj. R-Square, Pearson's r and residual sum of squares. A higher value of Adj. R-Square and Pearson's r indicate a model applicable to the release curve [21]. Conversely, a lower Residual Sum of Squares values highlight the better kinetic model [22].

Hemolysis assay

Hemolysis assay was performed on fresh blood drawn and used on the same day as the experiments. Rabbit blood was provided by the Instituto de Química Avanzada de Cataluña-IQAC. Following the method described by Pape et al. [23], red blood cells were washed three times with a solution of PBS pH 7.4. Different volumes of a niosomal solution (1190 μg/mL/ 5940.5 μM), ranging from 10 to 100 μL, were placed in an Eppendorf, to which 25 μL of erythrocyte suspension and phosphate-buffered saline were added for a total volume of 1 mL. The samples were mixed for 10 min at room temperature and then centrifuged for 5 min at 10,000 rpm. The percentage of hemolysis was determined by comparing the absorbance at 575 nm of the supernatant of the samples with that of the control totally hemolyzed with distilled water. Each analysis was performed in triplicate.

***In vitro* antibacterial activity**

To evaluate the antimicrobial activity of the thermosensitive niosomes, the MIC, defined as the lowest concentration of antimicrobial agents that inhibits the development of visible growth after 24 h of incubation at 37°C, was determined in vitro. The next representative Gram-positive and Gram-negative bacteria have been tested: Bacillus subtilis ATCC 6633, Staphylococcus epidermidis ATCC 12228, Staphylococcus aureus

ATCC 29213, Listeria monocytogenes ATCC 15313, Enterococcus faecalis ATCC 29212, Escherichia coli ATCC 25922, Acinetobacter baumannii ATCC 19606, Klebsiella pneumoniae ATCC 13048. The MIC values of the developed niosomes were determined using a broth microdilution assay at two different temperatures. Serial dilutions of niosomes in Mueller-Hinton broth (MHB) were prepared and 200 μL of these were dispensed into the corresponding wells of a 96-well polypropylene microtiter plate. Then, 10 μL of initial culture of each bacterial strain was added to obtain a final inoculum of about 5 × 10-5 colony forming units (CFU)/mL. The positive control wells contained MHB and the bacterial suspension without the niosomes, whereas the negative control wells contained MHB and the niosomes without bacterial suspension. Multiwell plates were incubated after sample inoculation at two different temperatures, 37°C and 42°C. After 24 hours, the MIC was visually determined as the development of turbidity indicates bacterial growth, reflecting an increase in cell number. To confirm the MIC observation, 20 μL of 0.015% w/v resazurin was added to each well and allowed to react for about 2 hours with the bacteria at the two temperatures. After the incubation period, the bacterial growth indicator changed from blue to pink, confirming the MIC value. Then the MBC (the antimicrobial concentration corresponding to at least a 3-log reduction in viable cells) was determined. A 10-μL aliquot of the MIC well and the two immediately preceding concentrations was seeded on Muller Hilton agar and incubated for 24 hours, at 37°C. The MBC was determined as the lowest concentration at which no colonies were observed on the agar plates.

Results and discussion

The aim of this work was to develop a thermosensitive nanodevice for localized antibiotic delivery. Unspecific antibiotic delivery has, indeed, important side effects such as sub-lethal concentrations at the site of infection, lack of targeting causing the disruption of intestinal flora and the appearance of multidrug resistance. The encapsulation of antibacterial agent in niosomes was widely pursued in the last years to improve their stability, biocompatibility, prolong the release and enhance antibacterial efficacy [24]. Considering the recent success of stimuli-responsive nanocarriers to improve antibiotic efficacy, we focused on the design of thermoresponsive niosomes for the control of TC release. For this goal, a eutectic mixture of lauric and stearic acid is used as thermoresponsive gatekeeper of vesicle bilayer. The choice of this type of fatty acids is

mainly due to that when combined at weight ratio 4:1 has a well-defined melting point at 39 °C.

Niosomes were prepared via film hydration approach by changing the molar ratios of non-ionic surfactant, CHOL and PCM in order with the goal towards obtaining a stable formulation at physiological temperature and a higher release in hyperthermic conditions. Niosomes visually appeared as milk and turbid dispersions, the typical aspect of vesicular formulations. The physicochemical properties of vesicles are reported in Table 2. The mean particle sizes ranged between 244.9 and 348.3, with a P.I. lower of 0.3 indicating a homogeneous and narrow size distribution (Figure 1). The increase of cholesterol content resulted in a decrease of vesicle size since surface free energy usually decreases with increasing hydrophobicity and therefore resulted in smaller vesicles [25]. A similar trend was also observed with the increase of PCM content in vesicle bilayers which further raises nanocarrier hydrophobicity. The formulations developed presented a good ability to encapsulate TC in aqueous core as suggested by the high values of EE% that ranged between 53.44 and 81.29 (Table 2). The drug loading led to important variation of particle size: a significant increase in the hydrodynamic diameter was indeed observed (Table 3). This trend is already reported in literature and it is due to the fact that TC has a negative charge and when is located in the aqueous compartment was free to move and cause electrical repulsion each other leading to an increase of vesicle size [26, 27].

Table 2. Composition (molar ratio) and physicochemical characterization of niosomes in terms of hydrodynamic diameter, P.I. and Z-potential. All formulations were prepared at 1 × 10−2 M of total lipid concentration. Values represent means ± S.D. (n=3).

Formulation	Span60	Chol	PCM	Size (nm)	P.I.	Z-potential (mV)
SP60	1	-	-	348.3±6.8	0.250	-28.3 ± 0.87
SP60PCM	1	-	0.5	327.3±3.6	0.220	-30.6 ± 0.92
SP60PCM2	1	-	0.7	270.0±4.5	0.237	-34.8 ± 0.83
SP60CH	0.5	0.5	-	311.1±4.9	0.270	-35.7 ± 0.76
SP60CHPCM	0.5	0.5	0.5	270.7±8.7	0.281	-37.7 ± 1.18
SP60CHPCM2	0.5	0.5	0.7	244.9±6.8	0.225	-29.3 ± 0.84

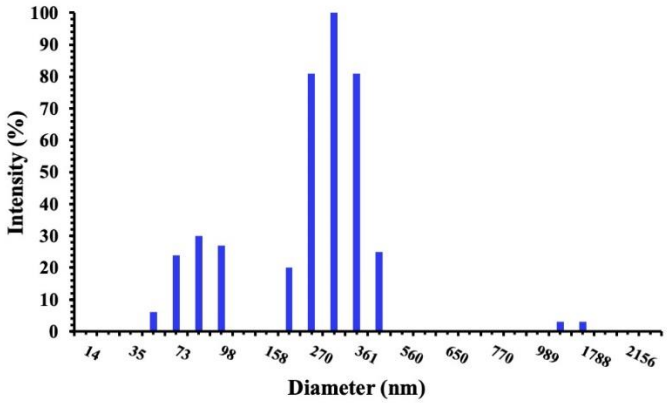

Figure 1. Intensity size distribution of SP60CHPCM2 by DLS analysis.

Table 3. Physicochemical characterization of niosomes loaded with TC in terms of hydrodynamic diameter, P.I., Z-potential and encapsulation efficiency (EE%). Values represent means ± S.D. (n=3).

Formulation	Size (nm)	P. I.	Z-potential (mV)	EE%
SP60	375.0± 7.9	0.175	-26.1 ± 0.58	66.36±3.79
SP60PCM	352.5± 5.7	0.192	-23.5 ±1.97	53.44±6.57
SP60PCM2	355.3± 8.5	0.245	-23.0 ±0.889	81.29±8.95
SP60CH	488.3± 4.3	0.184	-26.1 ±0.520	71.84±5.36
SP60CHPCM	316.4±7.5	0.263	-27.9 ± 0.503	54.86±6.82
SP60CHPCM2	353.3± 9.5	0.275	-26.6 ± 0.611	66.78±4.77

Despite its nonionic character the SP60 niosomes showed a large negative Z-potential value. The incorporation of the fatty acid mixture gave rise to lower Z-potential values due to the negative charge of these compounds. Anyway, all formulation exhibited large negative Z-potential values which help to increase the stability of these formulations due to electrostatic interactions. The TC loaded niosomes (Table 3) had higher values, but they are still enough negatives to maintain the stability. All these niosomes (free and TC loaded) presented low polydispersion index (0.174-0.281) which also can contribute to enhance the stability of these aggregates. The size and morphology of the SP60CHPCM2 niosomes have been also study using TEM. This niosomes showed the best *In vitro* cumulative release profile of TC (see next section), because that it has been chosen to carried out these studies. As shown in TEM image (Figure 2), SP60CHPCM2 niosomes were uniformly spherical and homogeneous in shape and the size concordant with that evaluated by DLS.

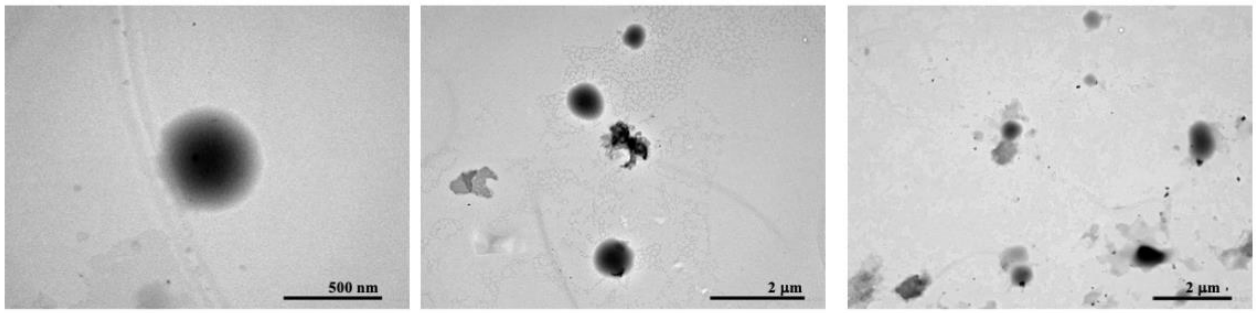

Figure 2. Representative TEM images of SP60CHPCM2

Next, we used differential scanning calorimetry (DSC) to evaluate the response of the developed formulation to temperature and the melting profiles for all the samples are showed in Figure 3.

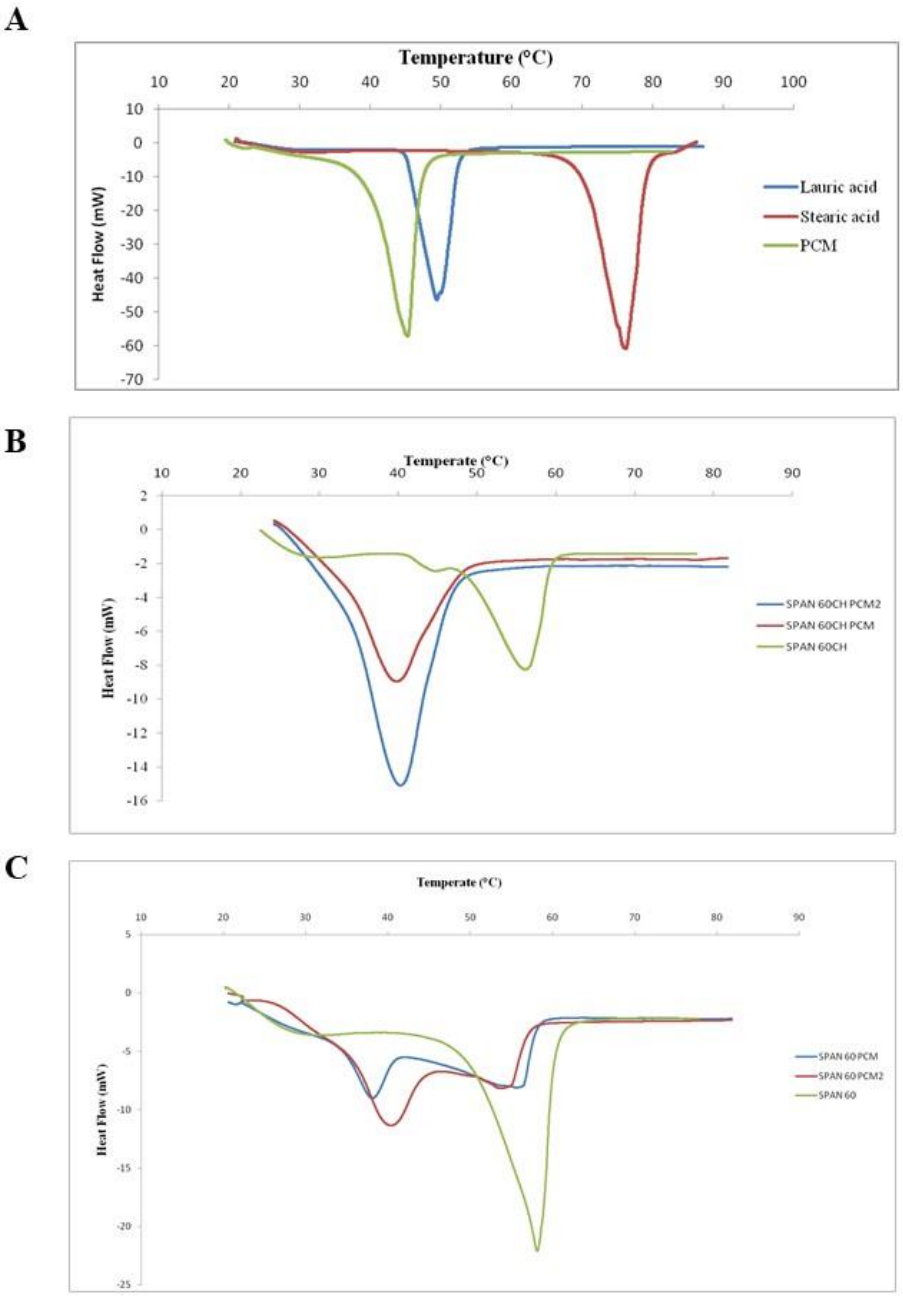

Figure 3. DSC thermograms of (A) PCM physical mixture, (B) SP60CH niosomes whit and without PCM mixture and (C) SP60 niosomes whit and without PCM mixture

Figure 3 A shows the DSC profile corresponding to the pure fatty acid and its mixture. As expected, the melting point of the PCM is lower than that corresponding to the two components. The melting point of the SPAN60 and SPAN60CH was around 55 ºC and the introduction of PCM in the vesicle bilayer of these niosomes conferred them a melting point around 40 ºC.

The thermo-responsive properties of the developed nanodevices were investigated performing drug release experiments at two different temperatures corresponding to the

physiological (37°C) and hyperthermic temperature (42°). Ideal drug delivery systems for antibiotic delivery should ensure no premature drug leakage during blood circulation but quickly release at the target sites.

Preliminary studies were done to achieve the best surfactant/PCM ratio that gives the formulation with suitable thermoresponsive properties. The inclusion of PCM in vesicles prepared without cholesterol conferred to the systems thermoresponsiveness dependent on the amount of eutectic mixture added in the bilayer. As shown in Figure S1, SP60PCM2TC, with the higher amount of PCM, achieved the total release of entrapped drug after only 4 h at hypertermic temperature, while SP60PCM release the 93 % of TC after 7 h. The release observed at 37 °C for these formulations is more slow, about 60% at 24 hours both systems. These results confirm our hypothesis that the inclusion of a eutectic mixture in vesicle bilayer with melting point of 39 °C allows to achieve a control of release dependent on temperature. Anyway, a significant leakage of TC already at 37 °C was observed making these devices less efficient and increasing the risk for systemic toxicity. Therefore, we decided to incorporate cholesterol in the bilayer since its ability to increase niosomes stability and decrease the leakage of encapsulated content in the bloodstream [28, 29]. Figure 4 shows the TC release experiments corresponding to the niosomes containing cholesterol. We investigated if the cholesterol incorporation affects thermoresponsive properties of the developed niosomes. As shown in Figure 4, TC release profile from SP60CH vesicles shows only a little increase with the temperature change from 37 to 42°C. The cumulative release of TC is respectively 45.21 and 59.72 % at 37°C and 42°C after 24 h. On the contrary, a significant increase of the release is observed for vesicles that present PCM mixture in their bilayer. SP60CHPCM and SP60CHPCM2 achieved a release equal to 65.40 and 54.04 % in 24h at physiological temperature. When the temperature increase at 42 °C, a fast and rapid release occurred resulting in the release of the total amount of drug encapsulated in only 7 and 2 h respectively for SP60CHPCM and SP60CHPCM2. Consequently, a clear temperature-dependent release pattern was observed highlighting the nanocarrier stability at physiological temperature and the increased release ability at phase-transition temperature, enhancing the local drug concentration at the infection site. So, cholesterol incorporation in the bilayer did not influence temperature triggered release properties of the developed vesicle but limits the TC release in physiological conditions. The best release profile was observed for SP60PCM2 that was more stable at 37 °C and released the drug rapidly when the temperature was higher than the phase transition temperature. Because of the obtained

results, stability studies and antimicrobial activity were conducted only considering SP60PCM2 vesicles.

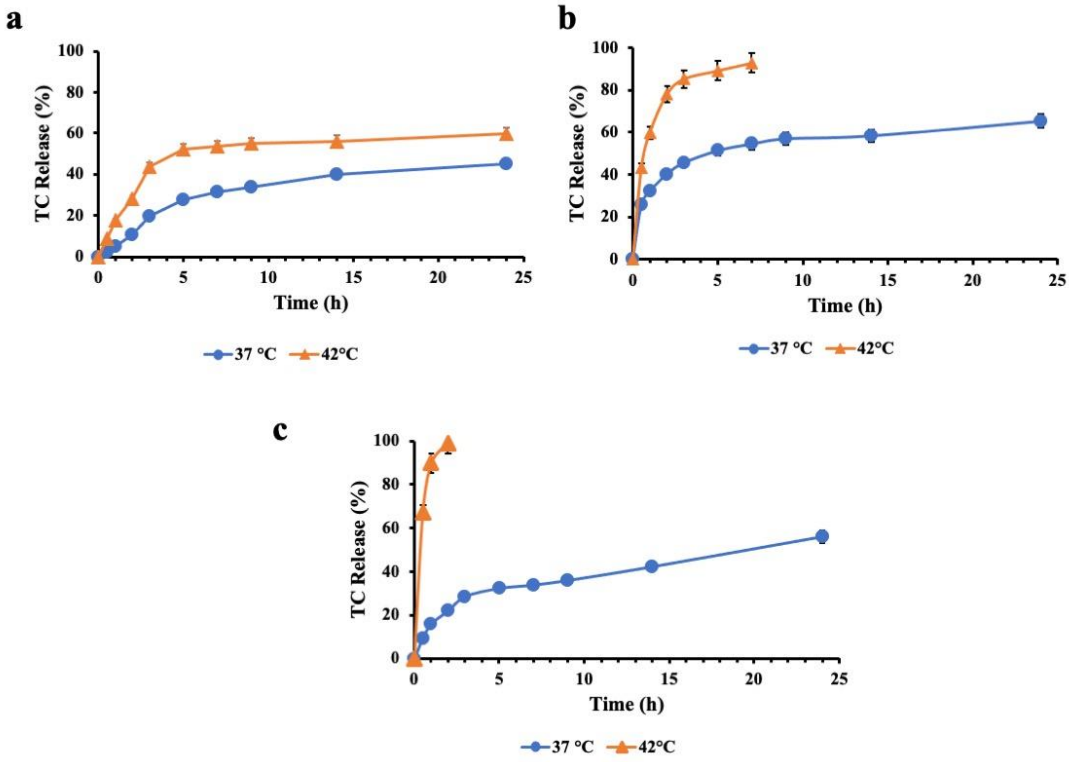

Figure 4. *In vitro* cumulative release profile of TC from SP60CH (A), SP60CHPCM (B) and SP60CHPCM2 (C) at physiological (37°C) and hyperthermic temperature (42°C).

The results data of TC release at the two different temperatures were then fitted into several kinetics models and linear form for understanding mechanism of drug release. We summarized all the kinetic parameters obtained in Table S1 and the results demonstrated that only Peppas-Sahlin and the Weibull models show acceptable fitting results. Moreover, it was found that the TC release from non termoresponsive systems (SP60 and SP60CH) was best explained by the Peppas-Sahlin model. The values of Adj. R-Square equal to 0.99647and the Residual Sum of Square equal 0.00176 were respectively higher and smaller than those of the other models as described in Table S1. Conversely, the patter release from vesicle that present in their bilayer the thermoresponsive PCM mixture at 42 °C in addition to Peppas-Sahlin model were also best fitted by the Weibull model as suggest by the high value of Adj. R-Square and very low Residual Sum of Square data. The stability of niosomes is important to assess their potential applications. In fact, one of the maul problems of liposomes is that they are not stable aggregates given that their low chemical stability of the phospholipids [30]. Stability studies of the developed vesicles stored at room temperature were carried out for 3 months and highlighted that vesicles were stable at room temperature and no sedimentation, creaming or flocculation

was observed. To gain more detailed information, the changes in particle size, PDI values, and Zeta potential were monitored as reported in Table 4, only small variations in particle size and EE % throughout 3 months of storage occurred suggesting that these formulations are suitable for drug delivery applications.

The stability studies of niosomes formulations were also assessed in various medium simulant biological conditions (Figure 5, S2, S3) since complex mixtures with a certain pH, ionic strength and often the presence of organic matter can influence the stability and, thereby, alter the efficacy.

Table 4. Storage stability of SPAN60CHPCM2 stored at room temperature up to 3 months evaluated measuring diameter, P.I., ξ-potential, D.L. at specific time points. Data are expressed as mean of three different experiments ± SD.

Time (days)	Size (nm)	P. I.	Z-potential (mV)	EE%
0	353.3 ± 9.5	0.275	-26.6 ± 0.61	66.78±4.77
15	326.4± 9.8	0.255	-27. 1 ± 1.01	65.34±3.44
30	391.0± 6.3	0.276	-26.0 ±0.52	65.11±3.75
45	382.8± 8.7	0.310	-27.2 ±0.52	64.99±6.78
60	379.4± 3.6	0.286	-25.5 ± 0.42	62.59±5.85
90	384.9± 4.4	0.274	-24.5 ± 0.53	63.01±4.98

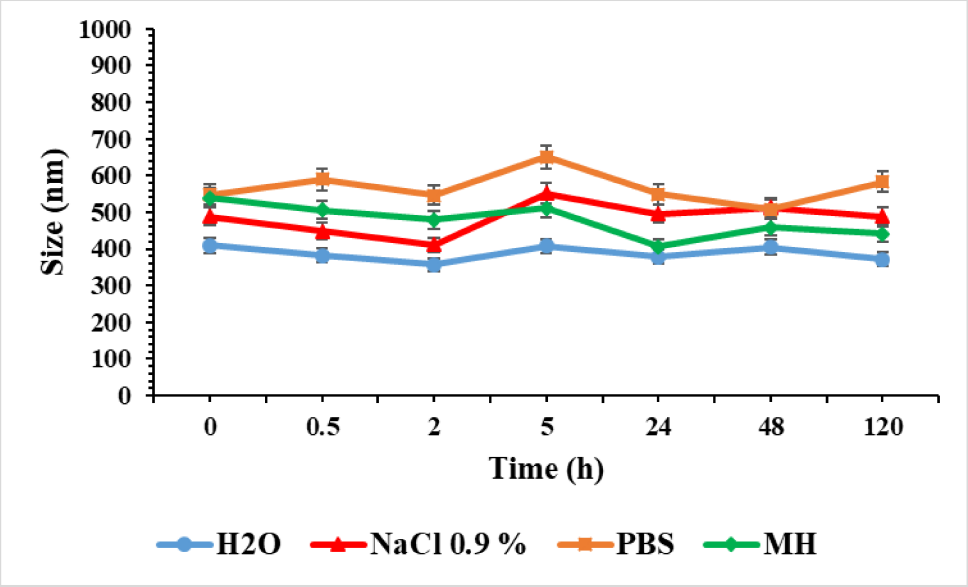

Figure 5. Measurements of average size (nm), (b) polydispersity index (PDI), and (c) Z-potential (mV) of SPAN60CHPCM at 37°C and at different time (0, 0.5, 5, 24,48,120 h) of incubation in H_2O, PBS, NaCl 0.9% and MH. Replicates of three different batches were considered and results are mean values ± SD.

No significant alterations in dimensions and ζ-potential within 120 h were observed in the different conditions tested. Only, niosomes diameter in PBS and NaCl 0.9% is slightly larger than that in water, which can be ascribed to the salt absorption on particle surface.

So it is possible to conclude that niosomes are stable in physiological conditions and the culture medium used for antibacterial assays. This suggests that the system is stable, and is therefore suitable for antibacterial applications.

Antimicrobical activity

The antimicrobial activity (MIC and MBC) of empty and TC-loaded niosomes were evaluated at two different temperatures (37°C and 42°C) against some representative Gram-positive and Gram-negative bacteria. This study was carried out to investigate the antimicrobial performance of the developed nananodevices and to identify if there is some enhancement of antibacterial efficacy with the temperature.

The experiments were carried out only on SP60CHPCM2 that, as reported above, presents the better thermoresponsive properties and the results are shown in Table 5 and 6. For comparison purposes the MIC and MBC values of free TC and empty niosomes were also measured.

Table 5. MIC values (μM) of free TC, empty and TC-loaded niosomes: BS (*B. subtilis*), SE (*S. epidermidis*), SA (*S. aureus*), LM (*L. monocytogenes*), EF (Enterococcus faecalis), EC (*E. coli*), AB (*A. baumannii*) and KA (*Klebsiella pneumoniae*) at 37°C and 42°C.

MIC	**37°C**			**42°C**		
	SP60CHPCM2	**SP60CHPCM2 TC**	**TC**	**SP60CHPCM2**	**SP60CHPCM2 TC**	**TC**
BS	>2970	0.77	1.62	371.26	0.77	1.62
SE	>2970	112.81	207.94	371.26	14.10	103.97
SA	>2970	3.52	3.25	742.57	3.52	3.25
LM	>2970	7.05	3.25	>2970	3.108	1.62
EF	>2970	28.20	25.99	>2970	14.01	12.99
EC	>2970	7.05	6.49	>2970	3.52	6.49
AB	>2970	7.05	6.49	>2970	3.52	3.25
KA	>2970	14.1	6.49	>2970	14.1	6.49

Table 6. MBC values (μM) of free TC, empty and TC-loaded niosomes: BS (*B. subtilis*), SE (*S. epidermidis*), SA (*S. aureus*), LM (*L. monocytogenes*), EF (Enterococcus faecalis), EC (*E. coli*), AB (*A. baumannii*) and KA (*Klebsiella pneumoniae*) at 37°C and 42°C.

MBC	**37°C**			**42°C**		
	SP60CHPCM2	**SP60CHPCM2 TC**	**TC**	**SP60CHPCM2**	**SP60CHPCM2 TC**	**TC**
BS	>2970	0,77	1.62	742.57	0,77	>6.49
SE	>2970	>49,74	>415.88	1485.14	>49,74	>103.97
SA	>2970	>24,87	>103.97	1485.14	>24,87	103.97
LM	>2970	>24,87	6.49	>2970	3,108	3.25
EF	>2970	>49,74	>207.94	>2970	>49,74	51.98
EC	>2970	>24,87	>25.99	>2970	>24,87	>25.99
AB	>2970	> 24,87	>25.99	>2970	24,87	12.99
KA	>2970	> 49,74	>51.98	>2970	>49,74	>25.99

At the higher concentration tested, 2970 μM, the empty niosomes did not showed antimicrobial activity against any of the tested bacteria. Only a weak activity was observed at 42 ºC against some of the Gram-positive microorganisms at very high concentrations possibly due to lauric acid presence in vesicle bilayer which has been reported to have antimicrobial properties [31]. Notice that at 42 ºC the fatty acid state has changed, this can give rise to a better bioavailability of this compound and consequently to a better antimicrobial activity. The experimental results in our study confirmed the antimicrobial activity of free TC against Gram-positive and Gram-negative bacteria with MIC values in the range 0.6-30 μM in accordance with that reported in the literature [32, 33]. It was obtained a very big MIC value against the *S. epidermidis* which agree with previous studies that observed that, compared with other antibiotics, tetracyclines exhibited low antimicrobial effectivity against different *S. epidermidis* strains [34]. In fact, Aelenei et al. [35] reported that the *S. epidermidis ATCC* 12228, strain use in this work, is resistant to this antibiotic. The MBC values of TC are much higher than the MICs. The mode of action of tetracycline implies the binding to the bacterial ribosome and thereby interfering with protein translation. The result of this type of interaction is generally bacteriostatic rather than bactericidal [36]. At 37 ºC it was observed that TC encapsulated in niosomes maintain its antimicrobial efficiency against the tested bacteria. Even a slightly better inhibition effect was observed against BS and SE strains with MIC reduction from 1.62 to 0.77 and from 207.94 to 112.81, respectively (Table 5). Instead, a significant decrease of MBC values was observed for TC-loaded niosomes respect ones obtained with free drug against all of the tested bacteria except for LM, indicating a good ability to completely kill bacteria (Table 6). For example, MBC value of TC-loaded niosomes against *S. aureus* (7.05 μM) was considerably higher than that of the free drug

equal to 103.97 μM. This enhanced antibacterial activity may be due to a change in the mode of action of the encapsulated TC against bacteria due to the better permeability and fusogenic properties of niosomes and/or the interaction of the other niosomes components. Indeed, it has been demonstrated that encapsulation of antibiotics in vesicles can improve their pharmacokinetic profiles and increase its accumulation at the infection site minimizing its cytotoxicity and protecting them from peripheral degradation [37].

Moreover, the developed niosomes showed an interesting temperature-dependent antibacterial activity against some bacterial strains. In fact, the temperature increase to 42°C further improves the activity of the niosomes against *S. Epidermis*, with lower MIC value equal to 14.10 μM respect that obtained at 37 °C equal to 112.81 μM. A moderate temperature-dependent trend of antibacterial activity was also observed for EC and AB strains. For example, MBC values for *E. coli* and *A. baumannii* at 37°C were 7.05 and 7.05 and were reduced to 3.52 by temperature increase. It is noticeable that using this niosomal formulation one resistant bacteria has become to a sensitive one. This shows that through this type of technology it is possible to reuse antibiotics that were no longer effective against certain resistant bacteria, then, it can be an interesting approach to combat the emergence of resistant bacteria. This shows again that encapsulation of TC in thermoresponsive niosomes also permitted the antimicrobial activity of the drug to be exerted at a lower concentration than that of the free drug without affecting the treatment outcomes and reducing side effects.

The experimental results demonstrate that the inclusion of a eutectic mixture in vesicle bilayer not only affects release but also the antibacterial activity. The enhanced activity at 42°C of the TC-loaded niosomes for some of the tested bacteria can be ascribed to better ability to release its content at temperature above the melting point of eutectic mixture, increasing drug concentrations at the infection site and offering a better killing effect. Taken together, encapsulating the antibiotic into a thermoresponsive nanocarrier provides good biosafety, prevents premature release, allows to release antibiotics more precisely and eliminate bacteria more effectively, which make these devices appealing for further development into a clinical agent to prevent serious bacterial infections.

In this regards the literature contains a lot of formulations containing antibiotics encapsulated in liposomal formulations that improve the antimicrobial activity of the drug [38]. In this respect, a TC-liposomal formulation has been already approved by the FDA to treat the *Chlamydia trachomatis* [39]. However, liposomes show certain disadvantages: low solubility, short half-life, low chemical phospholipid stability and high production

cost. Gentamicin loaded niosomes were also prepared using a non-ionic surfactant (Tween 60, tween 80 or Brij 35), cholesterol and a negative charge inducer, dicetyl phosphate. Niosomes composed of Tween 60, cholesterol, and dicetyl phosphate were the most effective in terms of prolongation of in vitro drug release [40].

In this work we have prepared, for the first time, a stable thermosensitive tetracycline-niosomal system using economical starting materials. It has been assessed that the realize of the antibiotic at 42 ºC is higher than at 37 ªC which could improve the effectivity of antibiotics against some resistant bacteria.

To evaluate the biosafety of the newly developed nanocarriers (empty and TC-loaded), hemolysis assay was performed on human erythrocytes. It was found that both empty and TC loaded vesicles were hemocompatible, causing negligible release of hemoglobin from erythrocytes even at the highest concentration tested. We observed only a slight hemolytic activity equal to 11.37±1.99 % and 19.97± 1.99 % of empty and drug-loaded systems at the concentration of 119 μg/mL of LA. These values indicate that the therapeutic index of these systems (hemolysis/MIC ratio) is very high which indicates the high biocompability of these formulations. The non-toxicity of free and TC-loaded niosomes makes these new antimicrobial systems highly desirable as safe nanocarriers for biomedical applications.

Conclusions

In the present study, we developed a novel platform based on thermoresponsive niosomes with the purpose to control TC delivery in the treatment of bacterial infections. The systems produced showed good physicochemical properties and entrapment efficiency, stability and tunable thermo-responsive properties. The developed niosomes result able to prevent premature release of TC in physiological conditions, while they have shown a fast release at 42 °C. This thermoresponsive release was also associated with an enhanced antibacterial efficacy in hypertermic conditions that allows, so, to use low antibiotic doses maintaining therapeutic outcomes and reducing the adverse side effects of common antimicrobial agents. The present smart platform may hold promise for fighting against various bacteria-induced diseases.

Supplementary materials

Figure S1. *In vitro* cumulative release profile of TC from SP60 (A), SP60PCM (B) and SP60PCM2 (C) at physiological (37°C) and hyperthermic temperature (42°C).

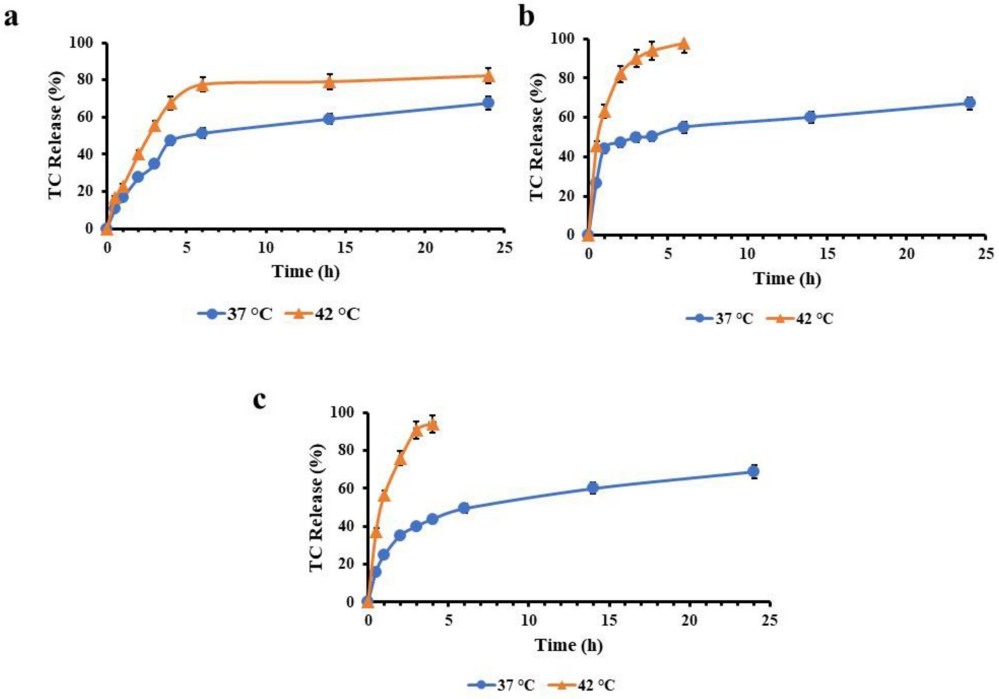

Figure S2. Measurements of polydispersity index (PDI) of SPAN60CHPCM at 37°C and at different time (0, 0.5, 5, 24,48,120 h) of incubation in H_2O, PBS, NaCl 0.9% and MH. Replicates of three different batches were considered and results are mean values ± SD.

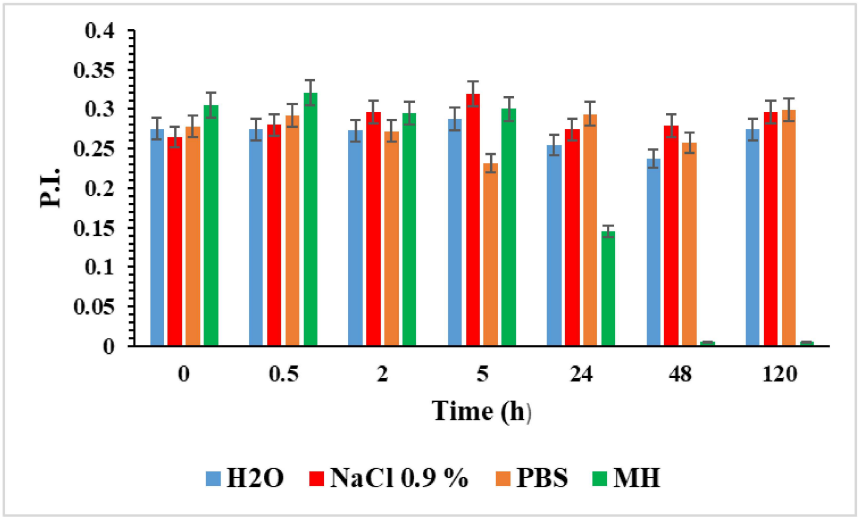

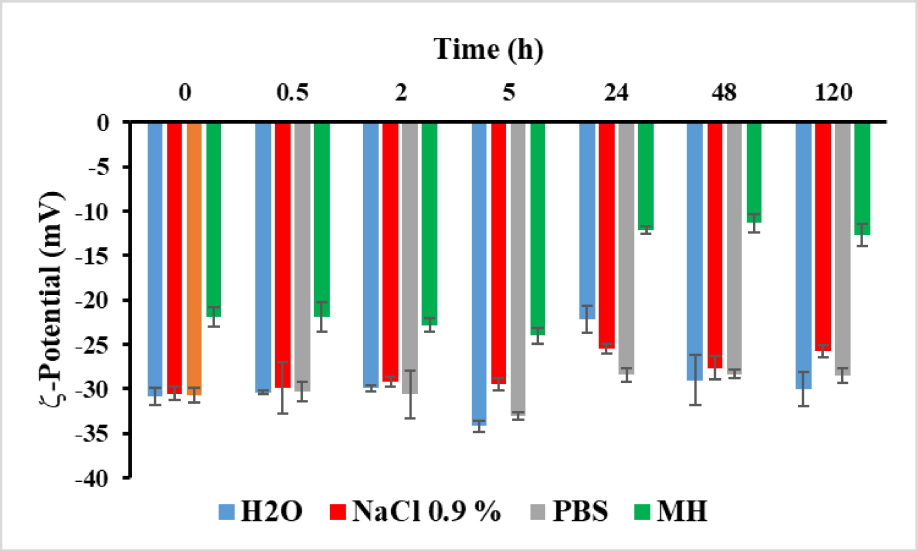

Figure S3. Measurements of Z-potential (mV) of SPAN60CHPCM at 37°C and at different time (0, 0.5, 5, 24,48,120 h) of incubation in H_2O, PBS, NaCl 0.9% and MH. Replicates of three different batches were considered and results are mean values ± SD.

Table S1. The release kinetics model fitting parameters of TC release from the developed formulations.

SP60					
KINETIC MODEL	**T**	**R^2**	**ADJ. R-SQUARE**	**PEARSON'S R**	**RESIDUAL SUM OF SQUARE**
First order	37°C	0.80081	0.76097	-0.89488	0.14926
	42°C	0.61806	0.54167	-0.78617	0.82589
Korsmeyer-Peppas	37°C	0.91327	0.89593	0.95565	0.22795
	42°C	0.84664	0.81597	0.92013	0.36034
Peppas-Sahlin	37°C	0.98784	0.98297	-	0.01431
	42°C	0.99748	0.99647	-	0.00176
Weibull	37°C	0.94415	0.93299	0.97168	0.22089
	42°	0.88818	0.86582	0.94243	0.50738
SP60PCM					
First order	37°C	0.75889	0.71066	-0.87114	0.08458
	42°C	0.98567	0.9809	-0.99281	0.05592
Korsmeyer-Peppas	37°C	0.82995	0.79594	0.91102	0.08396
	42°C	0.94688	0.9336	0.97308	0.02355
Peppas-Sahlin	37°C	0.98771	0.9814	-	0.02313
	42°C	0.99969	0.99954	-	0.00121
Weibull	37°C	0.87774	0.85329	0.93688	0.11167
	42°C	0.99975	0.99968	0.99975	0.00060
SP60PCM2					
First order	37°C	0.8852	0.86224	-0.94085	0.07219
	42°C	0.98567	0.9809	-0.99281	0.05592
Korsmeyer-Peppas	37°C	0.9461	0.93532	0.97268	0.07471
	42°C	0. 984	0.97338	0.98997	0.01201
Peppas-Sahlin	37°C	0.99921	0.99889	-	0.00101
	42°C	0.99858	0.99764	-	0.00387

Weibull	37°C	0.97771	0.97325	0.98879	0.05084
	42°C	0.99368	0.99158	0.99684	0.01401
SP60CH					
First order	37°C	0.78604	0.74325	-0.88659	0.05482
	42°C	0.51704	0.42045	-0.71906	0.28478
Korsmeyer-Peppas	37°C	0.88692	0.86431	0.94177	0.79899
	42°C	0.80612	0.76735	0.89784	0.59907
Peppas-Sahlin	37°C	0.96181	0.94653	-	0.01653
	42°C	0.97669	0.96736	-	0.02855
Weibull	37°C	0.90512	0.886887	0.9517	0.78060
	42°C	0.833	0.7996	0.91269	0.73374
SP60CHPCM					
First order	37°C	0.75812	0.70974	-0.8797	0.09704
	42°C	0.94298	0.92873	-0.97107	0.17698
Korsmeyer-Peppas	37°C	0.94688	0.93626	0.97308	0.03264
	42°C	0.92584	0.91842	0.96221	0.03216
Peppas-Sahlin	37°C	0.99782	0.99695	-	0.00333
	42°C	0.99029	0.99148	-	0.04439
Weibull	37°C	0.96268	0.95521	0.98116	0.04082
	42°C	0.99687	0.99583	0.99843	0.00134
SP60CHPCM2					
First order	37°C	0.91163	0.89396	-0.9548	0.02951
	42°C	0.92921	0.91152	-0.96396	0.20456
Korsmeyer-Peppas	37°C	0.95525	0.9463	0.97737	0.09069
	42°C	0.98445	0.98056	0.99219	0.01046
Peppas-Sahlin	37°C	0.99748	0.99647	-	0.00176
	42°C	0.99986	0.99972	-	0.00016
Weibull	37°C	0.97506	0.97007	0.98745	0.06977
	42°C	0.9966	0.99547	0.9983	0.00146

Reference

[1] N.E. Eleraky, A. Allam, S.B. Hassan, M.M. Omar, Nanomedicine fight against antibacterial resistance: an overview of the recent pharmaceutical innovations. Pharmaceutics. 12(2020) 142. https://doi.org/10.3390/pharmaceutics12020142

[2] S.J. Lam, E.H.H. Wong, C. Boyer, G.G. Qiao, Antimicrobial polymeric nanoparticles. Prog. Polym. Sci., 76 (2018) 40-64. https://doi.org/10.1016/j.progpolymsci.2017.07.007

[3] J.K. Patra, G. Das, L.F. Fraceto, E.V.R. Campos, M.P. Rodriguez-Torres, L.S. Acosta-Torres Diaz-Torres, R. Grillo, M.K. Swamy, S. Sharma, Nano based drug delivery systems: Recent developments and future prospects. J. Nanobiotechnol. 16 (2018) 1-33. https://doi.org/10.1186/s12951-018-0392-8

[4] X. Yang, B. Xie, H. Peng, G. Shi, B. Sreeniva, J.Guo, C. Wang, Y. He, Eradicating Intracellular MRSA via Targeted Delivery of Lysostaphin and Vancomycin with Mannose-Modified Exosomes. J. Controlled Release. 329 (2021)454−467. https://doi.org/10.1016/j.jconrel.2020.11.045

[5] F. Fenaroli, U. Repnik, Y. Xu, K. Johann, S. Van Herck, P. Dey, F.M. Skjeldal, D.M. Frei, S. Bagherifam, A. Kocere, Enhanced Permeability and Retention-Like Extravasation of Nanoparticles from the Vasculature into Tuberculosis Granulomas in Zebrafish and Mouse Models. ACS Nano. 12 (2018) 8646−8661. https://doi.org/10.1021/acsnano.8b04433

[6] Y. Huang, L. Zou, J. Wang, Q. Jin, J. Ji Stimuli-responsive nanoplatforms for antibacterial applications. Wiley Interdiscip. Rev. Nanomed. Nanobiotechnol. 14(2022), e1775. https://doi.org/10.1002/wnan.1775

[7] V.A. Spirescu, C. Chircov, A.M. Grumezescu, E. Andronescu, Polymeric nanoparticles for antimicrobial therapies: An up-to-date overview. *Polymers*,*13* (2021) 724. https://doi.org/10.3390/polym13050724

[8] S. Mura, J. Nicolas, P. Couvreur, Stimuli-responsive nanocarriers for drug delivery. Nat. Mater.12 (2013), 991−1003 10.1038/nmat3776

[9] M.A.C. Stuart, W.T.S. Huck, J. Genzer, M. Müller, C. Ober, M. Stamm, G.B. Sukhorukov, I. Szleifer,
Emerging applications of stimuli-responsive polymer materials. Nat Mater. 9 (2010) 101–13. https://doi.org/10.1038/nmat2614

[10] Q. Zhang, X. Chen, H. Shi, G. Dong, M.Zhou, T. Wang, H. Xin Thermo-responsive mesoporous silica/lipid bilayer hybrid nanoparticles for doxorubicin on-demand delivery

and reduced premature release. Colloids Surf. B: Biointerfaces, 160 (2017) 527-534. https://doi.org/10.1016/j.colsurfb.2017.10.005

[11] W.H. Abuwatfa, N.S. Awad, W.G. Pitt, G.A. Husseini,. Thermosensitive polymers and thermo-responsive liposomal drug delivery systems. Polymers, 14(2022) 925. https://doi.org/10.3390/polym14050925

[12] J. Qiu, D. Huo, J. Xue, G. Zhu, H. Liu and Y. Xia, Encapsulation of a Phase-Change Material in Nanocapsules with a Well-Defined Hole in the Wall for the Controlled Release of Drugs, Angew. Chem., Int. Ed., 58(2019) 10606–10611. https://doi.org/10.1002/anie.201904549

[13] Y Yuan, N Zhang, W Tao, X Cao, Y He, Fatty acids as phase change materials: a review. Renew Sust Energ Rev. 29 (2014) 482-498. https://doi.org/10.1016/j.rser.2013.08.107

[14] C. Zhu, D. Huo, Q. Chen, J. Xue, S. Shen, Y. Xia (2017). A eutectic mixture of natural fatty acids can serve as the gating material for near-infrared-triggered drug release. Adv. Mater. 29(40) 1703702. https://doi.org/10.1002/adma.201703702

[15] J. Qiu, D. Huo, Y. Xia, Phase-change materials for controlled release and related applications. Adv. Mat. 32 (2020) e2000660. doi:10.1002/adma.202000660

[16] J.E. Hunter, J. Zhang, P.M. Kris-Etherton, Cardiovascular disease risk of dietary stearic acid compared with trans, other saturated, and unsaturated fatty acids: a systematic review. Am. J. Clin. Nutr. 91(2020) 46-63. https://doi.org/10.3945/ajcn.2009.27661

[17] S. Xie, L. Zhu, Z. Dong, Y. Wang, X. Wang, W.Z. Zhou, Preparation and evaluation of ofloxacin-loaded palmitic acid solid lipid nanoparticles. Int J Nanomed. 6 (2011) 547-555. https://doi.org/10.2147/IJN.S17083

[18] A. Rusu, E.L. Buta, The development of third-generation tetracycline antibiotics and new perspectives, Pharmaceutics. 13 (2021) 2085. https://doi.org/10.3390/pharmaceutics13122085

[19] M. Zhang, Z. Cai, G. Zhang, D. Zhang, X. Pan, Abiotic mechanism changing tetracycline resistance in root mucus layer of floating plant: the role of antibioticexudate complexation, J. Hazard. Mater. 416 (2021) 125728. https://doi.org/10.1016/j.jhazmat.2021.125728

[20] R. Gouda, H. Baishya, Z. Qing, Application of mathematical models in drug release kinetics of carbidopa and levodopa ER tablets. J. Dev. Drugs, 6 (2017), 1-8. DOI:10.4172/2329-6631.1000171

[21] A. Jain, S.K. Jain, In vitro release kinetics model fitting of liposomes: An insight. Chem. Phys. Lipids 201 (2016) 28-40. https://doi.org/10.1016/j.chemphyslip.2016.10.005

[22] V. Rousson, N.F. Goşoniu ,An R-square coefficient based on final prediction error. *Stat. Methodol. 4* 82007)331–340. https://doi.org/10.1016/j.stamet.2006.11.004

[23] W.J. Pape, U. Pfannenbecker, U. Hoppe. Validation of the red blood cell test system as in vitro assay for rapid screening of irritation potencial of surfactants Mol. Toxicol. 1 (1987) 525– 536.

[24] M. Mehrarya, B. Gharehchelou, S. Haghighi Poodeh, E. Jamshidifar, S. Karimifard, B. Farasati Far, A. Seifalian, Niosomal formulation for antibacterial applications. J. Drug Target.*30*(2022) 476-493. https://doi.org/10.1080/1061186X.2022.2032094

[25] F. Nowroozi, A. Almasi, J. Javidi, A. Haeri, S. Dadashzadeh. Effect of surfactant type, cholesterol content and various downsizing methods on the particle size of niosomes. Iran. J. Pharm. Res. 17(2018) 1–11. 31011337

[26] L. Tavano, N. Picci, G. Ioele, R. Muzzalupo, Tetracycline-niosomes versus Tetracycline Hydrochloride- niosomes: How to Modulate Encapsulation and Percutaneous Permeation Properties. J. Drug 1 (2017) 1-6. doi: https://doi.org/10.24218/jod.2017.6.

[27] V.B. Junyaprasert, V. Teeranachaideekul, T. Supaperm, Effect of charged and non-ionic membrane additives on physicochemical properties and stability of niosomes. AAPS pharmscitech. *9* (2008) 851-859. DOI: 10.1208/s12249-008-9121-1

[28] B. Nasseri, Effect of cholesterol and temperature on the elastic properties of niosomal membranes.

Int. J. Pharm 300(2005) 95-101. https://doi.org/10.1016/j.ijpharm.2005.05.009

[29] TM Allen, LG Cleland. Serum-induced leakage of liposome contents. Biochim Biophys Acta Biomembr .*597*(1980), 418-426. https://doi.org/10.1016/0005-2736(80)90118-2

[30] S. Kulkarni, B. Prabhakar, P. Shende, Stabilization of lipid vesicles: Upcoming strategic insights for product development. Journal of Molecular Liquids, 348 (2022) 118430. https://doi.org/10.1016/j.molliq.2021.118430

[31] L. R. Beuchat, D. A. Golden, Antimicrobial Occurring Natually Naturally in Foods different molecular weight. Carbohydrate Polymers, 54 (1989). 527-530.

[32] C. Rodríguez-Melcón, C.Alonso-Calleja, C. García-Fernández, J. Carballo, R. Capita, R. Minimum Inhibitory Concentration (MIC) and Minimum Bactericidal

Concentration (MBC) for Twelve Antimicrobials (Biocides and Antibiotics) in Eight Strains of Listeria monocytogenes. Biology 2022, 11(2022) 46. https://doi.org/10.3390/biology11010046

[33] Grossman TH. Tetracycline Antibiotics and Resistance. Cold Spring Harb Perspect Med.6 (2016)a025387. 10.1101/cshperspect.a025387

[34] L. D. Sabath, C. Garner, C. Wilcox, M. Finland, Susceptibility of Staphylococcus aureus and Staphylococcus epidermidis to 65 antibiotics. Antimicrobial Agents and Chemotherapy, 9 (1976), 962-969.

[35] P. Aelenei, C. M. Rimbu, E. Guguianu, G. Dimitriu, A. C. Aprotosoaie, M. Brebu, A. Miron, Coriander essential oil and linalool–interactions with antibiotics against Gram-positive and Gram-negative bacteria. Letters in applied microbiology, 68(2019), 156-164.

[36] D.E. Brodersen, W. M. Clemons, A. P. Carter, R. J. Morgan-Warren, B. T. Wimberly, V. Ramakrishnan . The structural basis for the action of the antibiotics tetracycline, pactamycin, and hygromycin B on the 30S ribosomal subunit. Cell. 103(2000) 1143-54. doi: 10.1016/s0092-8674(00)00216-6. PMID: 11163189

[37] M. Ferreira, M. Ogren, J.N.R. Dias, M. Silva, S. Gil, L. Tavares, F. Aires-da-Silva, M.M. Gaspar, S.I. Aguiar, Liposomes as Antibiotic Delivery Systems: A Promising Nanotechnological Strategy against Antimicrobial Resistance. Molecules. 26(2021) 2047. https://doi.org/10.3390/molecules26072047

[38] L.Maja, K. Željko, P. Mateja,, Sustainable technologies for liposome preparation. The Journal of Supercritical Fluids, 165 (2020) 104984.

[39] R. Ghosh, M. De,Liposome-Based Antibacterial Delivery: An Emergent Approach to Combat Bacterial Infections. ACS omega, 8(2023), 35442-35451.

[40] D. Seleci,, M. Seleci, J.G. Walter, F. Stahl, T. Scheper, Niosomes as nanoparticular drug carriers: fundamentals and recent applications. Journal of nanomaterials, 2016.